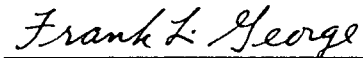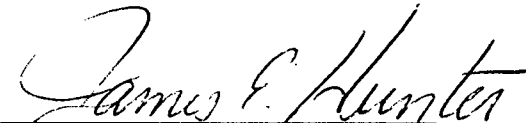## NOTICE

When Government drawings, specifications, or other data are used for any purpose other than in connection with a definitely related Government procurement operation, the United States Government thereby incurs no responsibility nor any obligation whatsoever; and the fact that the government may have formulated, furnished, or in any way supplied the said drawings, specifications, or other data, is not to be regarded by implication or otherwise as in any manner licensing the holder or any other person or corporation, or conveying any rights or permission to manufacture, use, or sell any patented invention that may in any way be related thereto.

This report has been reviewed by the Office of Public Affairs (ASD/PA) and is releasable to the National Technical Information Service (NTIS). At NTIS, it will be available to the general public, including foriegn nations.

This technical report has been reviewed and is approved for publication.

FRANK L. GEORGE
Flying Qualities Group Leader
Control Dynamics Branch

JAMES E. HUNTER, Chief
Control Dynamics Branch
Flight Control Division

FOR THE COMMANDER

H. MAX DAVIS, Assistant for
Research and Technology
Flight Control Division
Flight Dynamics Laboratory

"If your address has changed, if you wish to be removed from our mailing list, or if the addressee is no longer employed by your organization please notify AFWAL/FIGC, Wright-Patterson AFB, OH 45433-6553 to help us maintain a current mailing list.

Copies of this report should not be returned unless return is required by security considerations, contractual obligations, or notice on a specific document.

REPORT DOCUMENTATION PAGE

1a. REPORT SECURITY CLASSIFICATION	1b. RESTRICTIVE MARKINGS
Unclassified	

2a. SECURITY CLASSIFICATION AUTHORITY	3. DISTRIBUTION/AVAILABILITY OF REPORT
	Approved for Public Release; Distribution Unlimited.
2b. DECLASSIFICATION/DOWNGRADING SCHEDULE	

4. PERFORMING ORGANIZATION REPORT NUMBER(S)	5. MONITORING ORGANIZATION REPORT NUMBER(S)
AFWAL-TR-86-3093	

6a. NAME OF PERFORMING ORGANIZATION	6b. OFFICE SYMBOL (If applicable)	7a. NAME OF MONITORING ORGANIZATION
AF Wright Aeronautical Labs	AFWAL/FIGC	

6c. ADDRESS (City, State and ZIP Code)	7b. ADDRESS (City, State and ZIP Code)
Wright-Patterson AFB, OH 45433-6553	

8a. NAME OF FUNDING/SPONSORING ORGANIZATION	8b. OFFICE SYMBOL (If applicable)	9. PROCUREMENT INSTRUMENT IDENTIFICATION NUMBER

8c. ADDRESS (City, State and ZIP Code)	10. SOURCE OF FUNDING NOS.			
	PROGRAM ELEMENT NO.	PROJECT NO.	TASK NO.	WORK UNIT NO.
11. TITLE (Include Security Classification) Proceedings of the Twenty-Second Annual Conference on Manual	62201F	2403	05	69

12. PERSONAL AUTHOR(S)
Frank L. George (Conference Chairman)

13a. TYPE OF REPORT	13b. TIME COVERED	14. DATE OF REPORT (Yr., Mo., Day)	15. PAGE COUNT
Annual	FROM 15Jul86 TO 16Jul86	1986 December	

16. SUPPLEMENTARY NOTATION

17. COSATI CODES			18. SUBJECT TERMS (Continue on reverse if necessary and identify by block number)
FIELD	GROUP	SUB. GR.	Human operator models Physiological measurements
01	03		Displays and visual effects Human-machine systems
05	05		System design

19. ABSTRACT (Continue on reverse if necessary and identify by block number)

The Twenty-Second Annual Conference on Manual Controls emphasized human-machine system design methodology and the impact of automation on the human-machine interface.

20. DISTRIBUTION/AVAILABILITY OF ABSTRACT	21. ABSTRACT SECURITY CLASSIFICATION
UNCLASSIFIED/UNLIMITED ☒ SAME AS RPT. ☐ DTIC USERS ☐	Unclassified

22a. NAME OF RESPONSIBLE INDIVIDUAL	22b. TELEPHONE NUMBER (Include Area Code)	22c. OFFICE SYMBOL
Frank L. George	(513) 255-8497	AFWAL/FIGC

DD FORM 1473, 83 APR   EDITION OF 1 JAN 73 IS OBSOLETE.

Block 11 (Continued)

Control

TWENTY-SECOND

ANNUAL

CONFERENCE

ON

MANUAL

CONTROL

CONFERENCE CHAIRMAN:

        Frank L. George
        Air Force Wright Aeronautical Labs

CONFERENCE ORGANIZERS:

        1Lt. Lisa B. McCormack
        Air Force Wright Aeronautical Labs

        Douglas N. See
        Air Force Wright Aeronautical Labs

FOREWORD

This volume, published with the support of the Air Force Wright
Aeronautical Laboratories, contains the proceedings of the TWENTY-SECOND
ANNUAL CONFERENCE ON MANUAL CONTROL held at the Belton Inn, Dayton,
Ohio, July Fifteenth and Sixteenth, 1986. All papers accepted for the
Meeting are represented in this volume. In a few cases, authors were
unable to attend and present accepted papers, or authors who presented
papers failed to provide manuscripts for the proceedings. Those cases
are noted in the Table of Contents. Both formal papers, generally
representing completed work, and informal papers which might represent
work in progress were presented.

This was the Twenty-Second in a series of Conferences dating back
to December 1964. These earlier meetings and their proceedings are
listed below:

First Annual NASA-University Conference on Manual Control, The
University of Michigan, December 1964. (Proceedings not printed.)

Second Annual NASA-University Conference on Manual Control,
Massachusetts Institute of Technology, February 28 to March 2, 1966,
NASA-SP-128.

Third Annual NASA-University Conference on Manual Control, Univer-
sity of Southern California, March 1 through 3, 1967, NASA-SP-144.

Fourth Annual NASA-University Conference on Manual Control, The
University of Michigan, March 21 through 23, 1968, NASA-SP-192.

Fifth Annual NASA-University Conference on Manual Control,
Massachusetts Institute of Technology, March 27 through 29, 1969,
NASA-SP-215.

Sixth Annual Conference on Manual Control, Wright-Patterson AFB,
Ohio, April 7 through 9, 1970, proceedings published as AFIT/AFFDL
Report, no number.

Seventh Annual Conference on Manual Control, University of Southern
California, June 2 through 4, 1971, NASA-SP-281.

Eighth Annual Conference on Manual Control, The University of
Michigan, May 17 through 19, 1972, AFFDL-TR-72-92.

Ninth Annual Conference on Manual Control, Massachusetts Institute
of Technology, May 23 through 25, 1973, proceedings published by MIT, no
number.

Tenth Annual Conference on Manual Control, Wright-Patterson AFB,
Ohio, April 9 through 11, 1974, AFIT/AFFDL Report, no number.

Eleventh Annual Conference on Manual Control, NASA Ames Research
Center, May 21 through 23, 1975, NASA TM X-62,464.

Twelfth Annual Conference on Manual Control, University of Illinois, May 25 through 27, 1976, NASA TM X-73, 170.

Thirteenth Annual Conference on Manual Control, Massachusetts Institute of Technology, June 15 through 17, 1977, proceedings published by MIT, no number.

Fourteenth Annual Conference on Manual Control, University of Southern California, April 25 through 27, 1978, NASA CP-2060.

Fifteenth Annual Conference on Manual Control, Wright State University, March 20 through 22, 1979, AFFDL-TR-79-3134.

Sixteenth Annual Conference on Manual Control, Massachusetts Institute of Technology, May 5 through 7, 1980, proceedings published by MIT, no number.

Seventeenth Annual Conference on Manual Control, University of California at Los Angeles, June 16 through 18, 1981, JPL Publ. 81-95.

Eighteenth Annual Conference on Manual Control, Wright-Patterson AFB, Ohio, June 8 through 10, 1982, AFWAL-TR-83-3021.

Nineteenth Annual Conference on Manual Control, Massachusetts Institute of Technology, May 23 through 25, 1983, MIT publication, no number.

Twentieth Annual Conference on Manual Control, Ames Research Center, Moffett Field, California, June 12 through 14, 1984, NASA CP-2341.

Twenty-First Annual Conference on Manual Control, Ohio State University, Columbus, Ohio, June 17 through 19, 1985, NASA CP-2428.

The topics "human-machine system design methodology" and "the impact of automation on the human-machine interface" received special emphasis at the Twenty-Second Conference meeting.

Frank L. George
Air Force Wright Aeronautical Labs

CONTENTS

SESSION 1: <u>MODEL BASED ANALYSIS AND SYSTEM DESIGN</u>

Moderator: Dr. David K. Schmidt, Purdue University

MODELING THE EFFECTS OF SYSTEM DELAYS AND LAGS
ON TRACKING PERFORMANCE

William H. Levison
A.W.F. Huggins

BBN Laboratories Incorporated
10 Moulton St.
Cambridge, Massachusetts 02238

ABSTRACT

A laboratory experiment was performed to explore the effects of pure time delay on tracking performance in a simulated pitch-axis control task. Plant dynamics containing no pure delay term other than an irreducible simulator delay of 35 msec served as the baseline condition; the remaining experimental conditions contained added delays of 120, 240, and 360 msec. Time delay had consistent, large, and statistically significant effects on rms tracking error and operator frequency response for trained subjects. No consistent transfer-of-training effects were found.

Optimal control model (OCM) analysis with parameters adjusted to match the zero-delay results replicates the basic performance trends, but the predicted error score is less sensitive to delay, and the predicted stick and stick-rate scores are more sensitive to delay, than found experimentally. This finding is consistent with analysis of previous experimental studies, where we find that a model whose parameters are adjusted to match tracking performance with wide-band laboratory plant dynamics tends to yield optimistic performance predictions when the controlled dynamics contain significant lags. Sensitivity studies performed with the OCM suggest that human operators adopt a relatively more robust control strategy, when controlling plants with significant lags or delays in order to reduce the sensitivity of performance to fluctuations in the operator's response strategy.

INTRODUCTION

As flight control and management tasks become more complex, aircraft simulators -- especially those used by the military --are being required to simulate increasingly complex perceptual environments. Specification of such simulators, whether for engineering studies or for pilot training, requires a judicious balance between the need for simulation fidelity and cost effectiveness.

Considerations of both cost and flexibility have led to the widespread use of digital computation in simulating various aspects of the flight environment, including the simulation of aircraft response dynamics and visual scene cuing. Because the digital

3

simulator is largely a sequential processor of information, various distortions in the perceptual/response environment can arise. Much of this distortion can be represented as the introduction of delay in the presentation of information and/or the response of the vehicle. When whole-body ("platform") motion cues are provided, the problem is often compounded by bandwidth limitations of the motion simulator, plus the lack of synchrony between platform and visual scene cues. The existence of significant simulation delays and related imperfections may seriously compromise the training and research effectiveness of an aircraft simulator.

Work has recently been performed to develop the optimal control model (OCM) for manned systems as an analytic tool to aid in the development of specifications for advanced simulators (Levison, Zacharias, and Sinacori, 1982; Levison, McMillan, and Martin, 1984; Levison and Warren, 1984). While the results of this effort have been encouraging, and the OCM has been found to be a generally good predictor of performance trends, improvements in the absolute predictive accuracy of the model will enhance its utility as a design and evaluation tool.

The objective of the study described in this paper was to determine the requirements for enabling the model to predict the effects of system delays and lags with a consistent set of independent parameters. Specific tasks included (1) review of the existing database, (2) a laboratory study of time delay effects, and (3) evaluation of the concept of robust control as a guideline for understanding and predicting manual control behavior. Further details of the work described below are provided by Levison and Huggins (1986). The reader is assumed familiar with the structure and parameterization of the OCM (Kleinman, Baron, and Levison, 1970, 1971; Levison, 1982).

REVIEW OF EXISTING DATABASE

A review of existing data was conducted in a previous study by Levison (1983) to explore the potential relationship between control-task parameters and independent ("pilot-related") OCM parameters. With the aid of an automated scheme for identifying model parameters on a least-squared-error basis (Levison, 1981), qualitatively good matches were obtained for all data sets. However, sizeable changes in the best-fitting "motor time constant" and/or "time delay" parameters were found across the set of tasks. These model parameter variations could not be ascribed simply to insensitivity of the matching procedure, nor to an insensitivity of tracking performance to parameter values.

The database explored in this earlier study was obtained from different studies and was subject to a number of factors other than control-task differences that would lead us to expect variations in model parameters among experiments. Such factors included (1) different subjects; (2) different subject backgrounds (e.g. military pilot, commercial pilots, non-pilots); (3) different experimental laboratories; (4) different personnel conducting the experiments; (5) different training methods. Analysis of these results, while not conclusive, suggested that experimental factors of this type could not alone explain model parameter variations. If model-parameter differences were due solely to differences in subject populations and to other factors of the type listed above, then we would have expected to find (1) consistent parameters for the same subject groups, and (2) little correlation between model parameters and task

4

differences. The analysis presented in Levison (1983), however, showed the opposite trend. Parameters varied within groups of subjects performing different tasks, and the time–delay and motor–time–constant parameters seemed to increase with increasing effective vehicle response time. Furthermore, preliminary exploration with alternative modeling philosophies suggested that these trends could be ascribed in part to deficiencies in the operator's "internal model" of the task environment.

We felt that the results of the previous study warranted a closer look at the database and at modeling trends derived from this database. In this section of the paper we review the existing·database from a different perspective. Instead of exploring the relation between best–fitting model parameters and task parameters , we now adopt a fixed set of model parameters and explore ways in which model predictions differ from experimental measurements as the task is varied. The results of this analysis, combined with the results of the previous study, are intended as a basis for exploring refinements to the OCM and/or to the modeling philosophy that will allow more accurate predictions of task–related performance trends.

Model predictions presented here were obtained using a fixed set of model parameters that were found to match performance in a set of relatively simple, wide–band, laboratory tracking tasks. This selection is somewhat arbitrary: we could just as well have selected one of the more complex tasks as a baseline and improved the overall appearance of the model's predictive capabilities by "splitting the difference" between the relatively simple and relatively complex tasks.

The objective of this analysis, however, is not to demonstrate the ability of the OCM to match data, but to look closely at the trends of fixed–parameter model predictions as task complexity is varied. We feel that such trends are best observed by anchoring the model at one end of the task–complexity spectrum and accentuating model/data differences that might exist at the other end.

The general philosophy guiding this analysis is based on the following assertions:

1. The OCM will be a more useful predictive tool if model parameters identified with basic human information processing limitations can be related primarily to the capabilities of the human operator and to external factors that influence this state (motivation, background, level of training, etc.), and not to parameters of the external task.

2. Any consistent task–related trends in predictive capability with a fixed–parameter model (or in parameter values with a best–fit parameter model) reflect a cause–and–effect relationship that is in principle determinable but is not currently reflected in the model structure

3. The most desirable way to treat such trends, if they exist, is to modify the model structure or method of application to improve the ability of the OCM to predict performance trends across tasks of varying difficulty without modification of the "operator–related" independent parameters.

An alternative modeling philosophy –– one commonly used by other modelers –– is

to simply formalize the relationship between task parameters and so-called "independent" model parameters. Ideally (though not always), the model structure remains unchanged, and "pilot" parameters are selected from a chart or equation that indicates the best choices for the given task.

Data from previous tracking studies were analyzed to provide guidelines as to the type of model development required to improve predictive accuracy. The data consisted of time-domain statistics (typically, rms error, error-rate, control, and control-rate) as well as frequency-domain measures (pilot gain, phase-shift, and remnant spectrum). All data were obtained from single-axis, laboratory-type, steady-state tracking tasks using sum-of-sines inputs.

Data from the following nine tracking tasks (obtained from five separate studies) are reviewed here: (1) lateral-axis tracking, approximate position control (Levison, 1971); (2) pitch-axis tracking, rate control (Levison, 1971); (3) yaw-axis tracking, approximate acceleration control (Levison, 1980); (4) pitch-axis tracking, rate control filtered at 2 rad/sec by a second-order Butterworth filter (Levison, 1971); (5) pitch-axis tracking, rate control filtered at 1 rad/sec by a second-order Butterworth filter (Levison, 1971); (6) roll-axis tracking with simulated high-performance fighter dynamics, fixed-base (Levison, Lancraft, and Junker, 1979); (7) the same, moving base; (8) roll-axis tracking, approximate third-order plant, fixed-base (Levison, Baron, and Junker, 1976); and (9) the same; moving-base.

As noted above, the previous model analysis was performed using automatic identification of model parameters, with an apparent task-related degradation in model parameters identified with operator information processing capabilities. Because the subject study was intended to consider possible broadening and/or modification of the basic modeling philosophy (including the use of non-veridical internal models), a different approach was followed in re-analyzing the data. Specifically, the parameter set that provided the best match to the first three tasks was used to provide model predictions for all nine tasks. It was anticipated that suggestions for further model development would arise in part from analysis of the differences between model predictions and experimental results, and from the way in which these differences correlated with task parameters.

Independent model parameters were fixed as follows. (1) motor time constant. 0.09 seconds; time delay: 0.17 seconds; motor noise/signal ratio. −50 dB relative to control-rate variance; and observation noise/signal ratio: −21 dB relative to the variance of the corresponding perceptual variable.

A comparison between model and experimental tracking performance is shown in Table 1. Performance is expressed in terms of between-subject average standard deviation (SD) scores. Since tracking variables were essentially zero mean, the SD scores are virtually equivalent to rms tracking error. Units for error and control variables, along with other information relating to the experiments, are given in Levison and Huggins (1986).

Mismatch between model and experiment are shown in two ways. The "%Diff" column represents the difference between the corresponding model and experimental scores,

6

Table 1: Comparison of Model and Experimental Tracking Scores

Task	Conditions	Tracking Error		Modeling Error	
		Exptl	Model	%Diff	SD Diff
1.	Position Control	.772	.772	0%	0.0
2.	Rate Control	.985	1.01	+3%	0.3
3.	Acceleration Control	2.00	1.29	−35%	2.4
4.	Rate Control Filtered at 2 Rad/Sec	0.241	0.134	−44%	10.5
5.	Rate Control Filtered at 1 Rad/Sec	0.190	0.071	−63%	25.0
6.	Roll−Axis Simulation, Fixed Base	5.71	3.72	−35%	5.4
7.	Roll−Axis Simulation, Moving Base	2.68	3.05	+14%	1.5
8.	Third−Order Plant, Fixed Base	30.5	22.1	−28%	2.3
9.	Third−Order Plant, Moving Base	19.8	14.7	−26%	4.5

normalized with respect to the experimental score, expressed as percent. The "SD Diff" column shows the absolute value of the mismatch normalized by the between−subject standard deviation of the tracking error to give an indication of the statistical significance of the model/data differences.

A substantial difference (15% or more) is shown between predicted and experimental tracking error scores for six of the nine tasks. In all six cases, the mismatch appears to be significant (i.e., the mismatch is greater than two experimental standard deviations), and the fixed−parameter model is optimistic with respect to actual performance. The major trends shown in Table 1 are as follows:

o Mismatches are generally greater for high−order plants than for low−order plants. Specifically, model/data differences are greater for the acceleration−control, the third−order plant, and the filtered rate control system than for the simple proportional− and rate−control tasks.

o Reducing the plant bandwidth increases the mismatch. The 63% difference between predicted and experimental tracking error for the 1 rad/sec filtered plant was the largest mismatch for the nine tasks.

o Mixed results are obtained concerning the effects of whole–body motion cuing on the predictive accuracy of the fixed–parameter model. For the simulated fighter roll–axis tasks (Tasks 6 and 7), the mismatch was 35% for fixed–base and only 14% for moving–base results. For the third–order plant (Tasks 8 and 9), motion cuing did not materially affect the relative accuracy with which the tracking error score was predicted.

Before commenting on possible sources of model/experiment differences, let us review frequency response data. Figures 1a through 1i compare model predictions with experimental results. Experimental results are shown as filled circles, whereas model predictions as shown as smooth curves. A "gain" (i.e., amplitude ratio) of 0 dB represents 1 unit of control response amplitude per unit of tracking error amplitude. For five of the nine figures, 0 dB remnant represents one unit of control response power not linearly related to the external SOS forcing function. For the remaining four figures (1a, 1b, 1d, and 1e), remnant has been linearly transformed to an equivalent noise process injected at the pilot's input (tracking error) and normalized with respect to error variance.

The following model/data comparisons show that the fixed–parameter model replicated the general trends of the data across the various experimental tasks quite well. Specifically, the model predicted the nature of the substantial task–related changes in the frequency dependencies of the gain, phase and remnant curves. In the following discussion, we focus on some of the quantitative differences resulting from application of a fixed–parameter model.

Figures 1a and 1b reveal qualitatively good model matches to data from the position– and rate–control experiments. Figure 1c shows good model/data correspondence over most of the frequency range. Experimental remnant, however, was substantially greater than predicted at the lowest two measurement frequencies, and low–frequency pilot gain was a bit lower than predicted. Apparently, this discrepancy was sufficient to account for the 36% difference between predicted and measured tracking error. (It is also possible that control–response behavior was less linear for the acceleration–control task. Data are not available to test this hypothesis.)

On balance, the fixed–parameter model predicted higher gain and wider bandwidth than observed experimentally for the two filtered rate–control tasks (Figures 1d and 1e). The experimental remnant was generally greater than predicted at low frequencies and smaller than predicted at high frequencies. This sharper fall–off with increasing frequency is consistent with the notion that the subject is using acceleration information (Levison, 1971). However, if one were to include acceleration information as a perceptual input and not degrade other pilot parameters, model/experiment differences would increase.

As noted earlier in the discussion of performance scores, the presence or absence of motion had a considerable effect on the ability of the fixed–parameter model to

8
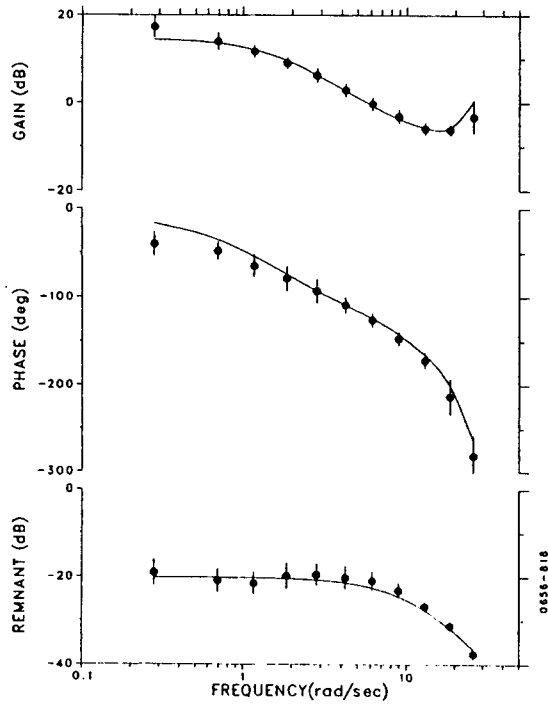
a. Position Control
b. Rate Control
c. Acceleration Control
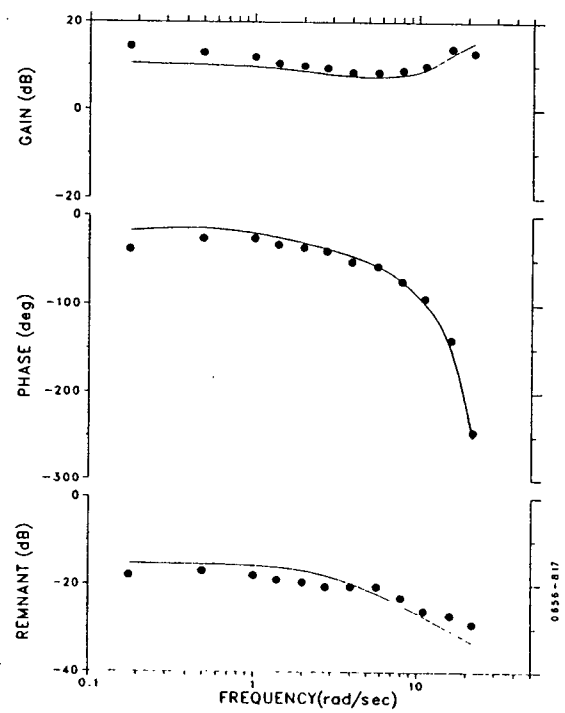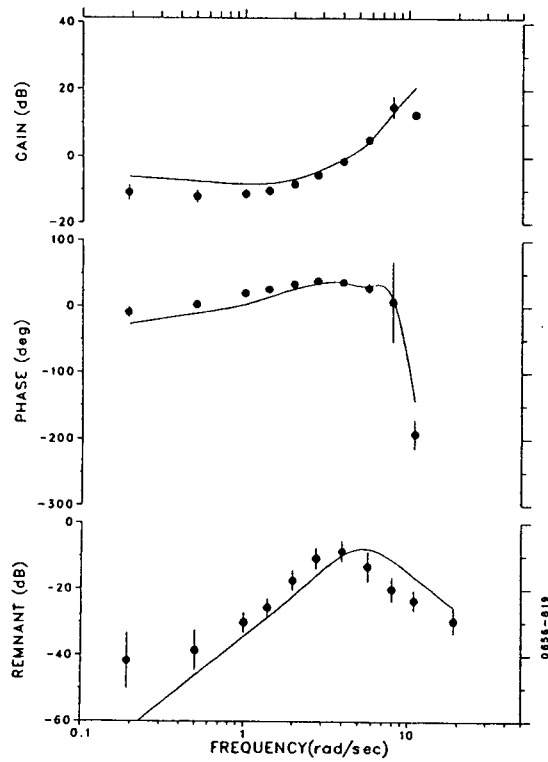
Figure 1: Pilot Frequency Response:

9

d. Control Filtered at 2 Rad/Sec
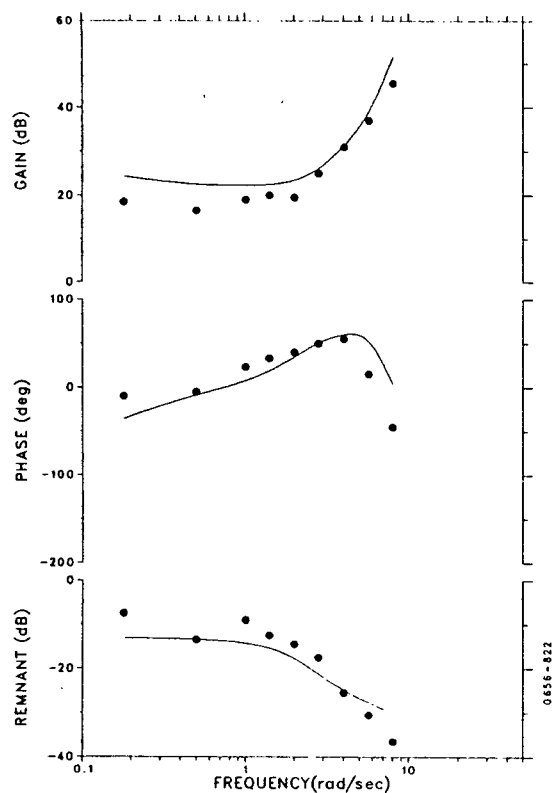
e. Rate Control Filtered at 1 Rad/Sec
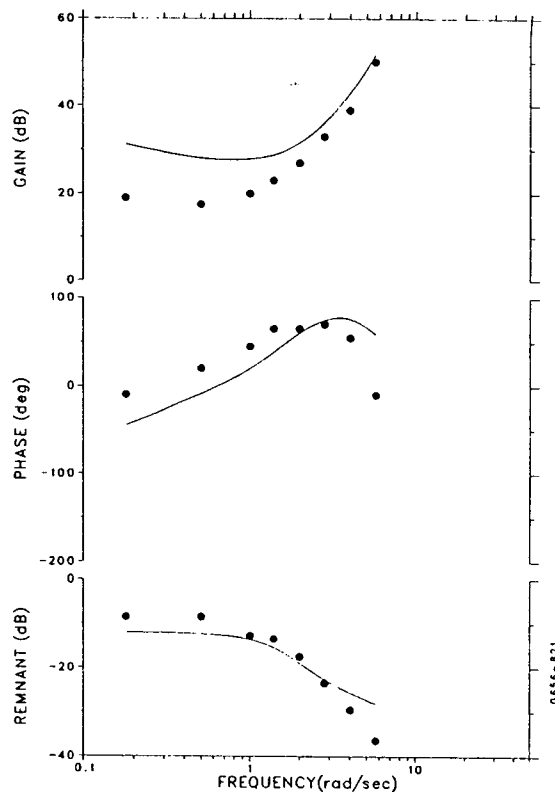
f. Simulated Fighter Roll-Axis Task, Fixed Base
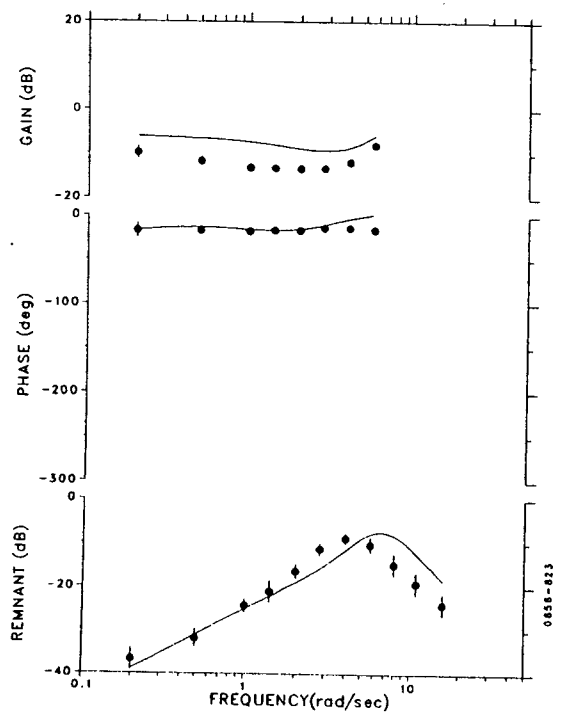
Figure 1. (continued)

10

g. **Simulated Fighter Roll-Axis,**
   Moving Base
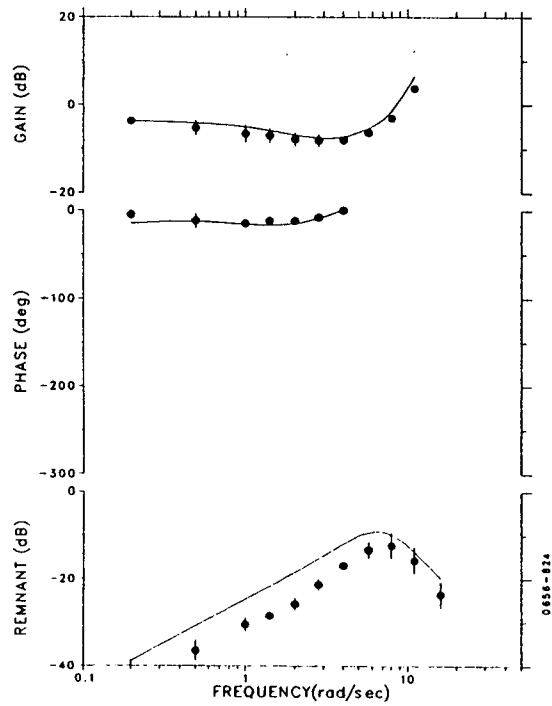
h. **Approximate Third-Order Plant,**
   Fixed-Base
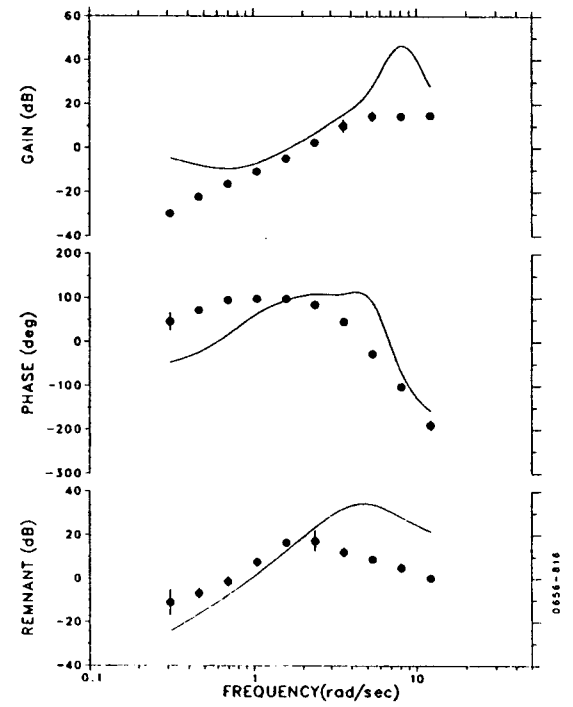
i. **Approximate Third-Order Plant, Moving Base**
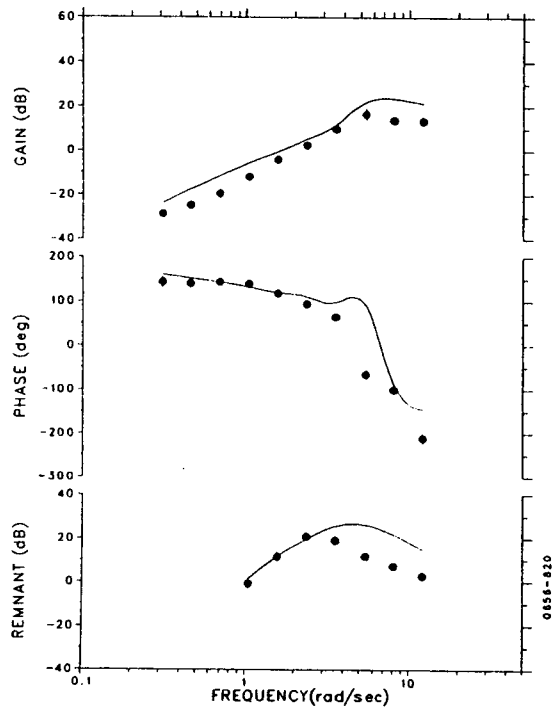
Figure 1. (concluded)   11

match the data obtained in the simulated fighter roll-axis tasks. Predicted pilot gain was around 6 dB greater than measured pilot gain for the fixed-base task (Figure 1f), revealing a substantially optimistic model prediction. On the other hand, Figure 1g shows that for the moving-base task, very good predictions were obtained for the pilot describing function, but the model predicted a higher than measured level of pilot remnant. For this task, then, the model yields an overall pessimistic prediction of pilot response behavior using nominal parameters.

Visual inspection of Figures 1h and 1i (third-order tracking task) seems to indicate a closer match to the data for the moving-base task, but the effects are less dramatic than for the roll-axis task.

The results presented above lend at least qualitative support to the hypothesis that model predictions tend to be relatively more optimistic compared to pilot performance when tracking dynamics are relatively sluggish (e.g., higher order, lower bandwidth) and/or when the perceptual cuing environment is lacking in critical information (e.g., visual-only cuing vs. visual+motion cuing). This trend has led to previous speculation that operator performance in tasks of high complexity or impoverished cuing is more severely impacted by imperfections in the operator's internal model of the task environment than when plant dynamics are wide-band and adequate cuing is available (Levison, 1983).[1] The experimental results reported herein are not as definitive as one might wish with respect to limitations on the operator's internal model, however, because of other experimental factors that may be confounded with the effects of task complexity and perceptual cuing. (See Levison and Huggins, 1986, for further discussion of confounding factors.)

EXPERIMENTAL STUDY

A small experiment to explore the effects of time delay on tracking performance was conducted. The primary motivation for this study was to provide data -- heretofore lacking from our database -- that would allow a direct test of the model's ability to predict the effects of simulator delays. A secondary motivation was to explore the effects of task complexity in a consistent experimental environment.

Description of Experiments

The experiment was designed with two goals in mind. The first was to provide asymptotic performance data for four time delays for comparison with model predictions. The second goal was to determine whether or not subjects who have practiced a tracking task with delay present perform better or worse on the zero-delay task than subjects who have spent the same amount of time tracking without delay. (There was no expectation that asymptotic performance would be better with plant delay than without. both analytical models and experimental results consistently

---

[1]Such imperfections may be the result of the pilot's inability to develop a better model of the vehicle response dynamics during training because the task and/or cuing environment do not provide sufficient feedback.

12

indicate that tracking performance degrades with increasing system response delays. The issue here was whether training for the no-delay case would be enhanced or hindered by the presence of simulator delays early in training.)

The task explored in this study was target-following with a compensatory display of tracking error, implemented as a slightly modified version of the Performance Analyzer described by Zacharias and Levison (1979). The subject used forward and backwards movements of a force control stick to minimize the vertical movements of a horizontal line displayed on a 10 cm oscilloscope at eye level about 110 cm in front of him. A full-scale (5 cm) displacement of the line subtended an angle of 0.045 rad (2 degrees 36 mins of arc). The plant dynamics were set to approximate the pitch-control response of a vehicle model used in a previous study by Levison and Warren (1984) to represent the pitch-axis behavior of an F-16 aircraft flying at low altitudes and high speeds.

The transfer function of the actual plant dynamics used in this task was:

$$\frac{P}{U}(s) = \frac{20}{(s + 2.5)s} e^{-s(T_s + T_e)} \tag{1}$$

where U is the Laplace transform of the pilot's stick input in pounds, P is the transform of the plant response in centimeters, "s" is the Laplace frequency variable, T_s is the irreducible simulation delay (about 35 msec), and T_e is the delay added to the plant response (the major experimental variable).

The simulated "target" was provided by a sum-of-sines input, with amplitudes and frequencies selected to simulate a zero-mean, second-order Gaussian noise process having two real poles at 0.5 rad/sec. The rms input was 4 cm. Recall that the subject did not observe target motion; rather, he was shown only the tracking error, defined as the difference between target and plant position.

One "zero-delay" and three nonzero-delay conditions were studied. The nominally zero-delay condition in fact incorporated a delay (T_s) of about 35 ms, of which 20 ms was due to the digital simulation, and the remainder was due to the anti-aliasing filter at 10 Hz. The three delays (T_e) chosen were nominally 120 ms, 240 ms, and 360 ms, not including the 35 ms due to the simulation and filter. Four male subjects served. They were students recruited from local universities, and reported no defects of vision or of manual dexterity. Each served for 6 or 7 1-hour sessions on separate days, and was exposed to at least 32 training runs under each of the four delay conditions, and then a final test block of 20 runs, five at each delay. Each tracking run lasted 90 seconds. The first 8 seconds were treated as warmup, and were not scored. The subject was told his score after each run to maintain motivation. The score corresponded to 100 times the standard deviation of the error signal (i.e. the displacement of the controlled line from the midpoint of the display).

Effects of Delay on Performance

The learning curves yielded by the test subjects failed to show any clear transfer effects.[2] Specifically, they failed to support the hypothesis that subjects trained on a more difficult task (nonzero system delay) would exhibit different initial performance, or train at a different rate, on the less difficult reference task (zero delay) than would subjects trained on the reference task. In contrast to this (negative) result, Fisher et al. (1986) found some evidence of enhanced training with time delays around 0.1 sec. It should be noted, however, that the BBN study was designed primarily to allow a within-subject analysis of delay effects, and that transfer differences would have had to be dramatic to be revealed in this study.

Average performance metrics in terms of closed-loop rms performance scores and operator frequency response for the trained subjects are presented below. For each tracking trial, within-trial standard deviation scores were computed for tracking error, error rate, "stick" (the pilot's control input), and stick rate. Because the external forcing function was a zero-mean process, these variables typically had negligible mean components, and the standard deviation (SD) scores were virtually equivalent to rms deviations.

The SD scores were first averaged across ten trials for each subject, each delay condition, the within-subject means were then averaged across the four test subjects to yield population means and standard deviations for the four system variables. These population statistics are shown in Figure 2.

System delay had a consistent effect on tracking error; the SD score increased monotonically with increasing delay, approximately doubling from smallest (zero) to the largest (360 msec) added delay. A similar trend was found for the error rate score, although the percentage change was less than for the error score. No consistent effects of delay on stick or stick rate scores were observed.

Subject-paired, two-tailed t-tests were performed on the four performance metrics to determine the statistical significance of delay-related differences. Tests were performed for all six possible combinations of delays compared two at a time. Delay-related differences in the error score were highly significant (alpha <0.01) for all pairs of delays. Four of the comparisons also revealed highly significant differences in error rate score. As one would expect from Figure 2, delay had no significant effect on either stick or stick rate score.

Effects of delay on operator frequency response are best illustrated in Figure 3, which compares mean frequency response for the zero and 360 msec delay conditions. Statistics for the operator describing function ("gain" and "phase") were obtained by averaging cross-power spectral measurements and converting these statistics to units of dB and degrees as described by Levison (1985a). Remnant means and standard deviations were obtained by operating directly upon the remnant estimates in dB. For

---

[2]Learning curves, as well as data for individual subjects, are presented in Levison and Huggins (1986).
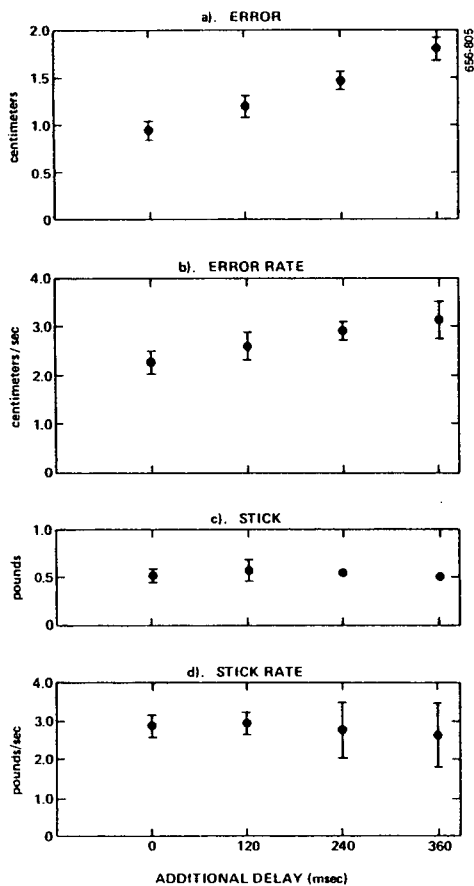
Figure 2: Effects of Delay on Average SD Scores

Average of 4 subjects, 10 trials/subject.
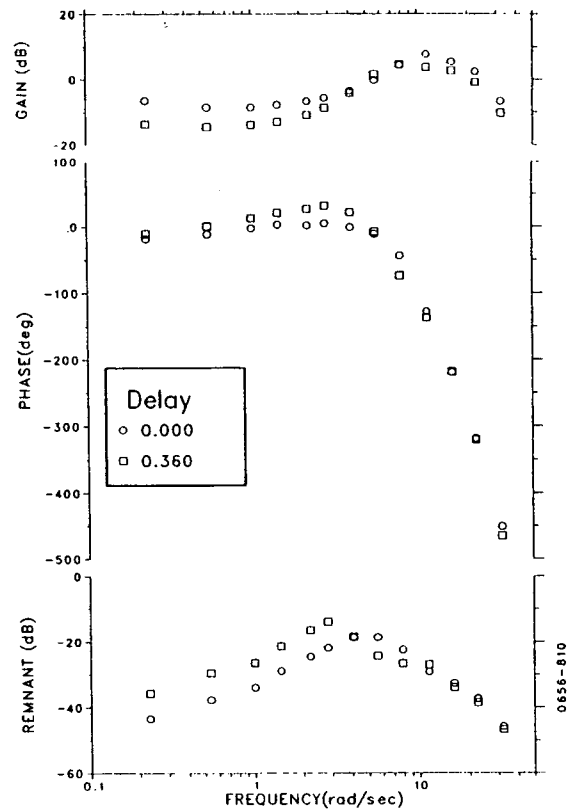
Figure 3: Effects of Delay on Average Operator Frequency Response

Average of 4 subjects, 10 trials/subject.

all frequency response curves shown in the remainder of this paper, 0 dB gain corresponds to a control response of 1 pound force per centimeter of tracking error; 0 dB remnant represents a power spectral density of stick remnant of one $pound^2$ per rad/sec. Remnant is computed from the actual closed-loop control response and does not reflect an equivalent "open-loop" or "injected" remnant.

Delay effects were found mainly at the lower measurement frequencies, where significant system delay led to decreased pilot gain, increased pilot remnant, and increased phase shift. High-frequency effects appeared to be negligible, except for a slight reduction in the frequency of peak gain -- an effect that has been observed before in the presence of delay (Johnson and McRuer, 1985). Frequency-response measures for the intermediate delay conditions generally fell within the bounds shown in Figure 3.

As we show in the following discussion of model analysis, these changes are expected as the operator's response is adapted to deal with the added system delay. Because of increased man/machine phase lag, gain must be reduced to maintain closed-loop stability. The operator generates more phase lead in an attempt to partially

compensate for the lag introduced by the time delay The increased low frequency remnant for the 360- msec delay condition is a natural consequence of the presence of the delay and does not necessarily indicate that the operator has become an inherently "noisier" information processor. (Recall that remnant is a measure of closed-loop control response and is thus shaped by the overall man/machine response characteristics.) Analysis of operator remnant (Levison and Huggins, 1986) failed to reveal symptoms of a move-and-wait strategy.

Model Analysis

Pre-experiment analysis, using independent "pilot-related" model parameters representative of those derived from wide-band laboratory tracking tasks as described earlier, yielded accurate predictions of performance trends. In terms of predicting absolute tracking errors, however, the pre-experiment model analysis proved to be optimistic. Figure 4 shows that predicted scores (solid curve) were about 70% of the experimental SD error scores. An automated identification scheme was subsequently employed to readjust independent model parameters to provide the best overall match to the SD scores and frequency-response measures for the zero-delay case. The re-adjusted parameters were : motor time constant. 0.122 sec, time delay: 0.177 sec; observation noise/signal ratio. −18.8 dB, and motor noise/signal ratio. −44.0 dB.
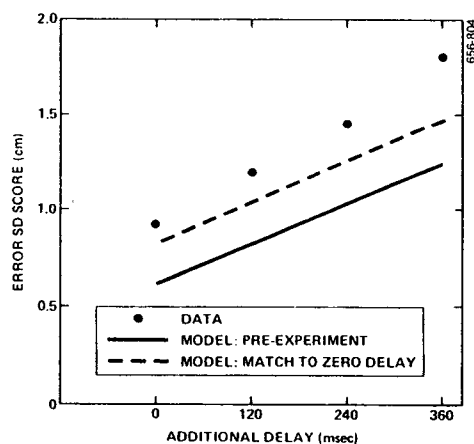
Figure 4:   Effects of Delay on Predicted and Experimental Tracking Error

Average of 4 subjects, 10 trials/subject.

With model parameters held fixed at these new values, model predictions were obtained for the three remaining delay conditions to determine whether delay effects could be replicated with a fixed set of operator-related parameters. Figure 4 shows that, while the model predicted an increase in the error SD score with delay (dashed curve), the increase was not quite as great as that observed experimentally. The model underestimated the error score for the zero delay case by about 12% of the

measured tracking error[3], this model/data difference increased to about 19% for the 360 msec delay.

Larger relative differences between model and data were found for the stick—related scores (not plotted). The predicted and measured stick and stick—rate scores were within 5% for the zero delay case. For the 360 msec delay task, however, the model predicted a stick SD score about 18% greater than measured, and the predicted stick—rate score was about 54% greater than measured.

These results, then, are consistent with previous studies which have shown that fixed—parameter model predictions tend to be increasingly optimistic relative to actual man/machine system performance as lags and/or delays are added to the system. The apparent failure of the subjects to increase their response activity with delay as predicted by the model is consistent with previous model analyses that show a decrease in the "motor time constant" parameter with increasing vehicle lags or delays.

Predicted and measured operator frequency response are compared in Figure 5. The model replicates the major experimental trends at low frequencies. The increased low—frequency remnant induced by system delay may be largely explained by a fixed operator noise, relative to signal, being processed by different closed—loop dynamics.

The fixed—parameter model does not completely replicate the effects of delay, but before discussing model/data differences further, let us first compare measured and predicted gain crossover frequencies and phase margins for the zero and 360 msec delay conditions. Table 2 shows that predicted and experimental crossover frequencies were nearly identical, but that the model tended to underestimate phase margins. (A better match to phase margin was obtained for the 360 msec delay condition, even though a better match to tracking error was obtained for the zero delay case.)

Model/data discrepancies are different in character below and above crossover. At frequencies below crossover, model gains are somewhat higher than measured gain for both delay conditions, and the phase shift is a bit more negative. The model matches the low—frequency remnant curve for the zero delay case, but underestimates remnant for the 360 msec condition. At frequencies above crossover, the model matches all three frequency—response metrics rather well for the zero delay case, but exhibits a greater peak gain, a less smooth phase response, and larger remnant than found in the data for the 360 msec delay.

On the basis of the results so far, we conclude that the subjects were not able to adapt their response behavior to system delay as efficiently as the fixed—parameter OCM adjusted for wide—band tracking tasks. The relatively optimistic predictions of the model concerning the effects of time delay on tracking error (once the model is

---

[3]Because the model—matching algorithm adjusted independent parameters to provide a best joint match to four SD performance scores, plus gain, phase, and remnant, a perfect match was not obtained to the error SD score.
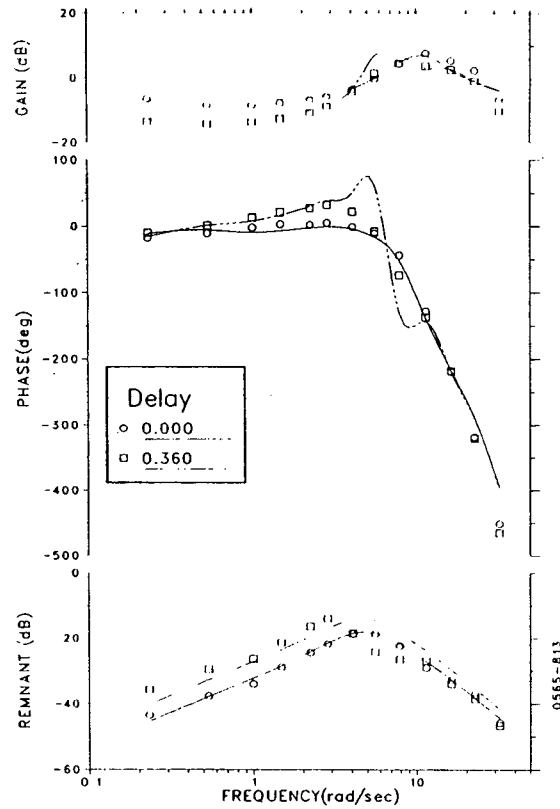
Figure 5: Comparison of Predicted and Measured Operator Frequency Response
Average of 4 subjects, 10 trials/subject.

Table 2: Gain Crossover and Phase Margin

	Crossover Freq. (rad/sec)		Phase Margin (degrees)	
	T=0	T=.360	T=0	T=.360
Experiment	2.8	1.7	40	40
Model	2.8	1.9	26	35

calibrated for the subjects) appear to be due to (1) the lower remnant exhibited by the model at frequencies below crossover, (2) a wider response bandwidth than seems to have been exhibited by the subjects, and (3) the model's ability to more efficiently fine-tune its response at frequencies above crossover.

18

EVALUATION OF THE ROBUST CONTROL CONCEPT

Various modeling concepts were explored in an effort to discover a consistent explanation for the observation that human operator performance degrades, relative to performance predicted by a fixed-parameter optimal-control model, with increasing system lag and delay. Greatest attention was devoted to two concepts: (1) low-order internal modeling, and (2) robust control.

Following suggestions offered in a previous study (Levison, 1983), a small modeling study was conducted to test the hypothesis that model/data deviations were due to the operator's inability to generate a veridical internal model of the task dynamics. Specifically, we explored the assumption that the operator was restricted to a second-order internal model of plant dynamics, given an explicit display of only tracking error.

This approach yielded apparently successful results when applied to the time-delay data described above (Levison and Huggins, 1986). Nevertheless, we were unable to apply it to the data obtained in the earlier study of an approximate third-order plant (Levison, Baron, and Junker, 1976). The obvious difficulty here was that a second-order model could not be made to resemble a third-order response; clearly, we would have to allow the operator to formulate a third-order internal model in order to perform this control task. Now, if we were to allow third-order modeling here, consistency would suggest that we allow third-order modeling for the time-delay tasks as well, in which case the "low-order" internal model would reflect minimal degradation in operator response capabilities for the time-delay tasks.

Because of the apparent inconsistencies engendered by this approach, subsequent analysis was devoted to testing the "robust-control" hypothesis. As noted below, this approach is consistent with the notion that the operator's internal model may fluctuate about a model that is correct on the average. That is, we consider variational rather than bias errors in the internal model.

One of the criticisms leveled against control-system design methods based on standard linear-quadratic-gaussian (LQG) optimal control techniques is that the performance of the resulting control system tends to be highly sensitive to the parameters of the system being controlled (Doyle and Stein, 1981). That is, performance may indeed be optimal when the parameters of the plant are exactly known, but may degrade rather sharply if the plant parameters differ from their assumed values. Straightforward application of LQG theory, then, may result in a control system that is rather "unforgiving". Consequently, some work has been devoted to the design of control systems that sacrifice optimal performance in favor of a "robust" control system that tolerates modest deviations between actual and assumed plant parameters.

This work suggests an approach to the modeling of human operator behavior; namely, that the human will sacrifice performance for a more robust response strategy when closed-loop performance is sensitive to errors in his internal model of the plant and/or his control strategy. A robust control strategy could be required when the operator's internal model of the task differs from the actual task, when his control

19

strategy differs from the desired control strategy, or when either the internal model and/or control strategy are correct on the average but fluctuating in time.

Because experimental measurements obtained from manual control studies do not facilitate a differentiation between errors in the internal model and errors in the control strategy, we shall use the term "response-strategy errors" to mean either or both of these two sources of non-ideal operator behavior. This type of "error", then, represents the difference between the operator's response strategy and that predicted by a straightforward application of LQG optimization techniques -- it is not the same as tracking error.

Recall that previous analysis indicated an apparent increase in the motor time constant model parameter for systems with significant phase lags (Levison, 1983). Since this parametric change in the OCM results in a reduced operator gain, it may well reflect an intentionally more conservative and robust control strategy rather than a degradation in the operator's response capabilities. In order for this hypothesis to lead to a consistent explanation of observed behavior, it is necessary to show the following.

1. Tracking tasks in which performance is best modelled by degraded "pilot parameters" are those for which predicted closed-loop performance is particularly sensitive to response-strategy errors when modeled by the OCM using fixed parameters appropriate to the wide-band tracking tasks.

2. The sensitivity of performance to such errors can be reduced by increasing the motor time constant.

In order to explore the robust-control hypothesis, response-strategy errors were modelled in two ways: (1) by forcing an improper response gain through manipulation of the plant gain in the operator's internal model, or (2) by adding significant "motor noise" to the operator's commanded control rate. The first manipulation provides a simple test of the effects of slow variations in the operators response strategy. (A more accurate test -- not computationally feasible with current model structures -- would be to randomly and slowly vary all parameters of the response, not just the gain.) The second manipulation provides a simple approximation to the effects of rapid fluctuations in the response strategy. The results of these tests are reviewed briefly below; additional details are given by Levison and Huggins (1986).

Sensitivity to deviations in operator gain was determined as follows for selected tasks:

o Baseline performance was determined using the correct internal model of the plant gain.

o Effects of high operator gain were determined by predicting closed-loop response for an internalized plant gain of 0.8 times the true plant gain

o Effects of low operator gain were determined by model analysis using an internalized plant gain 1/0.8=1.25 times the true gain.

20

Except for changes in internal-model gain, values for independent model parameters were the same as those used to perform the re-analysis of previous tracking data.

The sensitivity to motor noise was determined as follows:

1. Independent model parameters were adjusted as in the previous analysis. In particular, the motor time constant was set to 0.09 seconds.

2. "Baseline" performance predictions were obtained with negligible motor noise.

3. Performance predictions were obtained with a motor noise covariance of 0.001 times the baseline commanded control-rate variance.

4. If the addition of motor noise caused predicted rms error to increase by over 50%, the motor time constant was incremented by 0.03 seconds. Other independent model parameters were kept fixed.

5. Steps 2-4 were repeated until the addition of motor noise caused an increase of under 50% in predicted rms tracking error.

The particular motor noise scale factor used in this sensitivity test was selected to provide an interesting range of performance sensitivities; it was not selected on theoretical grounds.

The best correlation between predicted performance sensitivity and model/data departure is obtained by averaging the results of the two sensitivity tests. In Table 3 we present average sensitivities computed by first averaging the normalized error scores obtained for the high- and low-gain predictions, and then averaging this result with the corresponding normalized error score from the motor-noise sensitivity study using a 0.09 sec motor time constant. This table includes results from six tasks performed previously -- selected to span the range of modeling errors -- plus the zero-delay and 360-msec delay tasks explored in the time-delay study.

To facilitate comparison of sensitivity trends with model-error trends, the tasks are listed in order of increasing fixed-parameter modeling error. The only exception to this scheme is placement of the roll-axis, moving-base results: recall that for this case only, experimental tracking performance was actually superior to that predicted by the fixed-parameter model (See Table 1.) Modeling errors arising from application of the (optimistic) fixed-parameter model to the recent time-delay data were -33% and -31%, respectively, for the 0-msec and 360-msec delays.

The rank ordering of the average sensitivity of performance to response-strategy error corresponds generally with the rank-ordering of the fixed-parameter modeling errors. Specifically, simple position and rate control show least performance sensitivity and least modeling error, filtered rate control ranks highest in both categories, and acceleration control ranks second highest in both categories.

There are two major deviations between rank-ordering of modeling error and

Table 3: Average Predicted Response Sensitivity

Task	Average Sensitivity
Position control	1.04
Rate control	1.11
Pitch-axis, 360 msec delay	1.51
Pitch axis, 0 msec delay	1.28
Roll-axis, Moving Base	1.23
Roll-axis, Fixed Base	1.26
Acceleration control	1.62
Rate filtered at 1 rad/sec	2.08

performance sensitivity. First, performance sensitivity is greater for the 360-msec delay task than for the 0-msec delay task (which is not surprising), but these two tasks show almost identical fixed-parameter modeling errors when modeling errors are computed on a fractional basis (as has been done for Table 1). If, however, modeling error were to be computed on an absolute basis (which would make sense only for comparisons of tasks involving the same plant dynamics and input spectra), the 360-delay task would reveal a substantially higher modeling error.

Second, the predicted sensitivity for the roll-axis tracking task is relatively unaffected by the consideration of motion cuing, whereas modeling errors were quite different for fixed- and moving-base analysis. For the roll-axis data we suggest that the inclusion of whole-body motion cues provided the operator with sufficient information to minimize the occurrence rather than the effect of response-strategy errors, and thus allowed the operator to perform with a reduced margin for error. In effect we assume that platform motion provides a sensitive cue to roll-axis acceleration, and that deviations in the short-term statistics of this acceleration variable are more quickly detected than fluctuations in short-term roll or roll-rate statistics. These assumptions will require other than a steady-state model for verification.

On balance, the results of the foregoing sensitivity study show that tasks for which measured performance departs from performance predicted with a fixed-parameter model are also tasks for which predicted performance is sensitive to response-strategy errors. As shown in Table 4, the sensitivity study performed by manipulating motor also reveals that the sensitivity is reduced when the motor time constant is reduced -- a result that is needed to support the "robust-control" hypothesis.

Table 4: Sensitivity of Closed-Loop Performance to Motor Noise

Task	Motor Time Constant (sec)			
	0.09	0.12	0.15	0.18
Position control	1.05	—	—	—
Rate control	1.17	—	—	—
Pitch-axis, 360-msec delay	1.90	1.67	1.58	—
Pitch-axis, 0 msec delay	1.50	1.43	—	—
Roll-axis, moving base	1.20	1.14	—	—
Roll-axis, fixed base	1.27	1.19	—	—
Acceleration control	1.63	1.40	—	—
Rate filtered at 1 rad/sec	2.25	1.75	1.56	1.45

In summary, the results of the sensitivity studies generally support the hypothesis

that the operator adopts a robust control strategy that is more tolerant of response-strategy errors than is the strategy predicted by the fixed-parameter OCM. Sensitivity of rms tracking error to response-strategy error tends to correlate with departure of experimental results from fixed-parameter model predictions, and predicted sensitivity is reduced by a more conservative control strategy imposed on the model by an increase in the motor time constant.

SUMMARY

The learning curves yielded by the test subjects failed to show any clear transfer effects.

Time delay had consistent, large, and statistically significant effects on the asymptotic tracking error standard deviation (SD) score. Error increased by roughly a factor of 2 between the lowest and greatest delay condition. The error rate SD score also increased monotonically with delay, although by a smaller relative amount. Delay had no consistent effects on stick and stick rate scores.

System delay influenced primarily the low-frequency portion of the operator's frequency response, producing reduced pilot gain, increased phase shift, and increased closed-loop stick remnant. Individual differences between the best- and worst-performing subjects were considered small enough to justify pooling the results of the subject population. Analysis of fractional remnant power failed to support the hypothesis that introduction of delay would produce a tendency for the operators to adopt intermittent control behavior.

Pre-experiment model analysis performed with relatively "optimistic" parameters based on previous analysis with low-order systems yielded a good prediction of performance trends in terms of the percentage increase in error with delay. The actual error SD scores predicted by this analysis were about 70% of the experimental scores.

Subsequent model analysis with parameters adjusted to match the zero-delay results replicated the basic performance trends, but the predicted error score was less sensitive to delay, and the predicted stick and stick-rate scores were more sensitive to delay, than found experimentally. Comparison of the revised fixed-parameter model predictions to measured frequency response suggested that the superior model performance was due to lower low-frequency remnant, greater response bandwidth, and possibly some high-frequency "fine tuning" of the describing function not exhibited by the subjects.

Two modeling concepts were explored as potential mechanisms for enhancing the predictive capabilities of the OCM: low-order internal modeling, and robust control. The latter concept appeared to be the more promising. Sensitivity analysis conducted by varying the operator's control gain and motor noise were consistent with the hypothesis that (1) the addition of significant lags and/or delays to a system increases the sensitivity of closed-loop performance to fluctuations in the operator's response strategy, and (2) as this response sensitivity increases, the operator adopts a more conservative average response strategy.

23

ACKNOWLEDGEMENT

REFERENCES

1. Doyle, J.C., and Stein, G., "Multivariable Feedback Design: Concepts for a Classical/Modern Synthesis", IEEE Transactions on Automatic Control, Vol. AC-26, No. 1, February, 1981.

2. Fisher, T.J., Riccio, G.E., and McMillan, G.R., "The Effects of Simulator Delays on the Acquisition of Flight Control Skills", Proc. of the Tenth Biennial Psychology in the Department of Defense Symposium, USAF-TR-86-1, U.S. Air Force Academy, Colorado Springs, Co., 1978.

3. Johnston, D.E., and McRuer, D.T., "Investigation of Limb Sidestick Dynamic Interaction with Roll Control", AIAA Paper No. 85-1853-CP, Proceedings of the AIAA 12th Atmospheric Flight Mechanics Conference, Snowmass, Colorado, August 19-21, 1985.

4. Kleinman, D.L., Baron, S., and Berliner, J.E., "MCARLO: A Computer Program for Generating Monte-Carlo Trajectories in a Time-Varying Man/Machine Control Task", Technical Report TD-CR-77-2, U.S. Army Missile Research and Development Command, Alabama, June 1977.

5. Kleinman, D.L., Baron, S., and Levison, W.H., "A Control Theoretic Approach to Manned-Vehicle Systems Analysis," IEEE Transactions on Automatic Control, Vol. AC-16, pp. 824-833, No. 6, December 1971.

6. Kleinman, D.L., Baron, S., and Levison, W.H., "An Optimal-Control Model of Human Response, Part I. Theory and Validation." Automatica, Vol.6, pp. 357-369, 1970.

7. Levison, W.H., "Some Computational Techniques for Estimating Human Operator Describing Functions", Proc. of the Twenty-first Annual Conference on Manual Control, Ohio State University, June 17-19, 1985(a).

8. Levison, W.H., "Application of the Optimal Control Model to the Design of Flight Simulation Experiments," SP-634. Flight Simulation/Simulators, Society of Automotive Engineers Paper No. 851903, Aerospace Technology Conference and Exposition, CA, October 1985(b).

9. Levison, W.H., "Effects of Control Stick Parameters on Human Controller Response", Report 5510, Bolt, Beranek and Newman, Incorporated, Cambridge, MA, January 1984.

10. Levison, W.H., "Development of a Model for Human Operator Learning in Continuous Estimation and Control Tasks", AFAMRL-TR-83-088, Air Force Aerospace Medical Research Laboratory, Wright-Patterson Air Force Base, Ohio, December 1983.

11. Levison, W.H., "The Optimal Control Model for the Human Operator: Theory, Validation, and Application," in Frazier, M.L., and Cromble, R.B., (eds): Proceedings of the Workshop on Flight Testing to Identify Pilot Workload and Pilot Dynamics, AFFTC-TR-82-5, Air Force Flight Test Center, Edwards Air Force Base, CA, May 1982.

12. Levison, W.H., "Effects of Whole-Body Motion Simulation on Flight Skill Development", Report No. 4645, Bolt Beranek and Newman Inc., Cambridge, MA, October 1981 (ADA 111-115).

13. Levison, W.H., "The Effects of Display Gain and Signal Bandwidth on Human Controller Remnant", AMRL-TR-70-93, Aerospace Medical Research Laboratory, Wright-Patterson Air Force Base, Ohio, March 1971.

14. Levison, W.H., Baron, S. and Junker, A.M., "Modeling the Effects of Environmental Factors on Human Control and Information Processing", AMRL-TR--76--74, Aerospace Medical Research Laboratory, Wright Patterson Air Force Base, Ohio, August 1976.

15. Levison, W.H., and Huggins, A.W.F., "Modeling the Effects of Simulator Delays and Lags on Tracking Performance", Report No. 6245, BBN Laboratories Incorporated, Cambridge, MA, June 1986.

16. Levison, W.H., Lancraft, R.E., and Junker, A.M., "Effects of Simulator Delays on Performance and Learning in a Roll-axis Tracking Task", Proc. of the Fifteenth Annual Conference on Manual Control, Wright State University, Dayton, Ohio, March 20-22, 1979.

17. Levison, W.H., McMillan, G.R., and Martin, E.A., "Models for the Effects of G-Seat Cuing on Roll-Axis Tracking Performance," Proc. of the Twentieth Annual Conference on Manual Control. NASA-ARC, CA, June 1984.

18. Levison, W.H. and Warren, R., "Use of Linear Perspective Scene Cues in a Simulated Height Regulation Task," Proc. of the Twentieth Annual Conference on Manual Control, NASA-ARC, CA, June 1984.

19. Levison, W.H., Zacharias, G.L., and Sinacori, J.B., "Design of an Experiment to Study the Pilot's Use of Visual and Motion Cues in a Height-Regulation Task," Technical Report No. 5028, Bolt Beranek and Newman Incorporated, Cambridge, MA, December 1982.

THE APPLICATION OF MAN-MACHINE MODELS IN MARITIME RESEARCH

J. Perdok, C. van der Tak and P.H. Wewerinke
MARITIME RESEARCH INSTITUTE NETHERLANDS (MARIN)
P.O. Box 28
6700 AA Wageningen
The Netherlands

Abstract

In maritime research simulation techniques are used in different stages of the design process of ports, channels and inland waterways. Many questions concerning the behavior of the man-ship system, port lay-out, external disturbances (current, wind, waves) and aids to navigation (buoys, beacons, land marks etc.) can be answered by an adequate use of ship manoeuvring simulators. The attractiveness of ship manoeuvring simulators lies in the possibility to include the man in the loop as an important source of variability in the system behavior. Major drawbacks of real time simulation are the costs and time involved in executing a research program.

Presently MARIN is investigating how and to what extent man-machine models can be used to answer questions in the context of maritime research. These models already have proven their usefulness in other areas (e.g. flying, driving).

The paper describes the application of the optimal control model to a nautical problem. The subject of the study was the analysis of the safety of coal transport with barges pulled by tug boats, passing a bridge in a bendy river. In the project the sensitivy of the system configuration to wind, tow line orientation, and the system state at the start of the simulation was evaluated.

The results show the value and usefulness of man-machine models in maritime research.

1. INTRODUCTION

Optimal control theory has been successfully applied to model and analyse the control processes involved in car driving (Ref. 1) and flying (Ref. 2).

The application of this theoretical framework to the control of sailing ships is, however, relatively new. One reason for this may be the non linear equations of ship motions, which are in conflict with the linear character of optimal control theory.
In practice, however, the ship dynamics can be quite satisfactorily represented by a set of linear equations. The same applies to the environmental disturbances (wind, waves, current).

Another reason may be the somewhat conservative attitude in the maritime industry towards new developments and trends.

Whatever reason there may be it seems worthwhile to investigate the possibilities of applying modern optimal control theory to the nautical control task.

In the nautical control task four levels of control can be distinguished which involve different choices (see also Ref. 3).

The highest level of control refers to the choice of a destination. This choice is generally based on economical factors and is usually made by the shipowner.

The next level of control refers to the choice of a certain route, given the destination and the actual location. This is usually done by the master. Economical and safety factors play a major role. The output of this level of control can best be compared to a nominal trajectory or a reference track which is used in the later stages of control.

The third level of control refers to the choice of courses to be steered and RPM settings to be applied. The choices are based on deviations from the reference track and are usually made to minimize the track deviations. In open sea this level of control is usually executed by an officer of the watch (mate), while this task in confined waterways (e.g. approaches to ports) is performed by a pilot who is familiar with the local circumstances and has considerable experience in handling all kinds of ships.

This level of control requires continuous anticipation and can best be classified as a pursuit tracking task (Ref. 4).

On the lowest level of control choices are made concerning the rudder angles to be applied in order to minimize course error. In sea navigation this task is usually performed by a helmsman. This level of control can best be classified as compensatory tracking since the helmsman is compensating the course error without anticipation.

This division of control tasks is not strict, however. Some pilots tend to give rudder orders. In that situation they perform both a pursuit tracking and a compensatory tracking task.

Furthermore this description of different control levels performed by different persons does not apply to inland navigation. Here all levels of control can be in the hands of one person.

The two higher levels of control can be considered as a given input to the optimal control model (nominal trajectory with start and end point) while the two lower levels are the subject of the optimization process.

In the following chapter a description is presented of the different components of the man-ship system in his natural environment.

Chapter 3 contains a short review of the optimal control model.

In Chapter 4 the application of the optimal control model to a nautical problem is described. Chapter 5 contains some concluding remarks.

2. THE COMPONENTS OF THE MAN-SHIP SYSTEM

Figure 1 shows the basic elements of the man-ship system in relation to the environment.

Six relationships can be distinguished between the elements. Relationship No. 1 refers to the information about the environment to the human controller. Two kinds of information can be distinguished. Information which can be used to estimate the position (leading lines, buoys, beacons, land marks, etc.) and information about external disturbances. The information about external disturbances can either be viewed directly (e.g. the height of the waves) or by reading the values of instruments (e.g. wind velocity and direction).

Relationship No. 2 refers to the direct control of the environment. At first glance this may look a little bit strange, but this relationship represents the possibility to avoid for instance strong winds, high current velocities and bad visibility conditions. Ports all over the world have their own admission policies which are based on maximum allowable values of external disturbances.

Relationship No. 3 represents the information about the controlled system. This information can be obtained by looking at the instruments: compass, sal log, Doppler log, rate of turn indicator, radar. Information about the state of the controlled system, that can be obtained by visual inspection of the outside world, is already represented by relationship 1.

Relationship No. 4 represents the control actions of the navigator. Control actions can be performed by changing the rudder or RPM settings. In addition tug boats can be used in approaching a port and in special manoeuvres. Some vessels are equipped with bow and/or stern thrusters which can be used to generate a lateral velocity and/or a yawing moment.

Relationship No. 5 represents the influences of the environment which act on the controlled system. The most important influences, or external disturbances are current, waves, wind, bank suction and bottom effects.

Relationship No. 6 refers to the influence of the controlled ship on the environment. From a hydrodynamic point of view the disturbances in the current flow around the ship have to be considered here.

3. DESCRIPTION OF THE MAN-MACHINE MODEL

3.1. Introduction

In order to be useful in (maritime) research the man-machine model has to satisfy a number of requirements.

First of all the system elements and relationships described in Chapter 2 must be part of the model.

Secondly, knowledge about human factors regarding perception, information processing, neuro motor behaviour and selective attention has to be represented in the model.

Thirdly, the model must be flexible to allow for modifications and extensions to incorporate new developments in psychology, hydrodynamics and new trends regarding organisation and task performance in the maritime industry.

The optimal control model meets these requirements and is attractive since its structure has much in common with models of human information processing in modern psychology.

The following paragraphs give a brief review of the model. First of all a short system description is presented, followed by a description of model analogues of perception, information processing, response selection and response execution. See references 2, 5 and 6 for a more detailed description.

3.2. System description

The controlled process is represented by the following linear equation (see also Figure 2):

$$\dot{x} = Ax + Bu + Ew \qquad (1)$$

In this equation x is the vector of system states (heading, position variables, rate of turn, etc.).

u is the vector of control inputs (rudder angle setting, RPM setting etc.).
w is the vector of system disturbances (wind, waves, current, etc.). A, B and E are matrices which translate the vectors x, u and w to changes in the system state.

In this equation the matrix B represents relationship 4 of Figure 1, while relationship 5 is represented by matrix E.

3.3. Perception

The perception variables (y) are assumed to be related to the state (x) and control (u) variables according to

$$y = Cx + Du \tag{2}$$

The perception variables in this stage are not interpreted by higher mental functions.

The equation (2) expresses that, for instance, visual angles and instrument readings are computed on the basis of the state and control variables.

This equation represents the relationships 1 and 3 of Figure 1. One stage further in information processing the perceptions (y_p) are distorted by noise (V_y):

$$y_p = y + V_y \tag{3}$$

with:

$$V_{yi} = \frac{P_o \sigma^2_{yi}}{f_i K^2_i} \tag{4}$$

35

The noise term comprises the influences of the signal to noise ratio (P_o), the signal variance (σ^2_{yi}), the fraction of attention (f_i) dedicated to a particular source of information and the gain associated with the signal threshold (K). The index i refers to the elements of y.

The signal to noise ratio has been found to be fairly constant (-20 db) in different tasks (Ref. 2).

The signal variance (σ^2_{yi}) is computed and continuously updated in the simulation process.

The gain factor K is related to the perception threshold as shown in Figure 3. The gain factor is large (maximum is 1) if the threshold is small and the signal variance is large. In addition the noise term is lowered since K is in the denominator of V_{yi}. On the other hand the gain factor will be close to zero, with consequently a large noise term, if the threshold is high and the signal variance is low.

The fractions of attention (f_i) are computed to minimize the performance index J (see paragraph 3.5.). The fraction of attention concept takes into account that the human information processing capacity is limited and that a controller of a system has to divide his attention between a limited number sources of information.

3.4. Information_processing

Information processing in the model is the estimation of the new system state according to:

$$\dot{\hat{x}} = A \; \hat{x} + K \; (Ce + V_y) \tag{5}$$

36

In this equation A, x, C and V_y are already known. The vector e comprises the estimation errors, in fact x-$\hat{x}$. K is the so-called Kalman gain factor. So, if K is small not much use is made of new information. On the other hand, if K is large much emphasis is placed on the new information.

The gain factor K can be written as:

$$K = \Sigma \ C'V_y^{-1} \tag{6}$$

in which Σ is the variance of the estimation error (e). It can be seen that K is large if Σ is large and V_y is small. So in other words if the quality of information is good (V_y is small) and the need for information is high because of large estimation errors (large Σ), then K is large.

3.5. Response selection

Control response are computed according to:

$$u_c = -L \ \hat{x} \tag{7}$$

The optimal gains, L, which operate on the estimated state variables are computed by minimizing the performance index J:

$$J = E \ \{ y'Q_y \ y + u'Q_u \ u + \dot{u}' \ Q_{\dot{u}} \ \dot{u} \} \tag{8}$$

Here Q_y, Q_u and $Q_{\dot{u}}$ are the weights. These weights enable the investigator to define the task objectives of the controller. The weights are applied in such a way that maximum allowable values of y, u and $\dot{u}$ result in unity. This is accomplished by weighting with the reciprocal of the squared maximum allowable values. So, if a sailing vessel has a margin of 100 m at

starboard and port side within which to stay the weight for this variable would be 0.0001.

3.6. Response execution

The human control response is executed according to:

$$T_N \dot{u} + u = u_c + V_u \qquad (9)$$

Herein is u_c the commanded control, u is the actual control input, T_N is a matrix with time lags and V_u is neuro motor noise. With T_N it is possible to model gradual changes in control responses, instead of jumping from one control value to another. It is assumed that well trained navigators will try to avoid very drastic changes in control behaviour.

V_u on the other hand represents the imperfect knowledge to generate a particular response. A helmsman, for instance, does not perfectly know which rudder angle to select in order to attain the right course in the most efficient manner (Ref. 7).

The control input, u, is fed into the system equation and the model is updated and the whole sequence of perceiving, information processing, response selection and response execution starts again (see Figure 2).

So far relationships 1, 3, 4 and 5 of Figure 1 have been mentioned. Relationship 6 is inherent in the system equation. Relationship 2 is the subject of investigation in most research applications, since the effects of external disturbances are extremely important to determine admission policies.

4. CASE STUDY: MODEL ANALYSIS OF THE APPROACH TO A BRIDGE BY TOWED BARGES

4.1. Introduction

A study was executed to get a better insight into the risk of colliding to a bridge over the Mahakam River, Kalimantang (Indonesia). The bridge has been built within 1000 m from a bend in the river. Current velocities are between one and two m/s.

The model analysis was executed to investigate the performance of a system consisting of a tug boat pulling a barge, stabilized by another tug boat. This configuration can be considered as relatively difficult to handle. Both the effect of variable wind and the curve in the river in front of the bridge are investigated. The manoeuvres considered are in the same direction as the current.
The following paragraphs contain a general system description, a description of the task and finally the results of the model analysis.

4.2. System description

4.2.1. The barge-tug boat system

The model used in the model analysis is based on the following assumptions:

1. Course keeping is performed with the rudders of the tug boats only and a constant velocity of the tug barge unit.

2. Only small variations around the equilibrium, thus no higher order terms of lateral speed (v) and rate of turn (r, yawing).

3. The centre of gravity lies on $0.5 \, L_{pp}$.

39

Based on these assumptions the following mathematical model has been derived:

$$(m+m_y) \; \dot{v} = -mur + Y_{Ur} + Y_{Uv}Uv + Y_R + Y_C + Y_D \qquad (10)$$

$$(J_{zz} + m) \; \dot{r} = N_{Ur}Ur + N_{Uv} \; Uv + N_R + N_C + N_D \qquad (11)$$

with:

m = mass

m_y, m = added mass terms

u = longitudinal velocity

v = lateral velocity

U = ship's velocity ($\sqrt{u^2 + v^2}$)

r = rate of turn

J_{zz} = moment of inertia.

Y_{ur}, Y_{uv}, N_{ur} and N_{uv} are coefficients

V_R and N_R are the force and moment executed by the rudder.

Y_C and N_C are the force and moment executed by the cables.

Y_D and N_D are the force and moment executed by disturbances in the equilibrium.

This model is valid for both tug boats and the barge.
Two configurations of tug boat and barge were tested in the model analysis (see Figure 4).
The major difference between the configurations concerns the way of connecting the cables.
In configuration 1 the tug boat is pulling with the aid of one single line connected midship. In configuration 2 a so-called bridle is used. This difference in cabling was accounted for in the model.

Using the model assumptions the equations were linearized yielding a set of linear pertubation equations.

40

4.2.2. Wind

A constant wind delivers forces and moments on the ship. In case of constant wind the windforces and moment will not change.
The navigator will sail with a constant drift angle, which can be considered as the equilibrium. In reality, however, the wind fluctuates. A (linearized) Davenport spectrum (Ref. 8) has been used to model the variation in wind. The mean wind velocity was 12 m/s.

4.2.3. Current

Based on survey data the current can be modelled as a constant current. The magnitude of the current in addition to the forward velocity of the ship determines the time the navigator has available to bring the ship to the desired track coming out the curve. Current velocities (V_c) used were 1 and 2 m/s, in a direction parallel to the river side.

4.2.4. Visual perception

It was assumed that the dominant visual cue was derived from observing the bridge opening and especially from two pillars which mark the passage at both sides. The pillars at either side were located 12 m apart in longitudinal direction.
The difference in the projected visual images of the two pairs of pillars, expressed in visual angles, was used as the visual cue. The relationship between the perceptual cue and the system state (lateral deviation from the track) was linearized.

4.3. Task description

The task considered is to control the tug boats in such a manner that a desired trajectory is obtained. This desired

41

trajectory is defined as the straight path passing the bridge through the middle of the passage (width = 100 m).

Not only the deviation of this desired path (primarily of the barge but also of the tug boats) is of interest. Also the heading of the barge and the tug boats are important to minimize path deviations. Further the control will be limited and economized i.e. the control deflections and rapid movements will be minimized.

These aspects are translated in the model in terms of a performance index which the human operators are assumed to optimize. The relative weightings of these variables is chosen on the basis of "allowable limits", i.e. for path deviations 40 m (corresponding to the width of the passage of the bridge), for the heading of the barge 10 deg., and of the tug boats 20 deg., for the rudder deflections 30 deg. and for the rudder movements 10 deg. per second.

Finally, it is assumed that the control is in such a way that the heading of the cables is kept within 30 degrees.

4.4. Results

Two types of analysis were performed: a steady state model analysis and a range varying analysis which gives the state variables as a function of time.

The steady state model analysis concerns the effect of variable wind on the performance of the system which is in a stabilized position on the centre line of the passage of the bridge. Another source of system deviations is due to randomness in controlling the total system. Based on this analysis it was concluded that the effect of variable wind and human variability on system performance is small and will not contribute to an appreciable probability of hitting the bridge (probability of about $2 * 10^{-8}$).

In the range varying model analysis the effect of the curve of the river on the probability of hitting the bridge is indirectly investigated by considering various initial situations.

Based on the geographical situation derived from a map it is assumed that the configuration has an initial lateral deviation of 100 m at 1 km before the bridge (due to current, overshoot, etc.) and, in addition the barge and the last tug boat had a deviation in heading angle of 20 degrees, relative to the course of the track. Apart from this average deviation a variation in these deviations (in terms of the initial standard deviation) of 1/5 of the mean is assumed.

The results of case 1 (= configuration 1) are shown in Figure 5. The mean lateral deviation and (added to this mean) one standard deviation are given as a function of the time elapsed. Case 1 has a forward velocity with respect to the water of 3 m/s. In the case of a current velocity of 1 m/s, the distance of 1000 m corresponds to a time of 250 seconds. As shown in the figure this implies a mean lateral deviation of about 25 m and a standard deviation of about 5 m. So hitting the bridge is a real possibility (3σ with B = 18; $P \approx 0.0007$; 1 on 1400 passages). The situation becomes even more dramatic when the current velocity is increased to 2 m/s. The mean deviation is now more than 50 m.

The results for case 2 (= configuration 2) are summarized in Figure 6. Three conditions are considered. The first one is the same as for case 1 (position and heading deviations). As the forward velocity of this configuration is 2 m/s with respect to the water, the distance of 1000 m (thus the position of the bridge) corresponds now with 330 s when the current velocity is 1 m/s. The lateral deviation is about 8 m, on the average, and seldom much more than 10 m. So this situation does not seem to cause real problems. However, when a current velocity of 2 m/s is assumed, the bridge is passed at a time of 250 seconds. Now, the mean lateral deviation is almost 20 m

and the standard deviation is about 4 m. Although the corresponding hit probability is still small, this result indicates a problem area.

Since the forward velocities of case 1 and case 2 differ a direct comparison (on time basis) does not make sense. Therefore the system performance of both cases is shown as a function of distance in Figure 7. This figure shows that the performance of configuration 1 is worse.

The second initial condition for case 2 assumes only initial position deviations. In this case the deviations do not increase any more (as for condition 1 because of the initial heading deviations) but diminish after some time. Although the differences with the first condition are substantial during the initial period, after about 200 s these differences are less than 10 m. So 'details' in the assumed initial conditions have minor effect on the system performance in the vicinity of the bridge. For a more precise (absolute) interpretation of the results one has to know more precise the real initial condition.

The third condition considered is related to the first one. Initial positions and headings are assumed, but now not implemented as a mean value (corresponding with a specific ship movement) but simulated in terms of a statistical condition: an initial standard deviation of lateral position and heading (corresponding to a given real life variability in these parameters after the curve).
An initial standard deviation of 50 m (implying that initial lateral deviations are only a few per cent of the cases larger than 100 m) is considered. Figure 6 shows that for a current velocity of 1(2) m/s the standard deviation of the lateral position at the passage of the bridge is less then 5 (10) m.

The following conclusions were drawn from the model analysis:

a. Once the total system is in a stabilized position on the centre line in front of the bridge the probability of hitting the bridge is negligible.

b. The effect of deviations in lateral position and heading, due to the curved river, on system performance is prolonged and substantial because of the slowly responding system.

c. The effect of the geometry of the cables on the system performance is significant.

d. The effects of the sailing velocity and the current velocity on the lateral deviations have to be considered carefully.
High velocities may result in risky manoeuvres.

5. CONCLUDING REMARKS

The application of optimal control theory as presented in this paper shows how useful information concerning nautical problems can be obtained with this model approach.

In addition it is possible with this model to obtain information on workload and selective (fractions of) attention (Ref. 2). Especially the measures of fractions of attention are very useful in designing fairway lay-outs and in the optimization of navigational aids.

To apply the model to a very general class of nautical problems including bendy rivers and fairways the model will be extended (see Ref. 9). So far human control behaviour has been investigated and modelled in the restricted sense of continuous regulating against random disturbances so as to minimize the system state.

The model will be extended by incorporating control behaviour at a higher mental level involving planning (finite time, pre-programmed, open loop control) and decision making.

6. ACKNOWLEDGMENTS

REFERENCES

/1/ Blaauw, G.J. "Car driving as a supervisory control task", Ph.D. Thesis, Institute for Perception, Soesterberg, The Netherlands, 1984.

/2/ Wewerinke, P.H. "Visual scene perception process involved in the manual approach". National Aerospace Laboratory NLR, Amsterdam, The Netherlands. Report NLR TR 78130 u., 1978.

/3/ Schuffel, H. "Proposed procedures for determining man/ship performance at simulators", Proceedings of MARSIM'81, CAORF, New York, 1981.

/4/ McRuer, D.T. and Krendel, E.S., "The human operator as a servo system element", Journal of the Franklin Institute, 1959.

/5/ Baron, S. and Levison, W.H. "Display analysis with the optimal control model of the human operator", Human Factors, 1977, 19 (5).

/6/ Kleinman, D.L. and Baron, S. "Manned vehicle system analysis by means of modern control theory, NASA CR-1753, 1971.

/7/ Schuffel, H. "Human control of ships in tracking tasks", Ph.D. Thesis, Institute for Perception, Soesterberg, The Netherlands, 1986.

/8/ Davenport, A.G. "The application of statistical concepts to the wind loading of structures". Proc.Inst.Civ.Eng. 19, August, 1961.

/9/ Wewerinke, P.H. "Model of the human controller of a dynamic system". Paper presented at the 22nd Annual Conference on Manual Control, July 15-17, 1986, Dayton, Ohio (USA).

MAN/SHIP SYSTEM

CONTROL

1

2

3   4

ENVIRONMENT
(DISTURBANCES)

CONTROLLED
SYSTEM

5

6
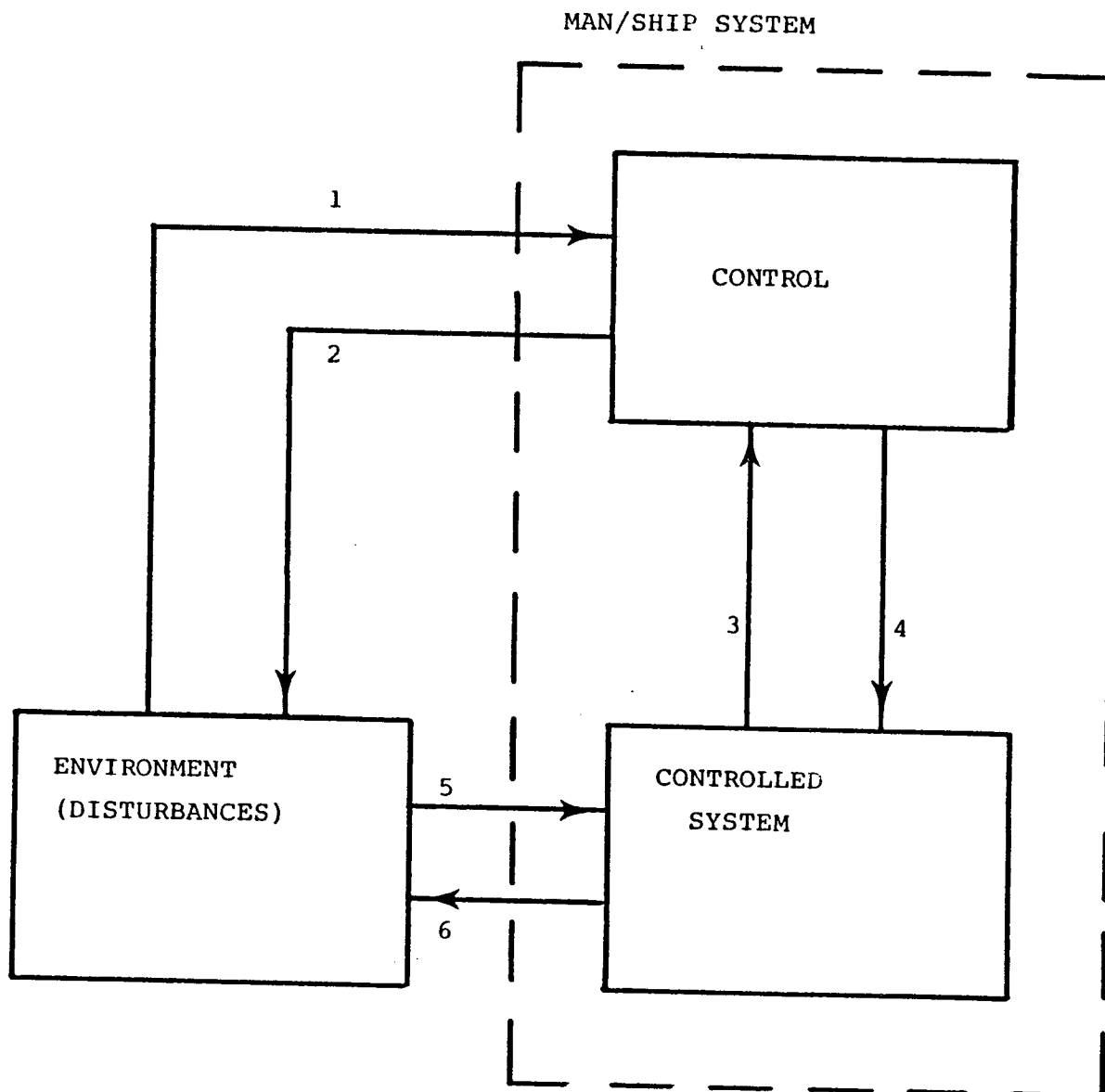
Figure 1: The man/ship system in relation to the
environment.

PERCEPTION

$$y = Cx+Du$$

$$y_p = y+v_y$$

$$y_p$$

INFORMATION PROCESSING

$$\dot{\hat{x}} = A\hat{x}+K(Ce+v_y)$$

$$\hat{x}$$

RESPONSE SELECTION

$$u_c = -L\hat{x}$$

$$u_c$$

RESPONSE EXECUTION

$$\tau_N\dot{u}+u=u_c+v_u$$

PERFORMANCE INDEX

$$J = E\{y'Q_yy + u'Q_uu + \dot{u}'Q_{\dot{u}}\dot{u}\}$$

CONTROLLED SYSTEM

$$\dot{x} = Ax + Bu + Ew$$

$$x$$

$$u$$
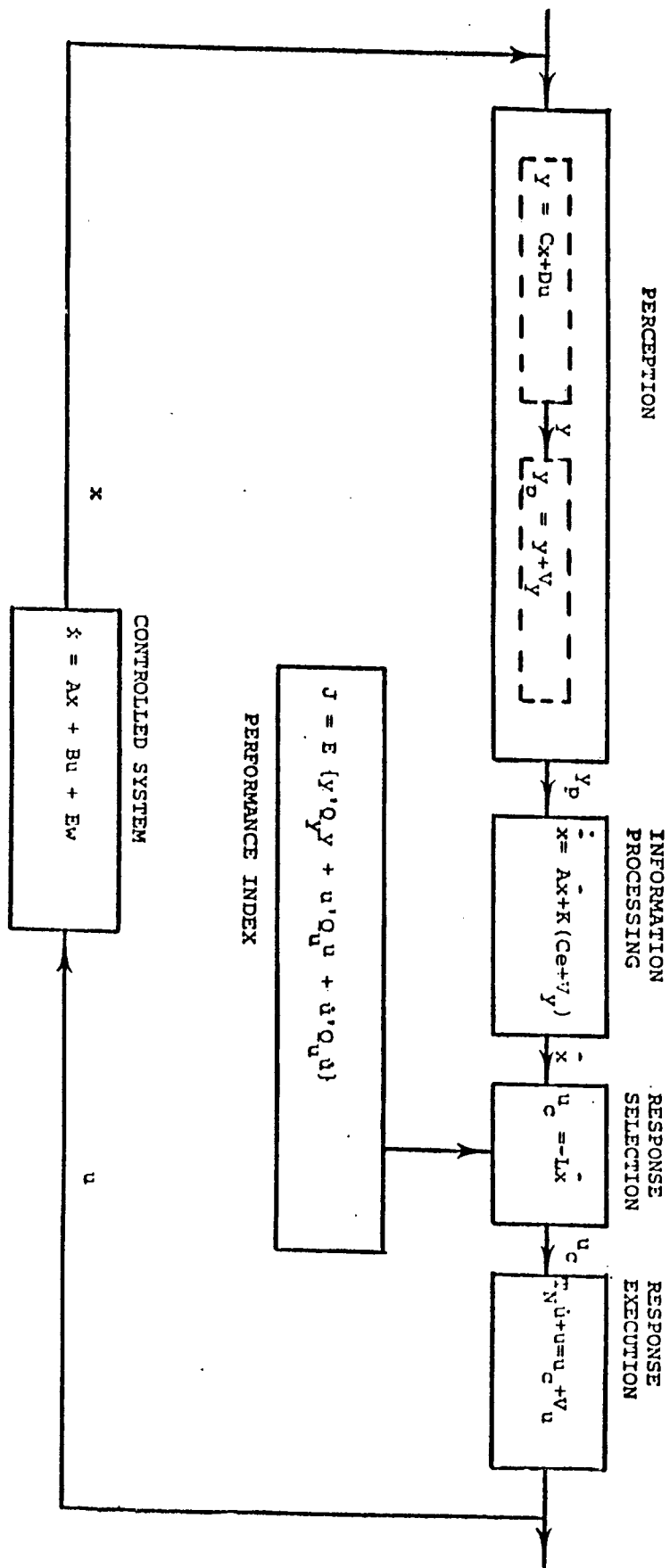
Figure 2: Man machine model.
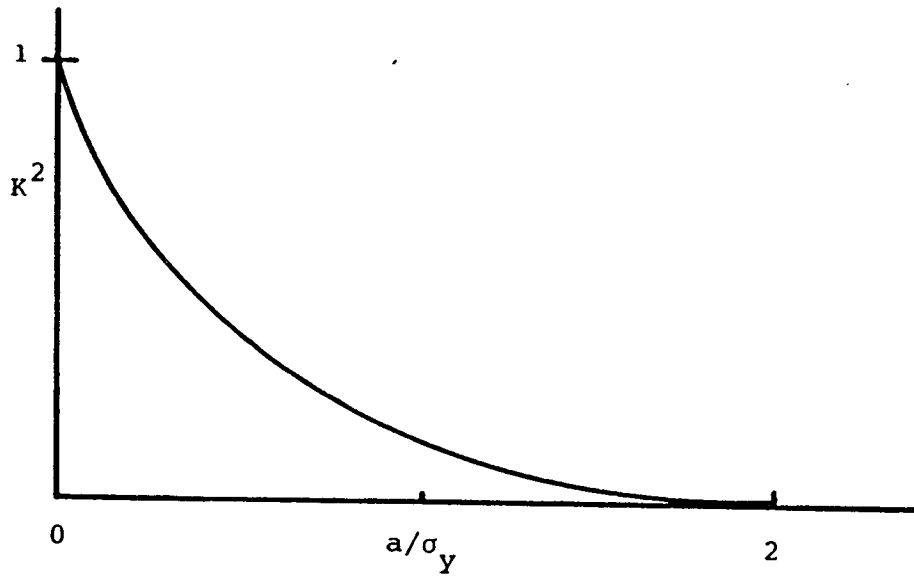
$$K^2 = N^2 (a, \sigma_y)$$
$$N(a,\sigma_y) = \sqrt{2/\pi} \int_{-\infty}^{-a/\sigma_y} \exp^{-u^2/2} du$$

a   = threshold

σ_y = signal variance

Figure 3: Relationship between K^2 and a/σ_y.

$1^2=20$

B = 12

L = 19.1
B = 5.4

1^1 = 20

L = 79

Configuration 1

$1^2=10$

B = 18.3

1^1 = 25

L = 64
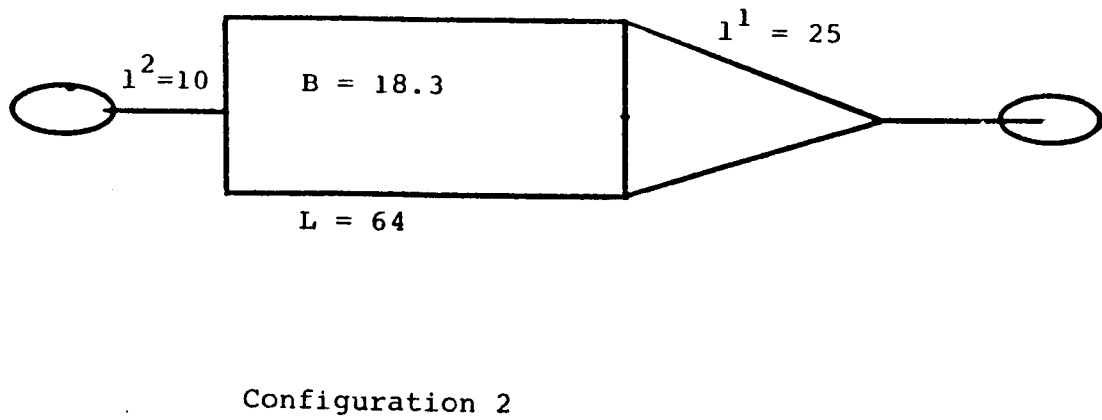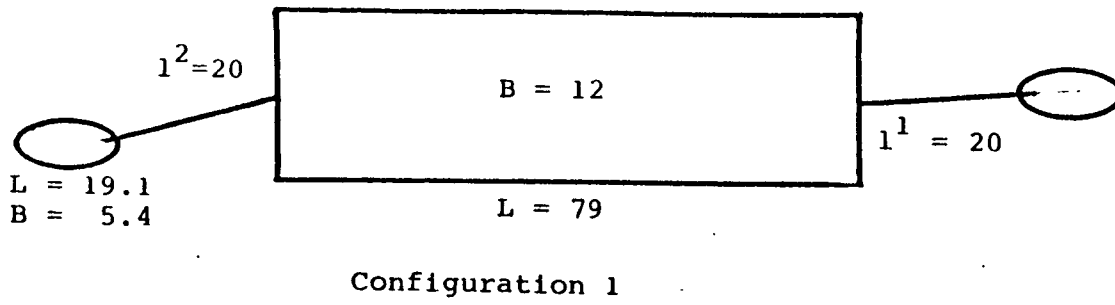
Configuration 2

Figure 4: The two configurations tested in the
model analysis.

LATERAL DEVIATION (m)
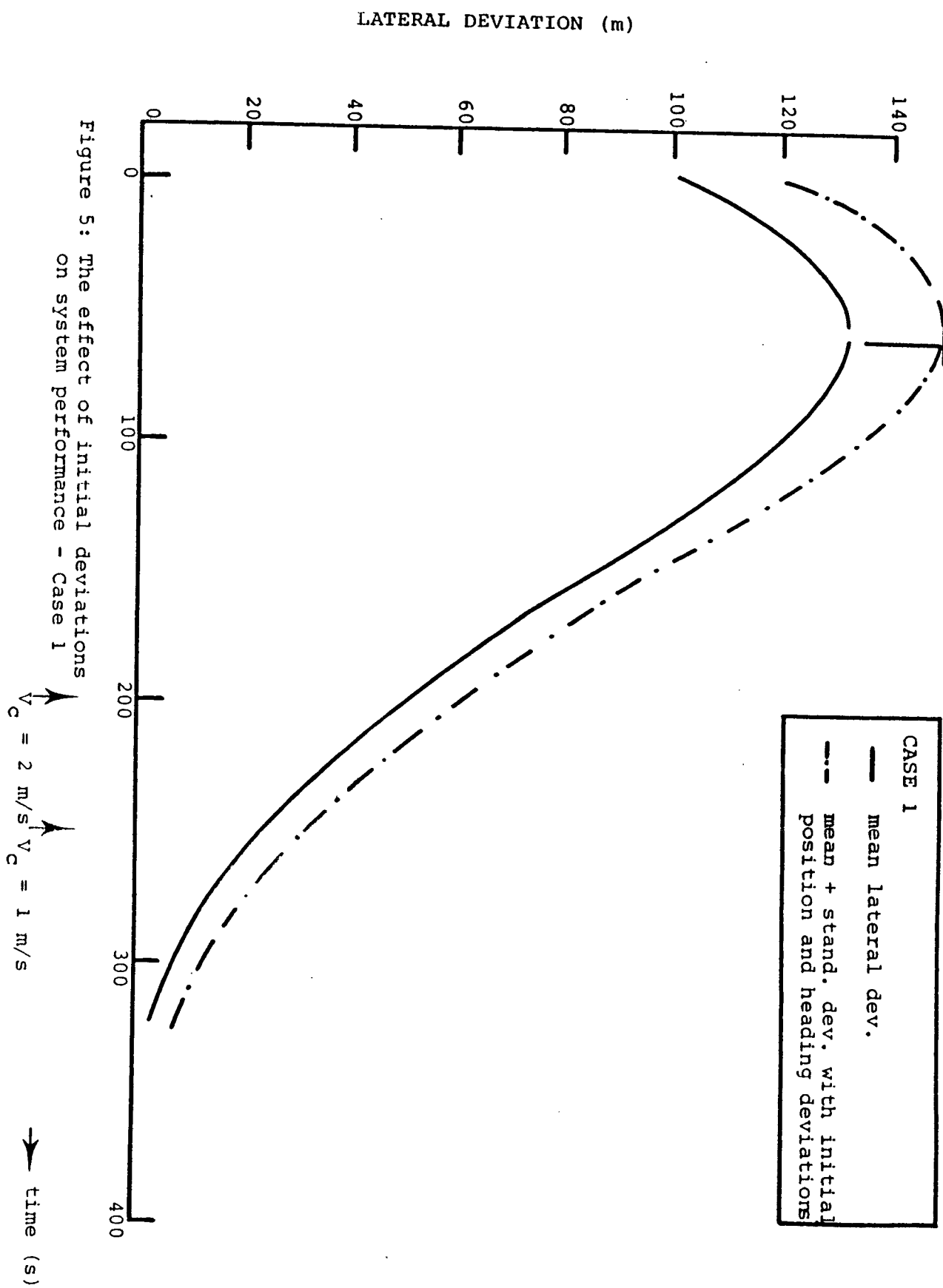
Figure 5: The effect of initial deviations
on system performance - Case 1

$\overleftarrow{V_c} = 2 \text{ m/s} \quad \overrightarrow{V_c} = 1 \text{ m/s}$

$\longrightarrow$ time (s)

CASE 1

——— mean lateral dev.

——·— mean + stand. dev. with initial
position and heading deviations

53

Figure 6: The effect of initial deviations on system performance - Case 2

CASE 2
(1) initial position and heading dev.
(2) only initial position dev.
(3) variability in initial position and heading

LATERAL DEVIATION (m)

time (s)

$V_C = 2\ m/s$ $V_C = 1\ m/s$

stand.dev. (1)

mean (1)

mean (2)

stand.dev. (2)

stand.dev. (3)

54

Figure 7: Comparing the effect of initial deviation for case 1 and case 2.

CASE 2

CASE 1

LATERAL DEVIATION (m)

range (m)

bridge

$V_c = 1$ m/s

mean

st.dev.

st.dev.

55/56

SESSION 2: HUMAN OPERATOR MODELS

Moderator: Dr. David K. Schmidt, Purdue University

Spatial Orientation from Pictorial Perspective Displays

Arthur J. Grunwald, Stephen R. Ellis and Stephen Smith

Aero-Space Human Factors Research Division
Ames Research Center, Moffet Field, Ca. 94035

Abstract

A mathematical framework has been described, developed in earlier work, for the process employed by a human observer of reconstructing a three-dimensional spatial situation from a perceived two-dimensional perspective image. The model is based on the assumption that the observer has some a priori knowledge of the size, shape or certain characteristics of the viewed objects, such as the existence of parallel or perpendicular lines or planes. It is assumed that this knowledge is used in a three-dimensional process to reconstruct a spatial situation which "best matches" with the perceived lines-of-sight. Sources of errors and inaccuracies are specified and their effect on model outputs are discussed. In this paper the model has been implemented with a display configuration abstracted from a perspective cockpit based air-traffic display. The display shows the ownship and surrounding environment from a "bird-eye" view above and behind the ownship. A series of experiments has been conducted to validate the model. In these experiments the pilot was to estimate the azimuth angle of an intruder with respect to the ownship. Systematic errors in the azimuth angle estimate have been found, which resemble the type of errors which would result from viewing the visual scene through telephoto lens. The model has been found to reproduce the general trends of the experimental results reasonably well. However, remaining disagreements between theoretical and experimental results indicate that apart from three-dimensional processing, as suggested by the model, some two-dimensional processing takes place in the plane of the image as well. The analytical model is expected to be a useful tool in analysing and developing pictorial perspective flight displays composed of a limited number of clearly outlined objects.

Introduction

Recent developments in microcomputer and electronic display systems technology, have led to new concepts for flight displays. Conventional displays, in which the navigation, guidance and control information is segregated over a variety of electro-mechanical flight instruments, are not able to meet the stringent demands of the increasingly dense air traffic environment. The pictorial flight display, which is commonly recognized as a promising candidate for an advanced integrated display, presents a natural and easily interpretable perspective image of the spatial situation of the aircraft and its surrounding environment. The choice of the viewpoint and field-of-view highly depends on the function to be performed. Thus, the viewpoint can be located either in the cockpit, producing a

through-the-windshield scene. e.g. as in the "tunnel" display of Ref. [1] used for path-following in the terminal area, or can be located slightly above and behind the aircraft, producing a bird-eye view, as in the "pathway-in-the-sky" display of Ref. [2], or can be far above and behind the aircraft, as in the airborn traffic display of Ref. [3]. Although these pictorial displays appear to be more natural for the pilot than symbolic displays such as horizontal or vertical situation displays, their schematic images generally lack the texture and detail present in real-world images, since they are usually composed of a limited number of lines or polygons. Their interpretation requires the mental reconstruction of a three-dimensional situation from the two-dimensional perceived image. The errors involved in this process largely depend on the correct choice of the relevant viewing parameters, such as viewpoint, field-of-view, level of detail, etc. Furthermore, the interpretation usually requires certain basic assumptions to be made about the characteristics of the displayed objects, i.e. certain points being located within one plane, the existence of parallel/perpendicular lines or planes, etc. The purpose of this paper is to model and analyse the process involved in reconstructing the spatial situation from the perceived two-dimensional image, to investigate how basic assumptions about the characteristics of the objects are used in the process, and to obtain a better understanding on how these parameters affect the estimation errors and accuracies.

Familiar objects provide an essential cue for the spatial orientation of an observer who processes visually perceived information. If the observer has some a priori knowledge of the perceived objects, like size, shape, or characteristics like parallel/perpendicular lines or planes, he is able to utilize this knowledge in estimating spatial positions and angular orientations of the object. It is well known that in low visual flight above uncultured terrain like bare sand dunes or water, distances and velocities are more difficult to estimate than above a cultured urban area, showing houses, roads, vehicles and man-made familiar objects. In previous work [4] an analytical model was formulated for estimating the viewpoint position from the perceived image of familiar objects, such as a rectangle or parallelepiped. The model was used for the development of visual aids in a helicopter hovering task above a moving ship-deck. An inertially stable square was displayed above the ship-deck in order to provide the pilot with the necessary inertial references for performing the hovering task. It was shown that in order for the pilot to use the displayed information, he had to make the basic assumption that the sides of the square were parallel. In this paper the model of Ref. [4] has been implemented to the more complex perspective air-traffic display, proposed, analysed and experimentally evaluated by Ellis et. al [3.5.6]. Seen from behind and above the ownship, the pilot has to identify potential intruders by estimating the azimuth and elevation angles of surrounding aircraft with respect to the ownship. Experimental results in these studies show the existence of a sinusoidal relationship between the error in the azimuth angle estimate and the true azimuth angle, while the magnitude of the error was found to depend on the combination of displayed field-of-view and eye-to-screen distance. McGreevy et.

60

al [5,6] attributed these systematic errors to two effects: the "virtual space" effect, resulting from the fact that the monitor image is not viewed from its center of projection, and the "2-D" effect, accounting for the fact that the observations are strongly affected by angles appearing between lines in the plane of the displayed image. The problem of pictorial distortions as a result of an incorrect viewpoint was earlier investigated by Farber and Rosinski [7]. Their model differed from the one of McGreevy et al. [5,6] only in the assumption under which the "virtual space" was created. However, with both models each point of the object is mapped into the virtual space individually, without considering the functional relationship between the points of the object. Consequently the object will appear distorted in the virtual space. In contrast to this, in this paper the computational process utilizes the known functional relationship between the coordinates of the object. All the points of the object are treated simultaneously, and rather than being distorted, the object will be dismatched with the lines-of-sight instead. The systematic estimation errors are analysed in view of inaccuracies and errors in the pilot's basic assumptions about the objects as well as random error components resulting from perceptual noise.

Geometry of the Problem

Fig. 1a shows the spatial viewing situation. The pilot is looking down at the traffic situation through the window W from the viewpoint location P which is above and behind the ownship. In this highly simplified case only the ownship, one intruder and the groundplane are shown. The ownship is indicated schematically by the reference cube R and the intruder by the target cube T. The groundplane is indicated by a grid consisting of a set of parallel and perpendicular irregularly spaced straight lines. In addition to the cubes, the line segments between the cubes and their projection on the groundplane RR' and TT', are shown as well. The pilot has to judge the relative position of the intruder with respect to the ownship in terms of the azimuth angle ψ_a and the elevation angle θ_a. We can distinguish between two cases: (1) the pilot is viewing a real-world situation; (2) he is viewing a picture of the situation. In the first case he perceives the directions of the lines-of-sight (LOS) between his eye and the coordinates of the objects. These LOS directions can be expressed as points on an imaginary unity sphere, centered about the pilot's eye position. In the second case only the intersections of the lines-of-sight with the window plane exist, rather than the original lines-of-sight. In case the pilot's eye is at the location from which the image was taken, (the center of projection), the lines-of-sight to the points on the image coincide with the original lines-of-sight. However, the eye being located in front of the center of projection, has the same effect as viewing the real-world scene through a telephoto lens and the eye being located behind the center of projection has the effect of viewing through a wide-angle lens.

The basic assumption which underlies the spatial perception model, is that the pilot uses the a priori knowledge of the objects to construct a three-

dimensional situation which best matches with the perceived lines-of-sight. For the task under investigation, the visual scene is separated into two objects: (1) the groundgrid, and (2) the formation of reference and target cubes. Regarding the groundgrid the pilot knows that the lines are parallel and perpendicular with respect to a main reference direction. However, the spacing between the lines is irregular and unknown to the pilot. The cube formation is outlined by the trapezoid $RR'T'T$ formed by the cube centers and their projection on the groundgrid. Here the pilot uses the knowledge that the four points are located in the azimuth plane, that the lines RR' and TT' are parallel and that the line RR' is perpendicular to the line $R'T'$. In addition to this he also knows that the points R' and T' are located in the plane of the groundgrid, and that the azimuth plane and the groundplane are perpendicular. Note that in this simplified case only the centerpoint location of the cubes is used, rather than the detailed cube description. The process of reconstructing the three-dimensional situation from the perceived lines-of-sight and on the basis of the a priori knowledge of the objects, involves the determination of unknown parameters such as the viewpoint location and viewing direction, the spatial orientation of the azimuth plane with respect to the groundplane, the estimation of the spacing between the lines in the groundgrid, and the dimensions of the trapezoid. This process is performed in three-dimensions and involves translations, rotations and the computation of distances to the lines-of-sight.

Sources of Errors and Inaccuracies

Ideally, the pilot will be able to choose a parameter setting, reconstructing a spatial situation, which fully matches with the actually perceived lines-of-sight. However, various sources of errors and inaccuracies will cause deviations. Two sources are considered: (1) perceptual inaccuracies which include (a) random errors and (b) systematic errors in the perception of the lines-of-sight and (2) errors or uncertainties in the memorized a priori knowledge of the object characteristics. The random errors in the perception of the lines-of-sight are modelled by randomly deflecting the LOS vector from its true direction by adding a LOS noise vector of a given constant magnitude to the LOS vector. This noise vector is located in a plane perpendicular to the true LOS and points in a random direction uniformly distributed between 0 and 360 degrees, with respect to a given reference, see Fig. 2a. As a result, the perceived perspective image will be distorted, as shown in Fig. 2b. The coordinates of the distorted image are randomly located on circles of equal radii, centered about the true coordinates. Systematic errors in the perception of the lines-of-sight include errors in the relative scaling of the perceived image. These errors are modelled by increasing or decreasing the relative size of the image, like this is done with the zoom operation of a camera lens. Errors in the memorized object characteristics are modelled by distorting the memorized shape by adding a shape noise vector to the stored object coordinates. In Fig. 2c shape noise is added to the stored definition of a square. In this example it is assumed that the observer utilizes the knowledge that the four

coordinates are located in one plane. Accordingly, the shape-noise vectors are located in this plane as well and point in a random direction, uniformely distributed between 0 and 360 degrees, with respect to a given reference.

The magnitude of the error sources can only be determined by experiments. For foveally viewed objects, the LOS noise magnitude will be determined primarily by objective physiological characteristics, such as visual acuity. However, image scaling errors and shape noise will highly depend on subjective characteristics, such as familiarity with the object or training.

Mathematical Formulation

Fig. 1b shows the coordinate systems for the spatial viewing situation of Fig. 1a. The main frame of reference is defined by the inertial reference system x^i, y^i, z^i, with the x_i axix pointing in the main reference direction. The two objects, i.e. the groundgrid (g) and the azimuth plane trapezoid (a), are described in the object coordinate systems x^g, y^g, z^g and x^a, y^a, z^a by the two sets of three-dimensional object coordinates $\underline{x}^g(\underline{c}_g)_j \equiv \{x^g, y^g, z^g\}_j$ where $j = 1,....,N_g$ and $\underline{x}^a(\underline{c}_a)_k \equiv \{x^a, y^a, z^a\}_k$ where $k = 1,...,N_a$, respectively. In order to model that only certain characteristics of the objects (g) and (a) are known rather than their exact shape, the coordinates $\underline{x}^g$ and $\underline{x}^a$ are expressed as a function of the unknown parameter vectors $\underline{c}_g$ and $\underline{c}_a$, which are to be estimated by the observer. In this case it is assumed that the observer has a priori knowledge of the existance of parallel/perpendicular lines or planes, which is modelled by the following linear relations:

$$\underline{x}^g(\underline{c}_g)_j = F_j + G_j \, \underline{c}_g \tag{1a}$$

$$\underline{x}^a(\underline{c}_a)_k = F_k + G_k \, \underline{c}_a \tag{1b}$$

where the matrices F_j, G_j, $j = 1...N_g$ and F_k, G_k, $k = 1...N_a$ are assumed to be memorized by the observer. The observer perceives the the objects in the eye-coordinate system x^e, y^e, z^e, oriented with the x^e axis pointing towards the reference cube, and with the y^e axis parallel to the $x^i oy^i$ horizontal plane, i.e. no roll is present. The perceived image is expressed in the eye-coordinate system as the two sets of unity vectors $\underline{u}_{g_j} \equiv \{u_{x_g}, u_{y_g}, u_{z_g}\}_j$, $j = 1,....,N_g$ and $\underline{u}_{a_k} \equiv \{u_{x_a}, u_{y_a}, u_{z_a}\}_k$, $k = 1,...,N_a$, coinciding with the lines-of-sight to each one of the object coordinates (LOS vectors). For simplicity the objects are presented by a wire-frame, i.e. hidden lines are not removed and it is assumed that the correspondence problem is solved, i.e. each line-of-sight is unambiguously associated with its corresponding object coordinate. The position of the origin of the object systems g and a in the i system, is given by the displacement vectors $\underline{d}_{g \to i} \equiv \{d_x, d_y, d_z\}_{g \to i}$ and $\underline{d}_{a \to i} \equiv \{d_x, d_y, d_z\}_{a \to i}$, respectively, and their angular orientation by the 3×3 direction cosine matrices $E_{g \to i}(\underline{\Omega}_g)$ and $E_{a \to i}(\underline{\Omega}_a)$ where $\underline{\Omega}_g \equiv \{\psi_g, \theta_g, \phi_g\}$ and $\underline{\Omega}_a \equiv \{\psi_a, \theta_a, \phi_a\}$ are the yaw,

63

pitch and roll Euler angles associated with the rotation from systems g and a to system i. Likewise, the position of the e system in the i system is given by $\underline{d}_{e \to i} \equiv \{d_x, d_y, d_z\}_{e \to i}$ and the angular orientation by $E_{e \to i}(\underline{\Omega}_e)$. The coordinates of the viewing location P can also be expressed in terms of the azimuth angle Ψ_0, elevation angle Θ_0 and range R_0 where:

$$\Psi_0 = \tan^{-1}\{d_y / d_x\}_{e \to i} \tag{2a}$$

$$\Theta_0 = -\sin^{-1}\{d_z / \sqrt{d_x{}^2 + d_y{}^2 + d_z{}^2}\}_{e \to i} \tag{2b}$$

$$R_0 = \{\sqrt{d_x{}^2 + d_y{}^2 + d_z{}^2}\}_{e \to i} \tag{2c}$$

Generally both the displacements and angular orientations of the object systems and eye system are unknown and are to be estimated by the observer. However, in this case, for simplicity, the groundgrid is placed such that the g system coincide with the i system, i.e. $\underline{d}_{g \to i} = \underline{0}$ and $E_{g \to i} = I$ (Identity matrix). The n dimensional vector of unknown parameters to be estimated by the observer is then given by:

$$\underline{\chi}^T = row\, [\underline{d}_{e \to i}, \underline{\Omega}_e, \underline{c}_g, \underline{d}_{a \to i}, \underline{\Omega}_a, \underline{c}_a] \tag{3}$$

where T denotes the transpose. For given $\underline{\chi}$ the j-th coordinate of object g and k-th coordinate of object a are successively transformed in the i and the e system according to:

$$\underline{x}_{g\,j}^i = \underline{x}^g(\underline{c}_g)_j \tag{4}$$

$$\underline{x}_{a\,k}^i = [E_{a \to i}(\underline{\Omega}_a)]\,\underline{x}^a(\underline{c}_a)_k + \underline{d}_{a \to i} \tag{5}$$

and

$$\underline{x}_{g\,j}^e = E_{e \to i}(\underline{\Omega}_e)^T\,[\underline{x}_{g\,j}^i - \underline{d}_{e \to i}] \tag{6}$$

$$\underline{x}_{a\,k}^e = E_{e \to i}(\underline{\Omega}_e)^T\,[\underline{x}_{a\,k}^i - \underline{d}_{e \to i}] \tag{7}$$

The matching situation in the $x^e\,oy^e$ horizontal plane is shown in Fig. 3. The objective is to find the unknown parameter vector $\underline{\chi}$ which yields eye-system transformed object coordinates (Eqs. 6 and 7) which "best match" the noisy perceived lines-of-sight. Ideally, all transformed object coordinates are located on their corresponding lines-of-sight, indicating that the reference objects are fully matched to the lines-of-sight. However, inaccuracies and errors in the perception of the lines-of-sight and the memorization of the familiar characteristics will cause deviations. For the j-th coordinate of object g the deviation of $\underline{x}_{g\,j}^e$ from $\underline{u}_{g\,j}$ is given by the j-th error vector $\underline{\epsilon}_{g\,j}$, obtained by subtracting $\underline{x}_{g\,j}^e$ from its projection on the corresponding LOS (see Fig. 3):

$$\underline{\epsilon}_{g_j} = \underline{u}_{g_j} \left[\underline{u}_{g_j}{}^T \underline{x}_{g_j}^e \right] - \underline{x}_{g_j}^e \tag{8}$$

or written shortly as:

$$\underline{\epsilon}_{g_j} = A_j \, \underline{x}_{g_j}^e \tag{9}$$

where:

$$A_j \equiv \left[\underline{u}_{g_j} \underline{u}_{g_j}{}^T - I \right] \tag{10}$$

The k-th error vector of object a, $\underline{\epsilon}_{a_k}$ is also obtained from Eqs. (9) and (10) by replacing the subscript g by a and j by k. Combing Eqs. (1a,b), (4-7), (9) and (10) yields:

$$\underline{\epsilon}_{g_j} = A_j \, E_{e \rightarrow i}(\Omega_e)^T \left[F_j + G_j \underline{c}_g - \underline{d}_{e \rightarrow i} \right] \tag{11}$$

$$\underline{\epsilon}_{a_k} = A_k \, E_{e \rightarrow i}(\Omega_e)^T \left[E_{a \rightarrow i}(\Omega_a) \{ F_k + G_k \underline{c}_a \} + \underline{d}_{a \rightarrow i} - \underline{d}_{e \rightarrow i} \right] \tag{12}$$

Eqs. (11) and (12) show that ϵ_{a_j} and ϵ_{g_k} are functions of the elements of the unknown parameter vector $\underline{\chi}$ and the matrices A_j and A_k, which incorporate the LOS vector observations. The matching problem can then be formulated as follows. Find the parameter vector $\underline{\chi}^*$ which minimizes the score:

$$J(\underline{\chi}) = J_1(\underline{\chi}) + J_2(\underline{\chi}) + J_3(\underline{\chi}) \tag{13}$$

where:

$$J_1(\underline{\chi}) = \frac{1}{2} \sum_{j=1}^{N_g} (\underline{\epsilon}_{g_j})^T \underline{\epsilon}_{g_j} \tag{14}$$

$$J_2(\underline{\chi}) = \frac{1}{2} \sum_{k=1}^{N_a} (\underline{\epsilon}_{a_k})^T \underline{\epsilon}_{a_k} \tag{15}$$

$$J_3(\underline{\chi}) = \frac{1}{2} \underline{\delta}^T R \underline{\delta} \tag{16}$$

where $\underline{\delta}$ is a linear combination of $\underline{\chi}$ according to:

$$\underline{\delta} = P + Q \underline{\chi} \tag{17}$$

The terms J_1 and J_2 are the dismatch scores of objects g and a, respectively. The term J_3 introduces a cost on a linear combination of $\underline{\chi}$ and expresses that the observer has the a priori knowledge that the unknown parameter vector $\underline{\chi}$ has to satisfy certain constraints, e.g. the object being in a certain position or angular orientation. In the case under investigation the base of the trapezoid is to be

located in the groundplane and the azimuth plane is to be perpendicular to the groundplane, i.e. $\underline{d}_{a \to i} = \underline{0}$ and θ_a and ϕ_a are zero. A Newton-Raphson scheme is chosen to solve this non-linear optimization problem. A detailed discription of the algorithm, is given in the Appendix.

Parametric Study

The objects used in this study were dimensioned in accordance with an ongoing real-world scene experiment, in which the azimuth angle was judged, between two model cubes positioned on a parking lot, viewed from the top of a four-story building. Accordingly, the groundgrid was of dimensions 5×5 meters, the height of the cubes above the groundgrid was 3.6 meters, the width of the cubes was 0.95 meters, and the distance from viewpoint to reference cube 28.24 meters. The target cube was positioned on a circle with a radius of 6 meters, centered about the reference cube. The azimuth angle between target and reference cube was measured in clockwise direction, with respect to the x^i axis. For convenience the x^i axis is considered pointed towards the north and the y^i axis towards the east.

The effect of the following parameters was investigated: (1) a zoom factor (f_z) for increasing or decreasing the relative size of the image, (2) the azimuth angle of the viewing location Ψ_0, (3) the height of the cubes above the groundgrid, and (4) the magnitude of the LOS noise and shape noise.

1. The effect of the zoom factor (f_z).
Fig. 4a shows the effect of increasing $(f_z > 1)$ or decreasing $(f_z < 1)$ the relative size of the image on the azimuth error, defined as estimated azimuth minus true azimuth. The scene is viewed straight from behind, i.e. the azimuth angle of the viewing location is zero. Both $f_z = 2.5$ (telephoto) and $f_z = 0.4$ (wide-angle), yield errors which vary sinusoidally with the true azimuth angle. Zero errors are obtained at 0, ±90 and ±180 deg azimuth, i.e. in the main direction $(x^i$ axis$)$ and perpendicular direction $(y^i$ axis$)$ of the grid, and maximum errors at about ±45 and ±135 deg azimuth. However, at +45 deg, $f_z = 2.5$ yields an overestimated and $f_z = 0.4$ an underestimated azimuth angle. Therefore, $f_z > 1.0$ produces a bias in the angle towards the y^i axis (east-west) and $f_z < 1.0$ towards the x^i axis (north-south). These results confirm the ones obtained previously by McGreevy and Ellis [5].

2. The effect of the azimuth angle of the viewing location Ψ_0.
The case for which $\Psi_0 = +15$ and $\Psi_0 = +30$ deg is shown in Fig. 4b. It is seen from the markedly reduced amplitude of the periodic curve, that viewing from aside reduces the bias produced by the zoom factor. It is also noticed that the curves shifted somewhat to the left, indicating that the zero errors are no longer occuring in the main and perpendicular grid directions.

3. The effect of the height of the cubes above the ground.
The dashed line in Fig. 4c represents the case in which the height above the ground is reduced to 0.1 meters. Since the shape of the trapezoid is no longer

useful, larger maximum errors than for height 3.6 meters are observed.

4. LOS and shape noise.

Each datapoint on the graphs of Figs. 5a,b show the standard deviation (SD) of the estimation errors of a set of 20 Monte-Carlo trials, where in each trial randomly oriented noise vectors were added to the lines-of-sight (LOS noise) or to the coordinates of the stored object (shape noise). The averages of the sets were found to be zero. Maximum values of the SD were found at ±90 deg azimuth, i.e. in y^i axis (east-west) direction and minimum errors at 0 and ±180 deg, i.e. x^i (north-south) direction.

Preliminary Experimental Tests

The images were generated with a Silicon Graphics, Inc. IRIS 2400 graphics terminal and presented on a raster scan color monitor. The image measured 28×28 centimeter and showed the groundgrid and cube formation of dimensions identical to the ones in the parametric study and parking lot experiment. At the right-hand side of the display two response dials were displayed, on which the pilot could adjust his estimates of the azimuth and elevation angle, by manipulating the buttons of the mouse. The pilot's eye was located at the center of projection of the image, which was 48 centimeter from the screen. Each experimental series contained 72 trials for viewing location $\Psi_0 = +22$ deg (left station) and 72 trials for $\Psi_0 = -22$ deg (right station). The true azimuth angle of the target with respect to the reference cube ψ_a was varied in steps of 5 deg, between -177 and +178 deg. The viewing location (left or right station) and ψ_a were picked randomly from the set. Although no time limit was set for the response to each trial, the response time was recorded. Four subjects participated in the experiment. Subject A performed 3 series and subjects C D and E two series each.

Fig. 6a shows the error in the azimuth angle estimate, (estimated minus true angle), averaged over all subjects, for the left and right station, respectively. For both stations the "sinusoidal" relationship between the error and the true azimuth angle, is clearly recognized. The errors are virtually zero in the main and perpendicular direction of the grid and the largest at ±45 and ±135 deg azimuth. Although the image is correctly viewed from the center of projection and no "virtual space" effect should occur, following McGreevy and Ellis [6,8], the systematic errors resemble the ones which would result from viewing the image through a telephoto lens, i.e. a bias exists in the azimuth angle estimate towards the y^i axis (east-west). The effect that viewing from aside has on the two-dimensional image is shown in principle in Fig. 6b. For the left station quadrants II and IV will appear to be "compressed" and quadrants I and III will appear to be expanded. For the right station quadrants I and III will appear to be compressed. Fig. 6a also shows that the maxima of the curve for the right station (dotted line) are markedly above the ones for the left station (solid line). This signifies that the bias in the azimuth estimate towards the east-west axis is stronger in the compressed quadrants than it is in the expanded ones. The dotted line in Fig.

6c shows the curve for the right station "mirrored" (both horizontal and vertical axis negated) and superimposed on the curve for the left station. Since the curves in Fig. 6c are nearly identical, the results for the left and right station can be considered as matching pairs, which are symmetrical with respect to the north-south axis.

Figs. 7a,b show the comparison between the analytical and experimental results. For the left station a "best match" is obtained for $f_z = 1.6$ and for the right station for $f_z = 1.85$. Fig. 7a shows that for the left station the analytical curve is somewhat above the experimental one, and for the right station somewhat below (Fig. 7b). A possible explanation for this disagreement might be that the processing is not entirely performed in three dimensions, as is suggested by the model, but that some processing takes place in the plane of the image as well. The experimental results show clear evidence of these image plane effects (2-D effects), i.e. the stronger bias towards the east-west axis in the compressed quadrants. However, the reason for this bias is presently being investigated. In general the 2-D effects can be modelled through the constraints on $\underline{\chi}$ by means of the term $J_3(\underline{\chi})$ of Eq. (16).

The standard deviation of the error, averaged over all subjects, was found to be at a minimal value of 3 deg for $\psi_a = 0$ and $\psi_a = 180$ deg and $\psi_a = \pm 90$ deg. However, the parametric study showed that at ± 90 deg azimuth the SD of the error resulting from LOS or shape noise, was at its maximum. Therefore, the variability found experimentally in the error, can not be attributed to LOS or shape noise only. This type of variability, having its minimum in grid axis directions, could results from a random component present in the fixed zoomfactor f_z.

Fig. 8 shows the response time, averaged over all subjects, as a function of the true azimuth angle, for the left and right station. Peak values for the response time appear at about ± 45 deg and ± 135 deg azimuth and the lowest values at about 0 and ± 90 deg. This shows that the direction judgement is the easiest in the main and perpendicular grid direction.

Summary

1. The analytical model is a useful tool in analysing and developing pictorial perspective displays with clearly outlined objects composed of a limited number of lines or polygons.

2. Fixed image scaling errors are responsible for the systematic errors in the estimates. Random variations in the image scaling, rather than LOS or shape noise, are expected to be responsible for the random variations in the estimation errors.

3. For a display, viewed correctly from the center of projection, systematic estimation errors will appear, resembling the errors which would result from viewing the true visual scene through a telephoto lens.

4. Therefore, in order to minimize systematic errors, the center of projection of the display should be somewhat in front of the eye position. i.e. the image should present a wider field-of-view than required by the correct viewing geometry. This confirms the results obtained earlier by McGreevy and Ellis [6,8].

5. Although the model reproduces the general trends of the experimental results, some unexplained differences are present. These differences provide evidence that part of the processing takes place in the plane of the image, rather than in three-dimensions, as suggested by the model. The differences are a subject of further study.

6. Judgement errors and response times are the smallest in the grid axis directions. Therefore the orthogonal groungrid is a useful element in perspective displays.

7. The presence of motion is expected to improve the estimates considerably and its incorporation in the model is a subject of further study.

References

1. Grunwald, A.J., "Tunnel Display for Four-Dimensional Fixed-Wing Aircraft Approaches," Journal of Guidance, Control, and Dynamics, Vol. 7, No. 3, May-June 1984, pp. 369-377.

2. Knox, C.E. and Leavitt, J., "Description of Path-in-the-Sky Contact Analog Piloting Display," NASA TM-74057, Oct. 1977.

3. Ellis, S.R., McGreevy, M.W. and Hitchcock, R.J., "Influence of a Perspective Cockpit Traffic Display Format on Pilot Avoidance Manoevers," AGARD Conference on Human Factors Considerations in High Performance Aircraft, Proceedings No. 371, May 1984.

4. Grunwald, A.J. and Negrin, M., "A Model for Human Spatial Orientation Using Familiar Object Cues," Proceedings of the 5-th Annual Conference on Human Decision Making and Manual Control, Berlin, W. Germany, June 1985.

5. McGreevy, M.W. and Ellis, S.R., "Direction Judgement Errors in Perspective Displays," 20-th Annual Conference on Manual Control, Ames Research Center, Moffet Field, Ca., June 12-14, 1984.

6. McGreevy, M.W., Ratzlaff, C.R. and Ellis, S.R., "Virtual Space and Two-Dimensional Effects in Perspective Displays," 21-st. Annual Conference on Manual Control, June 1985.

7. Farber, J. and Rosinski, R.R., "Geometric Transformations of Pictured Space," Perception, Vol. 7, 1978, pp. 269-282.

8. McGreevy, M.W. and Ellis, S.R., "The Effect of Perspective Geometry on Judged Direction in Spatial Information Instruments," Human Factors, In Press, 1986.

Appendix

A Newton-Raphson scheme has been chosen to compute the n-dimensional unknown parameter vector $\underline{\chi}$, which minimizes the score of Eq. (13). For the i-th iteration $\underline{\chi}_i$ is computed from $\underline{\chi}_{i-1}$ according to:

$$\underline{\chi}_i = \underline{\chi}_{i-1} - \left[\frac{\partial^2 J}{\partial \underline{\chi}^2}\right]^{-1}_{\underline{\chi}_{i-1}} \frac{\partial J}{\partial \underline{\chi}}\Bigg|_{\underline{\chi}_{i-1}} \tag{A.1}$$

The gradient vector is given by:

$$\frac{\partial J}{\partial \underline{\chi}}\Bigg|_{\underline{\chi}(i-1)} = \sum_{j=1}^{N_g} \underline{\epsilon}_{gj}^T \frac{\partial \underline{\epsilon}_{gj}}{\partial \underline{\chi}}\Bigg|_{\underline{\chi}_{i-1}} + \sum_{k=1}^{N_a} \underline{\epsilon}_{ak}^T \frac{\partial \underline{\epsilon}_{ak}}{\partial \underline{\chi}}\Bigg|_{\underline{\chi}_{i-1}} +$$

$$+ [P + Q\underline{\chi}_i]R \tag{A.2}$$

The $n \times n$ second derivative matrix is given by:

$$\frac{\partial^2 J}{\partial \underline{\chi}^2}\Bigg|_{\underline{\chi}_{i-1}} = \sum_{j=1}^{N_g} \frac{\partial \underline{\epsilon}_{gj}}{\partial \underline{\chi}}^T \frac{\partial \underline{\epsilon}_{gj}}{\partial \underline{\chi}}\Bigg|_{\underline{\chi}_{i-1}} + \sum_{k=1}^{N_a} \frac{\partial \underline{\epsilon}_{ak}}{\partial \underline{\chi}}^T \frac{\partial \underline{\epsilon}_{ak}}{\partial \underline{\chi}}\Bigg|_{\underline{\chi}_{i-1}} +$$

$$+ \sum_{j=1}^{N_g} \underline{\epsilon}_{gj}^T \frac{\partial^2 \underline{\epsilon}_{gj}}{\partial \underline{\chi}^2}\Bigg|_{\underline{\chi}_{i-1}} + \sum_{k=1}^{N_a} \underline{\epsilon}_{ak}^T \frac{\partial^2 \underline{\epsilon}_{ak}}{\partial \underline{\chi}^2}\Bigg|_{\underline{\chi}_{i-1}} + QR \tag{A.3}$$

The derivatives of $\underline{\epsilon}_{gj}$ and $\underline{\epsilon}_{ak}$ are:

$$\frac{\partial \underline{\epsilon}_{gj}}{\partial \underline{\chi}}\Bigg|_{\underline{\chi}_{i-1}} = \left[\frac{\partial \underline{\epsilon}_{gj}}{\partial \underline{d}_{e \to i}}, \frac{\partial \underline{\epsilon}_{gj}}{\partial \underline{\Omega}_e}, \frac{\partial \underline{\epsilon}_{gj}}{\partial \underline{c}_g}, \frac{\partial \underline{\epsilon}_{gj}}{\partial \underline{d}_{a \to i}}, \frac{\partial \underline{\epsilon}_{gj}}{\partial \underline{\Omega}_a}, \frac{\partial \underline{\epsilon}_{gj}}{\partial \underline{c}_a}\right]_{\underline{\chi}_{i-1}} \tag{A.4}$$

$$\frac{\partial \underline{\epsilon}_{ak}}{\partial \underline{\chi}}\Bigg|_{\underline{\chi}_{i-1}} = \left[\frac{\partial \underline{\epsilon}_{ak}}{\partial \underline{d}_{e \to i}}, \frac{\partial \underline{\epsilon}_{ak}}{\partial \underline{\Omega}_e}, \frac{\partial \underline{\epsilon}_{ak}}{\partial \underline{c}_g}, \frac{\partial \underline{\epsilon}_{ak}}{\partial \underline{d}_{a \to i}}, \frac{\partial \underline{\epsilon}_{ak}}{\partial \underline{\Omega}_a}, \frac{\partial \underline{\epsilon}_{ak}}{\partial \underline{c}_a}\right]_{\underline{\chi}_{i-1}} \tag{A.5}$$

where:

$$\frac{\partial \underline{\epsilon}_{g\,j}}{\partial \underline{d}_{e\to i}} = -A_j\, E_{e\to i}^{\ T}$$

(A.6)

$$\frac{\partial \underline{\epsilon}_{g\,j}}{\partial \underline{\Omega}_e} = A_j\, \frac{\partial E_{e\to i}^{\ T}}{\partial \underline{\Omega}_e}\left[F_j + G_j \underline{c}_g - \underline{d}_{e\to i}\right]$$

$$\frac{\partial \underline{\epsilon}_{g\,j}}{\partial \underline{c}_g} = A_j\, E_{e\to i}^{\ T}\, G_j$$

$$\frac{\partial \underline{\epsilon}_{g\,j}}{\partial \underline{d}_{a\to i}} = \underline{0}$$

$$\frac{\partial \underline{\epsilon}_{g\,j}}{\partial \underline{\Omega}_a} = \underline{0}$$

$$\frac{\partial \underline{\epsilon}_{g\,j}}{\partial \underline{c}_a} = \underline{0}$$

$$\frac{\partial \underline{\epsilon}_{a\,k}}{\partial \underline{d}_{e\to i}} = -A_k\, E_{e\to i}^{\ T}$$

$$\frac{\partial \underline{\epsilon}_{a\,k}}{\partial \underline{\Omega}_e} = A_k\, \frac{\partial E_{e\to i}^{\ T}}{\partial \underline{\Omega}_e}\left[E_{a\to i}\{F_k + G_k \underline{c}_a\} + \underline{d}_{a\to i} - \underline{d}_{e\to i}\right]$$

$$\frac{\partial \underline{\epsilon}_{a\,k}}{\partial \underline{c}_g} = \underline{0}$$

$$\frac{\partial \underline{\epsilon}_{a\,k}}{\partial \underline{d}_{a\to i}} = A_k\, E_{e\to i}^{\ T}$$

$$\frac{\partial \underline{\epsilon}_{a\,k}}{\partial \underline{\Omega}_a} = A_k\, E_{e\to i}^{\ T}\, \frac{\partial E_{a\to i}}{\partial \underline{\Omega}_a}\{F_k + G_k \underline{c}_a\}$$

$$\frac{\partial \underline{\epsilon}_{a\,k}}{\partial \underline{c}_a} = A_k\, E_{e\to i}^{\ T}\, E_{a\to i}\, G_k$$

The 3×3 direction cosine matrix for rotation from system e to i is given by:

$$E_{e\to i}(\psi,\theta,\phi) = \begin{bmatrix} c\,\theta\,c\,\psi & s\,\phi\,s\,\theta\,c\,\psi - c\,\phi\,s\,\psi & c\,\phi\,s\,\theta\,c\,\psi + s\,\phi\,s\,\psi \\ c\,\theta\,s\,\psi & s\,\phi\,s\,\theta\,s\,\psi + c\,\phi\,c\,\psi & c\,\phi\,s\,\theta\,s\,\psi - s\,\phi\,c\,\psi \\ -s\,\theta & s\,\phi\,c\,\theta & c\,\phi\,c\,\theta \end{bmatrix}$$

(A.7)

where c denotes cos and s denotes sin, and the subscript e is omitted from the Euler angles for clarity. The direction cosine matrix for rotation from system a to i is also given by Eq. (A.7) with the subscript e replaced by a. The 3×(3×3)

71

derivative of the direction cosine matrix is given by:

$$\frac{\partial E_{e \to i}}{\partial \underline{\Omega}}(\psi, \theta, \phi) = \left[\frac{\partial E_{e \to i}}{\partial \psi}; \quad \frac{\partial E_{e \to i}}{\partial \theta}; \quad \frac{\partial E_{e \to i}}{\partial \phi} \right] \tag{A.8}$$

where:

$$\frac{\partial E_{e \to i}}{\partial \psi} = \begin{bmatrix} -c\,\theta\,s\,\psi & -s\,\phi\,s\,\theta\,s\,\psi - c\,\phi\,c\,\psi & -c\,\phi\,s\,\theta\,s\,\psi + s\,\phi\,c\,\psi \\ c\,\theta\,c\,\psi & s\,\phi\,s\,\theta\,c\,\psi - c\,\phi\,s\,\psi & c\,\phi\,s\,\theta\,c\,\psi + s\,\phi\,s\,\psi \\ 0 & 0 & 0 \end{bmatrix} \tag{A.9}$$

$$\frac{\partial E_{e \to i}}{\partial \theta} = \begin{bmatrix} -s\,\theta\,c\,\psi & s\,\phi\,c\,\theta\,c\,\psi & c\,\phi\,c\,\theta\,c\,\psi \\ -s\,\theta\,s\,\psi & s\,\phi\,c\,\theta\,s\,\psi & c\,\phi\,c\,\theta\,s\,\psi \\ -c\,\theta & -s\,\phi\,s\,\theta & -c\,\phi\,s\,\theta \end{bmatrix} \tag{A.10}$$

$$\frac{\partial E_{e \to i}}{\partial \phi} = \begin{bmatrix} 0 & c\,\phi\,s\,\theta\,c\,\psi + s\,\phi\,s\,\psi & -s\,\phi\,s\,\theta\,c\,\psi + c\,\phi\,s\,\psi \\ 0 & c\,\phi\,s\,\theta\,s\,\psi - s\,\phi\,c\,\psi & -s\,\phi\,s\,\theta\,s\,\psi - c\,\phi\,c\,\psi \\ 0 & c\,\phi\,c\,\theta & -s\,\phi\,c\,\theta \end{bmatrix} \tag{A.11}$$

It should be noted that in the computation of the second derivative matrix of Eq.(A.3) the third and fourth terms on the right-hand side, carrying the second derivatives of $\underline{\epsilon}_g$ and $\underline{\epsilon}_a$, can be omitted. The computation of these terms is elaborate and their contribution to a faster convergence marginal. The iterative scheme of Eq. (A.1) is continued until the norm of the difference vector (second term on right-hand side of Eq. (A.1)) is sufficiently small. For the problem under investigation the dimensions of $\underline{c}_g$ and $\underline{c}_a$ were 4 and 3, respectively and thus $\underline{\chi}$ was of dimension $n = 19$. The scheme was found to converge to an absolute minimum from a wide range of initial dismatched settings of $\underline{\chi}$. Generally, between 6–12 iterations were required to reduce the norm of the difference vector to less than 10^{-14}.
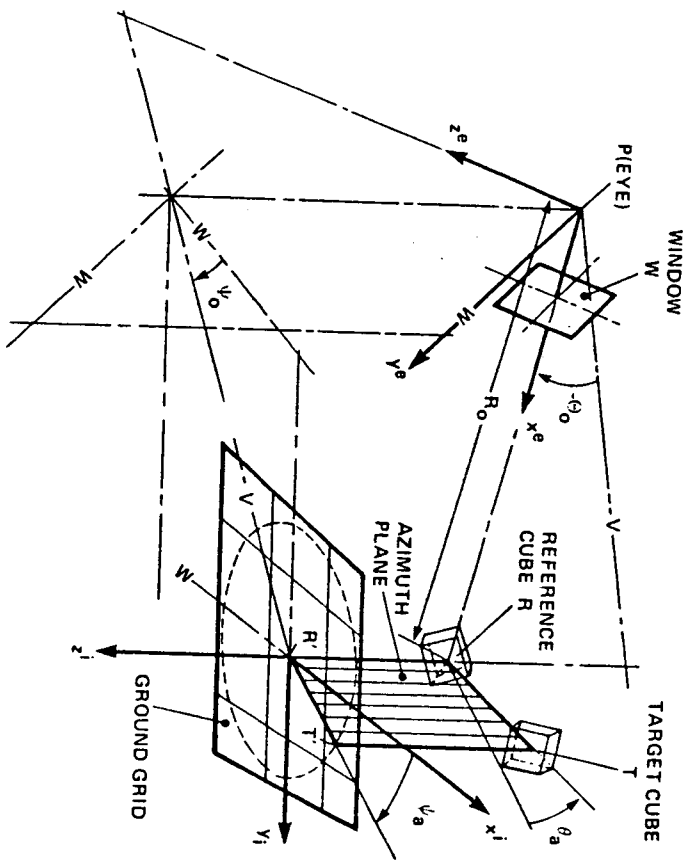
FIGURE 1a. : Spatial Viewing Situation
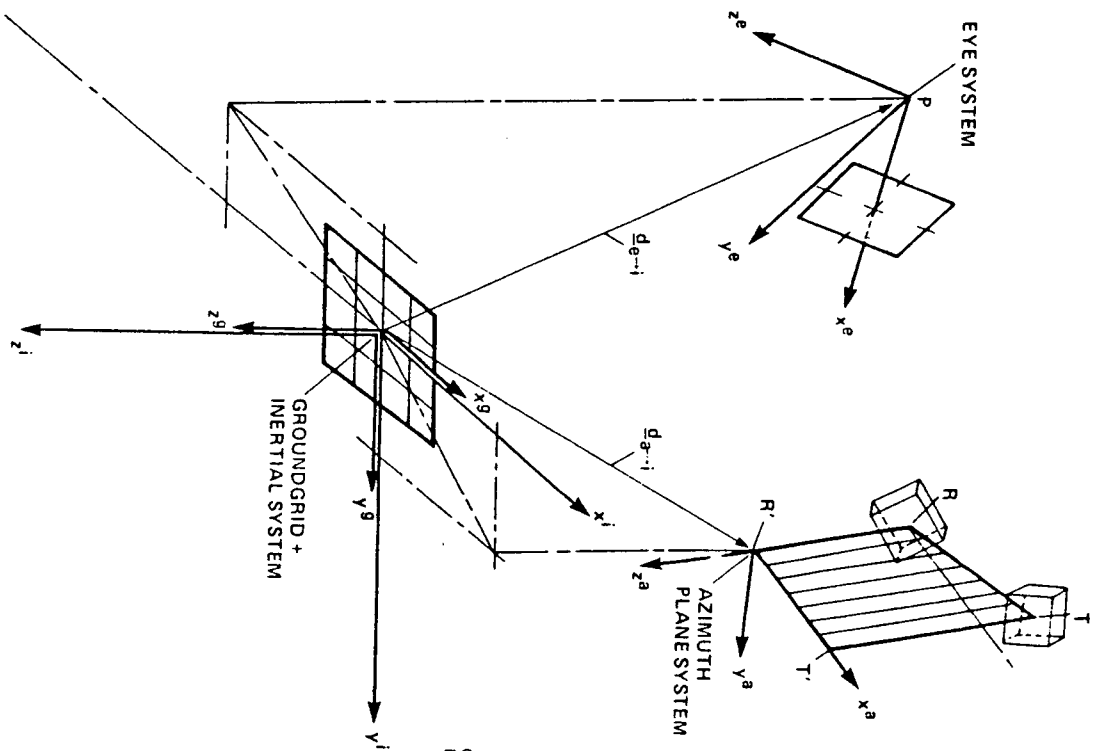
FIGURE 1b. : Coordinate Systems for Spatial Viewing Situation

73
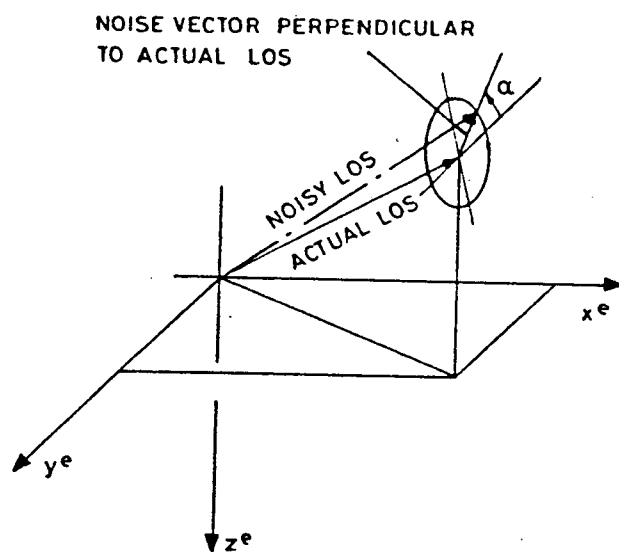
FIGURE 2a. : Line-of-Sight Noise
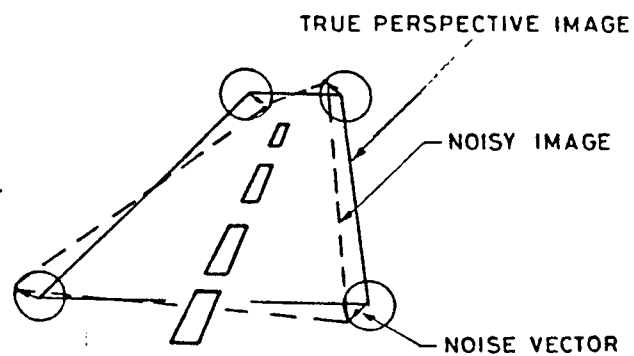
FIGURE 2b. : Line-of-Sight Noise Distorted Image
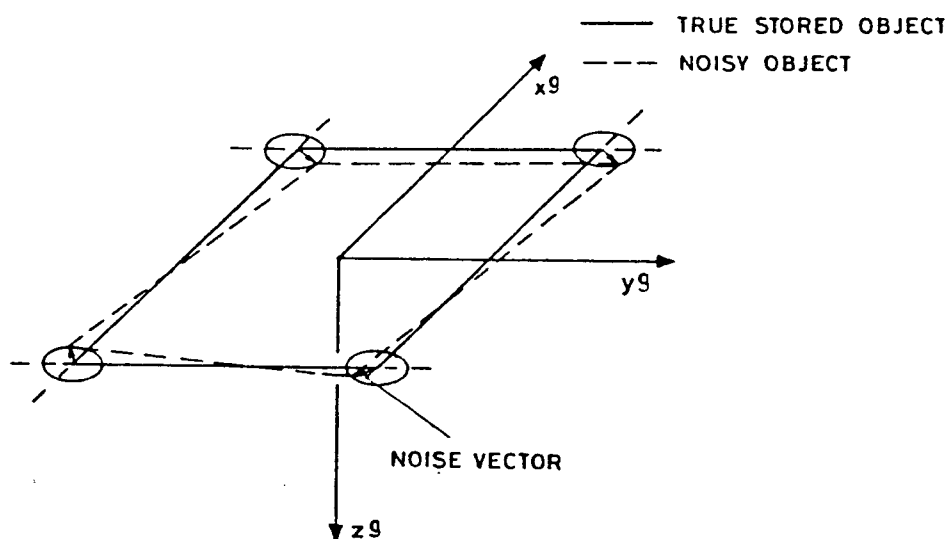
FIGURE 2c. : Shape Noise

74
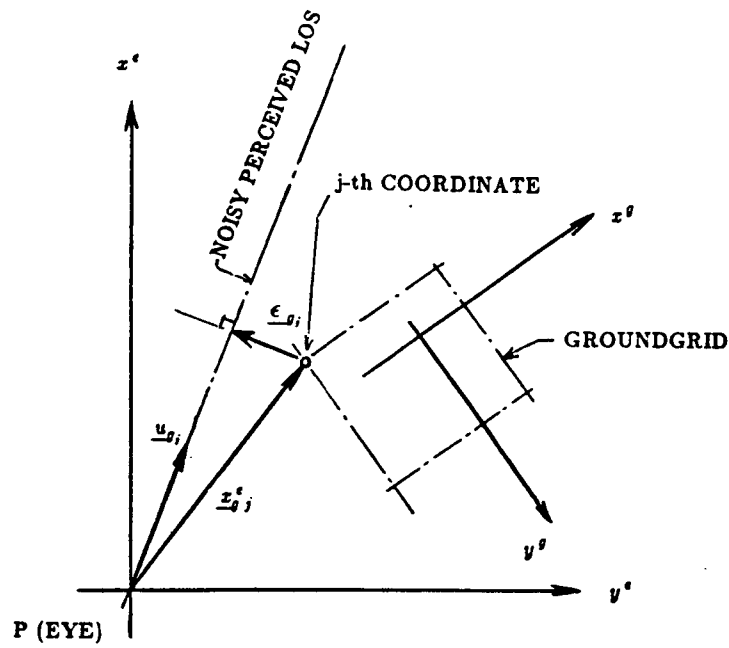
FIGURE 3. : Matching Situation in the $x^e \, oy^e$
Horizontal Plane
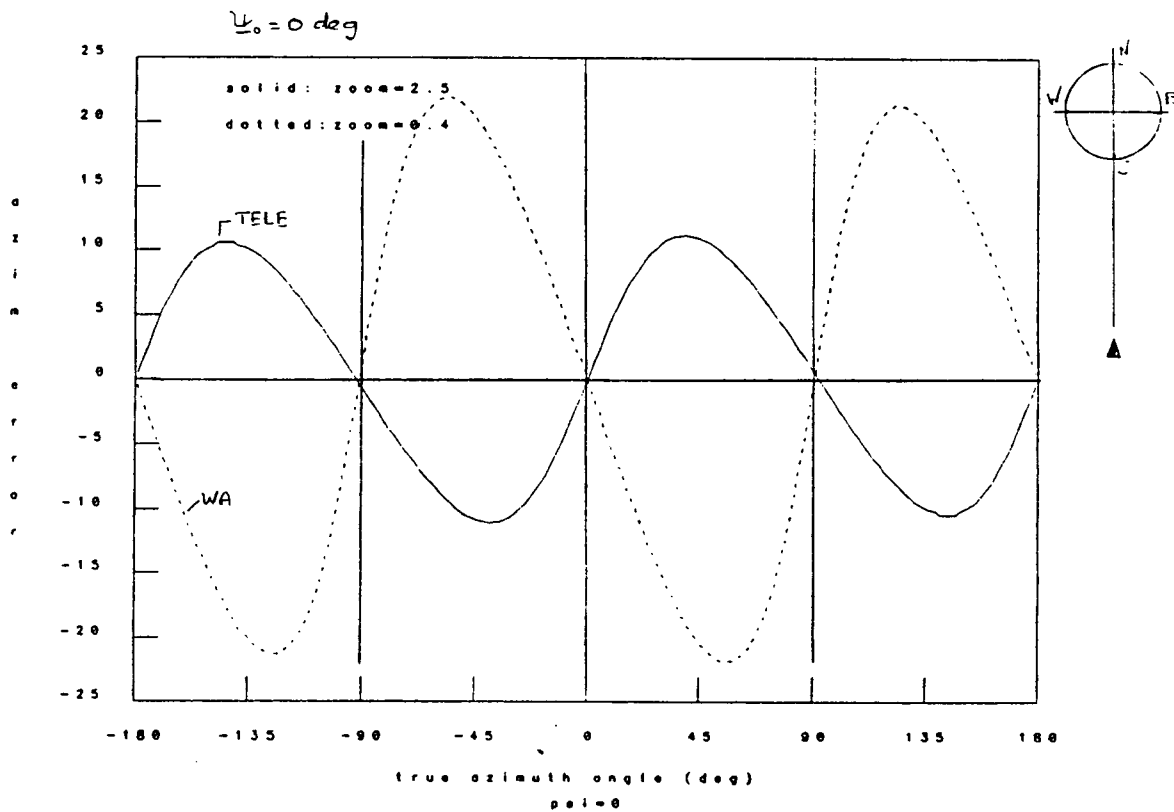
FIGURE 4a. : Azimuth Error as a Function of True Azimuth Angle;
$f_z = 2.5$ (Telephoto) and $f_z = 0.4$ (Wide-Angle)

75
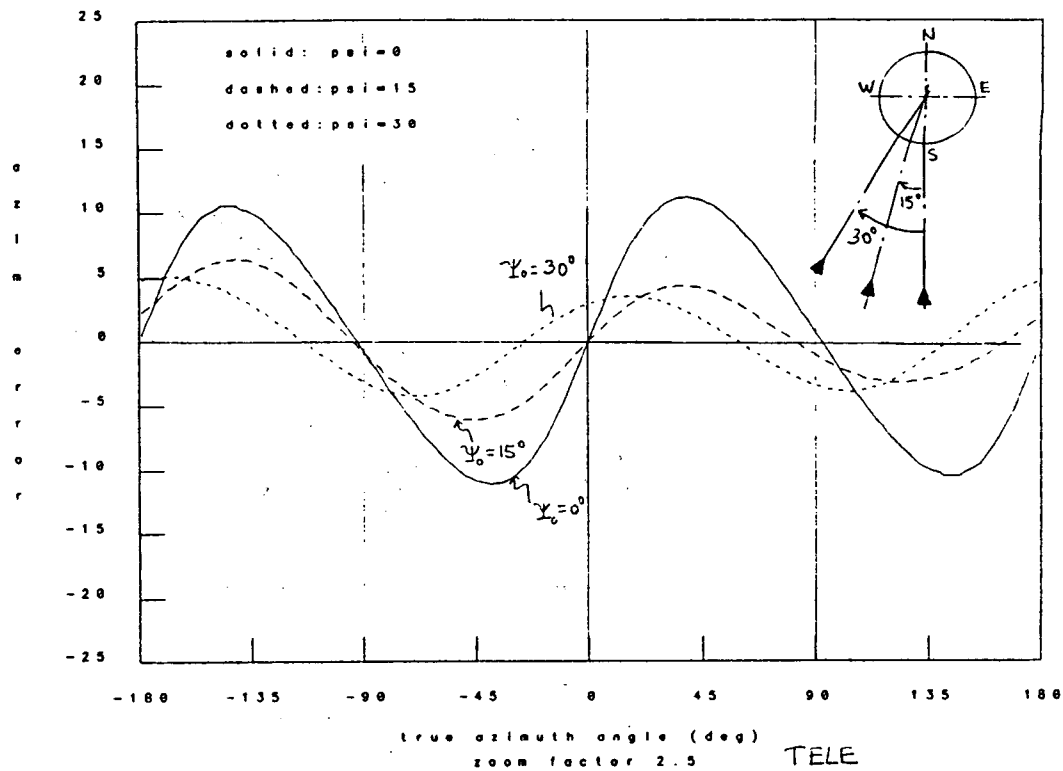
FIGURE 4b. : Azimuth Error as a Function of True Azimuth Angle;
The Effect of Ψ_0
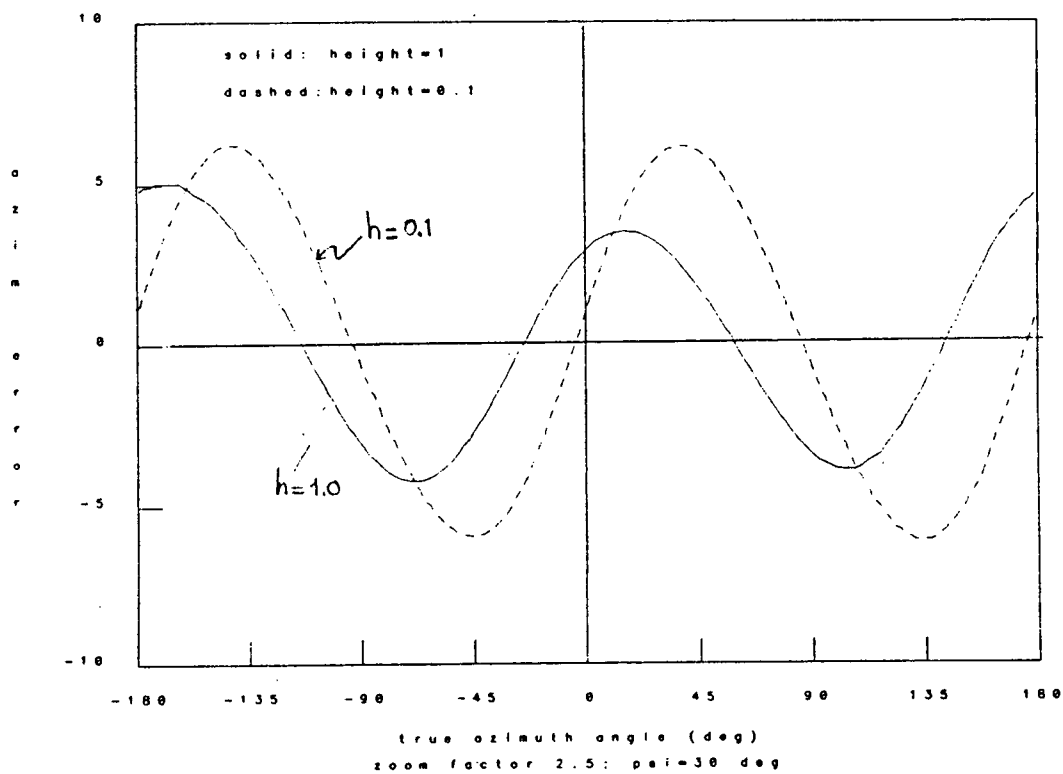
FIGURE 4c. : Azimuth Error as a Function of True Azimuth Angle;
The Effect of the Height of Object 2

76
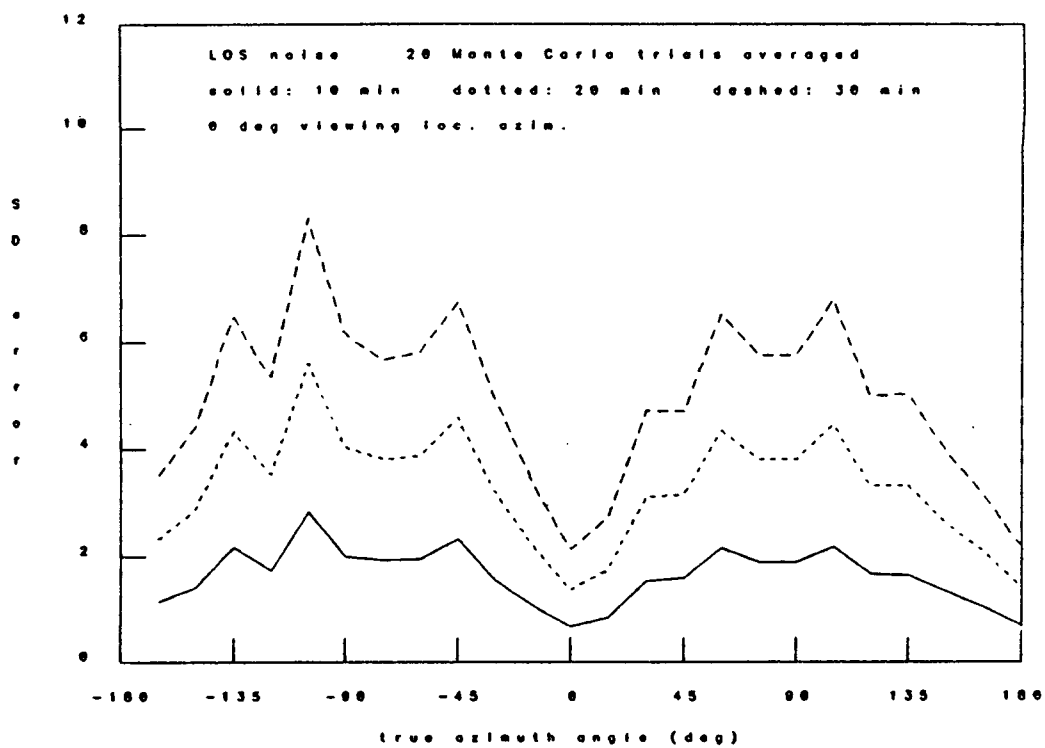
FIGURE 5a. : Standard Deviation of Azimuth Error as a Function
of True Azimuth Angle; LOS Noise
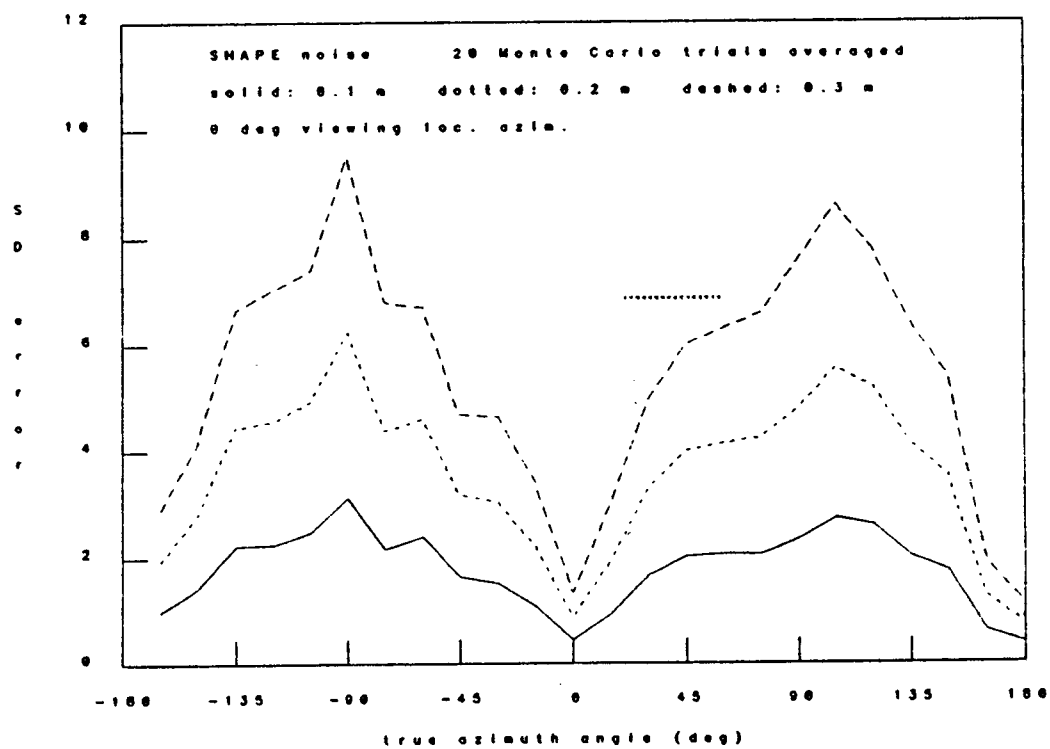
FIGURE 5b. : Standard Deviation of Azimuth Error as a Function
of True Azimuth Angle; Shape Noise

77
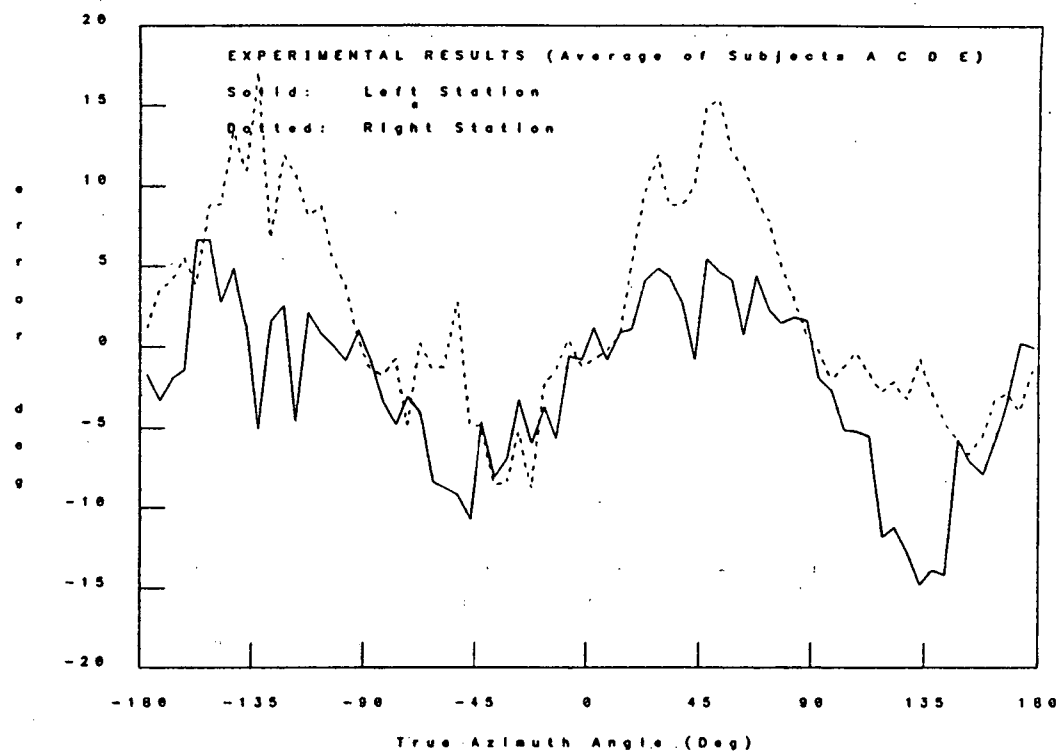
FIGURE 6a. : Experimental Results for Left and Right Station
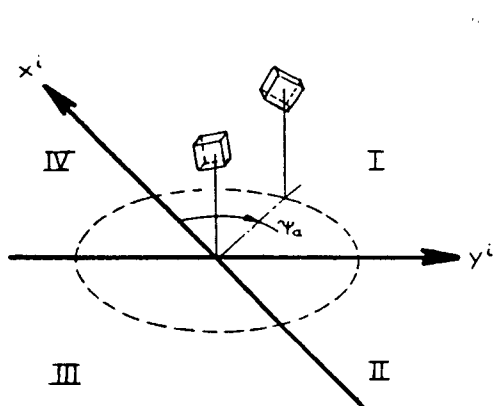
VIEW FROM LEFT STATION   VIEW FROM RIGHT STATION
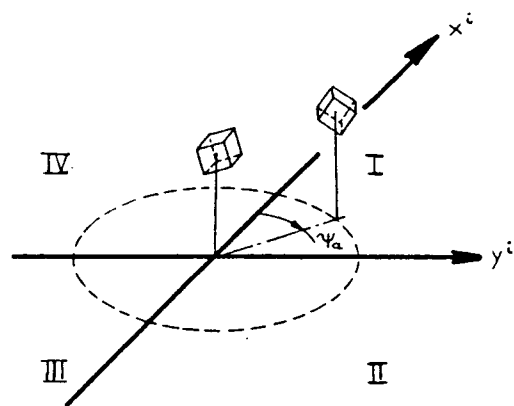
FIGURE 6b. : Effect of Viewing from Aside on Two-Dimensional Image
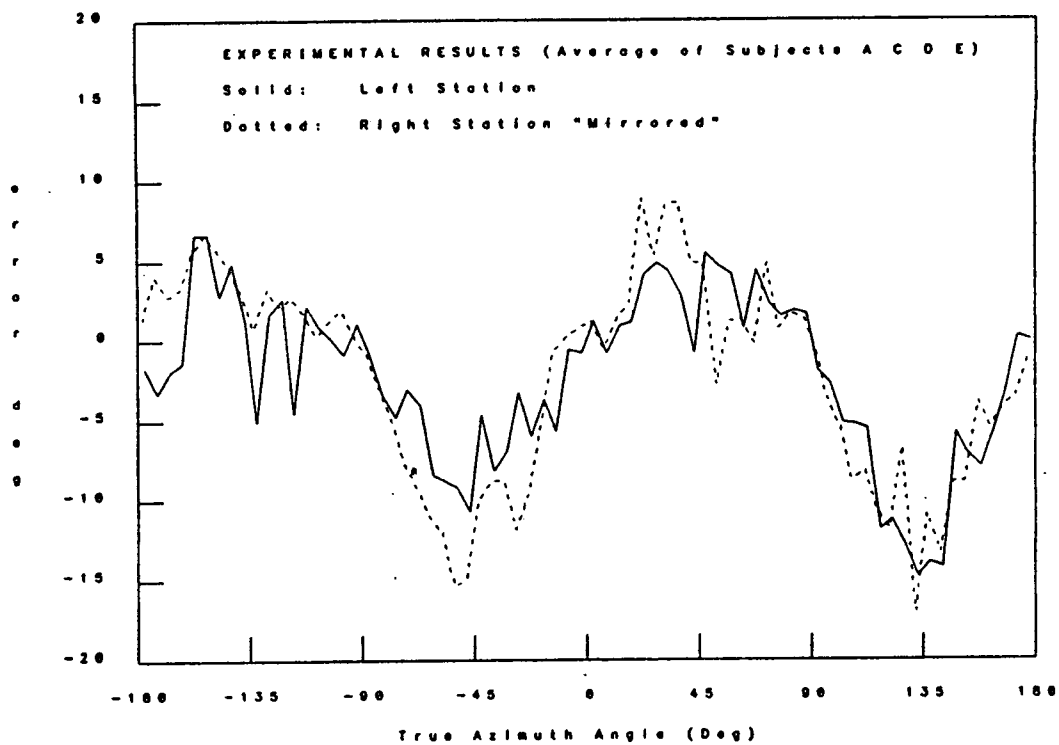
FIGURE 6c. : Experimental Results for Left Station and "Mirrored"
Results for Right Station
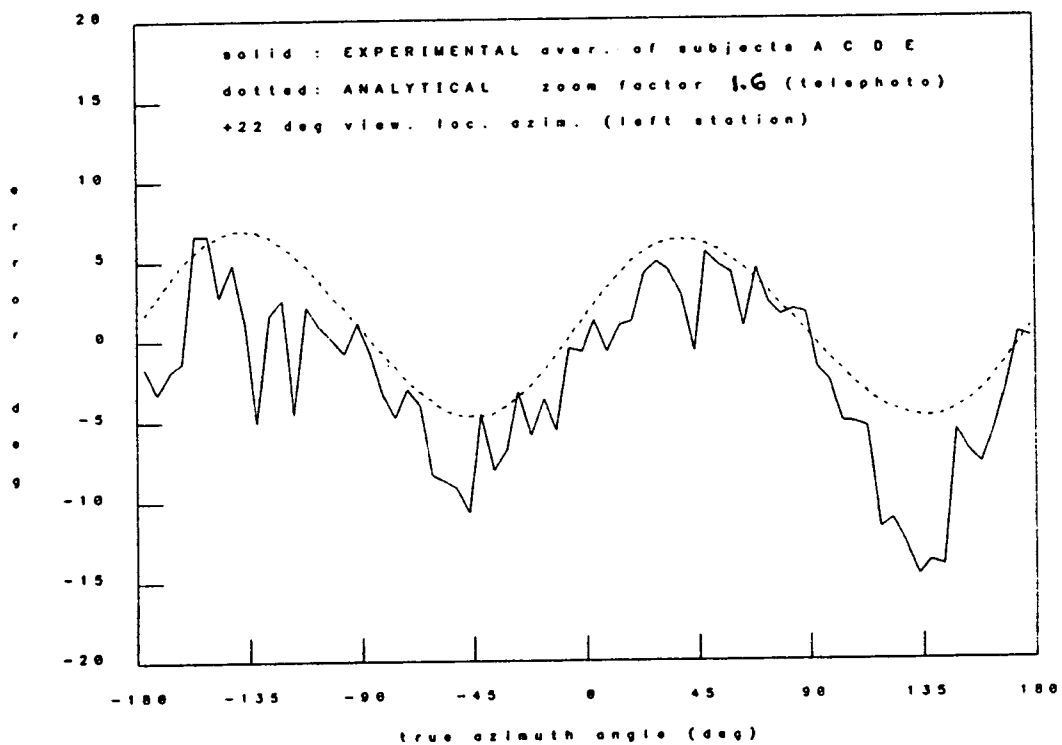
FIGURE 7a. : Experimental and Analytical Results for Left Station

79
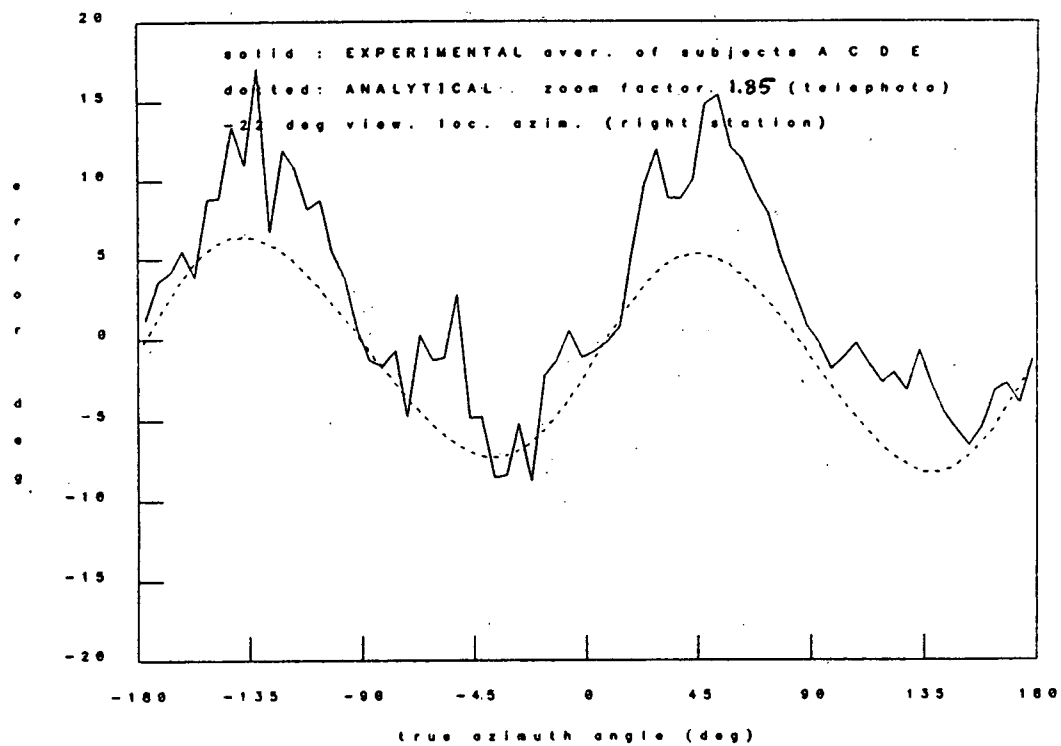
FIGURE 7b. : Experimental and Analytical Results for Right Station
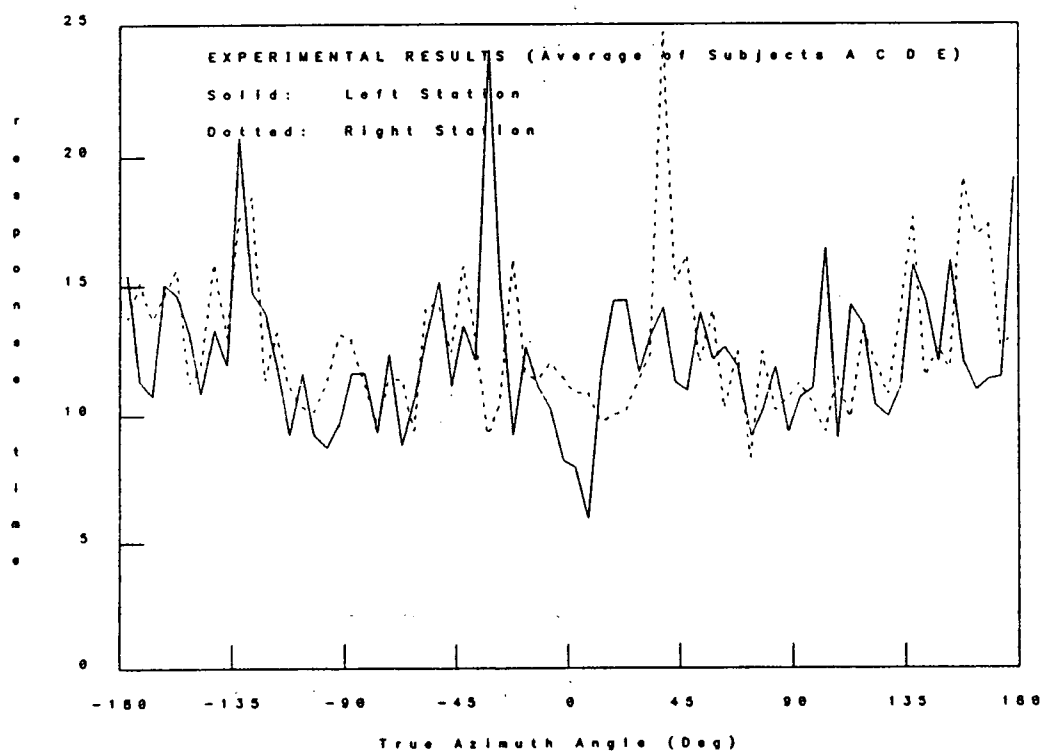
FIGURE 8. : Response Time as a Function of True Azimuth Angle

80

MODELLING THE PILOT'S USE OF FLIGHT SIMULATOR
VISUAL CUES IN A TERRAIN-FOLLOWING TASK

Greg L. Zacharias
Charles River Analytics Inc.
Cambridge, MA

Rik Warren
Armstrong Aerospace Medical Research Laboratory
Wright-Patterson AFB, OH

Gary E. Riccio
System Research Laboratories
Dayton, OH

An analytic pilot model was developed and exercised to integrate the results of a USAF AAMRL experimental program in flight simulator display research, and to account for the pilot's use of simulated visual cues in a terrain-following environment. The program effort was broken down into four basic tasks: 1) the specification of the flight task and experiment protocol; 2) the theoretical development of the analytic model; 3) the conduct of the experiment (by USAF); and 4) the model-based analysis of the resulting data. The flight task chosen was terrain-following flight, and the experiment focussed on the pilot's integration of linear perspective cues with texture flow cues. The pilot model included visual submodels of these two cueing mechanisms, and integrated them with the optimal control model (OCM) of the pilot, to account for overall display- driven closed-loop flight control behavior. Model-based analysis of the data served to integrate the results across a range of experimental conditions, and provide a unifying structure to account for the pilot's use of disparate visual cues in a realistic flight task. Specific findings were that linear cues alone and textural cues alone were adequate to support the task, but that the former provided for better terrain-following performance, when compared to the latter. Under combined cueing conditions, linear cueing dominated the display- driven response. Model-based analysis demonstrated an ability to closely match performance score and frequency response trends across all 12 conditions studied, with a minimal and consistent variation of model parameter values.

MODEL OF THE HUMAN CONTROLLER OF A DYNAMIC SYSTEM

P.h. Wewerinke[*]

D. ten Hove[**]

J. Perdok[**]

[*]
[**]   Twente Unviersity of Technology/MARIN, the Netherlands
Maritime Research Institute Netherlands (MARIN).

Contents

1. INTRODUCTION

In the last two decades considerable research effort has been devoted to the study of human involvement in dynamic systems. Especially human control behavior has been investigated but in the restricted sense of continuous regulating against random disturbances so as to minimize the system state deviation from a given reference state.

This paper presents a model of the human controller of a dynamic system involving not only regulating but also tracking a desired finite trajectory in some optimal sense. The first is characterized by short term, continuous, closed loop control. The latter concerns control behavior at a higher mental level involving planning (finite time, pre-programmed, open loop control) and decision making (to determine sequentially whether or not such a maneuver has to be initiated and/or stopped).

In this study it is assumed that the Human Operator (HO) derives information about the system from instruments and/or the outside world. This pictorial information provides the HO (directly or via a TV-camera/monitor system) with visual cues related to the present system state and the present and future desired system state.

The model describes both this complex visual information process (including an optimal visual scanning strategy) and the control and decision making behavior in terms (commensurate with those used for the task and system described in chapter 2) of stochastic optimal estimation, control and decision theory. It provides an integrated framework of the important and inter-related aspects of the afore-mentioned human control task. This is the subject of chapter 3.

Measures for system performance and control workload are indispensable for the evaluation of man-machine systems. This is contained in chapter 4.

The main conclusions are summarized in chapter 5.

It is anticipated that the model will be useful to investigate a variety of man-machine systems (nonlinear systems are represented by linearized

time-varying systems) e.g. in the increasingly important area of robo-
tics and in the handling of ships.

2. TASK ENVIRONMENT

The various aspects of the task which the HO has to fulfil are: the
dynamic system to be controlled, the environment in which the task has
to be performed, and the specifics of the task.

2.1 Dynamic System

A nonlinear, time-varying dynamic system can be represented by

$$X(k) = f(X(k-1),U(k-1),W(k-1),k) \qquad (1a)$$

$$Y(k) = f(X(k),U(k),k) \qquad (1b)$$

where $X(k)$ is the n-dimensional state vector at time k, f is the n-
dimensional vector function, U is the k-dimensional control vector, W is
the ℓ-dimensional disturbance vector, Y is the m-dimensional system
output vector and g is the m-dimensional vector function.

The standard procedure is followed to describe the nonlinear system
behavior (X) in terms of a state reference (X_0) and "small" pertur-
bations (x) around this reference; thus $X = X_0 + x$, $U = U_0 + u$, etc.
This linearization scheme yields a time-varying reference model and a
time-varying linear system description.

$$X_0(k) = f(X_0(k-1),U_0(k-1),W_0(k-1),k) \qquad (2a)$$

$$Y_0(k) = g((X_0(k),U_0(k),k) \qquad (2b)$$

and

$$x(k) = \Phi x(k-1) + \Psi u(k-1) + \Gamma w(k-1) \qquad (3a)$$

$$y(k) = Hx(k) \qquad (3b)$$

where $\Phi = \Phi(k,k-1) = \frac{\partial f}{\partial X}(X_0(k),U_0(k),W_0(k))$, being the Jacobian matrix of

f, is the state transition matrix,

$\Psi = \Psi(k,k-1) = \frac{\partial f}{\partial U}(X_0(k),U_0(k),W_0(k))$ is the control transition matrix,

$\Gamma = \Gamma(k,k-1) = \frac{\partial f}{\partial W}(X_0(k),U_0(k),W_0(k))$ is the disturbance transition matrix, $H = H(k) = \frac{\partial g}{\partial X}(X_0(k),U_0(k))$ is the measurement matrix and w is assumed to be a zero mean gaussian purely random sequence with covariance W.

This linearization scheme holds for relatively small x,u and w, which dictates the update rate of the reference and therefore of the foregoing Jacobian matrices.

2.2 Environment

It is assumed that the HO derives information about the system from instruments and the outside world. The latter provides information not only about the present state but also about the future desired state. This is shown in figure 1. The basic assumption is that the HO "knows" the nominal (or desired) visual scene, implying that the HO can observe deviations (x) from the desired state (x_d). Furthermore it is assumed that only one future (or forward*) point "at the time" is observed (corresponding with N steps ahead), implying that peripheral viewing is neglected, but the look distance ahead may be considered as a variable. The result is that visual cues can be observed which are (linearly, according eqs.(2b) and (3b)) related to the difference between the present state and the present desired state (which is assumed to be equal to the present reference) and the difference between the present state and one future desired state. Thus

$$y(k) = Hx(k) \tag{4a}$$

and $$y_0(k) = H_0[x(k)-x_d(k+N)] \tag{4b}$$

or $$y_1(k) = H_1x(k) + H_dx_d(k+N) \tag{4c}$$

---

* time- and distance ahead is uniquely related for a given constant (nominal) forward velocity.

with $\quad y_1 = \begin{bmatrix} y \\ \overline{y_0} \end{bmatrix}; \quad H_1 = \begin{bmatrix} H \\ \overline{H_0} \end{bmatrix}; \quad H_d = \begin{bmatrix} 0 \\ \overline{-H_0} \end{bmatrix}.$

2.3 Control task

The task considered is to achieve a desired trajectory (tracking task) in some optimal sense, i.e., controlling the state x over some fixed interval of time [0,N] by realizing a control sequence $\{u(k), k=0,1,\ldots,N-1\}$ which minimizes the performance measure

$$J_N(u) = E\left\{ \sum_{i=1}^{N} (x(i)-x_d(i))'Q_x(i)(x(i)-x_d(i)) \right.$$
$$\left. + u'(i-1)Q_u(i-1)u(i-1) \right\} \qquad (5)$$

In order to include $\dot{u}$-terms in eq.(5) define $x_e = \begin{bmatrix} x \\ u \end{bmatrix}$, $u_e = \dot{u}$ and eq. (5) is obtained with $x \rightarrow x_e$, $u \rightarrow u_e$, $Q_x \rightarrow Q_{xu} = \begin{bmatrix} Q_x & 0 \\ 0 & Q_u \end{bmatrix}$ and $Q_u \rightarrow Q_{\dot{u}}$.

In case x_d is given this optimal control problem is known (e.g. given in reference 3). In our case, however, x_d has to be derived (estimated) from the perceived visual cues. This is treated in the next section.

3. HUMAN CONTROL MODEL

The model of the human operator (HO) comprises various functional aspects which are shown in the block diagram of figure 2 and discussed in the following sections.

3.1 Perception and state estimation

It is assumed that the HO perceives the system outputs with a certain inaccuracy

$$y_p(k) = y(k) + v(k) \qquad (6)$$

with v(k) a linear independent, gaussian, purely random observation noise sequence with covariances (Ref.4)

$$V_j(k) = \frac{P_0 E\{y_j^2(k)\}}{\delta_j K(a_j, \sigma_{y_j})} \qquad (7)$$

with

P_0 the "full attention" noise ratio, $\delta_j\{0,1\}$ represents the look sequence (periphical viewing neglected), K the describing function gain (statistical representation of a threshold a_j for a given signal level σ_{y_j})

It is assumed that the HO utilizes the (learned) system dynamics and the observed information to estimate the state of the system. This estimation process (internal model of the system) can be described by

$$\hat{x}(k) = \Phi\hat{x}(k-1) + \Psi u(k-1) + Kn_1(k) \qquad (8a)$$

with

$$n(k) = y_p(k) - H\Phi\hat{x}(k-1) \qquad (8b)$$

and

$K(k) = P(k-)H'N^{-1}(k)$, $P(k-)$ is the estimation error covariance before the observation at time k is made and N is the covariance of the innovation sequence n.

This, and the following submodels are summarized in figure 3.

3.2 Continuous regulating

One part of the control task is to regulate against random disturbances. The optimal control is the standard solution of the LQG control problem (this amounts to the minimization of eq.(5) with $x_d = 0$), presented (e.g.) in reference 1.

The resulting (possibly time-varying) control gains are operating on the estimated state (see Appendix A). The resulting control is given by

$$u_1(k) = S(k)\hat{x}(k)$$ (9)

This part of the model is in the literature known as the optimal control model (Ref. 5). It has been a basic framework for many theoretical and experimental studies (e.g. Refs.6 and 7).

3.3 Intermittent maneuvering

Control behavior pertaining to some fixed finite interval of time involves the decision to start this period and to stop. (e.g. the decision that the state reference is changing from a straight path to a given finite trajectory). This decision process (on the basis of the observed information) determines the intervals of making intermittent control maneuvers.

3.3.1. Sequential decision making.

It is assumed that the HO utilizes his innovation sequence to determine whether a systematic deviation of the zero-mean system sequence is apparent due to a change in the desired system reference trajectory). This systematic deviation results in a non-zero mean innovation sequence (Ref. 8).

For this purpose the HO generates a "local" sample mean according to

$$\tilde{n}_1(k) = \frac{1}{M} \sum_{i=k-M+1}^{k} n_1(i)$$ (10)

where M is the number of samples used from the past.

Combining this with eq.(8) (but now utilizing all observations y_1) yields

90

$$\tilde{\hat{x}}(k) = \Phi\tilde{\hat{x}}(k-1) + \Psi\tilde{u}(k-1) + K_1\tilde{n}_1(k) \tag{11a}$$

$$\tilde{n}_1(k) = H_1\tilde{x}(k) - H_1\Phi\tilde{\hat{x}}(k-1) + H_d\tilde{x}_d(k+N) + \tilde{v}_1(k) \tag{11b}$$

Assuming that $\tilde{x}(k)$, $\tilde{u}(k-1)$ and $\tilde{v}_1(k)$ are small, $\tilde{n}_1(k)$ can be used to "detect" $\tilde{x}_d(k+N)$ and to estimate $x_d(k)$ and to respond to this desired trajectory.

A uniformly most powerful test (generalized likelihood ratio test, see reference 9) can be performed using the recursive expression for the (log of the) likelihood ratio

$$L(k) = L(k-1) + \frac{M}{2}\tilde{n}_1'(k)N_1^{-1}(k)\tilde{n}_1(k) \tag{12}$$

and compare this ratio with a threshold T according to

$$L(k) \underset{D_0}{\overset{D_1}{\gtrless}} T \tag{13}$$

The decision threshold T can be related to the decision error probabilities P_F ("false alarm") and P_M ("miss") according to

$$T = \ln(1-P_M)/P_F \tag{14}$$

The ensemble average of eg. (11) is used (with $\overline{x} = \overline{u} = \overline{v}_1 = 0$) to detect the (next interval of the) trajectory (on the average in K steps) according to (combining eqs. (12)-(14))

$$\overline{K} \doteq \frac{-2 \ln P_F}{E\{\tilde{n}_1'N_1^{-1}\tilde{n}_1\}} \tag{15}$$

At this time the HO initiates a maneuver to deal with the "detected" trajectory (interval).

3.3.2 Open loop maneuvering

Given the quadratic cost functional of eg.(5) the HO makes an optimal maneuver to track the desired trajectory $x_d(i)$, $i = k,...,k+N$.

Based on the information $\tilde{x}_d(i)$ he generates a control $u_m(k)$ which can be conceived as a planned strategy to follow $x_d(i)$ and obtain $x_d(k+N)$. In system theoretical terms this amounts to backwards integration of the desired control response (from $k+N$ to k) and then generating (forward in time) $u_m(k)$ to track the desired trajectory $x_d(k)$.

The mathematical formulation and solution of this problem is standard when x_d is given. For the ease of reference this is summarized in appendix A.

However, in our case x_d is not known (to the HO) but has to be derived from the (noisy) observations y_{p_1}, utilizing $\bar{n}_1(k)$ from eq.(11).

The ensemble mean of $\bar{n}_1(k)$ is easily obtained from eq.(11) (with $\tilde{v}_1(k) = 0$).

$$\bar{n}_1(k) = H_d \tilde{x}_d(k+N) + H_1 \bar{p}(k-)$$ (16)

where $p(k-)$ is the estimation error at time k before the observation at time k is included.

The accuracy with which this mean value (and thus $\tilde{x}_d(k+N)$ as $\bar{p}(k-)$ is generally much smaller than $\tilde{x}_d(k+N)$ is known is given by the ensemble covariance of $\bar{n}(k)$

$$\text{cov}(\bar{n}_1(k)) = E\{(\bar{n}_1(k)-\bar{n}_1(k))(\bar{n}_1(k)-\bar{n}_1(k))'\}.$$

The result is obtained from eqs.(11b) and (16), using the fact that $\tilde{n}_1 - \bar{n}_1$ is a white noise sequence.

$$\text{cov}(\bar{n}_1(k)) = \tilde{N}_1(k)/M \doteq N_1(k)/M$$ (17a)

where

$$N_1(k) = H_1 P(k-)H_1' + V_1(k) \qquad (17b)$$

From eqs.(16) and (17) the effect of M (number of past data) can be appreciated. A "large" value of M implies a "certain" estimate $(\bar{x}_d)$ of x_d ($cov(\tilde{n}_1)$ small) but with a relatively large difference between x_d and $\bar{x}_d$ (depending on the x_d sequence), and vice versa.

Now the foregoing results can be combined with the maneuver sequence derived in appendix A and given by

$$u_m(k) = A(k)u_m(k+1) + B(k)x_d(k) \qquad (18a)$$

where

$$A(k) = Q_u^{-1}(k)\Psi'S(k)Q_u(k) \qquad (18b)$$

and

$$B(k) = Q_u^{-1}(k)\Psi^{-1}Q_x(k) \qquad (18c)$$

with $k = k_0,\ldots,k_0+N$
and k_0 the detection time.

Eq.(18a) must be solved recursively from the final condition

$$u_m(k_0+N) = -B(k_0+N)x_d(k_0+N) \qquad (18d)$$

Thus replacing $x_d(k)$ by $\tilde{n}_1(k-N)$ yields for the maneuver sequence (from eqs.(11 and (18a)).

$$u_m(k) = A(k)u_m(k+1) + B^*(k)\tilde{n}_1(k-N) \qquad (19)$$

with

$$B^*(k) = B(k)(H_d'H_d)^{-1}H_d' \qquad (20)$$

After the maneuver (at time k_0+N) the system reference and the small perturbation model are updated according to

$$X_1(k_0+N) = X_{1-1}(k_0+N) + \hat{x}(k_0+N) \qquad (21a)$$

$$\Phi_1 = \frac{\partial f}{\partial X}(X_1, U_1), \text{ etc.} \qquad (21b)$$

In addition, the decision is made whether another (part of a) maneuver has to be executed or only regulating is required.

3.4 Visual scanning

Visual scanning is assumed to be governed by the strategy of the HO to minimize his total system uncertainty U which can be represented by

$$U(k) = tr[QP(k)] \qquad (22)$$

where $P(k)$ is the estimation error covariance and Q are weightings (or used for normalization purposes).

The effect of one look at time k is

$$\Delta U(k) = tr[Q\Delta P(k)] \qquad (23)$$

where (Ref. 9)

$$\Delta P(k) = P(k-) - P(k) \qquad (24a)$$

$$= P(k-)H'N^{-1}(k)HP(k-) \qquad (24b)$$

with

$$N^{-1}(k) = V^{-1}(k) - V^{-1}(k)HP(k)H'V^{-1}(k) \qquad (25)$$

Thus

$$\Delta U(k) = tr[G(k-)N^{-1}(k)] \qquad (26)$$

94

with

$$G(k-) = HP(k-)QP(k-)H'$$ (27)

look independent.

Now $N^{-1}(k)$ is a diagonal matrix if we assume only foveal viewing. This can be seen from eq.(7) which can be expressed as

$$V_j^{-1}(k) = V_{0_j}^{-1}(k-)\delta_j(k)$$ (28)

with

$$\delta_j : \{0,1\} \text{ the look sequence}$$

Foveal viewing implies that only one element of V^{-1} is non-zero and thus $n_{ji}^{-1} = -V_i^{-1} p_{y_{ij}} V_j^{-1} = 0$, where $p_{y_{ij}}$ is the ij-th element of HPH'.

Therefore also $N(k)$ is a diagonal matrix[*] with

$$N(k) = HP(k-)H' + V(k)$$ (29)

and thus

$$n_{ii}^{-1}(k) = (p_{y_{ii}}(k-) + V_i(k))^{-1}$$ (30)

Not looking at display element j ($\delta_j = 0$) implies $n_{jj}^{-1} = 0$, while looking at display element i yields $n_{ii}^{-1} = (p_{y_{ii}}(k-) + V_{0_i}(k-))^{-1}$.

Thus in general

$$n_{ii}^{-1}(k) = (p_{y_{ii}}(k-) + V_{0_i}(k-))^{-1}\delta_i(k)$$ (31)

Combining eqs.(26) and (31) yields

---

[*] The question of existence of $N(k)$ if $N^{-1}(k)$ is singular can be ~~the~~ circumvented by replacing the pertinent zeroes by (negligibly) small numbers.

$$\Delta U(k) = \sum_{i=1}^{NY} g_{r_i}(k-)\delta_i(k) \tag{32}$$

with

$$g_{r_i}(k-) = g_{ii}(k-)[p_{y_{ii}}(k-) + V_{0_i}(k-)]^{-1} \tag{33}$$

look independent.

Thus the maximum reduction in uncertainty is obtained for δ_j with max g_{r_j}.

Now the (ensemble) average effect of looking is

$$E\{\Delta U\} = \sum_{i=1}^{NY} E\{g_{r_i}\}P_i \tag{34a}$$

where P_i is the probability of attending to i or

$$E\{\Delta U\} = E_t\{g_r\} \tag{34b}$$

with E_t the average over the ensemble and over the display elements.

A "reasonable" scanning strategy to optimize (minimize) U is given by

$$P_i = E\{g_{r_i}\} / \sum_{i=1}^{NY} E\{g_{r_i}\} \tag{35}$$

resembling a first-order steepest descent gradient method to optimize U. Such an algorithm can also be applied directly. A useful expression for the gradient is in that case

$$\frac{\partial E\{\Delta U\}}{\partial P_i} = E\{g_{r_i}\} \qquad i = 1, \ldots, NY \tag{36}$$

With respect to maneuvering it is assumed that the HO looks ahead as frequently as necessary to "reconstruct" the desired trajectory x_d. This dictates the scan frequency of the pertinent cue(s) and thus (assuming an ergodic process) of the probability (P_m) of attending to the "maneuvering" cues y_0.

The remaining attention (or rather, the probability of attending, $1-P_m$) is divided optimally among the other visual cues y (e.g.) according to the scanning strategy of eq.(35).

4. PERFORMANCE AND WORKLOAD MEASURES

For our linearized, time-varying system with Gaussian inputs and outputs system performance can be adequately expressed in terms of the mean and covariance propagation (with time).

System performance related to regulating (against random inputs) involves only covariances of the system variables. Expressions are given in (e.g.) Ref.11.

Maneuvering performance can be derived from eq.(19). The mean maneuver sequence is simply

$$\bar{u}_m(k) = A(k)\bar{u}_m(k+1) + B^*(k)\bar{n}_1(k) \tag{37}$$

with $\bar{n}_1(k)$ obtained from eq.(16).

The ensemble covariance of u_m (variability) is obtained using eq.(17)

$$U_m(k) = A(k)U_m(k+1)A'(k) + B^*(k)\frac{N_1}{M}(k)B^*{}'(k) \tag{38}$$

The resulting (mean and covariance of the) system performance, x_m, is obtained using eqs.(3a), (19) and (21)

$$\bar{x}_m(k) = \Phi\bar{x}_m(k-1) + \Psi\bar{u}_m(k-1) \tag{39}$$

$$X_m(k+1) = \Phi X_m(k)\Phi' + \Psi U_m(k)\Psi' \tag{40}$$

using the fact that $\bar{w} = 0$ (assumption) and $E\{x_m u_m\} = 0$ (u_m is pre-programmed and thus uncorrelated with x_m).

Furthermore for many display-related (or, in general, visual informational) questions it is useful to establish the information contents of

the visual cues (e.g. the effect of a given display, a navigation aid, visibility conditions, etc.). This can be investigated on the basis of eq.(33) or eq.(36) in which g_{r_i} or $E\{g_{r_i}\}$ indicates how much system ucertainty can be reduced (by looking at element i).

HO workload can be determined using the workload model discussed in Ref.6. This model involves two psychological notions: "attention" and "arousal" in terms of the expression

$$W = S/P_0 \quad (dB) \tag{41a}$$

with

$$S = \partial J/\partial P_0 \quad (dB) \tag{41b}$$

The level of attention, or the fraction of information processing capacity, is represented by $1/P_0$ (Ref.12). The aspect of arousal is included in terms of the sensitivity S of task performance (cost functional J) to the momentary attention paid by the HO.
The workload model results have been shown to correlate excellently with subjective ratings and psychological measurements in a variety of control task situations (Ref.6).

5. CONCLUDING REMAKRS

In the foregoing chapters a model is presented describing rather detailed human control of a dynamic system. The model is an integration and an extension of previously developped (sub)models.
The main feature of the model is the intermittent control behavior during finite time intervals, thus involving decision making and planning. Another central element is that control is based on the perceived visual information from instruments and the outside world. Observing this visual scene is a complex process (e.g. involving preview) and intimately related to the control task. The model provides an adequate framework for the description of this interrelated process including a model for visual scanning.

After the implementation of the model and a preliminary model analysis it will be necessary to validate the model, especially the parts of the model related to intermittent control and visual scanning. This is recommended for future work.

6. REFERENCES

1. Meditch, J.S.
   Stochastic optimal linear estimation and control.
   McGraw-Hill, 1969.

2. Luenberger, D.G.
   Introduction to dynamic systems.
   John Wiley & Sons, 1979.

3. Elbert, T.F.
   Estimation and control of systems.
   Van Nostrand Reinhold Co., 1984.

4. Baron, S. and Levison, W.H.
   Display analysis with the optimal control model of the human operator.
   Human Factors, 19(5), 1977.

5. Kleinman, D.L. and Baron S.
   Manned vehicle system analysis by means of modem control theory.
   NASA CR-1753, 1971.

6. Wewerinke, P.H.
   Performance and workload analysis of in flight helicopter missions.
   NLR MP 77013 U, 1977.

7. Wewerinke, P.H.
   Visual scene perception in manual control.
   Journal of Cybernetics and Information Science, Vol. 3, No. 1-4, 1980.

8. Wewerinke, P.H.

    Model of the human observer and decision maker - Theory and validation.

    Automatica, vol. 19, No. 6, pp. 693-696, 1983.

9. Wewerinke, P.H.

    A model of the human decision maker observing a dynamic system.

    NLR TR 81062, 1981.

10. Gelb, A. (ed.)

    Applied optimal estimation.

    MIT press, 1974.

11. Kleinman, D.L. and Killingworth, W.R.

    A predictive pilot model for STOL aircraft landing.

    NASA CR-2374, 1974.

12. Levison, W.H. et al.

    Studies of multivariable control systems. A model for task inter-ference.

    NASA CR-1746, 1971.
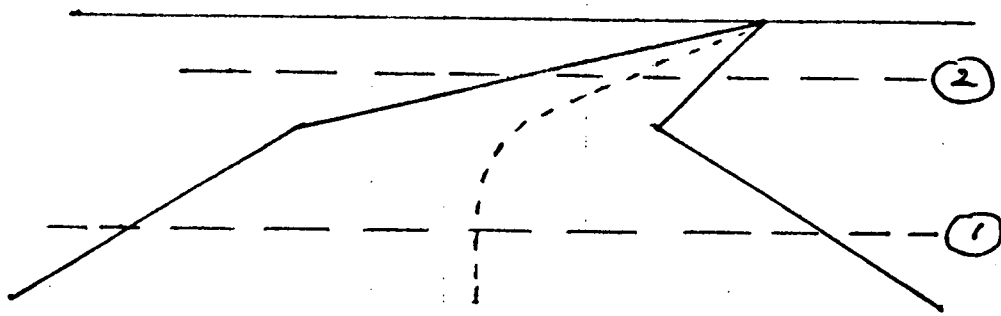
1a. Perspective view

$(x_d(k+N)$

x_2

$x(k)$

x_1
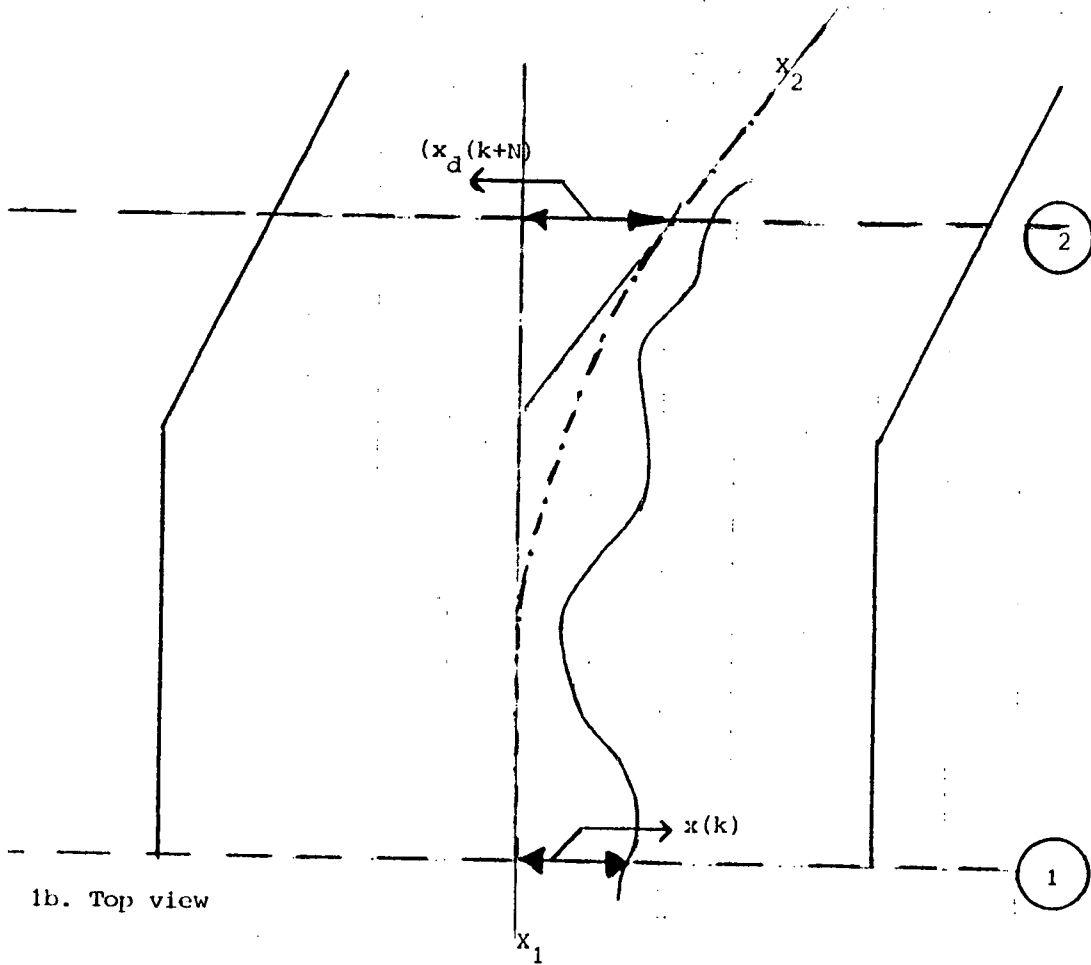
1b. Top view

Figure 1.   Visual scene information
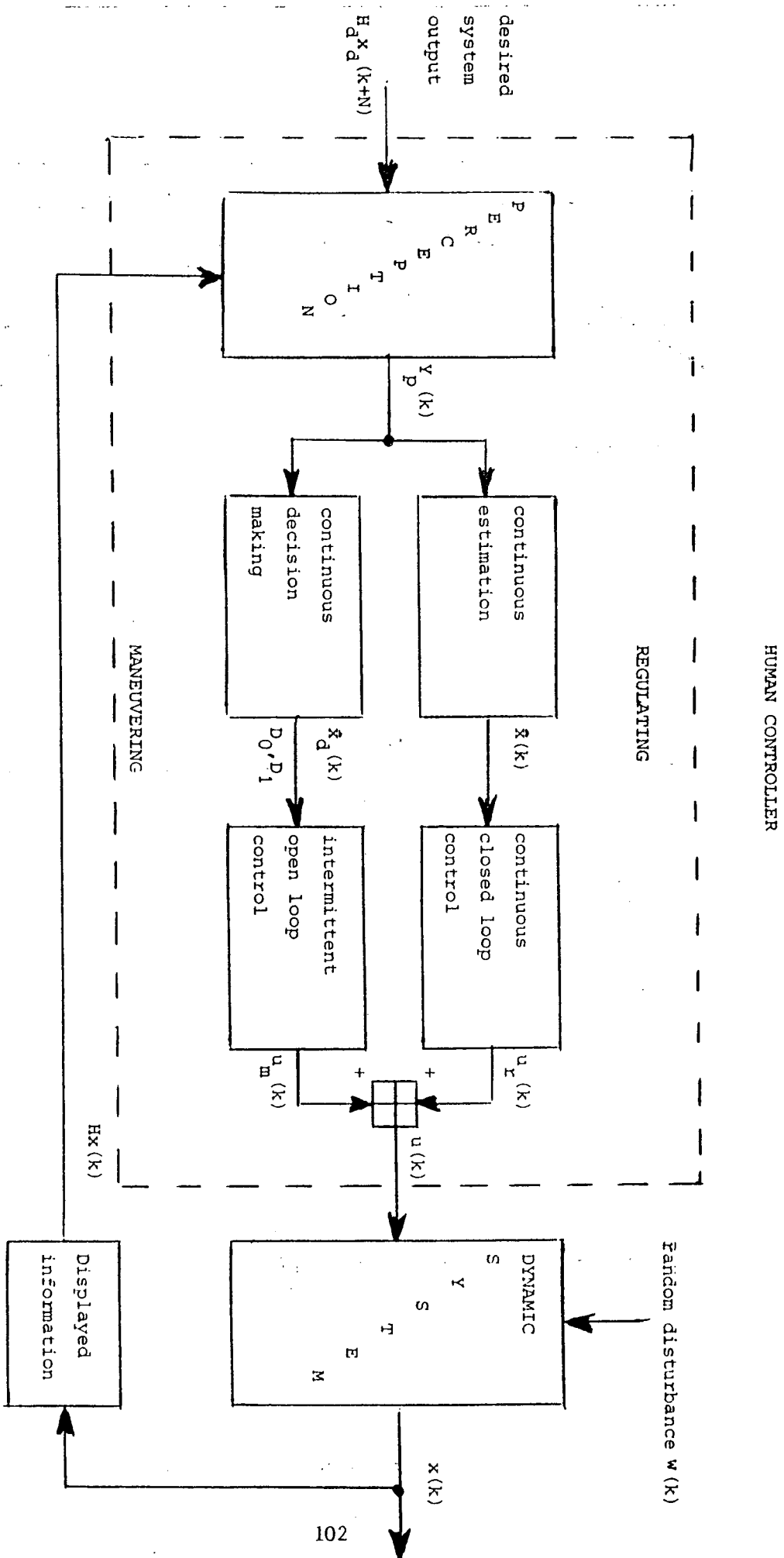
Fig. 2 Block diagram man-machine system
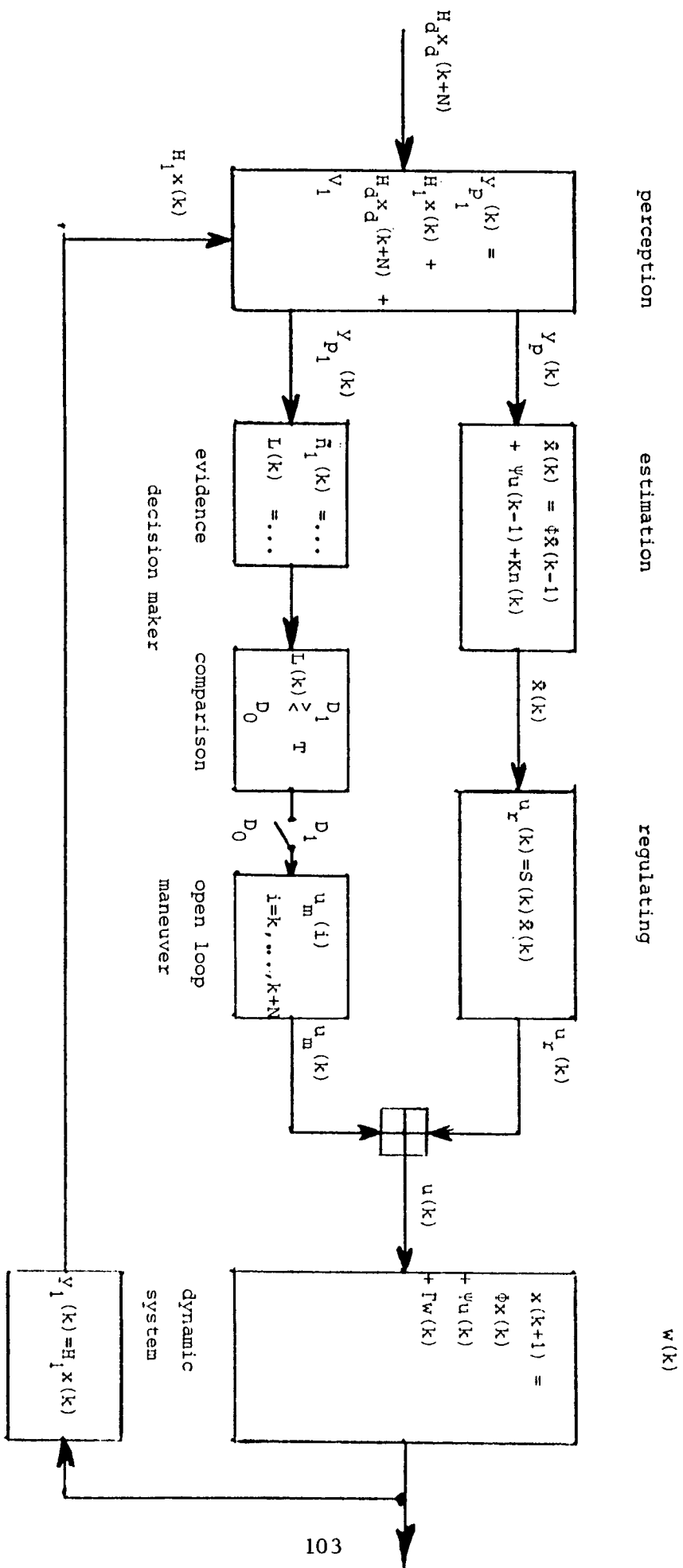
Fig. 3   Man-machine model

APPENDIX A: Solution of the finite time tracking problem

The problem is to control the state x of a linear(ized) system given by

$$x(k) = \Phi x(k-1) + \Psi u(k-1) + \Gamma w(k-1) \qquad (A.1a)$$

$$y(k) = Hx(k) + H_d x_d(k+N) \qquad (A.1b)$$

over some fixed interval of time by realizing a control sequence u(k) which minimizes the cost functional

$$J_N(u) = E\Big\{ \sum_{i=1}^{N} (x(i)-x_d(i))'Q_x(i)(x(i)-x_d(i)) +$$

$$u'(i-1)Q_u(i-1)u(i-1) \Big\}. \qquad (A.2)$$

First consider the solution of the standard (deterministic) linear regulator problem (thus with $x_d = 0$). The linear feedback control law is given by (Ref.1)

$$u_r(k) = S(k)x(k) \qquad (A.3)$$

where S(k) is determined recursively from

$$S(k) = -[\Psi'W(k+1)\Psi + Q_u(k)]^{-1}\Psi'W(k+1)\Phi \qquad (A.4)$$

with

$$W(k) = Q_x(k) + \Phi'W(k+1)[\Phi+\Psi S(k)] \qquad (A.5)$$

$$\text{with } W(N) = Q_x(N)$$

and

$$J_N(k) = x'(k)[W(k)-Q_x(k)]x(k) \qquad (A.6)$$

In case of a given (i.e. varying) state reference which has to be followed, the performance index (A.2) applies. The optimal control is now given by (e.g. reference 3).

$$u(k) = u_r(k) + u_m(k) \tag{A.7}$$

where

$$u_m(k) = Q_u^{-1}(k)\Psi'd(k) \tag{A.8}$$

and

$$d(k) = S'(k)\Psi'd(k+1) + Q_x(k)x_d(k) \tag{A.9}$$
$$\text{with } d(N) = -Q_x(N)x_d(N).$$

Thus the control is now extended with an open loop (feed forward) control. Eq.(8) has to be determined from $k = N,\ldots,1$ (backwards) to construct the control $u_m(k)$, $k = 1,\ldots,N$, yielding $x_m(k)$.

STALL: DEFINING A LOAD SATURATION POINT FOR SUPERVISORY CONTROL

by
G. P. Chubb
N. Wilcox
R. A. Miller
J. W. Park
SofTech, Inc.
3100 Presidential Dr.
Fairborn, OH 45324-2039

ABSTRACT

STALL is an acronym for Saturation of Tactical Aviator Load Limits. A load saturation point is defined as the intersection of light and heavy load limits. The model is an M-stream, closed-loop queuing system. Analytic and simulation implementations have been developed.

List of Symbols

λ - arrival rate of demands for service (the inverse of time between arrivals, usually expressed as an average)

μ - service rate for demands processing

ρ - utilization or efficiency (fraction busy; convertible to percent busy)

λ_{eff} - effective arrival rate, when multiple factors drive demand

λ_m - mission event arrival rate

λ_s - system event arrival rate

λ_p - emitted events or operator injected demand arrival rate

M - number of task streams or arrival processes

λ_i - one of the M arrival streams

INTRODUCTION

Workload guidelines (MIL-STD-H-46855) have recommended that required tasks occupy no more than 70 percent of the time available. This suggests that a 30 percent reserve capacity is desired as a design margin. Time available (T_A) is constrained by the mission time line, and time

107

required (T_R) is governed by task times. Two problems are typically encountered in simple comparisons like T_A/T_R. First, the time required values are really stochastic variables, not constants. Second, the task structure is often assumed to be some specified linear sequence of strictly determined activities. Typically, these task analyses do not account for anything but prime equipment operation and they ignore routine activities that crews normally engage in, like system supervision.

Moreover, no distinction is made between the duration an activity "should" take and the actual duration its does take. "Should" durations ought to reflect best case conditions predicated on design. Actual times ought to fluctuate, depending on assumptions about the situations or conditions under which task execution is attempted.

1.0 APPROACH

Queuing theory provides a suitable conceptual framework that is useful for gaining analytical insights into design issues related to how busy the human operator becomes under a stochastic demand pattern. Queuing theory also easily handles the fact that operators will exhibit stochastic service behavior as task demands are processed. Recent advances allow the classic assumptions of queuing theory to be relaxed to improve the correspondence between the model and the cockpit operations being described.

Viewing the pilot as a simple queuing system, the pilot becomes the server of customers. Those customers may be tasks, decisions, display changes, or some mix of these. While precise definition of customer is a significant and non-trivial issue, for our present purpose, it is assumed this can be done and that the arrival of these customers can be observed or determined by some combination of mission/system analysis. In particular, we presume that the distribution of interarrival times can be described by a particular function of computable statistics (like the average or the standard deviation). Arrival rate (λ) is then simply the reciprocal of interarrival time ($1/\lambda$).

The design problem is to determine what service rate is necessary and sufficient to handle customer processing. The stochastic pattern of customer arrivals and the pilot servicing of that demand makes it more difficult to specify what the limiting constraint on design should be. That is where queuing theory provides an analytic approach for specifying that upper bound--the point where demands lead to Saturation of Tactical Aviator Load Limits (STALL).

2.0 PRELIMINARY DEVELOPMENT

If customers arrive at rate (λ) and the pilot services them at rate (μ), it is clear that to avoid guaranteed failure, the rate of servicing

must be greater than the rate of customer arrivals, since the number of waiting customers is assured to increase continuously.

So we already know two things about our design. First, service rates must be as high as possible. If service rates cannot be made greater than the arrival rate, something has to be done about the surplus customers. Either they must be ignored or they must be directed to some other service facility, human or not.

If service rate equaled arrival rate, then efficiency (in the sense defined by queuing theory) would be 1.0. When this is the case, the backlog continues to build (forever), and arriving customers entering the end of the line face an increasingly longer wait. The index representing efficiency is:

$$\rho = \frac{\lambda}{\mu} \tag{1}$$

Suppose that a thirty percent reserve is desired; then seventy percent utilization is implied: $\rho = .7$. If we then assume the customer arrivals are either fixed or given as a design constraint to be met, the problem is to find the service rate that meets the stated requirements.

$$\mu \geq \lambda/\rho \tag{2}$$

This will ensure that, on the average, the demand λ will be met if utilization is 70 percent, so long as the average activity duration is $1/\mu$ or smaller.

This mean value analysis ignores variability, so it only provides results that work on the average, under steady state conditions. This is a necessary but insufficient condition for good design.

Then what is sufficient? That depends on setting some criterion for the allowable upper bound on response time. Response time depends on two factors: (1) how long customers wait for service, and (2) how fast they get serviced when the wait is over. If customers are not prioritized and are treated on a first-come, first-served basis (i.e., FIFO queue discipline), then the wait time depends on customer placement in the queue: average queue length affects average response time.

This distinction between task duration $(1/\mu)$ and response time is not typically treated in the classic approach to workload analysis by means of mission timelines and task analyses that estimate time required for crew activities.

If response time is inadequate and neither service nor arrival rates can be changed, then the only adjustment possible is to alter queue discipline, that is, to prioritize customers. Some get ignored temporarily (or permanently) in order to improve the response time to others. The effects of such strategies are not easily analyzed. Analysis typically requires simulation of the proposed queue discipline (priority

scheme). Since simulations execute more slowly than analytical models, and their coding needs to be verified and validated, it is useful to begin such studies by first simulating the FIFO strategy and by comparing run results to the closed-form analytic solution. This has been successfully pursued in STALL model development.

3.0 RE-EXAMINATION OF DEMAND

The interarrival pattern of demand has several components: (1) mission driven demands, (2) system driven demands, and (3) personal factors that add to that demand.

Queuing theory is a time based analysis. It has no inherent ability to treat the geometry (altitude, range, bearing, etc.) of the mission or engagement. Such factors must be treated separately and translated into a time based pattern of demands on pilot servicing. This is a non-trivial, but fairly straightforward analysis problem. Changes in the scenario or script that impact the geometry may also affect the timing considerations. However, within a particular class of scenario, many of the realizable scripts may be treatable as distributional variations rather than as completely new analyses. The event distributions may be different, or their parameter values may change, but the derivational approach may remain the same.

System mechanization will impact demands on the pilot in two ways. First, it may require pilot checks for feedback on whether prior actions were effective. Second, failures (physical or functional) also demand attention. Automation can alleviate psychomotor servicing requirements (action demands), but actually increase cognitive servicing requirements (scanning demands). Scanning is typically quicker than acting, but it is important to examine automation impacts carefully and to not assume that automation is the solution. As designed, automation may actually increase load by imposing greater scanning demand, instead of decreasing it through a reduced action demand.

Personal factors include satisfying desires that are not related to mission goals. They also include correcting detected mistakes, whether omissions or commissions, and their consequences (if any). Experimental evidence indicates that human error is inescapable and that design must be tolerant of that fact. Thus, the effective demand pattern consists of at least three factors, i.e.,

$$\lambda_{eff} = f\left(\lambda_m, \lambda_s, \lambda_p\right) \qquad (3)$$

where

λ_m - mission event rate: externally imposed demands

λ_s - system event rate: design induced demands

λ_p - rate of people-emitted events: operator injected demands

Clearly, designers can only control λ_s. They must accommodate λ_m and λ_p.

4.0 ALTERNATE REPRESENTATION OF DEMAND

There is another way to look at task demand. One can categorize the kinds of activities which might occur in a mission. Table 1 provides an example of possible demand categories. The categories could be rank ordered in terms of their perceived importance. Importance needs to consider conflicting goals and to presume that those conflicts can be resolved so that a unique ordering will result.

If the categories each had an equivalent arrival rate (which may be a poor assumption), then in theory, if servicing demands were overtaxed, presumably the least important demand should be the one dropped first. The most important demand would be dropped last. One question that might be asked is how many demand categories can be handled for a particular design concept? Ideally, one wants to handle all categories completely, but, if this cannot be done, then one prefers the design that can handle the most categories.

In this model, demand becomes

$$\lambda_{eff} = \sum_{i=1}^{i=M} \lambda_i = M \lambda \qquad (4)$$

The demand is $M \lambda$ only if all the λ_i are identical or if they may reasonably be assumed to be samples from a homogeneous population. If this assumption cannot be met, then it is better to treat the effective arrival rate as the aggregate sum of the collective set of arrival rates for the $i = 1, 2, ..., M$ categories.

5.0 EFFECTIVE SERVICE DESCRIPTIONS

Since the arrival process can be treated as a collection of demand generators creating an effective customer arrival rate, then service might also be treated as a collection of services replaceable or represented as an effective service rate (μ_{eff}). This construct then permits a formulation of networks of servicing actions. These are the elemental activities which may occur once the operator initiates servicing of arriving or waiting customers.

Several kinds of processes might exist within the operator as a service facility: (1) sequences, (2) probabilistic branches, and (3) loops. One kind of network element is very difficult to incorporate mathematically (but easy to include in simulations): logical control of sequencing, branching, or looping.

Sequences can represent simple skill-based behavior, like operating procedures or checklists. Branches can be used to represent more complicated activities, like rule-based behavior. Loops can be used to represent activities with uncertain duration, like knowledge-based behavior.

TABLE 1. THIRTEEN CATEGORIES OF LOAD

Acronym	Description
TF/TA	Terrain Following/Terrain Avoidance
TCM	Threat Counter Maneuver
MAL	Malfunctions
TDA	Target Detection and Attack
ACE	Audio Communication Exchange
TFD	Task Failure Demands
CDV	Check Display(s) and Verify
NAP	Navigation Action Points
OSO	Offensive System Operation
SMC	Sensor Management and Control
IMT	Information Management Tasks
CEH	Coupled Eye Hand Movements
RAC	Routine Assessment Checks
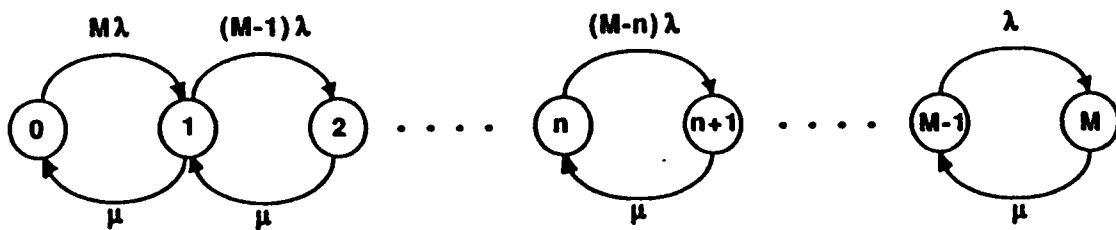
A-D-6064

Figure 1. State Transition Diagram

Sequences suggest a pattern of behavior that may vary in duration, but not in structure. Branches suggest options that are predefined. Branches may control execution of subsequences. Branching sequences may also be included as subelements of a sequence.

Loops are a special kind of branching in which one leg of the branch returns to an element earlier in a sequence. If the branch is controlled probabilistically, then the amount of time spent in the loop will vary, depending on how many times in succession that branch gets taken before the alternative(s) are selected instead.

The aggregate estimate of μ_{eff} must be computed by appropriate methods. Sequences are finite sums of random variables.

If the variables are identically distributed variables, the construction of an effective parameter value for the distribution of their sum is quite straightforward. Using the method of moments, first order approximations are possible even if the distributions are not identical. The computational problem is slightly more complicated for branching sequences.

Loops are random length sums of random variables and they present the most difficult problem computationally. Since the process effectively loops on itself, the variables in the sum are all identically distributed, but the number in that sum is itself a random variable. Consequently, the distribution of the sum typically cannot be determined exactly, but its first few moments can be described by differentiating the moment generating function and by evaluating the result when the argument is set to zero.

6.0 OPEN VS CLOSED QUEUING SYSTEMS

Most classic queuing models are of open systems. The customers arrive from an infinite population and effectively never return for further servicing. This is a reasonable representation for a very broad class of problems. It does not well represent certain kinds of problems that arise in aircraft operation.

Often, what happens is that the arrival of one demand precludes any future arrivals from that stream until the generated demand has been serviced; but, once serviced, the demand may reoccur. Typically, there are one or more streams of such cyclic demand. The problem then is to determine how many of these streams can be handled.

Let M be the maximum number of streams that may generate demands. Assume each stream generates arrivals at the same rate (λ). Then, if there are no customers in queue waiting for service, the effective arrival rate is M λ (since all streams have the same rate and there are M such streams). As soon as some arriving customer has to wait (because service is not yet completed for the previous arriving customer), the effective rate decreases to (M-1)λ. Figure 1 represents the state

diagram for this system. The state description consists of defining the probability distribution for the number of customers in the system. Once this state description has been defined (by analytic, simulation, or empirical methods), then the statistics for backlog (queue length), response time (servicing and waiting time), and throughput (customers per second) can be computed (by analysis) or generated (by simulation).

7.0 STALL: SATURATION OF TACTICAL AVIATOR LOAD LIMITS

STALL is a FORTRAN program that implements four very simple network models in a closed loop, M-stream system. It is based on a very compact mean value analysis algorithm and has an interactive prompting system to solicit parameter values from a user. Extensive help features are included to explain and interpret these entries for inexperienced users.

Preliminary application has demonstrated the feasibility of using STALL to represent an air-to-ground mission. Preliminary validation has been restricted to comparing analytic results to outputs obtained from more detailed modeling by using Systems Analysis Of Integrated Networks of Tasks (SAINT). SAINT is a FORTRAN-based simulation language used for modeling large, complex, manned systems. Results indicate that STALL is more robust for uncertainties in effective service rates than for arrival rates. STALL becomes relatively insensitive to violation of theoretical assumptions when the system is heavily saturated.

Empirical validation has been considered. The distinction between demand arrival and start of service presents a difficult measurement problem in practice. Moreover, definition of "customer" still poses formidable problems in the context of cockpit design applications. These are not insurmountable problems, but they are issues that still need additional consideration.

SESSION 3: <u>DISPLAYS AND VISUAL EFFECTS</u>

Moderator: Dr. William H. Levison, BBN Laboratories, Inc.

FREQUENCY RESPONSE OF THE VISUAL SYSTEM TO SIMULATED

CHANGES IN ALTITUDE AND ITS RELATIONSHIP TO ACTIVE CONTROL

Gary E. Riccio and Jeffrey D. Cress
Systems Research Laboratories, Inc.
Dayton, OH

A magnitude estimation technique was used
to evaluate the sensitivity of the visual
system to sinusoidal changes in pitch and
altitude. Perceptual describing functions
were derived from the magnitude estimates. The
perceptual describing functions were compared
to human-operator describing functions from an
altitude-control experiment. Describing
functions were analyzed for three types of
visual display. The results have implications
for the use of impoverished displays in flight
simulators.

INTRODUCTION

An important characteristic of visual displays in flight
simulation is that they can provide multiple sources of
information for the same aircraft state. This leads to several
questions that are relevant to the design and use of simulators:
What is the relative sensitivity of the visual system to the
redundant sources of information? What is the relative efficacy
of these sources of information for flight control? Is more
information better, or is there interference among redundant
sources of information?

We have addressed these issues by focusing on a two aircraft
states (pitch and altitude) and two methods of depicting this
state in a visual display. One method is to schematically
display a perspective angle that corresponds to an infinitely
straight roadway on flat and level terrain (Figure 1a). An
alternative is to display a flow field that corresponds to flat
and level terrain over which texture elements (dots) are randomly
scattered (Figure 1b). The roadway and the dots could be
presented either alone or in combination (Figure 1c).

We have studied these displays extensively in the context of
compensatory control tasks (Levison & Warren, 1984; Warren &
Riccio, 1985; Zacharias, Warren, & Riccio, 1986). In these
experiments, subjects were required to maintain an assigned
altitude in the presence of a pseudo-random disturbance. Both
the roadway display and the combined display were better than the
dots display for the control of altitude; the combined display
was slightly worse than the roadway display. Differences were
also found in the extent to which training with one display
transferred to an identical task performed with a different
display: While there was strong transfer between the roadway and

117
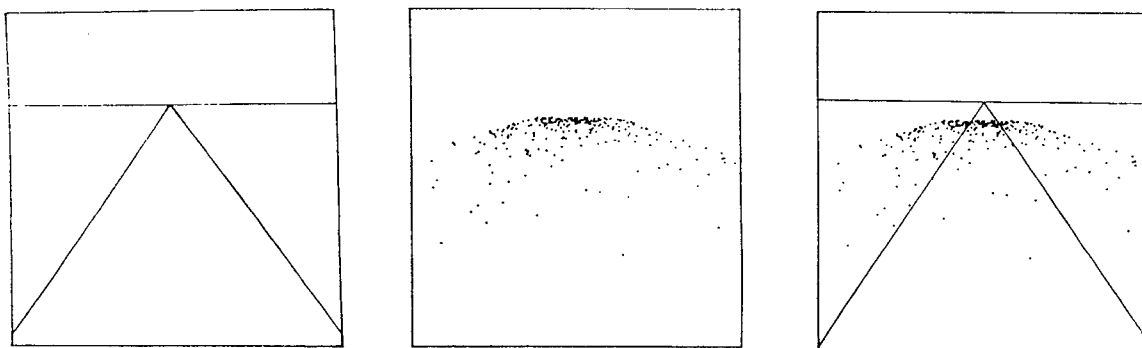
Figure 1. Visual displays.

combined displays, there was very poor transfer between either of these displays and the dots display.

There are four major conclusions from the active control studies: (1) Performance is better with the roadway display because it provides more useful altitude information than does the dots display. (2) Performance is slightly worse with the combined display than with the roadway display because the dots may have a slight masking effect on the roadway. (3) There is poor transfer of training from the combined display to the dots display because subjects selectively attend to the roadway when given the combined display. (4) There is poor transfer of training between the dots display and both the roadway and combined displays because different perceptual skills are involved in the pick up of altitude information in these displays. It would be prudent to include data on such relationships in a simulator's specifications. The use of the simulator should be guided by such data.

It may be useful to differentiate two components to the pick up of altitude information in the compensatory control task. One is the perception of changing altitude. The other is the perception of instantaneous altitude with respect to the assigned altitude; the assigned altitude was specified by the appearance of the display at the beginning of a trial. Subjectively, these seem to be distinct skills, and the latter seems to be more useful for detecting gradual departures from the assigned altitude.

Informal reports from the compensatory control studies suggested that performance was better with the roadway because it was easier to detect deviations from the assigned "altitude", which for the roadway was specified simply by a 30 or 60 degree angle. Moreover, subjects seemed to gradually drift away from the assigned altitude more frequently with the dots display. If this is the reason for the superiority of the roadway display, then there may be no difference between the roadway and dots displays with respect to the perception of changing altitude.

The present experiment evaluates, for each of the three displays, the sensitivity of the visual system to sinusoidal

118

changes in pitch and altitude as a function of the frequency of this change. These perceptual describing functions provide insights about the pick up of altitude information with the various displays. In addition, the perceptual describing functions are compared with the human-operator describing functions from a previous compensatory control study. The comparison provides some clues about the characteristics of control with the various displays.

METHODS

Observers

There were six participants in the experiment. All were paid for their participation. They had either normal or corrected vision. Ages ranged from 19 to 24 years. Three had previously participated in a compensatory control study that used the same displays (Warren & Riccio, 1985). None were pilots.

Apparatus

The experimental setup is schematically depicted in Figure 2. The longitudinal dynamics of a simulated F-16 aircraft were implemented on an EAI 2000 analog computer (see Zacharias, et al., 1986, for the dynamics of the simulated aircraft; see also Figure 3). The inputs to the simulated aircraft included a pitch-rate forcing function and pitch-rate control signals from an autopilot. The autopilot was also implemented on the analog computer. Outputs were states of the aircraft. These analog outputs were digitized and sent to a PDP 11/60 computer. The geometry for the visual scene was computed with an Analogic AP-400 array processor. The visual display was then generated with a DEC GT-40 (vector graphics) display processor and presented on a Hewlett-Packard high-speed phosphor monitor. The screen was 38 cm wide and 28 cm high. Viewing the display from approximately 38 cm resulted in a field of view that was 53 degrees wide.

ANALOG COMPUTER

GUST → (+) M ⊕ → F-16 → DIGITAL DISPLAY GENERATION → OBSERVER → MAGNITUDE ESTIMATE

STICK

AUTO PILOT
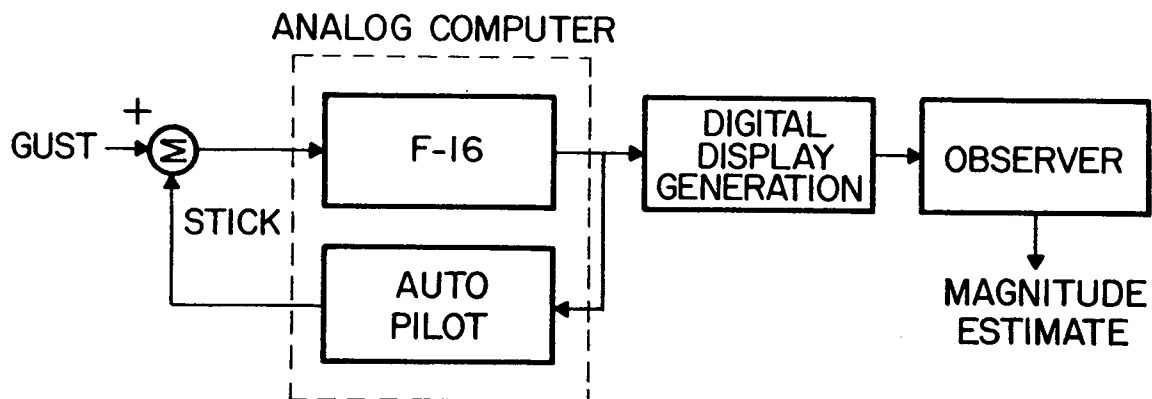
Figure 2. Experimental setup.
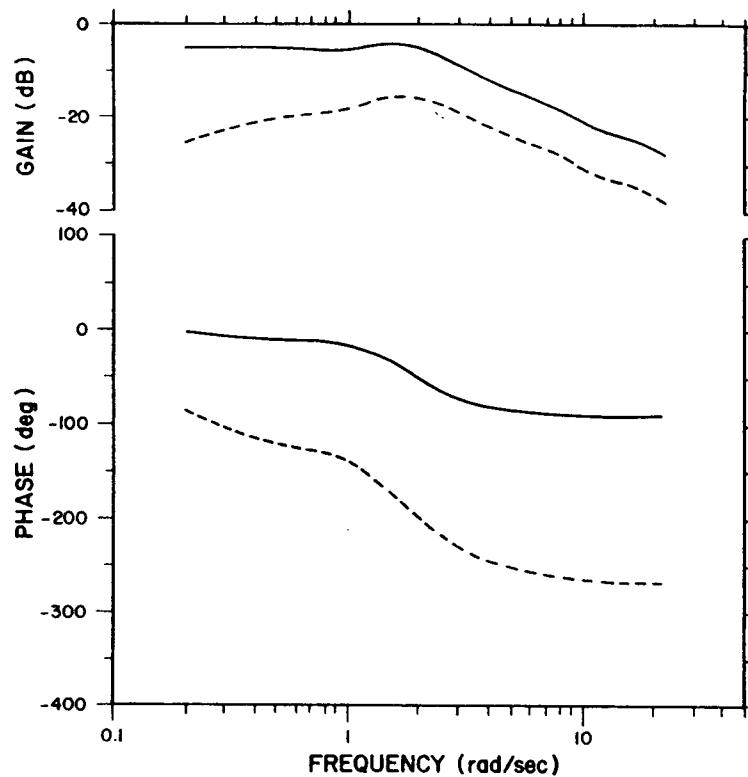
Figure 3. Open-loop describing functions for pitch-
rate/disturbance (dotted line) and pitch-rate/control-force
(solid line) for simulated aircraft (from Levison, Zacharias,
and Sinacori, 1982).

The computer-generated visual scenes contained two sources
of altitude information, either alone or in combination. One
source was a perspective scene of a roadway, and the other was
the flow field corresponding to a randomly textured terrain.
Three displays were constructed from these two scene components.

The roadway display. One display consisted of a schematic
view of a horizon and an infinitely straight roadway on flat and
level terrain (Figure 1a). The central perspective angle of the
road changed as a function of the altitude (road width was held
constant at 30.5 m). The vertical position of the horizon line
changed as a function of the pitch state of the aircraft. The
experimental room was darkened so that there would be no external
visual references for display components such as the horizon
line. The horizon was at eye level when the aircraft was level.

The dots display. Another display consisted of a
perspective scene of dots spread randomly over flat and level
terrain. The "data base" for the display contained 256 dots (or
texture elements) within an area on the simulated "island" of
terrain that was 1.22 km wide and extended 4.88 km in front of
the simulated aircraft. Consequently, the density of texture
elements on the simulated terrain was 43.0 dots per square km.

120

The forward motion of the simulated aircraft over the field of dots resulted in a flow field (i.e., optical streaming of dots). This revealed a dimension of movement that was not apparent with the schematic roadway. The simulated aircraft moved at a fixed forward velocity of 206 m/s. As each texture element moved beneath the simulated aircraft it was replaced by a new element randomly placed at the far edge of the texture island. This insured that the simulation did not run out of terrain over the course of an experimental trial and that roughly the same number of texture elements was always visible.

The perspective view of the terrain resulted in a gradient of optical texture from the bottom to the top of the display (Figure 1b). Several parameters of the optical texture gradient and flow field covaried with altitude. The optical covariates included the global texture density, the gradient in texture along the vertical axis of the display (Gibson, 1950), the global rate of texture flow (Owen, Warren, Jensen, Mangold, & Hettinger, 1981), and the structure in the directions of streaming in the flow field (Koenderink, 1986).

The vertical position of the far edge of the visible island covaried with the pitch state of the simulated aircraft. The edge of the field of dots provided a pseudo-horizon since the texture island was of finite extent. The location of the pseudo-horizon relative to the true horizon was altitude dependent. The true horizon was not present in this display. As with the roadway display, the darkened experimental room prevented the use of external visual references for the various display components.

The combined display. A third display contained both the field of random dots and the schematic roadway with the true horizon (Figure 1c). This display contained all the nested sources of information in the roadway and dots dislays. In addition, another source of information emerged from the relationship between the roadway and dots components of the combined display. The visible gap between the true horizon and the end of the texture island provided information about the altitude of the aircraft. The gap was an artifact of the texture island that was being simulated.

Factors affecting the displays. Within each trial, changes in the displays were caused by changes in the pitch and altitude states of the aircraft as influenced by the forcing function and control signals from the autopilot. The display changes had the same frequency composition as the easily calibrated forcing function since both the autopilot and the aircraft were linear. In most trials the changes in altitude and pitch were simple sinusoids. The forcing function was filtered through the aircraft and the autopilot so that observers would experience coordinated changes in altitude and pitch that were similar to those in the previous compensatory control experiments (Warren & Riccio, 1985). The relationship between the changes in pitch and altitude is depicted in Figure 4. The frequency and amplitude for the sinusoidal forcing functions, the average altitude of the aircraft, and the type of display were set before each trial.

121
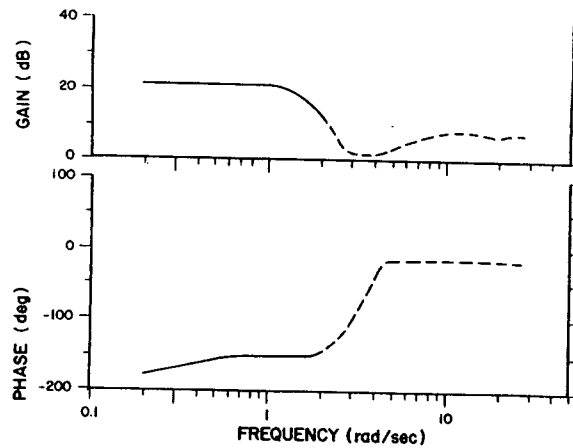
Figure 4. Describing function for altitude-change/pitch-change. Solid lines indicate frequency range of pitch/altitude sinusoids used in the present study. Dotted lines extend the range to include all frequencies in the sum-of-sines disturbance used in the compensatory control study.

Procedure

There were three classes of presentation: (1) sinusoidal change, (2) no change, and (3) pseudo-random change similar to that experienced in the compensatory control study. Most trials consisted of sinusoidal changes in pitch around level flight which resulted in sinusoidal changes in altitude around one of three "reference" altitudes. The three reference altitudes (13.7, 27.4, and 54.8 m) were chosen to span the range of "assigned" altitudes in the compensatory control experiments; the corresponding central roadway angles were 96.1, 58.2, and 31.1 degrees. The frequency and amplitude of the pitch/altitude sinusoids were constant throughout the trial.

Observers were presented with one of five frequencies (.18, pitch/altitude sinusoids. These were the lowest five frequencies in the sum-of-sines (SOS) forcing function used in the compensatory control experiments. These five frequencies accounted for 98.8% of the variance in altitude and 82.4% of the variance in pitch during autopilot control with the full sum-of-sines disturbance used in the compensatory control experiment; this was due primarily to the dynamics of the simulated aircraft.

Each frequency was presented at several different amplitudes of pitch/altitude change (Table 1). The lowest amplitude at each frequency was based on the corresponding threshold which was informally estimated before the experiment; this increased the comparability of magnitude estimates across frequencies. The amplitudes for each frequency were evenly spaced on a logarithmic scale of altitude change; adjacent amplitudes of altitude change differed by a factor of two. None of the amplitudes resulted in altitudes that were equal to or less than zero.

122

Table 1. Amplitudes of change in altitude and pitch are
presented at each frequency. Frequency is specified in radians
per second. The root-mean-square (rms) change in altitude is
specified im meters, and the rms change in pitch is specified in
degrees. The rms amplitudes for the corresponding frequencies in
the pseudo-random SOS presentations are included. The rms
amplitudes for the the combined effect of "all" 13 frequencies in
the SOS presentations are also provided.

Change	Freq.	---------- Single Sinusoids ----------						SOS
alt.	0.18	0.43	0.86	1.72	3.45	6.90		1.13
alt.	0.43	0.43	0.86	1.72	3.45	6.90		1.50
alt.	1.04	0.32	0.65	1.29	2.59	5.17		2.51
alt.	1.43	0.22	0.43	0.86	1.72	3.45	6.90	2.19
alt.	1.92	0.13	0.26	0.52	1.03	2.07	4.14	2.40
alt.	all							4.54
pitch	0.18	0.03	0.07	0.13	0.26	0.53		0.09
pitch	0.43	0.04	0.07	0.14	0.29	0.57		0.12
pitch	1.04	0.03	0.07	0.14	0.28	0.55		0.27
pitch	1.43	0.03	0.06	0.12	0.25	0.49	0.99	0.31
pitch	1.92	0.03	0.06	0.12	0.23	0.46	0.93	0.54
pitch	all							0.76

The trials varied in length between 15 and 17 s. There were
three factors that affected trial duration: (1) The simulated
aircraft was level at the beginning and end of the trial; that
is, an integer number of half cycles were presented at each
frequency. (2) Trial duration was not the same for all
frequencies because the frequencies of change were not harmonics
of each other. (3) Trial duration and its range across
frequencies were minimized.

Observers passively viewed the simulated aircraft motion that
was specified by the visual display. After each trial the
observer rated the "average magnitude of perceived motion,
excluding the forward motion of the simulated aircraft". With
these nonspecific instructions, both pitch and altitude changes
could influence the observers ratings; presumably changes in both
pitch and altitude affected compensatory control in previous
studies. They rated this motion on a open-ended integer scale.
Larger numbers indicated greater magnitude of perceived motion.
Negative numbers were not allowed and "zero" was used only when
there was no perceived motion.

The experiment consisted of two phases: familiarization and
testing. In the familiarization phase observers were exposed to
a subset of the presentations used in the testing phase. The
experimental parameters were systematically varied by changing
amplitude first (largest then smallest), frequency second
(highest, intermediate, then lowest), altitude third (lowest then
highest), and display last (roadway, dots, then combined).

Observers participated in eighteen sessions during the
testing phase. Each session lasted approximately 45 minutes.

Each session consisted of 45 trials: three sets of 15 trials separated by five-minute rest periods. Over two consecutive sessions observers were exposed to all (81) combinations of frequency, amplitude, and display, for a particular altitude. In addition, each pair of sessions contained six (baseline) trials with no pitch/altitude change and three (SOS) trials with the sum-of-sines forcing function used in the compensatory control experiments (two baseline trials and one SOS trial per display). The order of the 90 presentations was randomized separately for each pair of sessions.

Observers were exposed to the three altitudes over three successive pairs of sessions. The order, in which the three altitude conditions were experienced, was completely counterbalanced across the six observers. Observers participated in three replications of the six sessions over which all combinations of frequency, amplitude, display, and altitude were presented. Observers were presented with the three altitude conditions in different orders over the three replications.

Data Analysis

Data Reduction. The technique used for generating perceptual describing functions was adapted from Stevens & Marks (1980) and Flach, Riccio, McMillan, & Warren (in press). It assumed that the perceived magnitude of pitch/altitude change was proportional to a physical measure of that change taken to some power. The psychophysical power functions -- for each observer, display, altitude, and frequency -- were generated by computing the linear relationship between the logarithm of the amplitude of simulated aircraft motion and the logarithm of the corresponding magnitude estimate. The exponent of the power function for the untransformed variables was specified by the slope of the best-fitting regression line for the log-transformed variables. Regression analyses were performed using both altitude change and pitch change as measures of simulated aircraft motion.

The median magnitude estimate was then computed for each observer. Given homogeneity of regression slopes (exponents in the power functions), the median provides a scale-free intercept for the regression lines. Scale-free parameters for the psychophysical functions are desirable since there is no reason to believe that different observers use the same numerical scale. The amplitude of simulated aircraft motion that corresponded to each observer's median magnitude estimate was computed for each frequency, altitude, and display (Figure 5). The resulting data are iso-sensitivity amplitudes (ISA).

ISA can be viewed as the input magnitude required to achieve a specified output magnitude. The gain of a system is usually viewed as the output magnitude resulting from a specified input magnitude. It follows that plots of ISA versus frequency are analogous to describing functions. The analogy is more direct if the inverse of ISA is expressed as a function of frequency. This is because there is an inverse relationship between gain and ISA. The inverse of ISA can be considered as a measure of sensitivity or gain of the visual system.
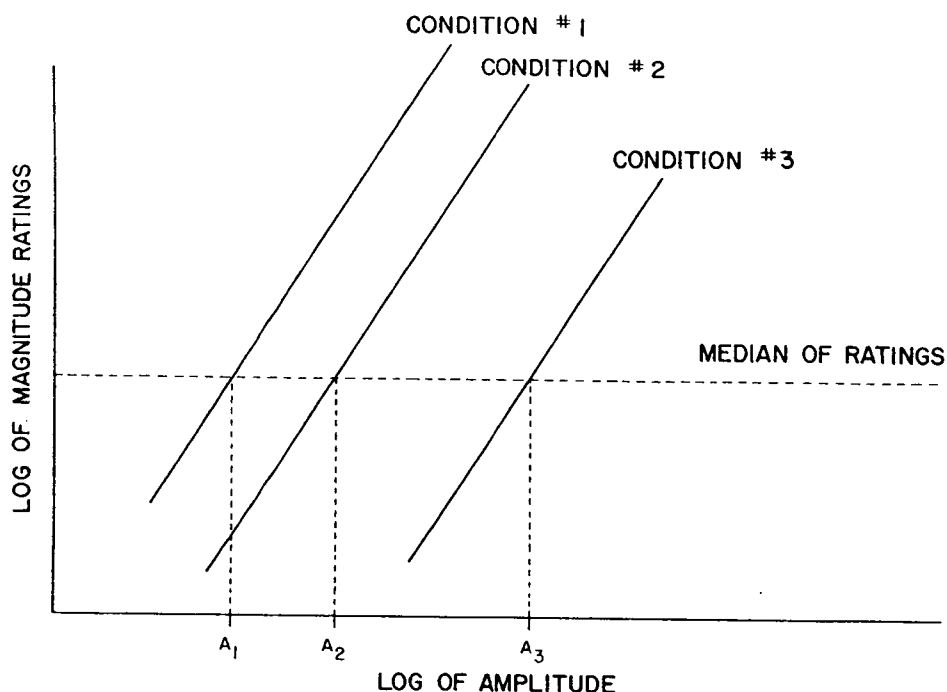
Figure 5. Hypothetical data showing the "magnitude matching"
technique for generating iso-sensitivity amplitudes (A_1, A_2, A_3).

Analysis of Perceptual Describing Functions. ISA was used
as the dependent variable in a nonadditive-model ANOVA. The
independent variables were observer, display, altitiude, and
frequency. Display, altitude, and frequency were all within-
observer variables. Bonferroni t-tests were used in multiple
comparisons among levels of the independent variables.
Perceptual describing functions were analyzed by performing
regression analyses with inverse-ISA and frequency.

ISA could be described in terms of altitude change or pitch
change (Table 1); there was a high correlation between pitch and
altitude change in this experiment (r=.935). However, the
displays differed in the way altitude changes were specified
(changes within the displays) but not in the way pitch changes
were specified (vertical movements of the display on the
monitor). In addition, altitude change was the criterion
variable in the compensatory control experiment that motivated
this investigation. For these reasons the analyses of ISA used
altitude change as the measure of simulated aircraft motion.

Comparison with Compensatory Control Data. Supplementary
data from a previous compensatory control experiment were also
analyzed (see Warren & Riccio, 1985, for details on the
experiment). Time histories, for the altitude error and for the
subject's control activity, from 24 post-training trials (four
replications from each of six subjects) were averaged for each of
the three displays and three altitudes. This was meaningful
since the forcing function was exactly the same for all trials.

125

Frequency spectra were derived by computing Fourier transforms for the eighteen average time histories.

The frequency spectra for control activity (subject's output) were divided by the corresponding spectra for altitude error (subject's input). This yielded "human-operator describing functions" for the nine experimental conditions. Regression analyses were performed on the describing functions (over the lowest five frequencies) to facilitate comparison with the perceptual describing functions from the present experiment.

RESULTS

Validity of the Psychophysical Technique

The magnitude estimates for the sinusoidal changes in pitch and altitude were compared to the median magnitude estimates for the SOS trials. This was done separately for each observer. 75% of the magnitude estimates for the pure sinusoids were less than the corresponding medians for the SOS trials. The technique was also applied to the baseline trials. 16% of the magnitude estimates were equal to or less than the the corresponding medians for the baseline trials. Consequently, psychophysical functions (and ISA) were based on perceived magnitudes of change that were broadly distributed from threshold levels to the levels experienced during a typical post-training trial in the compensatory control study. This increases the validity of comparisons between the present experiment and the compensatory control experiment.

Magnitude estimates can be related to changes in altitude or to changes in pitch. However, the amount of variance in the magnitude estimates that was due uniquely to altitude change was 3.3 times as great as that due uniquely to pitch change. The partial correlation between the log of the magnitude estimates and the log of altitude change is .120 (controlling for observer, display, altitude, frequency, and pitch change). The corresponding correlation for the log of pitch change is .066 (controlling for observer, display, altitude, frequency, and altitude change). The partial correlations provide some support for our assumption that altitude change is the primary observable in this study.

The psychophysical regression assumed that the relationship between (psychological) magnitude of motion and (physical) amplitude of altitude change was adequately described by a power function. The validity of this step was checked by evaluating the statistical significance of the linear correlation between the two log-transformed variables. The correlation was computed for each combination of observer, display, altitude, and frequency. The mean correlation was computed for each observer. The observer means were used to test the hypothesis that the overall correlation was greater than zero. The grand mean of correlations was .770, $t(5)=21.6$, $p<.0001$.

ISA is determined by looking at a point on each psychophysical function that corresponds to a particular subjective magnitude of motion. The results from the ANOVA on ISA are more meaningful, and are more generalizable, if they are

relatively insensitive to changes in the subjective magnitude
that is used as the reference. This would be the case if the the
psychophysical power functions (slopes from corresponding
regressions) were relatively homogenous. In fact, the 270 slopes
cluster fairly tightly around a mean value of 1.09 (standard
deviation = 0.45, skewness = -0.20, kurtosis = 7.78). Table 2
shows the mean slopes across levels of the main factors. The
homogeneity of slopes is also indicated by the partial
correlation between log magnitude and log altitude-change
(controlling for display, altitude, and frequency). The mean
partial correlation (over the six observers) is .749, t(5)=21.4,
p<.0001. The slopes must be homogenous for this correlation to
be close to the grand mean of simple correlations, r=.770.

Table 2. Exponents in the psychophysical power functions:
magnitude estimates related to amplitude of altitude change taken
to some power. Exponents were derived by·computing the slopes of
the linear regression between the log of psychological magnitude
and the log of physical amplitude. Power functions are provided
for each of the levels of the main factors in the experiment.
Frequency is specified in radians per second. Altitude is
specified in meters.

Frequency:	0.18	0.43	1.04	1.41	1.90
Exponents:	1.09	1.10	1.09	1.16	1.02

Display:	Combined	Dots	Roadway
Exponents:	1.11	1.09	1.08

Altitude:	13.7	27.4	54.9
Exponents:	0.97	1.17	1.13

Effects of the Experimental Manipulations

The mean (inverse) ISAs are presented in Figure 6, for each
frequency, display, and altitude. The results from the ANOVA on
ISA are summarized in Table 3. The effect of frequency is highly
significant. Bonferroni t-tests reveal significant differences
between all frequencies (critical difference = 1.72, p<.05). The
sensitivity of the visual system to pitch/altitude change
increases as frequency increases. The describing functions
(sensitivity as a function of frequency) were analyzed further
with quadratic regression (Table 4). In general, the describing
functions are adequately described by the linear component of the
regression. The mean slope of this linear trend is 3.18 decibels
per octave (db/oct). The mean slope of the human-operator
describing functions from the compensatory control experiment is
6.73 db/oct (Figure 6).
The effect of altitude is also highly significant.
Bonferroni t-tests show that while the two lowest altitudes are
significantly different, the two highest altitudes are not
(critical difference = 2.87, p<.05). Sensitivity of the visual
system to altitude change is inversely related to the mean

127
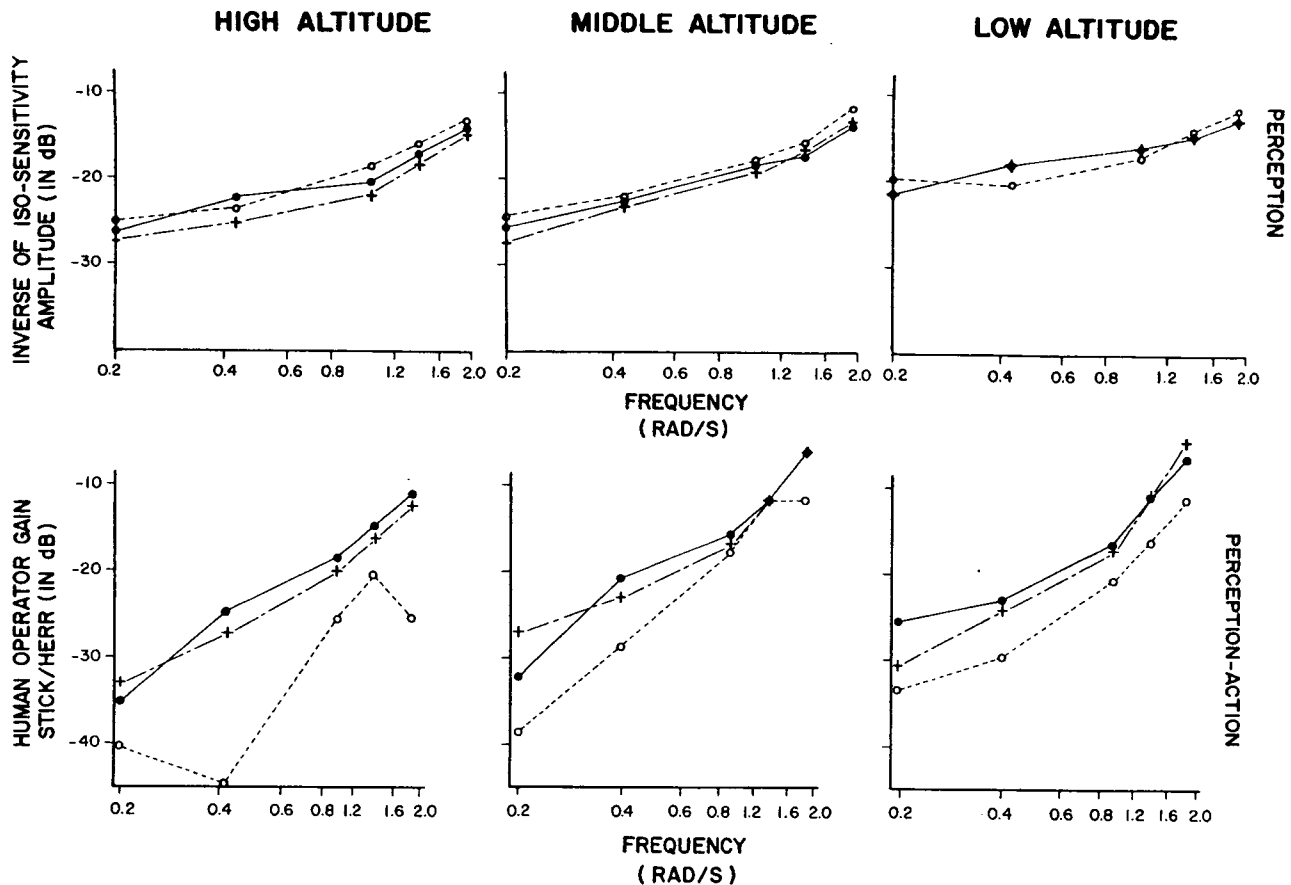
Figure 6. Upper panels show sensitivity as a function of
altitude, display, and frequency. Comparable human-operator
describing functions from a compensatory control experiment are
shown in the lower panels. Roadway data are indicated by the
solid line. Dots data are indicated by the dotted line. Data
for the combined display are indicated by dashes.

altitude. While such an effect is familiar in psychophysics,
quantitatively the relationship between sensitivity and altitude
does not follow a simple Weber, Fechner, or power function. All
these functions overestimate the difference in sensitivity
between the higher two altitudes (or underestimate the difference
between the lower two altitudes).

There is a significant interaction between altitude and
frequency. The slopes of the describing functions (as determined
by the linear component of the quadratic regression) for the
lowest altitude are about 27% lower than those for the other
altitudes. This is due to a greater sensitivity, at the lowest
altitude, to low frequencies of altitude change.

On the average, sensitivity of the visual system to altitude
change is greatest for the dots and least for the combined
display. However, the effect of display is not significant.
There is a significant interaction between display and frequency.
The describing functions for the dots, but not the roadway
display, reveal quadratic trends (Table 4). The dots display is

128

Table 3. Nonadditive model analysis of variance for iso-
sensitivity amplitude. Each source of variance that is marked by
an asterisk is the error term for the effect(s) listed
immediately above it.

Source of Variance	df	SS	F	p≤
Frequency	4	4371	136.21	0.0001
*Frequency x Observer	20	160	--	--
Display	2	60	3.19	0.0849
*Display x Observer	10	94	--	--
Altitude	2	627	17.64	0.0005
*Altitude x Observer	10	178	--	--
Frequency x Altitude	8	97	4.20	0.0010
*Freq x Alt x Obs	40	115	--	--
Frequency x Display	8	46	4.23	0.0010
*Freq x Disp x Obs	40	54	--	--
Altitude x Display	4	45	1.24	0.3247
*Alt x Disp x Obs	20	179	--	--
Freq x Alt x Disp	16	33	1.84	0.0400
*Freq x Alt x Disp x Obs	80	90	--	--
Observer	5	578	--	--

Table 4. Stepwise quadratic regression for perceptual describing
functions (Figure 6): log(inverse-ISA) is modelled as a
quadratic function of log(frequency). R-square is for the simple
regression that evaluates the linear relationship between
log(inverse-ISA) and log(frequency). Delta-R-square is for the
partial regression that evaluates the nonlinear relationship
between log(inverse-ISA) and log(frequency), after taking into
account the contribution of the linear relationship. Asterisks
indicate F-ratios for the respective regressions that are
statistically significant (p<.05, df=1,2).

	Altitude (m)					
	13.7		27.4		54.9	
	R^2	ΔR^2	R^2	ΔR^2	R^2	ΔR^2
Displays						
Combined	.9674*	.0005	.9752*	.0079	.9041*	.0768
Dots	.8342*	.1653*	.9124*	.0784	.9545*	.0444
Roadway	.9673*	.0006	.9738*	.0172	.9435*	.0204

129

superior at the lowest and highest frequencies.

There is a marginally significant three-way interaction between display, altitude, and frequency. While this effect is complex, it can be seen in Figure 6 and Table 4. The shapes of the describing functions for the three displays change in different ways as mean altitude decreases: The describing function for the dots display becomes more concave; concavity decreases for the combined display; and there are no marked changes for the roadway display.

Three of the six observers had previous experience with the displays in a compensatory control experiment. A preliminary ANOVA included the observers' experience as a variable. None of the effects involving experience were close to statistical significance ($p > .2$). Consequently, this variable was removed from the ANOVA summarized in Table 3.

DISCUSSION

Perception of Altitude Change

There seem to be no important differences among the three displays with respect to the overall sensitivity of the visual system to altitude change. One could argue that the magnitude estimates were determined by pitch changes which were specified in similar ways in the three displays (vertical movements of the horizon). However, this is unlikely for several reasons: (1) Altitude change accounts for more variance in the magnitude estimates than does pitch change. Pitch changes were probably difficult to see because they were very small and were specified by absolute movements on the display screen. On the other hand, altitude changes were sometimes quite large (relative to the reference altitude) and were specified by relative movements within the display. (2) There are three statistically significant effects due to manipulation of the reference altitude. While this manipulation has no effect on the appearance of pitch changes, it has very noticeable effects on the appearance of altitude changes.

It was suggested that the superiority of the roadway displays in the compensatory control experiments was due to more accurate perception of instantaneous altitude with respect to the assigned altitude. The data from the present experiment strengthen this hypothesis insofar as they provide evidence against the only likely alternative. Another psychophysical experiment is warranted. For example, observers could be presented with constant-altitude trials where their task would be to indicate whether the presented altitude was the same as or different from a previously presented reference altitude; ROC curves could then be constructed for the three displays.

The perceptual describing functions depicted in Figure 6 provide insight into the characteristics of the visual system. In general they indicate that the visual system becomes less sensitive to changes in altitude as the change becomes more gradual (i.e., of lower frequency). This is consistent with the hypothesis that another skill -- the perception of instantaneous

130

altitude relative to the assigned altitude -- becomes useful at
low frequencies of change. The slopes of the describing
functions indicate that, with respect to the pick up of
information about changes in altitude, the visual system can be
described neither as a differentiator (slope of 6 db/oct) nor as
a simple gain (slope of 0 db/oct), but as something intermediate.
Integer derivatives seem to be rare in the perception of natural
objects and events (Flach, et al., in press; Scott Blair, 1956).

The describing functions vary with both display and
altitude; that is, there are interactions between these variable
and frequency (Table 3). These interactions suggest that the
pick up of information about change in altitude utilizes
different perceptual skills for the roadway and dots displays.
This is plausible for two reasons: (1) angles and flow fields are
very different patterns of optical stimulation. (2) In previous
studies, we found very poor transfer of training between the two
displays (Warren & Riccio, 1985).

One salient feature of the three-way interaction between
frequency, display, and altitude is the relatively low
sensitivity for the combined display at the highest altitude.
This may be evidence for masking of changes in the roadway by the
flow field (the dots). Sensitivity of such an effect to altitude
and frequency is certainly not inconsisent with a masking
interpretation. These variables both influence the changes in
the roadway and dots displays. However, different procedures
would be required to elucidate the mechanisms of such masking.

Comparison of Perception and Control

In figure 6 the perceptual describing functions from this
experiment are compared with the human-operator describing
functions from a previous compensatory control experiment. Any
differences between corresponding describing functions from the
two experiments should be due to the characteristics of the
action (motor) system or to strategies for action (control
behavior).

One difference between the two sets of describing functions
is that the human-operator describing functions are steeper.
These curves suggest that the human operator can be described as
a differentiator of altitude. Since pitch angle is monotonically
related to change in altitude, the human operator could also be
described as a simple gain with respect to pitch. However, there
were statistically significant effects involving both display and
assigned altitude in the compensatory control experiments (Warren
& Riccio, 1985). It follows that pitch information must have
been less important than information about changes in altitude.

Another striking difference between the two data sets is
that the human operator has lower gain for the dots display than
for the other two displays; that is, compensatory actions are
less effective when feedback about performance is provided by the
dots display. This cannot be explained by the perception of
changes in altitude. We have suggested that the most likely
alternative involves the perception of instantaneous altitude
relative to the assigned altitude. How can this account for
differences in the human-operator gain over the frequency range

131

presented in Figure 6? There is evidence -- from informal reports and from inspection of several time histories -- that subjects gradually drifted away from the assigned altitude when viewing the dots display. Such drift is eventually noticed when the altitude error becomes large enough. We believe that on such occasions, subjects would momentarily depart from linear compensation, inject a strong control pulse, and move as quickly as possible to a more appropriate altitude.

The periods during which linear compensation is suspended would result in the lower gain observed in the human-operator describing function for the dots display. The nonlinear control pulse would lead to large increases in remnant (activity not linearly correlated with the forcing function). This has also been observed for the dots display (Zacharias, et al., 1986). It should also be noted that the stick signal reached saturation much more often with the dots display. Saturation resulted from large control pulses that exceded the limits of the analog computer.

Broader Implications

We have suggested (Warren & Riccio, 1985) that some experience with impoverished displays is desirable. The argument is that some real-world environments (such as deserts or oceans) are visually risky or impoverished, and that training with visually rich displays does not allow one to develop the perceptual skills required for visually impoverished enviroments. The results from the present study suggest that performance with "impoverished" displays may even be as good as that with "rich" displays in some situations. More research on the practical utility of impoverished displays seems warranted.

The results of this experiment demonstrate that passive psychophysical paradigms are useful adjuncts to experiments on active control. The magnitude matching data complemented the compensatory control data. Together they led to conclusions that would not have been possible with either of the experiments alone. Moreover, the data from passive psychophysical experiments can be useful in deriving predictive mathematical models for human-operator behavior. For example, the data can be useful in "calibrating" displays (Levison & Warren, 1984); that is, to determine the sensitivity of the perceptual systems to the information contained therein. Such procedures can also be useful in matching performance levels and control behavior, and possibly in optimizing transfer of training, between two devices (Flach, et al, in press).

132

REFERENCES

Gibson, J.J. (1950). The perception of the visual world. Boston: Houghton-Mifflin.

Flach, J.M., Riccio, G.E., McMillan, G.R. & Warren, R. (in press). Psychophysical methods for equating performance between altenative motion simulators. Ergonomics, 29.

Koenderink, J.J. (1986). Optic Flow. Vision Research, 26, 161-180.

Levison, W.H. & Warren, R. (1984). Use of linear perspective scene cues in a simulated height regulation task. Twentieth Annual Conference on Manual Control (Conference Publication 2341, pp. 1-24). Moffett Field, CA: NASA Ames Research Center.

Levison, W.H., Zacharias, G.L., & Sinacori, J.B. (1982). Design of an experiment to study the pilot's use of visual and motion cues in a height-regulation task (Tech. Rep. No. 5028). Cambridge, MA: Bolt, Baranek, & Newman.

Owen, D.H., Warren, R., Jensen, R.S., Mangold, S.J. & Hettinger, L.J. (1981). Optical information for detecting loss in one's forward speed. Acta Psychologia, 48, 203-213.

Scott Blair, G.W. (1956). Measurement of mind and matter. London: Philosophical Library.

Stevens, J.C. & Marks, L.E. (1980). Cross-modality matching functions generated by magnitude matching. Perception & Psychophysics, 27(5), 379-389.

Warren, R. & Riccio, G.E. (1985). Visual cue dominance hierarchies: Implications for simulator design. SAE Technical Paper Series (851946). Warrendale, PA: Society of Automotive Engineers.

Zacharias, G.L., Warren, R. & Riccio, G.E. (in press). Modeling the pilot's use of flight simulator visual cues in a terrain-following task. Proceedings of the 22nd Annual Conference on Manual Control (July, 1986; Dayton, OH).

ACKNOWLEDGEMENTS

STEREO DEPTH ILLUSIONS IN TELEOPERATION

Two converged cameras, viewing a workspace and presenting a stereo view to a teleoperator, can cause stereo depth illusions. Two critical variables are the intercamera angle, and the centering alignment of the image on the stereo monitor.

For a fixed viewing distance (1.2 meters), we have measured errors on the order of two centimeters of depth.

Larger intercamera angles cause greater depth illusions.

Image centering misalignments can be caused by the panning of, or by horizontal motions of, the cameras with respect to the work location. We have investigated both, and find greater depth illusions due to horizontal motions.

Thus, to insure higher precision in stereo depth teleoperation, one must take great care in the initial horizontal alignment of the cameras

Dr. Daniel B. Diner
Mail Stop 23
Jet Propulsion Laboratory
California Institute of Technology
4800 Oak Grove Drive
Pasadena, California 91109

VIDEO FEEDBACK FOR HUMAN CONTROLLED TELEROBOTS

Telerobotic systems are robotic manipulator systems operated by a human operator from a remote control station. The system relies on the operator to control and direct the task activities. The operator generates control signals from a hand control device while the task environment and manipulator actions are relayed to the operator by various sets of sensors, primarily visual. Task performance is highly dependent on the quality of the visual displays, depth information, and the angle of view. This paper examines these aspects of vision systems and discusses experiments comparing stereo vision systems with two monocular cameras and experiments examining the task dependency of view angle.

Eric Byler
Erik Eriksen
Grumman Space Systems
5/30/86

Reduction of Biodynamic Interference In

Helmet Mounted Sights and Displays

Mordekhai Velger

Aero-Space Human Factors Research Division
NASA Ames Research Center Moffett Field, CA 94035

Shmuel Merhav

Department of Aeronautical Engineering
Technion, Israel Institute of Technology, Haifa, 32000 Israel

Summary

An adaptive filtering technique for the reduction the effects of whole-body and head vibrations on helmet mounted displays and sights is proposed. The voluntary and involuntary head commands are estimated from the measured head motion. The estimated voluntary commanded head motion is used to drive a slaved device thus increasing its pointing accuracy. The estimated involuntary head commands are used for image stabilization in the Helmet Mounted Display to retain visual acuity of the viewer while subjected to platform vibrations. System modeling and computer simulations are presented. The results indicate the potential effectiveness of the method.

I. Introduction

Work on head coupled devices such as Helmet Mounted Sights or displays have been prompted by the growing need to reduce pilot workload in the increasing com-

plexity manual of control tasks. Such systems are needed either for pointing a device in the direction of the line-of-sight, or for displaying information to the pilot regardless of his viewing direction. In the first application, the system employs a cockpit-located transducer and a helmet mounted sensor from which the position of the head, and thus, the line of sight, is calculated. In such systems, whether it is a simple target aiming sight reticle or a more structured image display, a visual image is partially reflected from an optical surface in front of the eye and collimated to infinity. Head-coupled systems potentially offer a considerable advantage over conventional panel-mounted display and hand manipulator controlled systems. However, under conditions of vehicular vibrations, a major limitation of the helmet-coupled systems is apparent (1). Under these conditions the aiming accuracy, as well as, reading performance may be severely degraded due to two main factors: (i) Involuntary head motion due to vibrations; (ii) Impairment of visual acuity.

Visual acuity degradation in the presence of aircraft vibrations results from the reflexive eye movements induced by the stimulation of the vestibular system of the inner ear. The normal function of the vestibulo-ocular reflex (VOR) is to induce an eye movement which is opposite to that of the head, thus maintaining a stationary point of regard of the eye and enabling earth-fixed objects to be viewed during normal locomotor activities. However, for the display which moves with the head, the vestibular induced eye movement is undesirable because it produces a relative motion between the viewed image on the display and the eye. Hence, to preserve visual acuity, this vestibular reflex must be suppressed. The principal mechanism available for such suppression is the pursuit or fixation reflex of the visual control system. But the

visual control system is known to exhibit a severe performance degradation when either the angular velocity of the target movement exceeds approximately 60 deg/sec or exceeds a frequency of 1-2 Hz. Thus, under these conditions the control system of the eyes cannot compensate for these relative motions and visual acuity is degraded.

The natural approach for retaining the visual acuity in helmet mounted displays is to minimize the relative motion between the viewed image and the eye by shifting the image on the display in the same direction and magnitude as the induced reflexive eye movement. i.e. stabilize the image in the space. This approach was adopted by Wells and Griffin (2). They measured the rotational acceleration at the display and after integrating twice the signal was fed to the cathode ray tube so as to deflect the image in antiphase to the display movement. Using this method a considerable improvement in reading performance was achieved i.e., the number of numerals correctly read increased and the time to read these numerals, was lessened. However, the method of Wells and Griffin has two major deficiencies: (i) The use of angular acceleration as a source for the stabilization technique necessitates high-pass filtering of the input signal to remove d.c. components which might result in unbounded image shifting commands. The high-pass filter introduces phase leads in the shifting algorithm which limit the effectiveness of the method: (ii) The technique does not allow voluntary low frequency head commands. because they might result in unintentional large image motions. This limits the usefulness of the technique considerably, since most applications involve voluntary pilot head movements.

An attempt to preserve the aiming accuracy using a helmet mounted sight. in the presence of motion. is reported by Tatham (3). He experimented with three

techniques for improving aiming accuracy. The first technique, which was low-pass filtering on the head motion signal, achieved an improvement of 50% in the aiming accuracy. However, the drawback of this method is that a significant time delay was introduced into the system. The second method involved the pilot marking the instants he considered of more accurate aiming. This method showed no improvement in the aiming accuracy. In the third method, the helmet sight output was scaled down to provide less sensitivity to the involuntary head motion. However, since the one-to-one correspondence between head attitude angle and spatial aiming angles was not maintained, the target as well as an aiming cursor had to be shown on the display. Although a marked improvement in aiming accuracy was achieved in this method, the main advantages of the helmet mounted display were essentially not exploited.

It has recently been shown by Velger et al (4) that adaptive filtering techniques can significantly reduce the adverse effects of biodynamic interference in hand manipulation control tasks.

This paper presents a method for increasing the aiming accuracy of a helmet mounted sight and for its display stabilization under the conditions of motion and vibrations. The method employs adaptive filtering techniques for estimation of the voluntary and involuntary head attitude. The estimated voluntary head movements are used to drive the pointing device, while the involuntary head movements are used for the image stabilization scheme.

II. System Modelling and the Adaptive Filtering Concept

The model of the man-machine system, using a Helmet Mounted Display/Sight (HMD/HMS) on board a moving platform, is shown in Fig. 1. The scenario described in Fig. 1 is of a human operator pointing a device at a moving target using head movements. The head attitude relative to the platform θ_H, is measured by a head orientation tracking system. The measured head attitude θ_{Hm} is used as a command to the pointing device. The head involuntary commands θ_{HB}, appear as an additive noise to the voluntary head commands. The total head motion invokes eye movements θ_{EH} relative to the head. The adaptive filter employs the platform acceleration and the head orientation for estimating the involuntary head motion. These are used, after an appropriate transformation to shift the image on the HMD in the same amplitude but in antiphase to the head motion. Moreover, the adaptive filter provides estimates of the voluntary head commands which are directed to the slaved device. The acceleration signal is filtered by a band-pass filter before it is processed by the adaptive filter. The band-pass filter is used so that the adaptive filter processes signals only in the frequency range of 1-8 Hz. The low frequency filtering is required since humans often tend to adjust their posture in order to accommodate to a certain vehicle maneuver. This may be interpreted by the adaptive filter as a biodynamic interference. The high frequency filtering is included since in this range the VOR is ineffective and the eyes tend to follow the head movements. Hence, it is preferable that the image is not shifted on the display in the high frequency region.

III. The Adaptive Filter Algorithm

Several adaptive estimation algorithms were tested by computer simulations. The basic requirement from the adaptive filter was to enable estimation of the involuntary head motion with an error smaller than 2 mrad RMS and a sufficiently short convergence time. The adaptive filtering method that was found to be the most suitable for estimation of the voluntary as well as the involuntary head movements is a variant of the Instrumental Variable Approximate Maximum Likelihood (IVAML) method, Young (5).

The total head command (θ_H) is the sum of the voluntary head command (θ_{HC}) and the involuntary head motion (θ_{HB})

$$\theta_H(t) = \theta_{HC}(t) + \theta_{HB}(t) \tag{1}$$

In Eq. (1) and in the sequel t is discrete time. The voluntary head commands θ_{HC} are assumed to be uncorrelated with the involuntary commands. Typically θ_{HC} is a low frequency and large amplitude signal while, θ_{HB} is characterized by higher frequencies and smaller amplitudes. Assume the following input-output model for the biodynamic system

$$\theta_{HB}(t) = H(q^{-1})a(t) \tag{2}$$

Where $a(t)$ is the acceleration of the platform. $H(q^{-1})$ is a polynomial of order N_H and the following form:

$$H(q^{-1}) = h_0 + h_1 q^{-1} + \cdots + h_{N_H} q^{-N_H}$$

q^{-1} is the unit delay operator, i.e., $q^{-1}a(t) = a(t-1)$.

Substitute Eq. (2) in Eq (1) yields

$$\theta_H(t) = H(q^{-1})a(t) + \theta_{HC}(t) \tag{3}$$

Both the total head motion θ_H and the platform acceleration are measurable signals. The last term in Eq. (3) can be interpreted as a noise in the measurement equation. The formulation of Eq. (3) is a proper form to estimate the parameters of $H(q^{-1})$ using a standard least squares technique. However, because of the very low signal-to-noise ratio, the convergence rate may be very slow. This is overcome by using Instrumental Variables instead of the measured signals.

Let us model θ_{HC} as an auto-regressive process

$$\theta_{HC}(t) = \frac{1}{D(q^{-1})} \eta(t) \tag{4}$$

Where $\eta(t)$ is a zero-mean Gaussian white-noise process. $D(q^{-1})$ is a polynomial of order N_D of the following form:

$$D(q^{-1}) = 1 + d_1 q^{-1} + \cdots + d_{N_D} q^{-N_D}$$

Substitute Eq. (4) in Eq. (3) and multiply by $D(q^{-1})$ yields

$$D(q^{-1})\theta_H(t) = H(q^{-1})D(q^{-1})a(t) + \eta(t) \tag{5}$$

Define the following data vector

$$\xi(t) = [a(t) \ldots \ldots a(t-N_H)]^T \tag{6}$$

and the following N_H dimensional instrumental variable vector

$$\phi(t) = D(q^{-1})\xi(t) \tag{7}$$

145

Also define the scalar $\bar{\theta}_H$ as

$$\bar{\theta}_H(t) = D(q^{-1}) \theta_H(t) \tag{8}$$

and the following parameter vector

$$\pi_1 = [h_0 \ldots \ldots h_{N_H}]^T \tag{9}$$

Substitute the definitions (6)-(9) in Eq. (5). Then Eq. (5) becomes

$$\bar{\theta}_H(t) = \pi_1^T \phi(t) + \eta(t) \tag{10}$$

Now the noise term in the measurement equation is white. This is an important factor in achieving rapid convergence of the parameters in the algorithm described here. However. Eq. (10) as shown cannot be directly implemented since the parameters of the "whitening filter" $D(q^{-1})$ are unknown. The way to overcome this problem is to replace the polynomial $D(q^{-1})$ by its estimate. To estimate the polynomial $D(q^{-1})$ let us assume for a moment that the polynomial $H(q^{-1})$ is known. Then from Eq. (3) the voluntary head command is

$$\theta_{HC}(t) = \theta_H(t) - H(q^{-1}) a(t)^{\pm} \tag{11}$$

Since the polynomial $H(q^{-1})$ is unknown let us replace it by its recent estimate $\hat{H}(q^{-1})$. thus forming the model:

$$v(t) = \theta_H(t) - \hat{H}(q^{-1}) a(t) \tag{12}$$

We now define the data vector

$$\psi(t) = [-v(t-1). \ldots . -v(t-N_D)]^T \tag{13}$$

And a parameter vector

$$\pi_2 = [d_1 \ldots \ldots d_{N_D}]^T \tag{14}$$

The estimation process is performed recursively in two steps. In the first one the parameter vector π_1 is estimated by using the previous estimate of π_2. In the second step the parameter vector π_2 is estimated utilizing the recent estimate of π_1. This can also be interpreted as estimating in step 1 the involuntary head motion while in step 2 the voluntary head commands.

Step 1

Update the parameter vector π_1 according to

$$\hat{\pi}_1(t) = \hat{\pi}_1(t-1) + \gamma(t)L_1(t)e(t) \tag{15}$$

Where the prediction error $e(t)$ is

$$e(t) = \bar{\theta}_H(t) - \hat{\pi}_1^T(t-1)\,\phi(t) \tag{16}$$

$L_1(t)$ is the following gain vector of dimension N_H

$$L_1(t) = R_1^{-1}\,\phi(t) \tag{17}$$

The $N_H \times N_H$ covariance matrix R_1 is updated according to

$$R_1(t) = R_1(t-1) + \gamma(t)[\phi(t)\phi^T(t) - R_1(t-1)] \tag{18}$$

Where $\gamma(t)$ is a given gain sequence.

Step 2

Update the parameter vector $\hat{\pi}_2$ according to

147

$$\hat{\pi}_2(t) = \hat{\pi}_2(t-1) + \gamma(t)L_2(t)\epsilon(t) \tag{19}$$

Where the prediction error is

$$\epsilon(t) = v(t) - \psi^T(t)\hat{\pi}_2(t-1) \tag{20}$$

$L_2(t)$ is the following gain vector of dimension N_D

$$L_2(t) = R_2^{-1}\phi(t) \tag{21}$$

The $N_d \times N_d$ covariance matrix $R_2(t)$ is updated by

$$R_2(t) = R_2(t-1) + \gamma(t)[\psi(t)\psi^T(t) - R_2(t-1)] \tag{22}$$

The computation of the gain vectors $L_1(t)$ and $L_2(t)$ requires inversion of the matrices $R_1(t)$ and $R_2(t)$. There are several ways to compute the gain vector $L(t)$ without inverting the matrix $R(t)$. Since our application is to be implemented in real time we will use the so-called "Fast Algorithms" (6) to compute directly the gain vector $L(t)$. These algorithms require on the order of n, rather than n^2, operations per time step. The complete "Fast Algorithm" is presented in the Appendix.

IV. Description of the Simulation

A computer simulation of the system described in Fig. 1 was performed. The biodynamic model, taken from Riedel et al (7), is used to describe the rotational head response of a seated pilot to vertical acceleration. The model is formulated as a transfer function of order of 11

$$\frac{\ddot{\theta}_{HB}}{a}(s) = \frac{\kappa\left(s + \dfrac{1}{T_z}\right)\prod_{1}^{3}(s^2 + 2\varsigma_z\omega_z s + \omega_z^2)}{\left(s + \dfrac{1}{T_p}\right)\prod_{1}^{5}(s^2 + 2\varsigma_p\omega_p s + \omega_p^2)} \tag{23}$$

The poles and zeros of the transfer function are summarized in Table 1. A bode plot is shown in Fig. 2. The head orientation measuring system. is simulated as the Magnetic Position and Orientation Tracking System (MPOTS) and is described in Ref. 8. The platform acceleration a was modeled by a sum of 8 randomly phase shifted sines with frequencies ranging from 2.5 Hz to 12.5 Hz. The frequencies and amplitudes of the sine waves are given in Table 2. The RMS value of the acceleration for this input sequence is 1.5 $m/\sec^2$. The target motion c too is modeled by the sum of 8 sines ranging. between 0.016 Hz to 1 Hz. Their frequencies and amplitudes are given in Table 3.

It is assumed here that the target motion is uncorrelated with the platform motion. and that the operator precisely tracks the target. Thus. the control head commands can essentially be replaced by the angular target motion.

The adaptive filter in the simulation has $N_H = 24$ parameters in step 1. and $N_D = 4$ parameters in step 2. Both parameter vectors were initialized from 0.

V. The Simulation Results

Fig. 3 shows the head voluntary and total motion. The total motion consists of a low frequency large amplitude signal which represents the voluntary head commands. corrupted by a high frequency small amplitude biodynamic interference. The

signal representing the voluntary head motion, indicates the limited bandwidth of the human operator as well as the large control commands experienced in a typical tracking task. In spite of the distinct spectral separation between the two components of the total signal, the obvious approach of high-pass filtering the signal is not appropriate. This is mainly due to the very high voluntary to involuntary signal ratio. Consequently, the approach of high-pass filtering would cause significant distortions, especially due to residual phase shifts, which are incompatible with the stringent requirements for the stabilization of the image.

The results of the adaptive filtering are shown in Fig. 4 to Fig. 6. Fig. 4 shows the true and estimated biodynamic interference. It can be seen that after a short learning process the signal is estimated with very high accuracy. The voluntary head command estimation process is shown in Fig. 5. As before, the estimated voluntary head command is achieved with high accuracy. In Fig. 6 the difference between the estimated and true biodynamic interference is compared with the biodynamic interference. This signal describes the relative motion between the displayed image and the viewer's eye. It is shown that this relative motion is essentially zero thus, a good image stabilization is achieved, implying that the adaptive filtering scheme enables a substantial improvement of the legibility of a helmet mounted display.

Since that the estimation of the involuntary head command is highly dependent on the estimate of the voluntary head commands through the parameters of the filter $D(q^{-1})$, a question may arise about the quality of the estimate when the operator changes the nature of his control activity. This activity may often change rapidly from a random tracking mode to fixed direction of head orientation. This may require

rapid changes in the parameters of the filter $D(q^{-1})$. In order to examine the effect of a rapid change in the control activity of the operator. a simulation was performed where the control activity was changed according to the sequence shown in Fig. 7a. These commands were obtained by multiplying the previous control sequence (as shown in Fig. 7b) by the weighting function shown in 7c. The estimation results are shown in Fig. 8 and Fig. 9. It can be seen from Fig. 8 that the voluntary head command is still estimated with a very high accuracy in spite of the dramatic changes in the signal. Fig. 9. showing the biodynamic interference together with its estimation error $(\theta_{HB} - \hat{\theta}_{HB})$. The results indicate that the changes in the nature of the voluntary head commands essentially have no effect on the estimation of the involuntary head motion. This example shows that once the adaptive filter has converged to its asymptotic value. a good estimation of the voluntary and involuntary head commands will be maintained.

VI. Conclusions

The biodynamic model used predicts that platform accelerations in the level of 0.1g RMS result in head angular motion of 20 mrad RMS. It was shown in previous works (1.2) that these levels of accelerations may significantly impair the usefulness of helmet mounted displays/sights. The adaptive filtering technique based on the IVAML algorithm, enables the estimation of both the voluntary and involuntary head motion with an error smaller than 2 mrad. which is the accuracy of the measuring sensor. The method is not sensitive to head voluntary commands as earlier methods and does not require high pass filtering of the head orientation signal. Thus no phase

shifts in the estimated signals occur. The proposed filtering scheme. is equally effi-
cient in cases where either the biodynamic interference are not present or when no
voluntary control commands are generated by the operator.

Acknowledgement

Appendix

The problem is to compute the gain vector $L(t)$ given by

$$L(t) = \gamma(t)R^{-1}(t)\psi(t) \tag{A1}$$

Without inverting the $N \times N$ matrix R. which is given by

$$R(t) = R(t-1) + \gamma(t)[\psi(t)\psi^T(t) - R(t-1)] \tag{A2}$$

The vector $\psi(t)$ is defined as

$$\psi(t) = \begin{pmatrix} x(t-1) \\ \cdot \\ \cdot \\ \cdot \\ x(t-N) \end{pmatrix}$$

Then the algorithm for "fast" calculation of the gain matrix is (see Ref. 6 for details)

1. Initialize:

$$A(0)=0, \quad B(0)=0, \quad R^e(0)=\delta, \quad L(1)=0$$

2. Given $A(t-1)$. $B(t-1)$. $R^e(t-1)$. $L(t)$. update:

$$e(t) = x(t) + A^T(t-1)\psi(t) \tag{A3}$$

$$A(t) = A(t-1) - L(t)e^T(t) \tag{A4}$$

$$\beta(t) = L^T(t)\psi(t) \tag{A5}$$

$$\bar{e}(t) = [1-\beta(t)]e(t) \tag{A6}$$

$$R^e(t) = \lambda R^e(t-1) + \bar{e}(t)e^T(t) \tag{A7}$$

$$L^*(t) = \begin{pmatrix} \bar{e}(t)/R^e(t) \\ L(t) + A(t)\bar{e}(t)/R^e(t) \end{pmatrix} \tag{A8}$$

Partition $L^*(t)$ as

$$L^*(t) = \begin{pmatrix} M(t) \\ ---- \\ \mu(t) \end{pmatrix} \begin{matrix} N\ \ elements \\ --- \\ last\ \ element \end{matrix} \tag{A9}$$

Compute:

$$r(t) = x(t-n) + B^T(t-1)\psi(t+1) \tag{A10}$$

$$B(t) = \frac{B(t-1) - M(t)r(t)}{1 - \mu(t)r(t)} \tag{A11}$$

$$L(t+1) = M(t) - B(t)\mu(t) \tag{A12}$$

Where:

$A(t)$. $B(t)$. are n dimensional vectors. $e(t)$. $\beta(t)$. $\bar{e}(t)$. $R^e(t)$. $\mu(t)$. $r(t)$. are scalars.

References

1)   Benson. A.J.. and Barnes. G.R.. "Vision During Angular Oscillation: The Dynamic Interaction of Visual and Vestibular Mechanisms." Aviation Space Environ. Med. 49:340-345. Jan 1978.

2)   Wells, M.J., and Griffin, M.J., "Benefits of Helmet-Mounted Display Image Sta-

bilisation Under Whole-Body Vibration." Aviation Space Environ. Med. 55:13-

18, Jan 1984.

3)   Tatham, N.O., "The Effect of Turbulence on Helmet Mounted Sight Accura-

cies." AGARD CP-267, March 1980.

4)   Velger, M., Merhav, S. and Grunwald, A., "Effects of Adaptive Filtering in

Manual Control on Board Moving Platforms", TAE Report No. 583, Department

of Aeronautical Engineering, Technion Israel Institute of Technology, November

1985.

5)   Young, P., "Some Observations on Instrumental Variable Methods of Time-

Series Analysis." Int. J. of Control, Vol. 23, No. 5, pp. 593-612, 1976.

6)   Ljung, L., and Soderstrom, T., Theory and Practice of Recursive Identification,

The MIT Press, Cambridge Mass, 1983.

7)   Riedel, S.A., Magdaleno, R.E., and Jex, H.R., "User's Guide to BIODYN-80: An

Interactive Software Package for Modelling Biodynamic Feedthrough to a pilot's

hands, Head and Eyes." Systems Technology Inc., Tech. Rept. No. 1146-1,

Dec 1980.

8)   Raab, F.H., Blood, E.B., Steiner, T.O., and Jones, H.R., "Magnetic Position

and Orientation Tracking System." IEEE Trans. on Aerosp. Electron. Sys., Vol.

Table 1. Poles and Zeroes of the Biodynamic Model

	$\frac{1}{T} \cdot \varsigma$	ω
Zeroes	18.284	
	0.458	10.396
	0.098	16.203
	0.236	51.815
Poles	58.788	
	0.265	10.914
	0.203	12.943
	0.354	26.761
	0.151	29.611
	0.191	57.483

Table 2. Frequencies and Amplitudes of the Z-Axis Vibration Signal

Frequency (Hz)	2.5	3.15	4.0	5.0	6.3	8.0	10.0	12.0
Amplitude (m / sec^2)	1.9	1.69	1.53	1.5	1.5	1.5	1.87	2.34

Table 3. Frequencies and Amplitudes of the Target Motion Signal

Frequency (Hz)	0.016	0.08	0.16	0.24	0.32	0.48	0.64	0.95
Amplitude (deg)	5.7	5.7	5.7	4.58	2.86	1.72	0.57	0.29
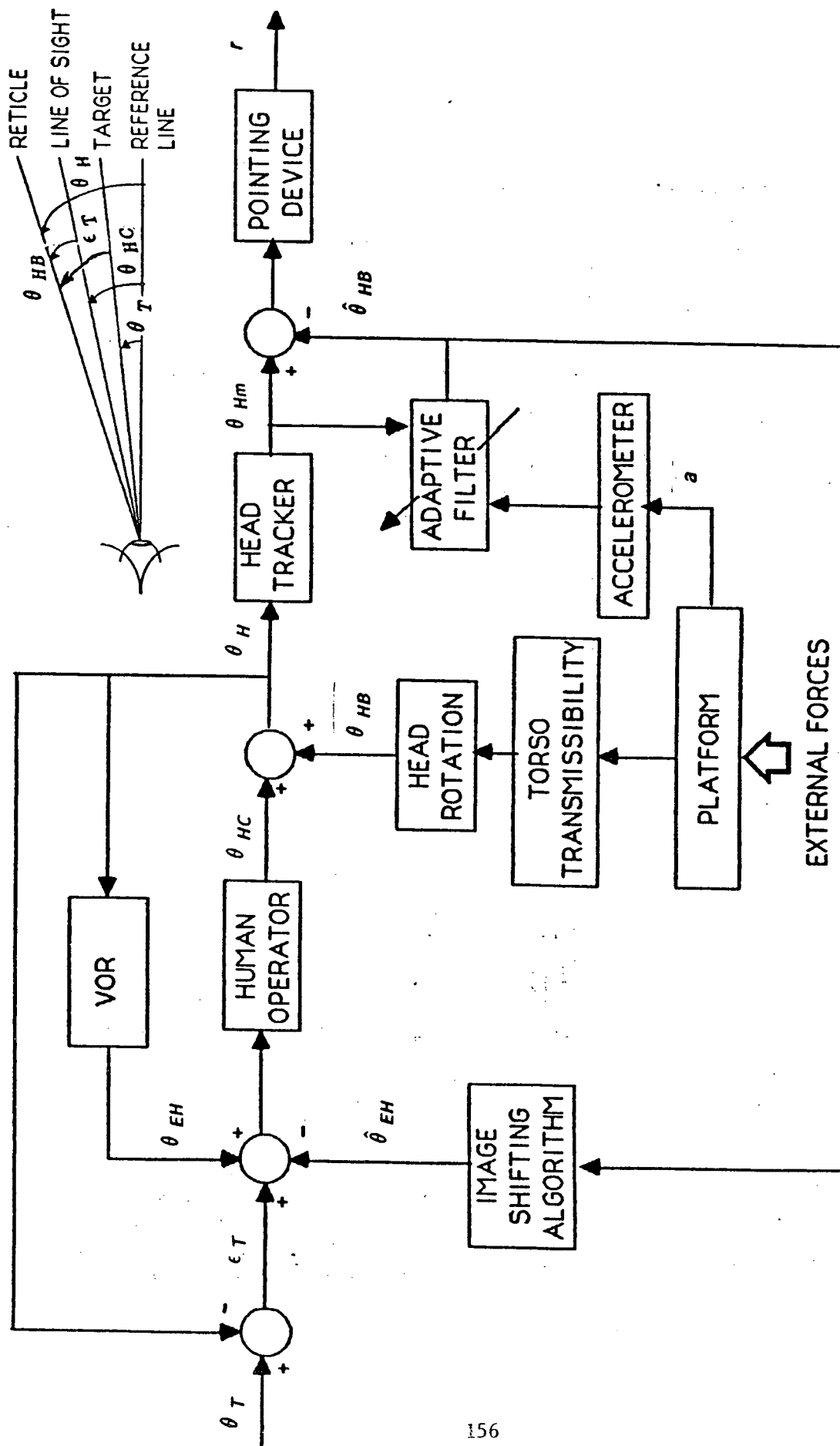
Fig. 1 System Modeling and Adaptive Filtering Concept
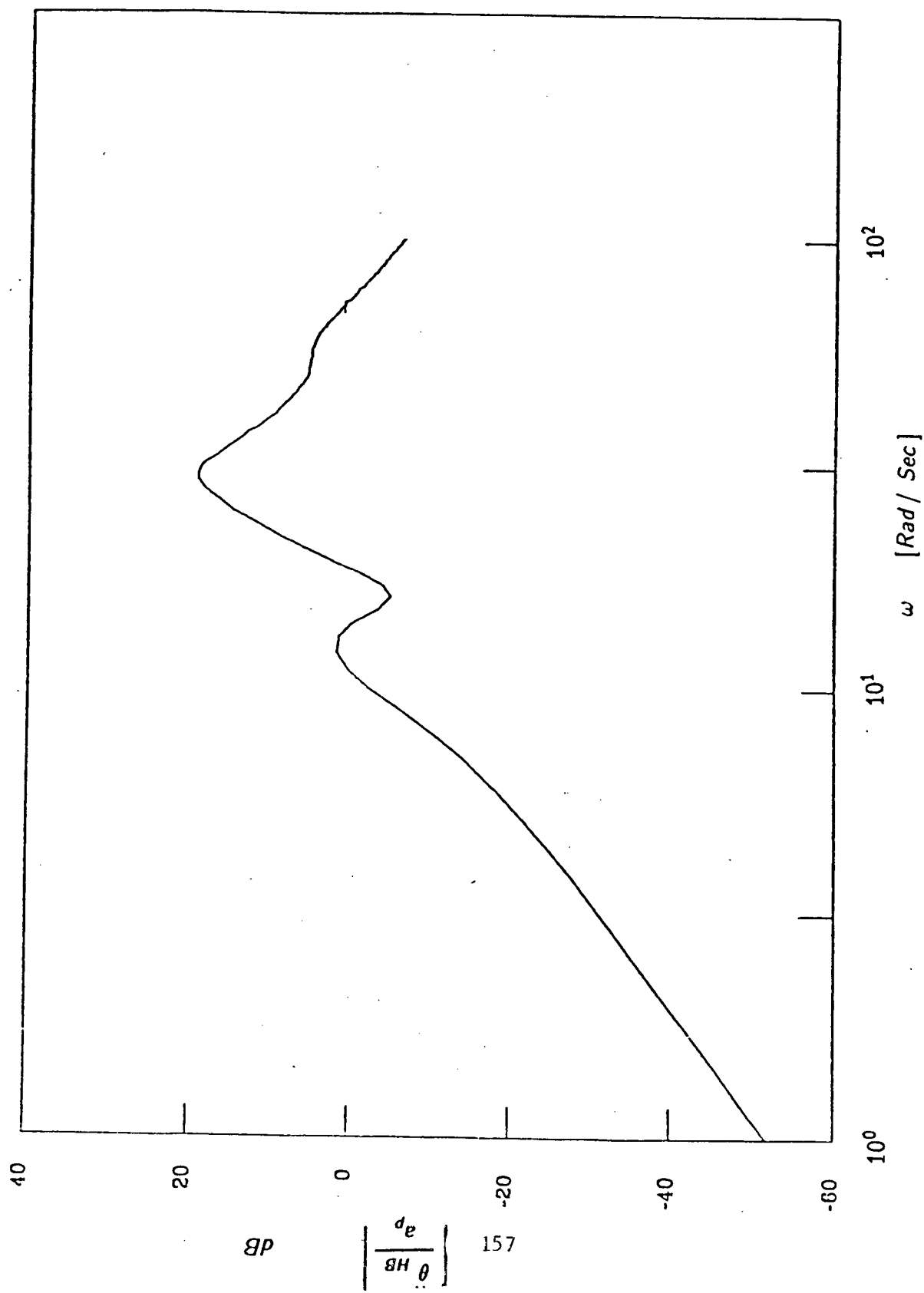
Fig. 2   Frequency Response of Head Angular Acceleration Due to Platform Vertical Acceleration

$$\left| \frac{\ddot{\theta}_{HB}}{a_p} \right|$$ dB

157

ω [Rad / Sec]

Fig. 3   Total (θ_H) and Voluntary (θ_{HC}) Head Motion

Solid = θ_H
Dashed = θ_{HC}

θ_H, θ_{HC} [Deg]

158

Solid = θ_{HB}
Dashed = $\hat{\theta}_{HB}$

$\theta_{HB}, \hat{\theta}_{HB}$ [Deg]

TIME (Sec)
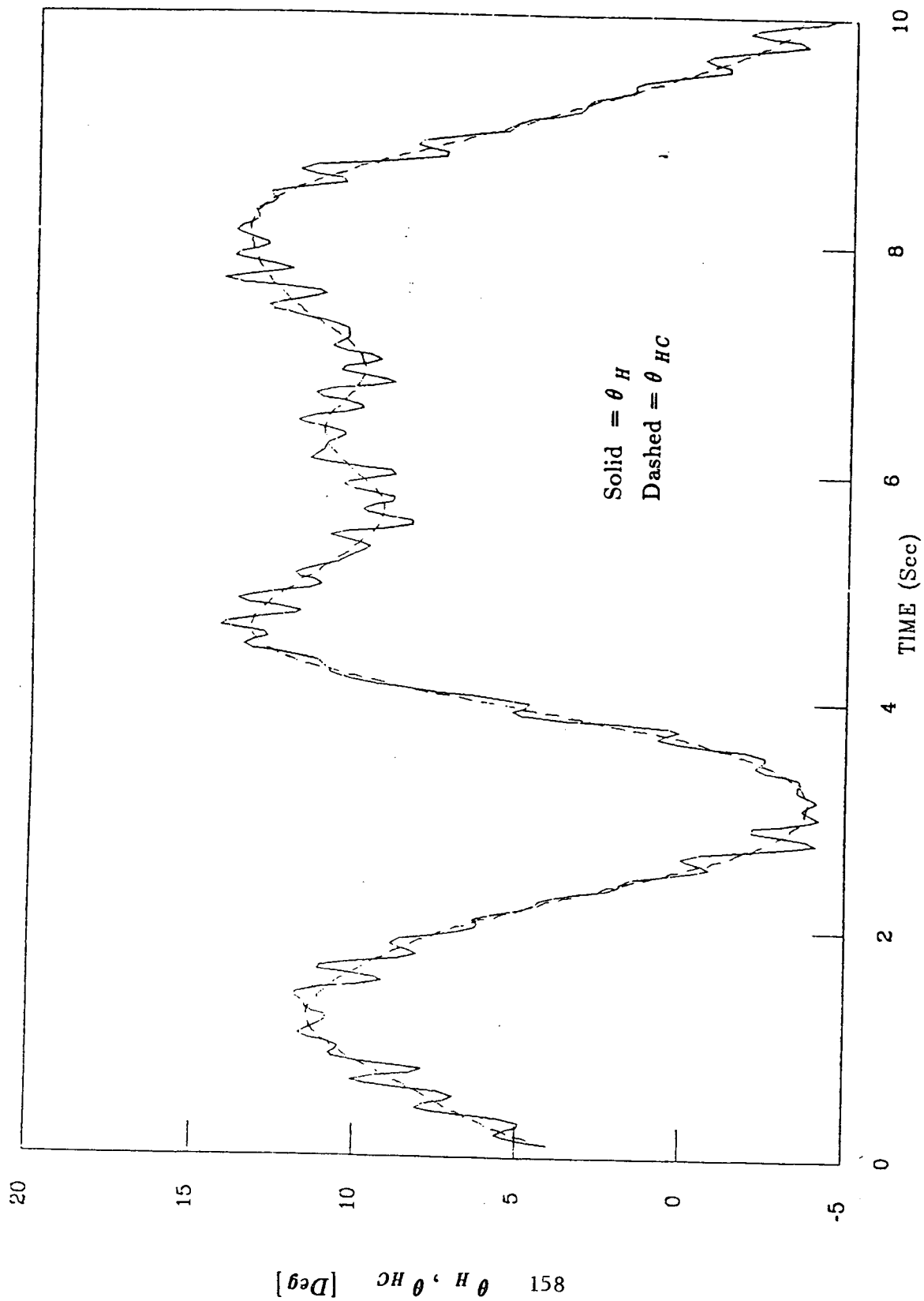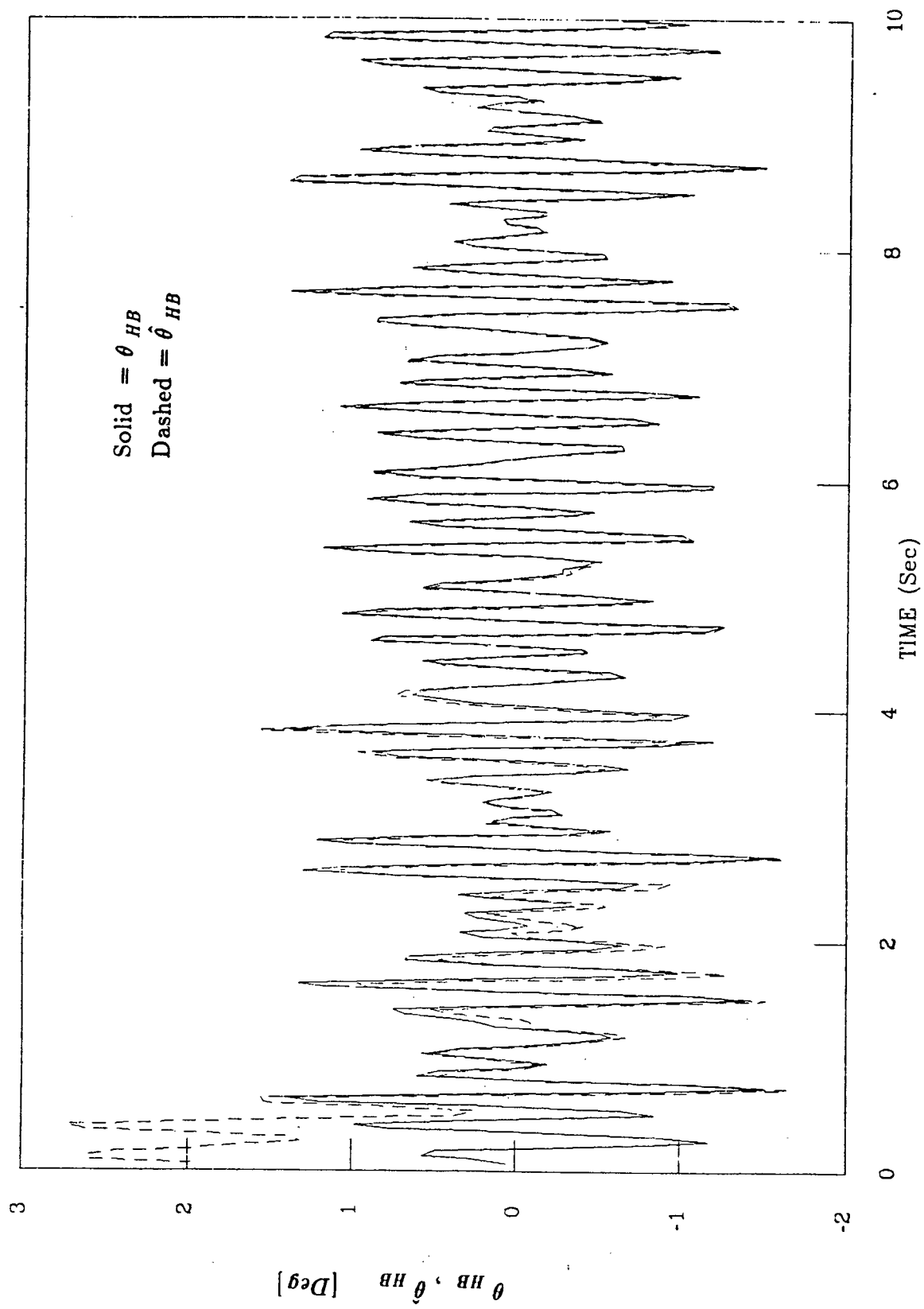
Fig. 4   True and Estimated Involuntary Head Command

159

Solid = $\hat{\theta}_{HC}$
Dashed = θ_{HC}

TIME (Sec)

θ_{HC} , $\hat{\theta}_{HC}$ [Deg]
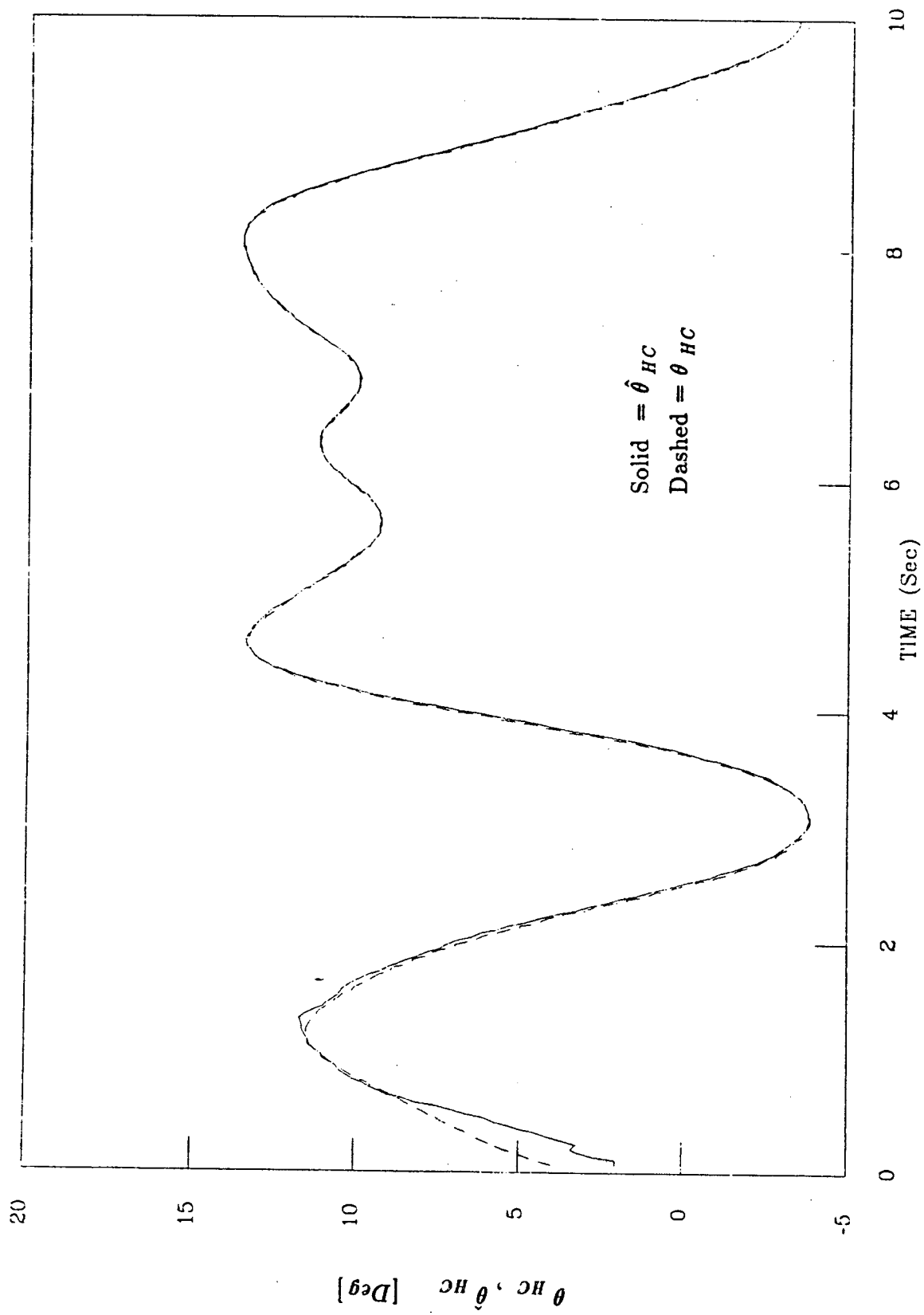
Fig. 5   True and Estimated Voluntary Head Command

160
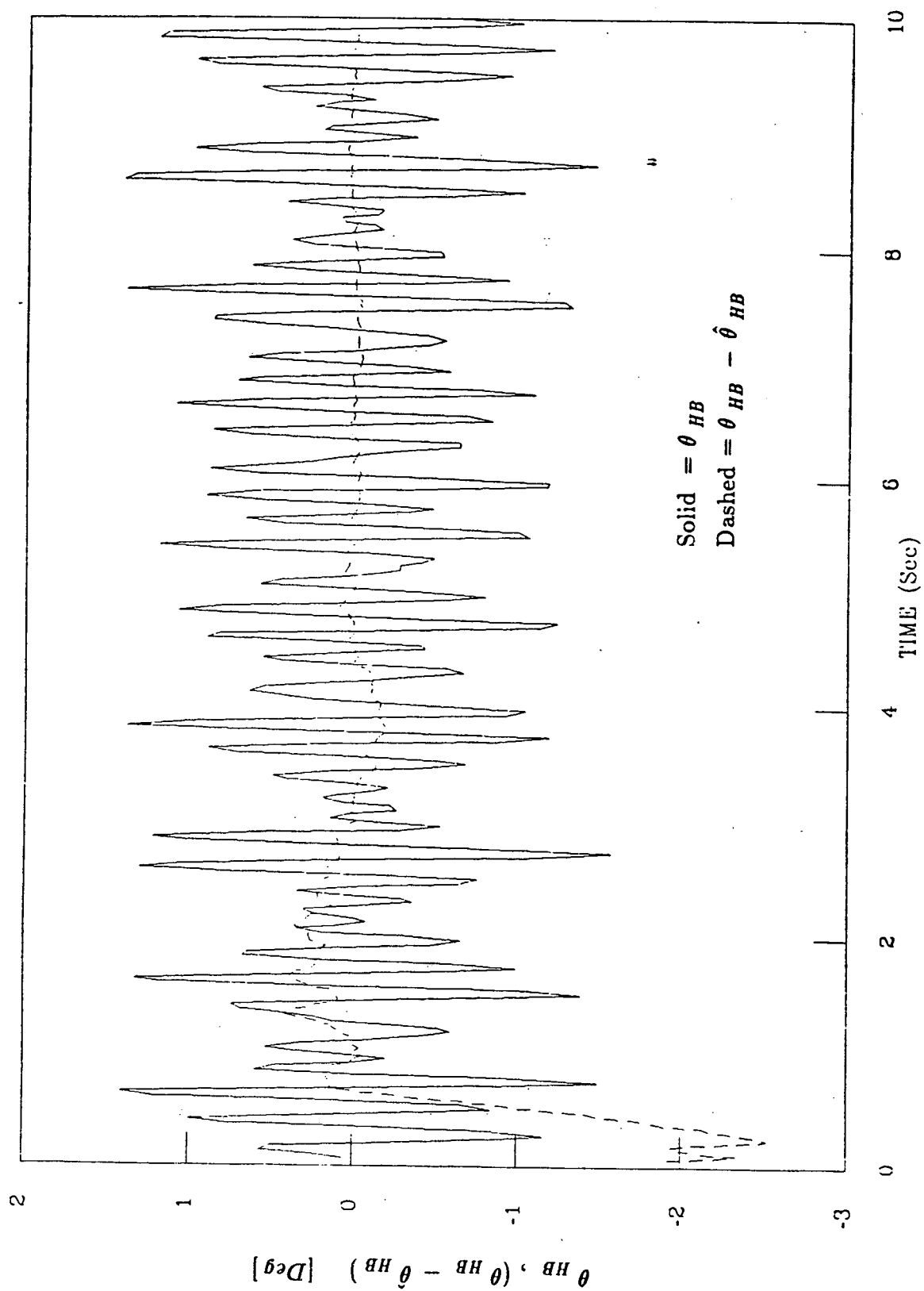
Fig. 6 True and Estimation Error of the Involuntary Head Command

θ_{HB} , $(\theta_{HB} - \hat{\theta}_{HB})$ [Deg]

TIME (Sec)

Solid $= \theta_{HB}$

Dashed $= \theta_{HB} - \hat{\theta}_{HB}$

161

30.00
20.00
10.00
0.00
-10.00
-20.00

$SF \times \theta_{HC}$ [Deg]

(a)

30.00
20.00
10.00
0.00
-10.00
-20.00

θ_{HC} [Deg]

(b)

2.000
1.200
0.400
-0.400
-1.200
-2.000

SF

(c)

0   10   20   30   40   50

TIME (Sec)

Fig. 7   Irregular Head Tracking Sequence

162

Fig. 8 True and Estimated Voluntary Head Command for Irregular Tracking

163
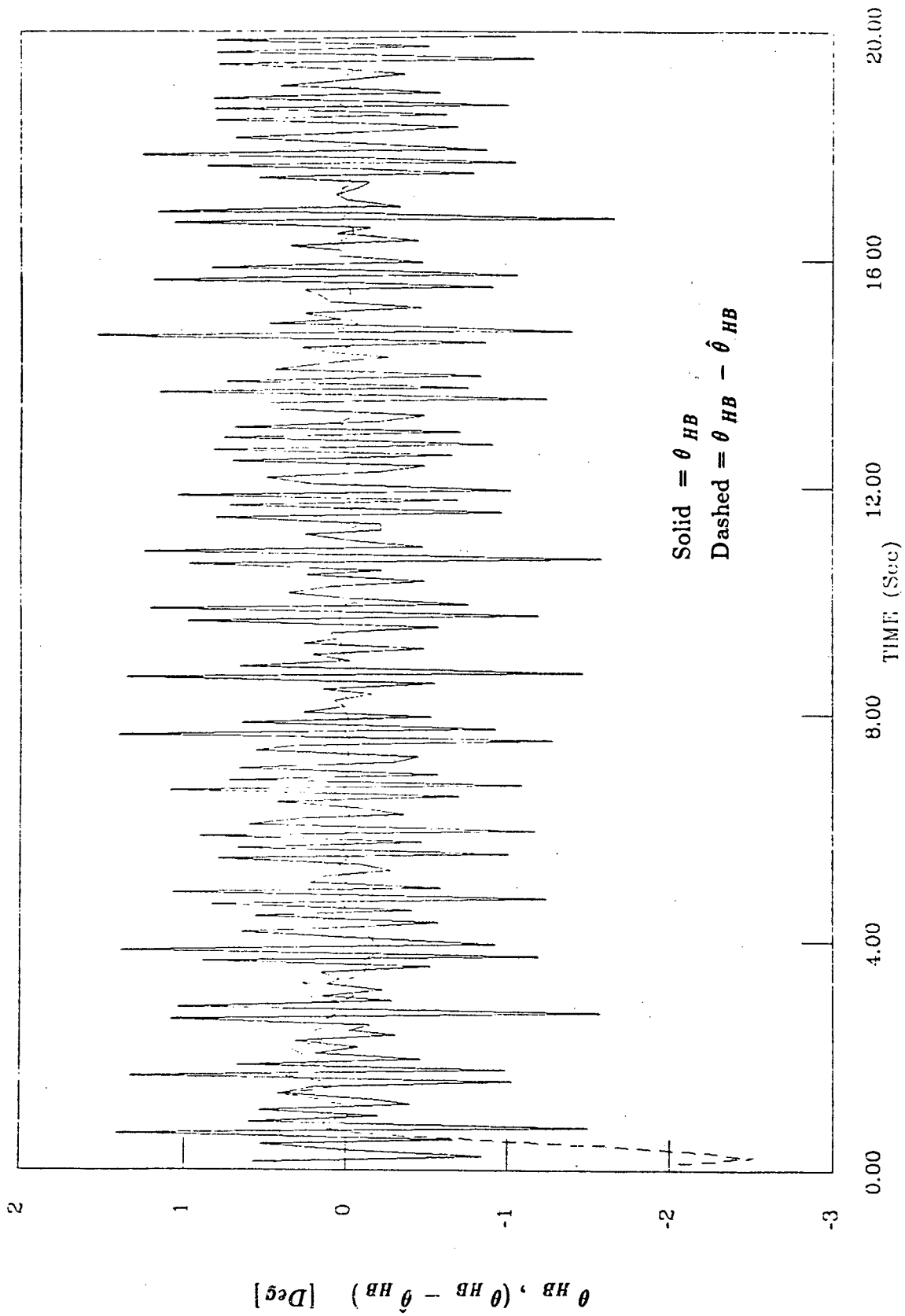
Fig. 9 True and Estimation Error of Involuntary Head Command for Irregular Tracking

Solid = θ_{HB}

Dashed = $\theta_{HB} - \hat{\theta}_{HB}$

θ_{HB}, ($\theta_{HB} - \hat{\theta}_{HB}$) [Deg]

TIME (Sec)

164

AN EXPLORATION OF A FITTS' LAW TASK

ON A LOGARITHMICALLY SCALED SCREEN

by

Wesley A. Olson and John M. Flach
University of Illinois at Urbana-Champaign
144 Mechanical Engineering Building
1206 West Green Street
Urbana, Illinois 61801

ABSTRACT

This study examines movement time and reaction time for a discrete tracking task in which display gain is dynamically changing as a function of cursor position. The dynamically changing gain resulted from a logarithmic scaling of display coordinates which magnified the region around the target. The results show that movement time with the logarithmic displays could be predicted using Fitts' Law. There was no MT advantage for the logarithmic displays relative to normal (constant gain) displays.
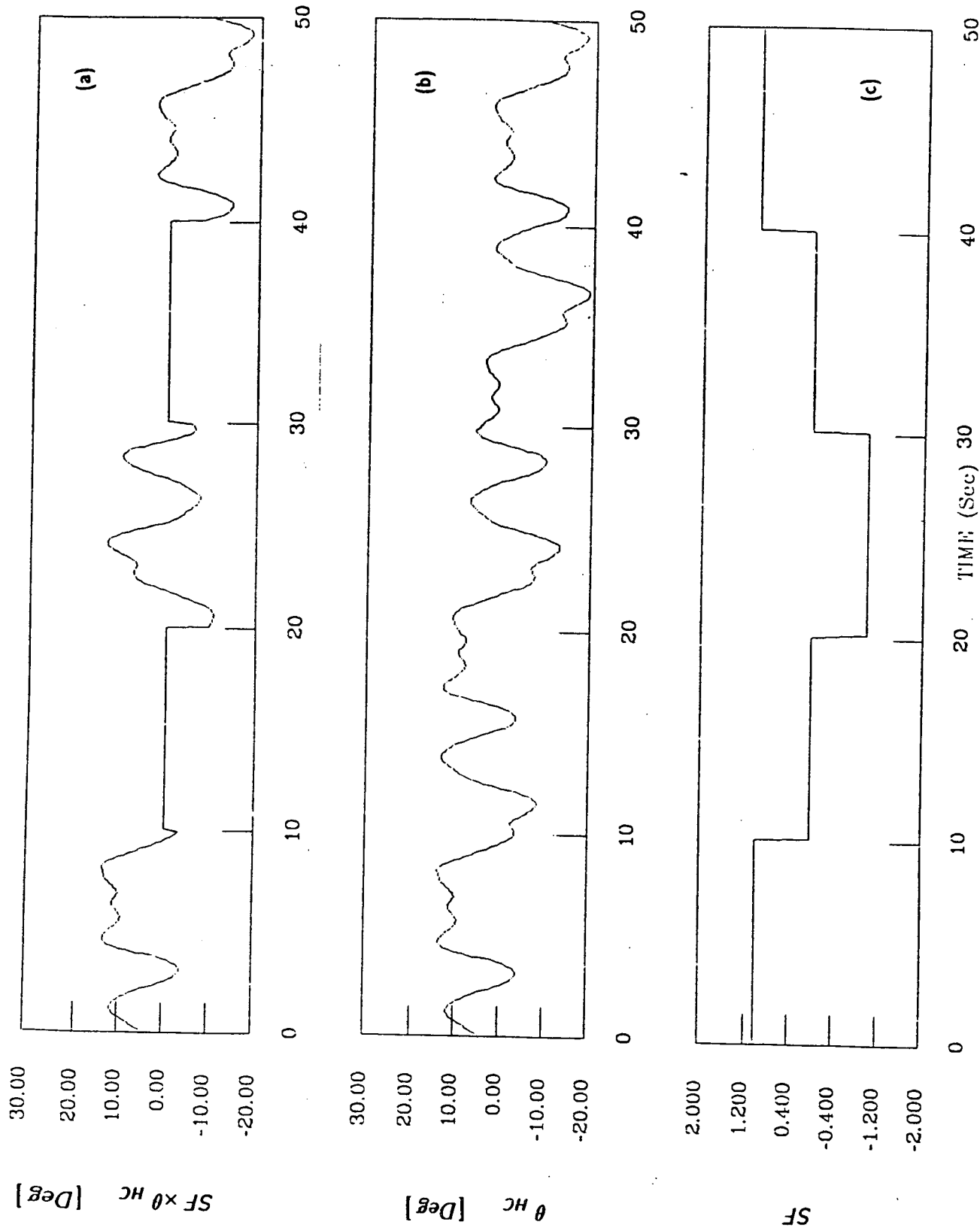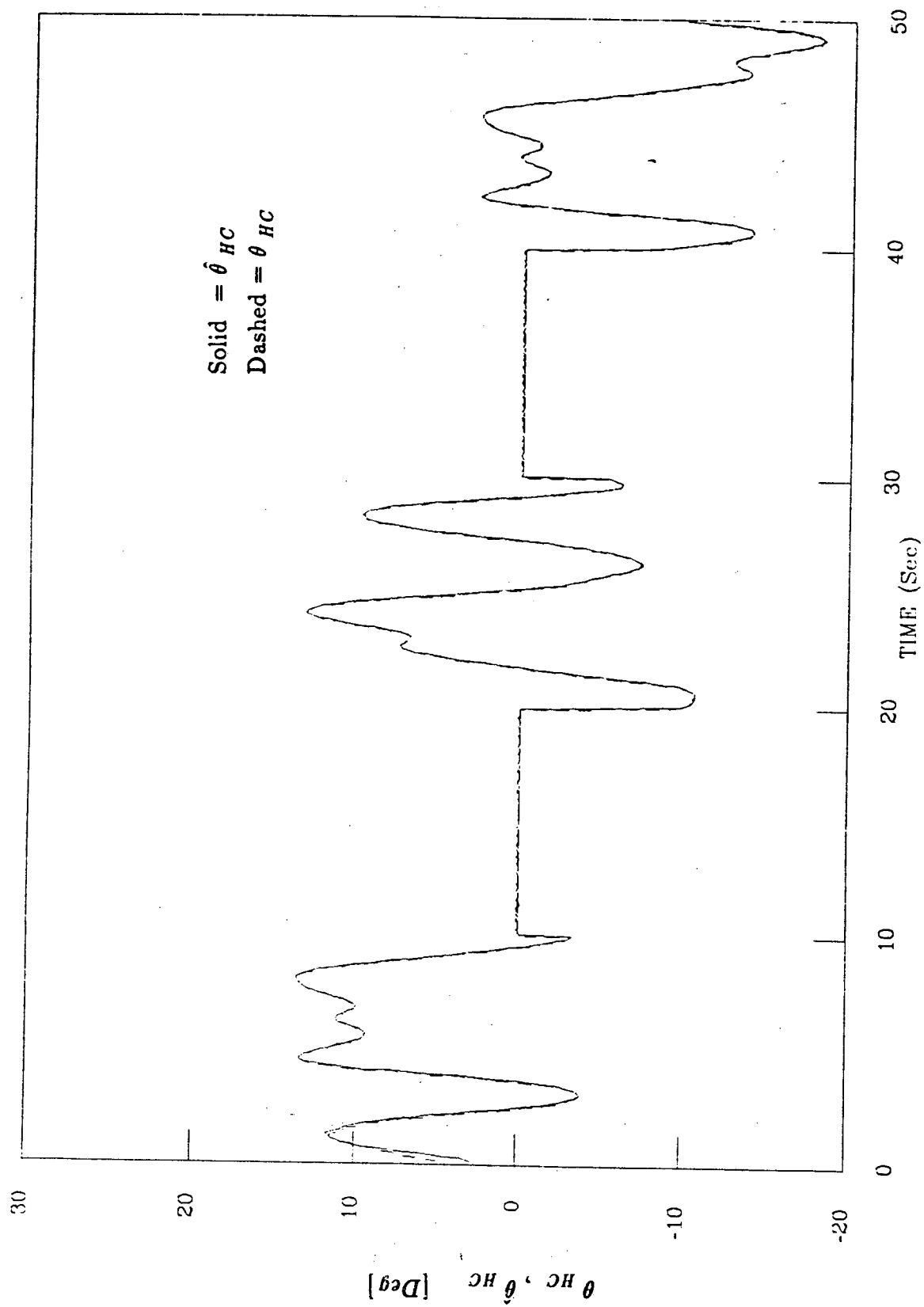
INTRODUCTION

The duration of movements to a fixed target can be predicted quite well by a function which has come to be known as Fitts' Law. This function is shown here as Equation 1:

$$MT = a + b \ (\log_2 2A/W) \tag{1}$$

where a and b are constants and A is the amplitude (distance to the target) and W is the target width. The term $\log_2 2A/W$ is generally referred to as the index of difficult (ID).

This function predicts movement time in reciprocal tapping tasks (Fitts, 1954), in discrete arm movement tasks (Fitts and Peterson, 1964), and has recently been investigated in cursor positioning tasks as a function of display gain (Buck, 1980), display dynamics (Jagacinski, Repperger, Moran, Ward, and Glass, 1980), and the interaction of gain and dynamics (Elvers and Kantowitz, 1986).

In this study, the ability of the above equation to predict movement time in a discrete cursor positioning task in which display gain is dynamically increased as a function of distance to the target will be investigated. The dynamically increasing gain is the result of mapping the normal, linear display coordinates onto a logarithmic scale. This mapping expands space around the target (magnifying target widths)

and contracts space distant from the target. There are two reasons for interest in this type of display. First, there is the possibility that the magnification of the target may result in reduced movement times for some situations. Thus, this would provide a method for aiding the operator in performing some classes of discrete positioning tasks. Second, the pattern of performance observed under this altered feedback condition might help in understanding the cognitive processes which are involved in the control of aiming movements.

METHOD

Subjects

Seven males and nine females aged 19 to 23 participated in this study. Subjects were paid for their participation at the rate of $3.50/hour. All subjects had normal vision. All but 1 subject were right handed. All subjects used their preferred hand.

Design and Procedure

The independent variables were display type (normal vs. logarithmic), rate of magnification (0.5 or 0.8), index of difficulty (ID=8.01, A=260 pixels, W= 2 pixels; ID=7.43, A=260 pixels, W=3 pixels; ID=7.02, A=260 pixels, W= 4 pixels), and order of display presentation (normal display first or logarithmic display first). Order of presentation and rate of magnification were manipulated between subjects. The crossing of these factors resulted in four experimental groups with 4 subjects per group. Each subject performed using both the normal and logarithmic screens and was tested at all three levels of ID. Thus, the experiment employed a 2 x 2 x 2 x 3 mixed design.

The dependent variables were movement time (MT) and reaction time (RT). RT was measured from onset of the target until the cursor passed a boundary 10 pixels from the starting point. Movement time was measured from the time the cursor passed the RT boundary until the beginning of the 1 sec capture period.

Each subject participated in 14 sessions---5 sessions using the normal display and 9 sessions using the logarithmic display. It was hoped that this would be sufficient to permit near asymptotic performance in the two display conditions. A session consisted of 6 blocks of 21 trials each. Each of the 3 levels of ID were presented in random order 7 times within a block. A session lasted approximately 40 minutes.

The task was a discrete positioning task. A cursor was moved from a constant starting point over a fixed distance to a target of variable width. At the start of each trial a cursor appeared on the left edge of the computer screen. After a random interval (mean duration of 4 seconds) two target lines appeared on the right side of the screen.

Subjects were instructed to move the cursor as quickly as possible to within the target area and hold it there for a 1 second capture period. Target capture was followed by a five second feedback display that showed both reaction time and movement time. A first order control system was used to manipulate the cursor.

Equipment and Stimuli

This experiment was controlled using an IBM/XT personal computer. Stimuli were presented on an IBM color monitor measuring 200 pixels high x 320 pixels wide (6 1/2" x 10"). The refresh rate was 30 Hz. The integration for the first order control was a trapezoidal approximation sampling at 120 Hz. A Measurement Systems spring loaded joystick (Model 542-G213) was used. Cursor velocity was proportional to stick displacement with each degree of stick displacement adding approximately 7 pixels/sec to cursor velocity.

The cursor was a red line 1 pixel wide x 80 pixels (2 3/5") high. At the start of a trial it appeared on the left edge of the screen. The target consisted of two green lines. Each line was 1 pixel wide x 100 pixels (3 1/4") high. The target center was always 260 pixels from the left edge of the screen. The target width varied as a function of ID and display scaling. Table 1 shows the target width for each of the various ID/display conditions.

Figures 1 and 2 show the mapping of the normal screen coordinates to the logarithmic screen coordinates. As can be seen in these Figures, the starting and target center positions were fixed. This mapping is defined in Equation 2 below:

$$S = (A/T) \ln [(B - X)/ B] \qquad \text{for } X \leq 260$$

$$S = 520 - (A/T) \ln [(X - (520 - B))/ B] \text{ for } X > 260 \qquad (2)$$

S = cursor position on scaled screen
X = cursor position on normal screen
T = constant used to determine rate of magnification
A & B = constants needed to maintain starting and center positions

When rate of magnification (T) was 0.5, A and B were set at -46.72 and 277.16 respectively. When rate of magnification (T) was 0.8. A and B were set at -46.72 and 263.07 respectively.

The logarithmic display scaling had two effects. One effect was to expand the target width as illustrated in Figures 1 and 2 and Table 1. The second effect was that the display gain dynamically increased as the target was approached. Table 2 shows the relative gain in the starting and target regions for the three display conditions. For the logarithmic displays, gain is low when the distance from the target is
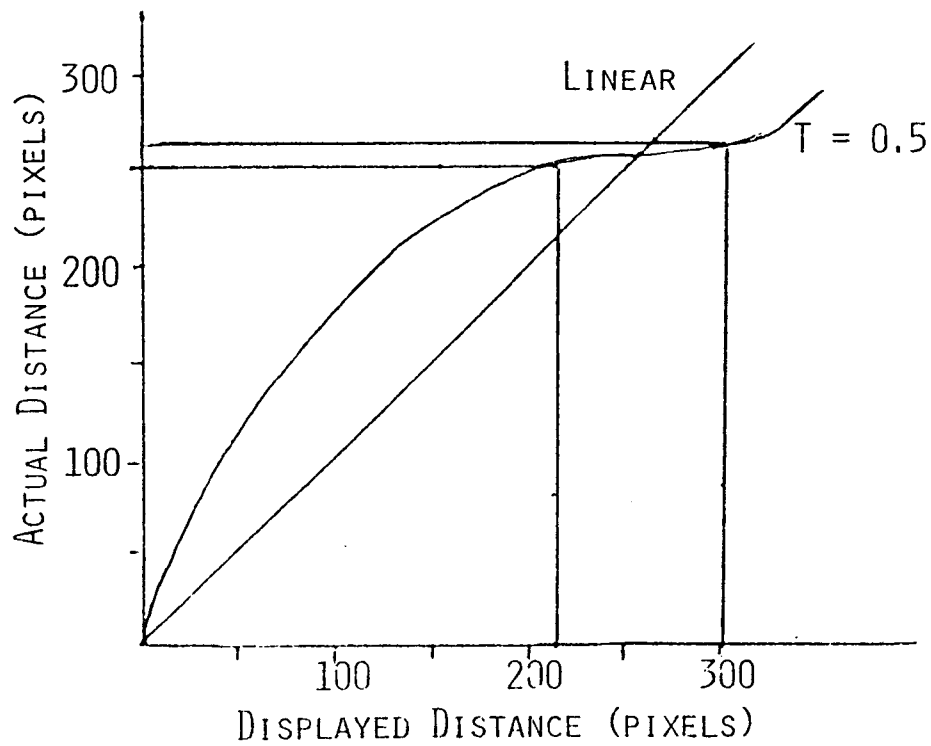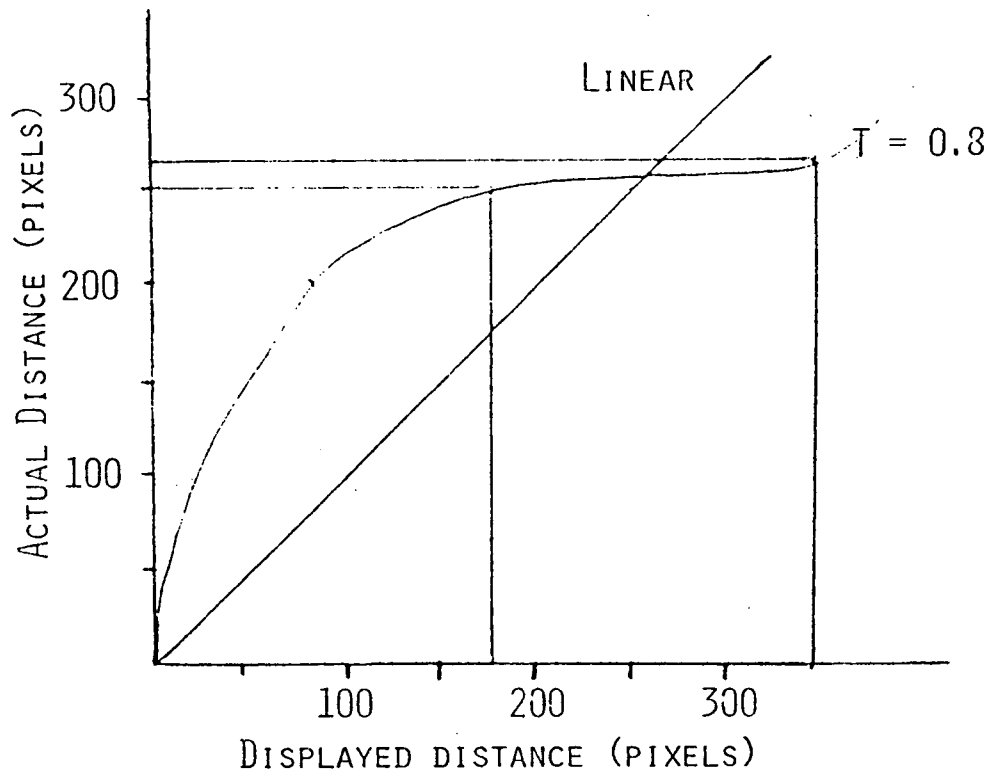
FIGURES 1 & 2.   ACTUAL VS. DISPLAYED DISTANCE FOR NORMAL
AND LOGARITHMIC SCREENS.

TARGET WIDTH

	2	3	4
0.8	13	33	47
0.5	6	11	16
0.4	4	8	11

TABLE 1. TARGET WIDTHS FOR DIFFERENT RATES OF APPROACH.

	INITIAL	TARGET
0.8	.222	16.52
0.5	.338	5.32
0.4	.401	3.64
NORMAL	1.000	1.00

TABLE 2. TARGET GAINS FOR DIFFERENT RATES OF APPROACH.

great and gain is high when the distance from the target is small. For the normal display, gain is constant.

RESULTS AND DISCUSSION

Figure 3 shows MT as a function of magnification rate, order, display, and ID. The data shown in Figure 3 was collected on the last session with each display. Medians across ID within a session were computed for each subject. These medians were then averaged across blocks to obtain scores for each subject. Each data point in Figure 3 is a mean averaged across the 4 subjects in each group. However, one subject's data was dropped from the T=0.5/Normal First Group because of abnormally slow responding.

Analysis of Variance showed a significant main effect for ID $(F(1,24) = 177.2, p<.001)$. As can be seen in Figure 3 there was an approximately linear increase in MT with increasing ID. This is exactly the relationship predicted by Fitts' Law. A striking feature of Figure 3 is the nearly parallel MT slopes as a function of ID for the normal and logarithmic displays. Equation 3 is the function which maps ID for the normal display to ID for the logarithmic display.

$$IDS = \frac{260}{260 - A/T \ln\{[B - ((260 - 260/2^{IDN}) + .5)]/B\} + .5}$$

where A, T, and B are display scaling constants for the logarithmic display and IDS and IDN are the IDs for the log and normal displays.

This mapping is illustrated in Figure 4. The mapping is nearly linear over the range of IDs tested in this study. This may account for the parallel slopes.

Although not statistically significant, there appears to be an effect due to the interaction of presentation order and display type $(F(1,12) = 2.59, p = .13)$. MT tends to be longer with the first display, regardless of the type. This indicates that, contrary to intentions, subjects were not at asymptote with either display type.

The data in Figure 3 indicate no MT advantage for the magnified targets (logarithmic display). Average MT was 2.10 sec for the normal display and 2.22 sec for the logarithmic display.

Analysis of variance of the RT data showed a significant interaction between display and ID $(F(2,24) = 3.72, p = .039)$. RT decreased as a function of increasing ID for the normal display, however increased for the logarithmic display. The decrease in reaction time as a function of ID for the constant gain display with a velocity control was also found by Elvers and Kantowitz (1986). There was also a
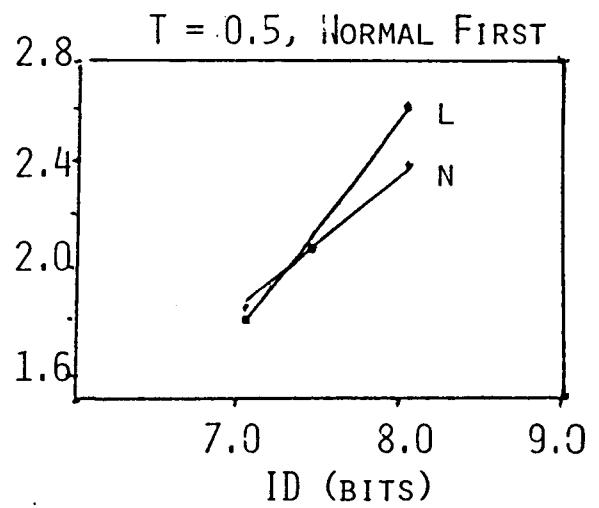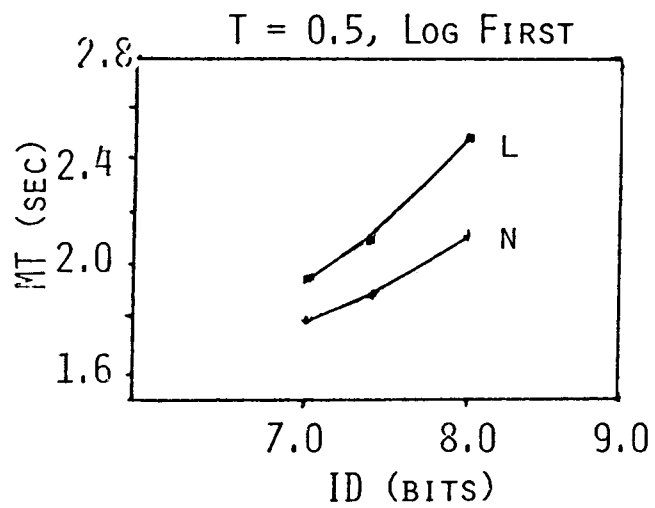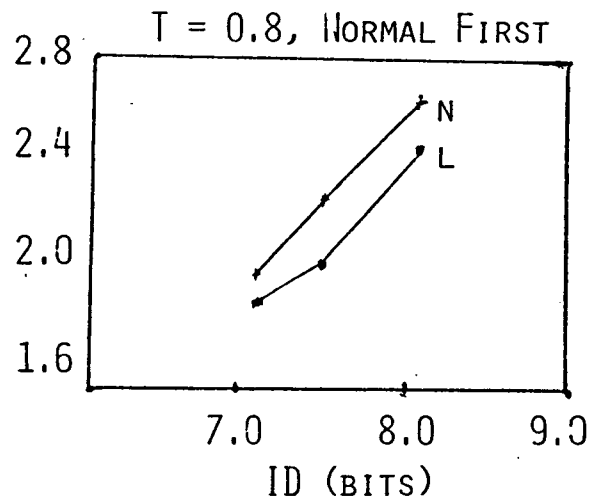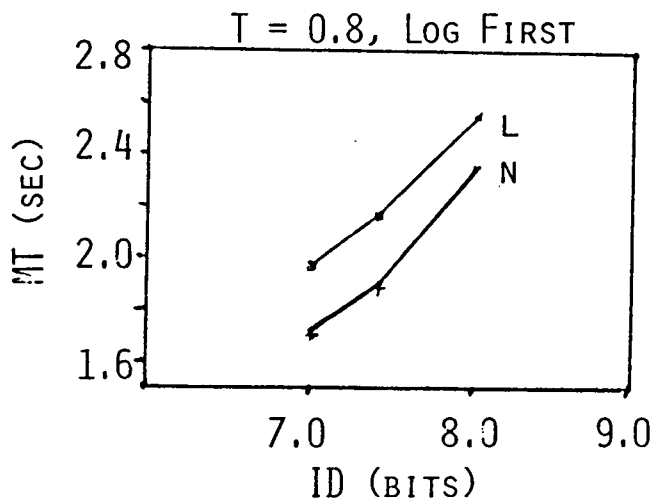
Figure 3. Median movement times for different rates of approach and orders of presentation.
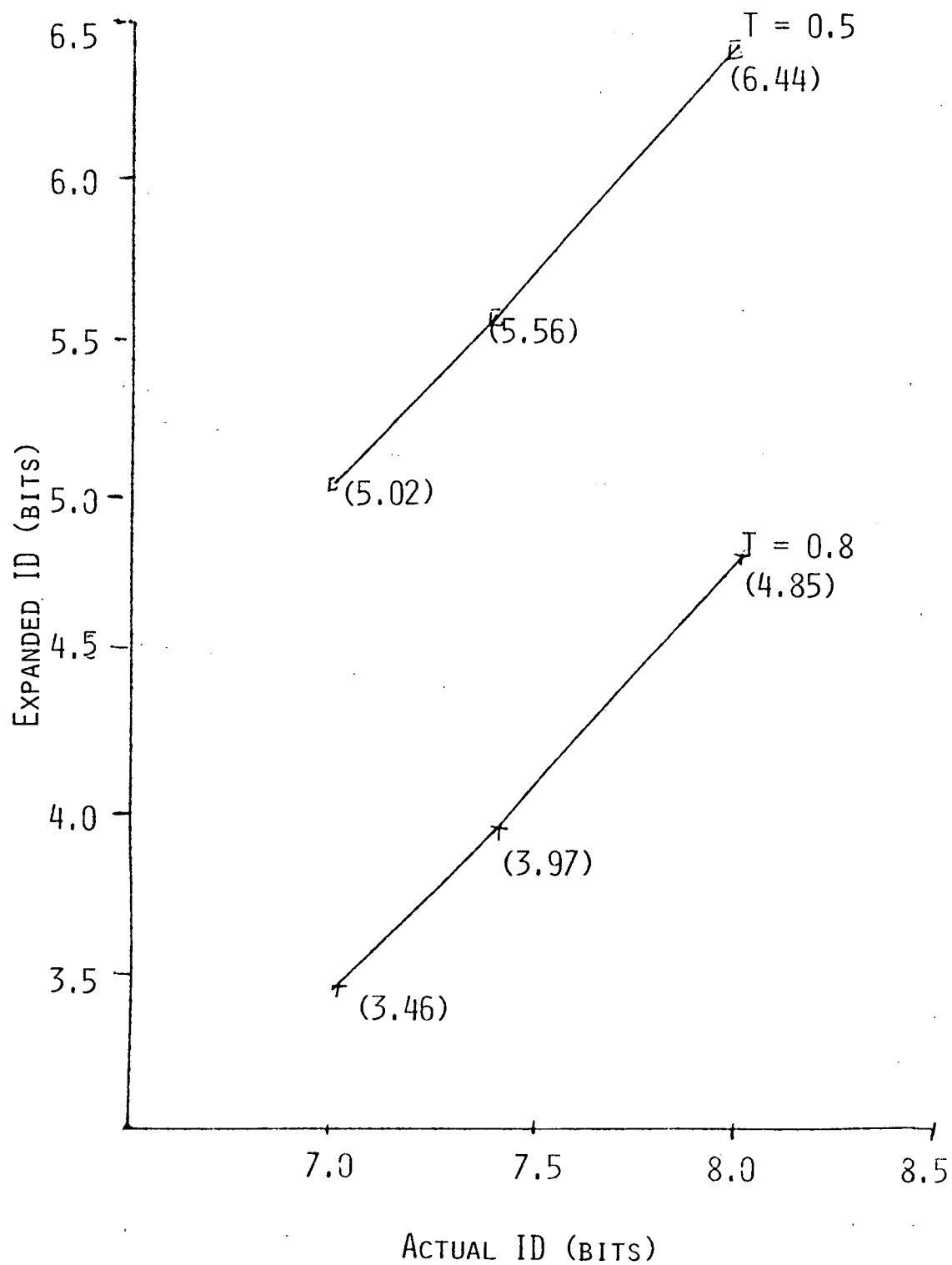
FIGURE 4. MAPPING OF ID FROM ACTUAL TO EXPANDED SPACE.

significant three way interaction between order, magnification rate, and ID $(F(2,24) = 4.24$, $p = .026)$. These interactions are shown in Figures 5 and 6.

CONCLUSIONS

The data from this study indicate that Fitts' Law predicts MT even when display gain is dynamically increased as the target is approached. There appears to be no advantage for the logarithmic display scaling at the magnification rates tested. Caution should be used in interpreting these results since subjects were not at asymptote with either the normal or the logarithmic displays.

An analysis of the movement time histories obtained in this study is planned. This will provide information about the microstructure of movements under the varying feedback conditions.

An additional study is planned to examine performance with a display having a magnification rate of 0.4. As shown in Table 1, this magnification rate will result in a magnification of the smallest target from 2 to 4 pixels. The results for the normal screen indicate that such a change in target width can reduce MT by more than 500 msec. However, this is for constant gain. It remains to be seen how the dynamically increasing gain will effect MT. Longer training periods will also be used in this additional study.

REFERENCES

Buck, L. (1980). Motor performance in relation to control display gain and target width. Ergonomics, 23, 579-589.

Elvers, G. & Kantowitz, B.H. (1986). Fitts' law with variations in control-display gain and order of control using an isometric controller. Paper presented at the Third Annual Mid-Central Ergonomics/Human Factors Conference, Miami University, Oxford, OH.

Fitts, P.M. (1954). The information capacity of discrete motor responses. Journal of Experimental Psychology, 47, 381-391.

Fitts, P.M. & Peterson, J.R. (1964). Information capacity of discrete motor responses. Journal of Experimental Psychology, 67, 103-112.

Jagacinski, R.J., Repperger, D.W., Moran, M.S. Ward, S.L., & Glass, B. (1980). Fitts' law and the microstructure of rapid discrete movements. Journal of Experimental Psychology: Human Perception and Performance, 6, 309-320.
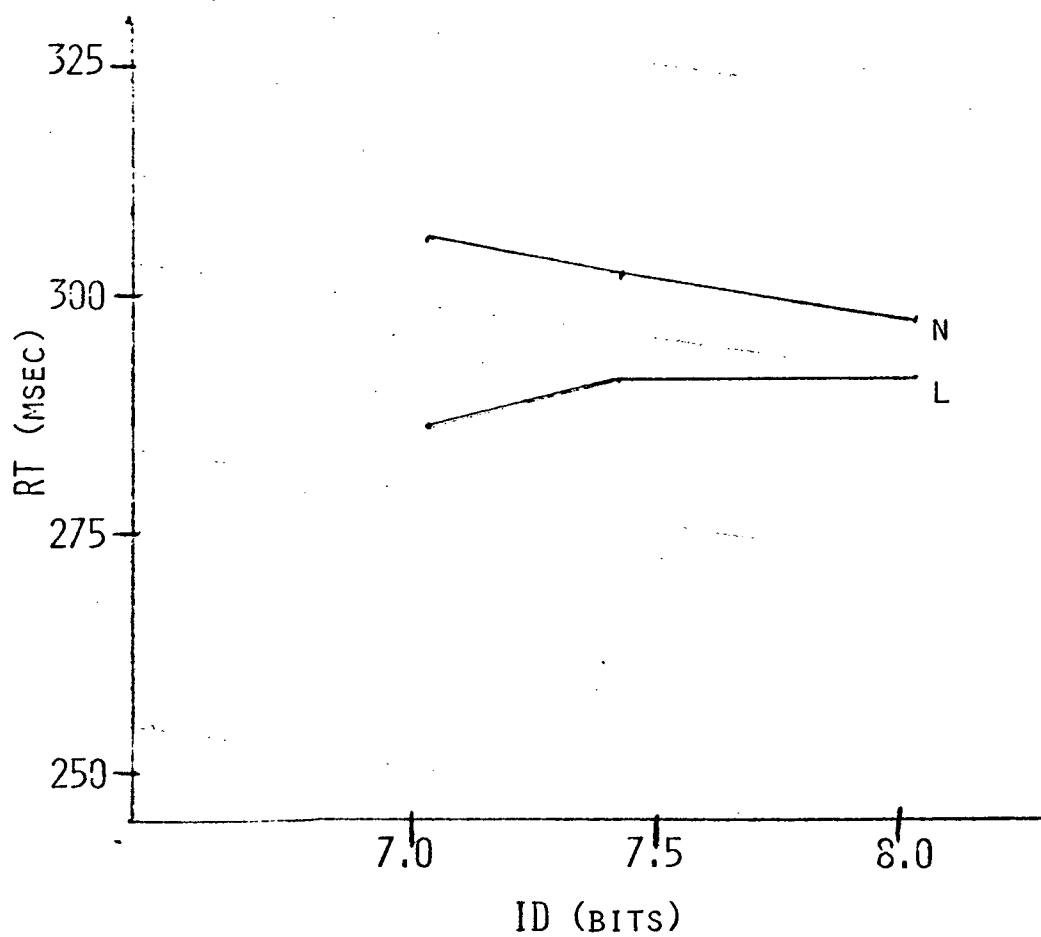
FIGURE 5. MEDIAN REACTION TIME VS. INDEX OF DIFFICULTY
SHOWING AN INTERACTION BETWEEN DISPLAY AND
INDEX OF DIFFICULTY.
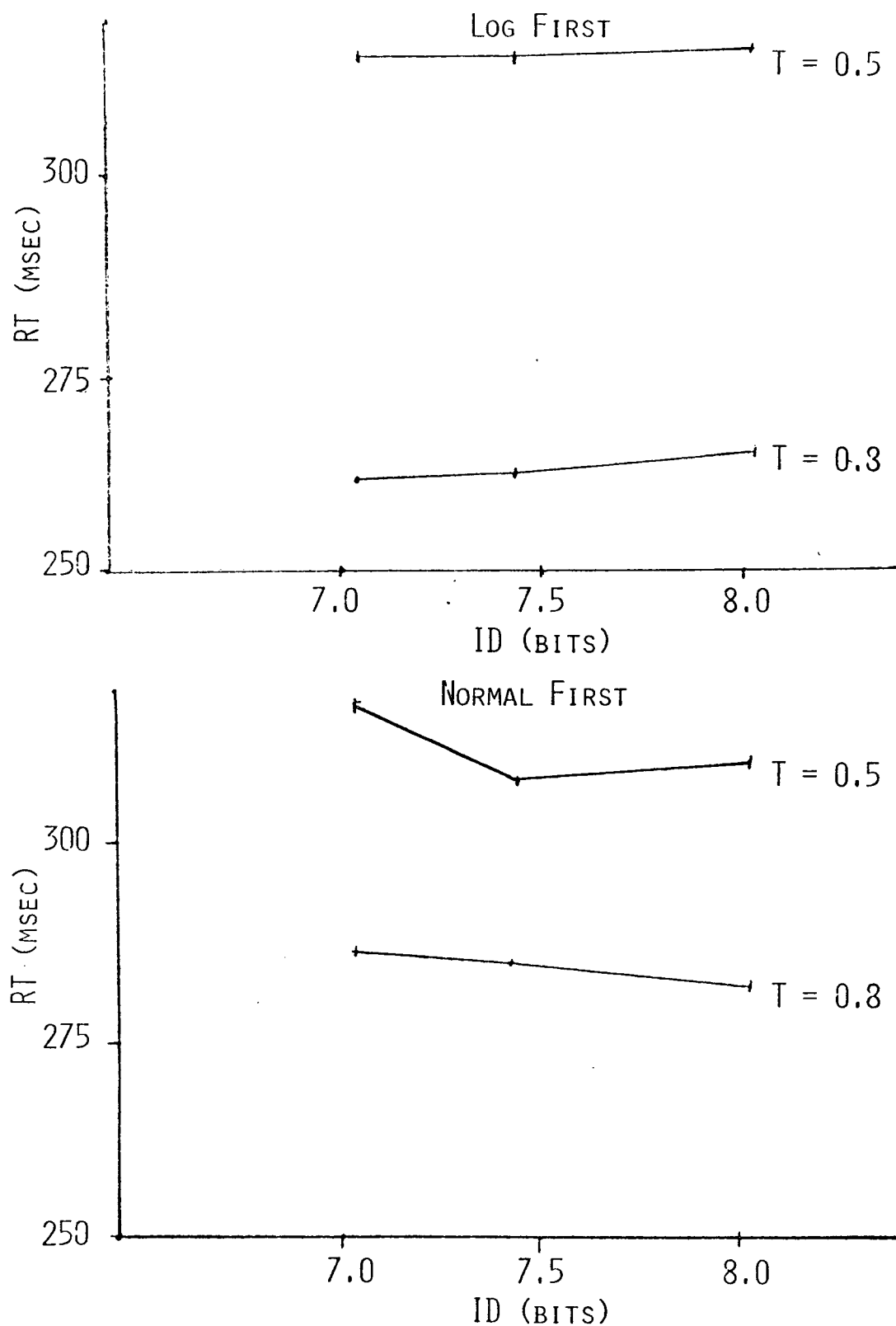
FIGURE 6. MEDIAN REACTION TIME VS. INDEX OF DIFFICULTY SHOWING
AN INTERACTION BETWEEN ORDER, RATE, AND ID.

EFFECTS OF UPDATE RATE, PRACTICE, AND DISPLAY CHARACTERISTICS IN CRITICAL EVENT DETECTION WITH DIGITAL DISPLAYS

Glenn A. Hancock, Larry C. Walrath, and Richard W. Backs

Human Performance Laboratory

McDonnell Douglas Astronautics Company - St. Louis
P.O. Box 516
St. Louis, Missouri 63166

ABSTRACT

A simulation procedure was used to evaluate display update rate in a multi-readout LCD digital display. Six right-handed male observers each received three update rates (4, 6, and 8 Hz), one per day on three successive days. Observers monitored the display and pressed a button whenever any readout exceeded a specified critical value. There was no evidence in our data for the superiority of one update rate over another. Possibly, increased difficulty at higher rates is offset by improved rate-of-change information provided by the more rapidly changing display. Critical values were detected significantly faster with each successive day of the experiment. Response time also decreased within each day, but this effect was not statistically significant. This suggests a continual improvement with practice, partially countered by fatigue-related attentional deficits as each session progressed. There were major differences among readouts unrelated to their number of significant digits. For the three main readouts, response speed was inversely related to the distance between the upper limit of the normal range and the critical value (when that distance is expressed as a proportion of width of the normal range). This effect seems to result from the greater discriminability provided by relatively large numerical changes.

INTRODUCTION

As more avionics displays are converted from analog to digital formats questions arise concerning the design parameters for digital displays. For example, should a digital display be LCD, LED, or CRT based? How fast should the display refresh? What kind of damping is needed? This report summarizes an experiment conducted to examine one of these issues -- LCD refresh rate for an upfront Engine Monitor Display (EMD). Additional information concerning physical layout of the EMD, that may be useful in addressing other design issues, was obtained.

The major question of interest concerned the optimal display refresh rate. For the purpose of this experiment, "optimal" rate was defined as the rate that facilitated subject performance in a reaction time task. In the task, subjects monitored a computer-simulated EMD operating at different refresh rates. They were required to detect the occurrence of numbers designated as critical values. Critical values were carefully selected from the caution or warning levels reported in the F-15 fight manual to approximate conditions occurring in an aircraft that require immediate attention. The refresh rates were 8 Hz, 6 Hz, and 4 Hz. Design variables included items such as type of displayed function and the side of the EMD on which the display appeared. Experimental control variables included group structure, controls for order and for practice effects, and the like.

METHOD

Subjects

Six full-time McDonnell Douglas Astronautics Company (MDAC) employees participated in the experiment. All participants were right-handed males between the ages of 24 and 42 years.

Display

The simulated EMD is shown in Figure 1. It was generated by an AED 767 graphics terminal and presented to the subject on a JVC Model TM-41 UA color video monitor. The full-scale display filled the entire 5 inch diagonal-measure screen of the monitor. The color of the display approximated standard aircraft blue-white and was presented upon a black background. Mean luminance of the display was 18.3 ftL and average
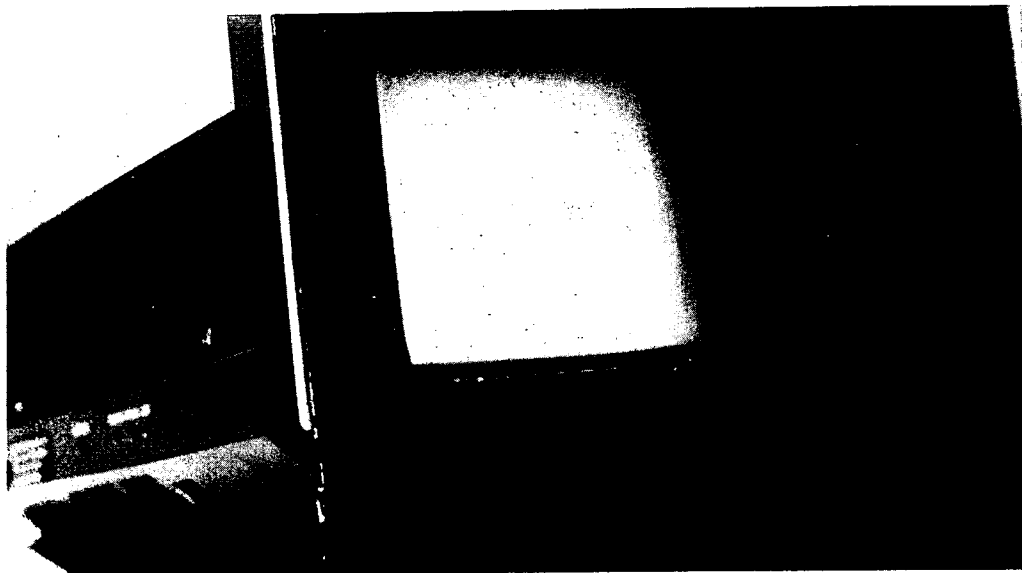
FIGURE 1. SIMULATED AIRCRAFT MONITOR DISPLAY

background luminance was 0.20 ftL. Ambient illumination was 1.0 ft-candle. The display was situated with the subject seated at approximately design eye height. The monitor was located at its approximate position and angle in the cockpit (i.e., 29 in. left of design eye on a 77° line 31.7 in. below design eye on a 63° line with the display face angled upward 15°).

Design

Independent Variables - The major independent variable of the experiment was the rate at which the information on the EMD was updated (screen refresh rate). Three refresh rates were used, 4 Hz, 6 Hz, and 8 Hz. Independent variables required by the physical layout of the EMD were: (a) the display function (i.e., RPM, Temperature, Fuel Flow, and Oil PSI; (b) the engine that the display monitored (i.e., the left or the right side of the display); and (c) the direction of the critical value of a display function (i.e., a maximum or minimum critical value). The only function for which the direction of the critical value was a variable was the Oil PSI display, all other displays had only a single, maximum, critical value. Experimental control variables required by the design were: (a) the experimental test day; and (b) the number of trial blocks within a experimental day.

Dependent Variables - Dependent variables were reaction time (RT) and error rates. RT was defined as the time in milliseconds from when a display reached a critical value to the first button press. Several different types of errors were defined: (a) anticipatory responses, responses made when a display function was approaching, but had not yet exceeded, the critical value; (b) extraneous responses, responses made when no display functions were approaching critical value; and (c) false alarm responses, extraneous responses made to a display function after another display function had already exceeded its critical value.

Experimental Design - The experimental design was a replicated Latin square with repeated-measures (Winer, 1962, page 571). Each subject received all three refresh rate conditions, one condition per day over three successive days. A Latin square design was used to balance the order effects of the experimental test day and display refresh rate variables. The three day-by-refresh rate orders were used. Two subjects were assigned to each row of the Latin square. Rows were randomly ordered and subjects were assigned to a row in the order in which they arrived for their first experimental session. One subject was assigned to each of the three rows of the Latin square before any of the rows were replicated.

Task

Software to control the experiment was locally developed in Fortran and executed on a Data General S/140 Eclipse minicomputer. The software determined the order in which the display functions reached critical value, the time it took to reach that value, the damping, the rate-of-change, and the direction-of-change for the display functions. It recorded subjects' responses and RTs.

179

Trial Balancing - An experimental session consisted of seven 32-trial blocks, a 1-block practice session during which data were not recorded and 6 experimental blocks. Each display function exceeded its critical value on 8 trials in each block, 4 trials on the right side and 4 trials on the left side of the EMD. For the Oil PSI displays, 2 of the 4 trials on each side surpassed the maximum critical value and 2 trials surpassed the minimum critical value. The 32 trials were randomly ordered within each block so that neither experimenter nor subject could predict which display function was about to exceed critical value. Any trial on which an error was made was repeated at the end of the block until 32 error-free trials were obtained.

Intertrial Interval - The ITI varied from trial-to-trial depending upon two independent factors: (a) a delay constant used for each trial; and (b) the amount of time between when a function reached critical value and when a subject completed his response. Each trial began with a fixed 2-sec interval, and after an additional delay of 1, 2, 3, or 4 sec a function would begin to move toward critical value. Therefore, without allowance for response time, the minimum ITI was 3 sec and the maximum ITI was 6 sec.

The length of the delay was balanced with the display functions. That is, each delay interval occurred once with each of the four side-by-display-function trials in each block. For the Oil PSI display, the 1 and 4 sec delays were assigned to the minimum critical value trials and the 2 and 3 sec delays were assigned to the maximum critical value trials. If a trial was repeated, the same delay constant was associated with all trial repetitions.

Rate-of-Change - The rate- and direction-of-change of the display functions was determined by adding a random number to the display total each time the screen was refreshed. The random number selected for the RPM and Oil PSI display was an integer between -1 and 1 inclusive, for the Temperature display it was an integer between -7 and 7 inclusive, and for the Fuel Flow display it was integer between -6 and 6 inclusive. Different random numbers were selected for right and left display functions.

Damping - The display functions did not necessarily increment or decrement with each screen refresh. A damping function was used to alleviate the flickering effect caused by continually incrementing or decrementing the displays by relatively small amounts. The amount of damping varied across display functions depending upon the possible rate-of-change for each display. Display functions were damped such that they did not change until the absolute value of the change was greater than or equal to a damping constant. The damping constant was 2 for the RPM and Oil PSI displays, 6 for the Temperature display, and 8 for the Fuel Flow display. Thus, with damping in effect, only the Temperature display could change on every screen refresh. This type of damping was necessary to produce more stable and realistic displays because the normal operating range for the RPM and Oil PSI displays consisted of only two significant digits while the Temperature and Fuel Flow displays consisted of three significant digits.

As a result of damping, display functions approaching critical value were easily recognizable. Therefore, a random surge of increments or decrements was introduced. A random number was selected so that the chance of initiating a surge was 5% at every screen refresh. If a surge was initiated, all displays incremented or decremented at three times their normal rate-of-change for a period of 3 sec, during which time no new surges could be initiated. The 3 sec length of the surges was constant for all screen refresh rates. The direction of the surges alternated between incrementing and decrementing, and all displays either incremented or decremented.

Critical Value Weighting - When a display was approaching critical value, the rate-of-change was weighted so that the amount of time needed to reach critical value was the same regardless of the screen refresh rate. If a surge occurred while a display function was approaching critical value, the weighted rate-of-change for the display approaching critical value was not tripled as were all of the other display functions. That is, the weighted rate-of-change increase toward critical value was the same, independent of surges, to assure the constancy of critical value changes across screen refresh rate conditions.

Procedure

Subjects were given detailed instructions concerning the nature of the task at the first experimental session, but were not specifically told about any of the independent variables. They were instructed to watch the EMD and whenever any of the display functions exceeded the critical value (see Table 1 for critical value(s) for each display function) to press a black button on the response box (Figure 2) as quickly as possible. Once the black button was pushed, the critical value was reset to a predetermined value, and the EMD was frozen. It remained frozen until the subject pressed the red button on the response box that corresponded to the display function that he thought had exceeded critical value. If a subject made any type of response error, the trial was repeated later on in the session.

Subjects were free to use any strategy to perform the task that would minimize both their response time and error rate. Each session began with 32 practice trials, during which subjects were allowed to ask questions to facilitate their understanding of the task. The practice trials were always at the same refresh rate as the experimental blocks. After the practice trials, there was a short break while the experimenter restarted the program. Then the experimental trials were administered without interruption. An entire experimental session took approximately 35 minutes. Each subject participated in three sessions, one for each refresh rate. At the end of the experiment, subjects were debriefed concerning the strategies they used to perform the task and what they thought the independent variables were.
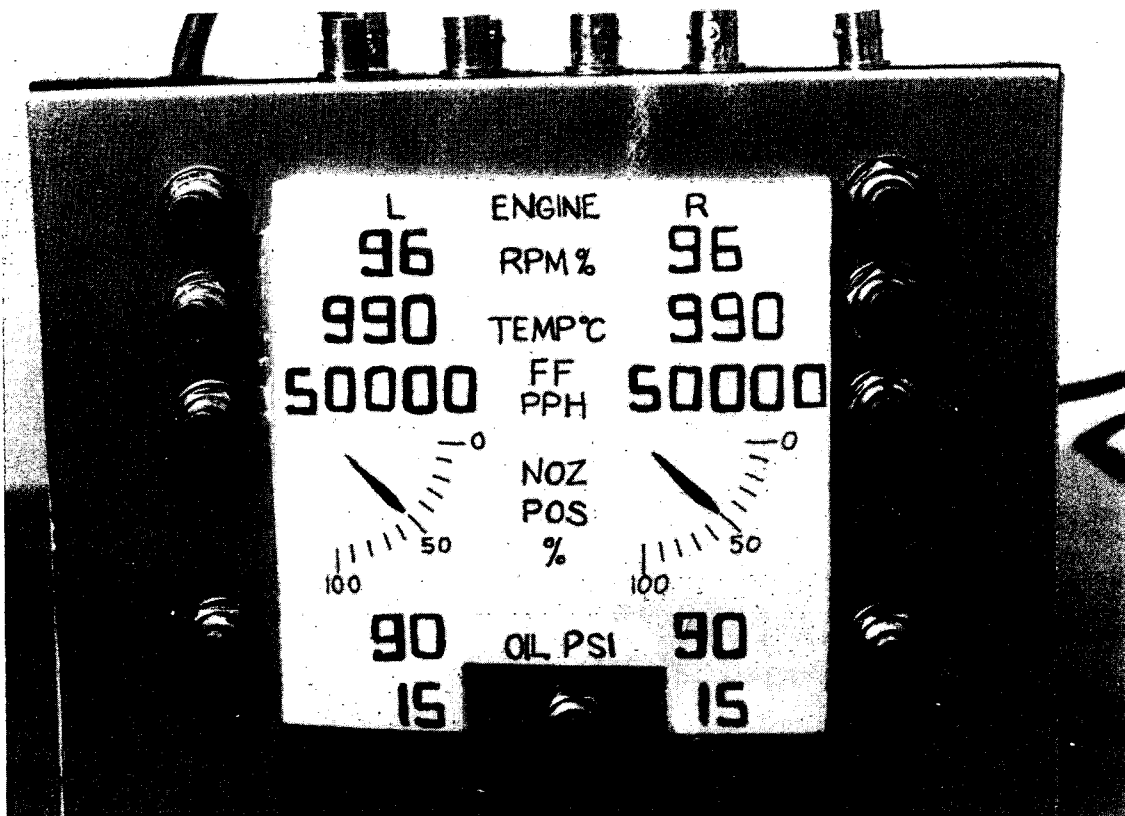
FIGURE 2. SUBJECT RESPONSE BOX

RESULTS

Each subject contributed 144 data points for analysis. These were obtained from the four display functions (RPM, Temperature, Fuel Flow, and Oil PSI, which will be referred to collectively as Function), the two sides of the display (right and left, referred to as Side), the three refresh rates for the display (4 Hz, 6 Hz, and 8 Hz, referred to as Rate), and the 6 blocks of trials that were presented at each rate (referred to as Block). The 144 data points were the median RTs of the 4 trials in each block for the display functions on the two sides of the EMD. Although several different types of errors were monitored, the only type that occurred often enough to be statistically analyzed was anticipatory response errors.

Three different analyses were performed on the RT data in order to answer questions concerning: (a) the overall effects of Function, Side, and Rate; (b) the effect of Block (i.e., within session effects); and (c) the effect of the direction-of-change of the Oil PSI display (i.e., whether it exceeded the maximum or minimum critical value, referred to as Direction). All three of these analyses have a common structure; that is, the Function, Side, Block and Direction effects all occur within the context of a Latin square analysis of Rate by test day (first, second or third experimental

session, referred to as Day). All analyses of variance (ANOVAs) were performed using the Statistical Analysis System (SAS Institute Inc., 1982) GLM procedure. For all significant main effects or two-way interactions, Duncan's Multiple Range post-hoc tests were performed using the SAS Duncan procedure. Significance level for all tests was set at $p < .05$. Since the Latin square portion of the analysis is the same in all three analyses, it will be discussed first.

Latin Square Analysis

The effect of Day is statistically significant ($F(2,4) = 24.81$). As can be seen in Figure 3, RT decreased significantly over all three experimental days. All pairwise comparisons were significant according to Duncan's Multiple Range Test. The decrease in RT occurred independent of the order of the refresh rate conditions. A significant group effect ($F(2,3 = 41.08$), indicates that mean RT, collapsed over all other variables, differs among the three groups. All three groups differ significantly from each other as determined by the Duncan's Test. The group difference may be due to the fact that each group constituted a different row of the Latin square and thus received the three refresh rate conditions in a different order over experimental days. However, at least two factors argue against this interpretation: a) there was no Rate x Day interaction, an effect that would correspond to the within-subjects portion of an order effect; and b) RT for all three groups improved similarly over days. All other Fs in the overall Latin square analysis, including that for rate, are less than 1.
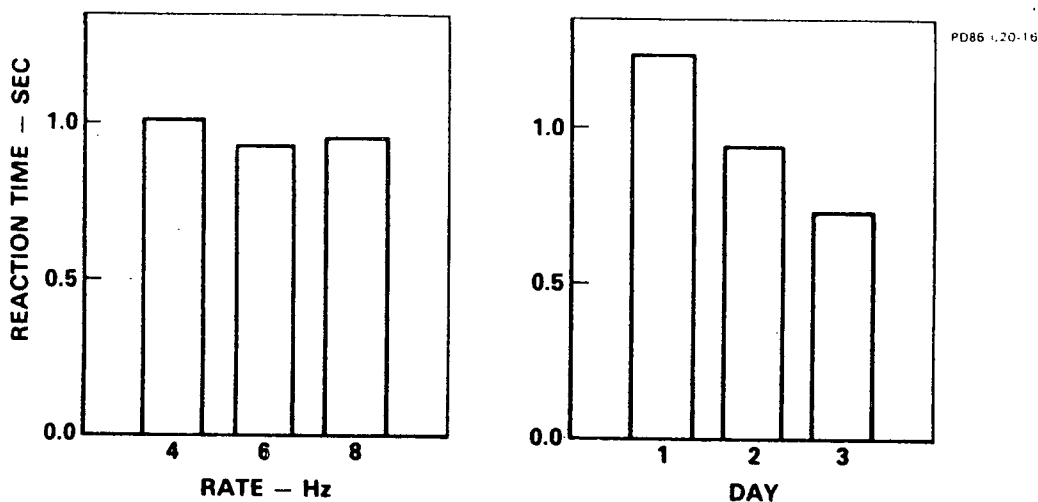
FIGURE 3. TIME TO DETECT CRITICAL EVENTS; RATE AND PRACTICE EFFECTS

Within Session Block Effects

No significant Block effects were observed. Fatigue did not seem to affect task performance. Mean RT actually decreases across Blocks 4, 5, and 6, even though task performance required a high degree of vigilance for an extended period of time. This observation, in combination with the strong Day effect, suggest partially offsetting effects of practice and fatigue within each experimental session.

Display Analysis

Analysis of RT data, designed to test the effects of display Function and Side, yielded two significant effects: the main effect of Function $(F(3,9) = 37.94)$ and the Function x Group interaction $(F(6,9) = 4.51)$. In addition the main effect of Side was marginally significant $(F(1,3) = 9.83,$ $p < .10)$. The means for the main effects are presented in Table 1. All comparisons among display function means differed significantly according to Duncan's Multiple Range Test; however, the Temperature and Oil PSI functions stand out from the others. Oil PSI was understandably more difficult to detect: 1) it was physically separated from the rest of the display functions and 2) it required that both maximum and minimum critical values be monitored. Because of these additional factors, Oil PSI is analyzed more thoroughly below.

PD86-020-18

	FUNCTION				
	RPM	TEMPERATURE	FUEL FLOW	OIL PSI	
CRITICAL VALUE	96 MAX	990 MAX	50000 MAX	90 MAX	15 MIN
NORMAL RANGE	30−72	545−800	12300−42500	38−62	38−62
NUMBER OF SIGNIFICANT DIGITS	2	3	3	2-½	2-½
DISTANCE TO CRITICAL VALUE	24	190	7500	28	23
PROPORTIONATE DISTANCE	.57	.75	.25	1.16	.96
MEAN RESPONSE TIME (RT) (MSEC)	974	546	1092	1473	1310
SIDE	LEFT	RIGHT	LEFT	RIGHT	LEFT	RIGHT	LEFT	RIGHT	LEFT	RIGHT
MEAN RT (MSEC)	876	1072	539	552	1069	1116	1300	1647	1258	1362

TABLE 1. RESPONSE TIME FOR CRITICAL ENGINE FUNCTIONS

184

It is more difficult to explain the very fast mean RT associated with the Temperature display. Possibly this results from the large discrepancy between the critical value (990) and the upper limit of the normal operating range (800) thus allowing subjects to more accurately predict when the display would reach its critical value.

As evident in Table 1 the left-to-right scanning bias is relatively large; however, this effect did not reach statistical significance. The Function x Group interaction was also significant, however, this effect does not lend itself to ready interpretation.

Oil PSI Analysis

As noted, Oil PSI display was analyzed separately in order to examine the effect of Direction. Raw data points for this analysis were the mean RTs of the two trials in each block for the maximum and minimum critical values of the Oil PSI display. In this analysis, only the main effect of Side $(F(1,3) = 44.29)$ reached statistical significance; however, the Side x Direction interaction was marginally significant $(F(1,3) = 9.03, p < .10)$. As can be seen in Table 1, response times were faster overall to the left Oil PSI display than to the right display. This mirrors that tendancy which was observed (but which failed to reach significance) in the overall analysis. The nature of the Side x Direction interaction can be clearly seen in the Table. Subjects were almost equally efficient in responding to both maximum and minimum critical values on the left side of the display, but were much slower in responding to the maximum critical value than the minimum critical value on the right side of the display.

Anticipatory Response Analysis

Unlike the RT data, no significant effects of Group or Day were observed for the anticipatory response frequency data. There was, however, a main effect of Function $(F(3,9) = 7.98)$. Anticipatory responses occurred significantly more often (according to Duncan's Multiple Range Test) for the Temperature display than for any other display. The Day x Function interaction was also significant $(F(6, 18) = 3.50)$. The source of this interaction was that there were more anticipatory response errors for the RPM display on Day 3 than Days 1 and 2 and fewer anticipatory responses for the Temperature display on Day 3 than on Days 1 and 2.

CONCLUSIONS

Refresh Rate

The major experimental question concerned the effect of screen refresh rate on performance in detecting display functions that had exceeded a specified critical value. The three different refresh rates used in this experiment, 4 Hz, 6 Hz, and 8 Hz, resulted in no significant differences in performance. This result is somewhat surprising in that, at first glance,

the task appeared to be very difficult. However, subjects' proficiency increased quickly, as evidenced by the large effect of experimental day where subjects' RT decreased significantly over days.

The lack of a significant refresh rate effect may be somewhat misleading. There is some indication that the task was, in fact, too easy. Although it required a high degree of vigilance over a period of 35 min, performance was remarkably consistent within an experimental session, as demonstrated by the lack of a significant effect of Blocks. Even though our subjects were highly motivated (they were coworkers of the experimenters), the task could be expected to produce effects of fatigue or boredom; yet performance actually improved slightly across experimental blocks within sessions.

In summary, the implication of the lack of both refresh rate and experimental block effects is that subjects are able to perform equally well in all three screen refresh rate conditions when they are highly motivated and are able to allocate all of their information processing capacity (that is, direct all of their attention) to the task. However, it is extremely unlikely that such a situation would ever exist in a cockpit, where monitoring the EMD is only one of many tasks that must be performed simultaneously. A more externally valid simulation would divide subjects' attention among a number of different tasks, one of which would be to monitor the EMD.

Display Variables

The analyses of the control variables provided some interesting results, especially the display function and side variables that described the physical layout of the display. For example, RT differed significantly among all four display functions. Considering for the moment only the RPM, Temperature, and Fuel Flow displays, there appears to be a relationship between RT and the difference between the upper limit of the normal operating range and the critical value. That is, RT was inversely related to the distance between the limit of the normal operating range and the critical value when that distance was expressed as a proportion of the width of the normal range. This does not result in a longer preparatory period while the observers watched the function approach critical value since we adjusted the rate-of-change for the simulated malfunctions so that each one made the transition from normal to critical in the same amount of time. The significant effect of function in this study, therefore, seems to result from the greater discriminability provided by relatively large numerical changes.

Reaction time for the Oil PSI display is considerably slower than for any other display function. When the Oil PSI display was analyzed separately from the other display functions, the left-to-right scanning bias was significant. Another factor to consider is that the Oil PSI display is the only display function that has both a maximum and a minimum critical value. Although there is no significant RT difference between the maximum and minimum critical values, the marginally significant interaction between display side and critical value direction suggest that this additional degree of complexity may contribute to the overall longer RT to the Oil PSI display.

Finally, there is the difference among display functions in anticipatory response errors. The greater error rate for the Temperature display than for all other display functions can be explained by the larger difference between the upper limit of the normal operating range and the critical value of the Temperature. This difference not only resulted in better response preparation and faster RT for the Temperature display, but also results in more errors of anticipation. However, overall the error rate is quite low and would probably be even lower with the addition of critical value indicators.

Group Differences

An unfortunate result in this study is the overall RT difference among Groups. As argued earlier, the Group difference appears to be simply a matter of individual differences. Since each group consists of only two subjects, the beneficial effects of random subject assignment are minimized. That is, with so few subjects chance differences between groups are readily possible. In fact, the two subjects with the slowest overall RT were assigned to Group 1 and the two subjects with the fastest overall RT were assigned to Group 3.

Future Directions

A follow-up study utilizing the secondary task technique could be very valuable. Requiring subjects to divide their information processing capacity among monitoring the EMD and other tasks may result in quite different conclusions about screen refresh rate effects. One could hypothesize that in such a task a clear advantage for one of the rates would be found. Post-experimental interviews with subjects revealed that many of them preferred a strategy that emphasized detecting pattern changes on the EMD rather than reading the digital value of the display functions. Based on this information one might hypothesize that an advantage would be found for the faster rate.

REFERENCES

SAS Institute Inc. (1982). SAS Users Guide: Statistics 1982 Edition. Cary, NC: SAS Institute Inc.

Winer, B. J. (1962). Statistical principles in experimental design. New York: McGraw-Hill.

EFFECT OF VARYING COCKPIT DISPLAY DYNAMICS
ON PILOT WORKLOAD AND PERFORMANCE

Lt Lisa B McCormack
Mr Frank L George

AFWAL/FIGC
Wright-Patterson AFB, OH

Research recently begun in the Flight Dynamics Laboratory investigating the effects of varying cockpit display dynamics on pilot workload and performance for a tracking task has produced some encouraging results. A series of four Air Force pilots 'flew' twelve display configurations for three simple aircraft transfer function models in a ground based simulator. Data such as RMS tracking error and stick activity indicate for a high intensity tracking task, pilots achieve better performances for high bandwidth, heavily damped displays. This research addresses the larger problem of achieving a higher level of pilot-vehicle integration for modern aircraft.

The purpose of this work was to examine the impact of dynamic elements of heads-up displays on pilot workload and performance. Here we discuss some results obtained in a fundamental in-house effort in this area.

We performed the analysis and experiment using a pursuit display and investigated the effects of varying time delay, bandwidth, and damping as well as the impact of degraded aircraft response on pilot workload and performance. The display dynamics consisted of a second order filter and a time delay. We selected three very simple aircraft models based on transfer functions and for our preliminary analysis, used the crossover model to simulate pilot dynamics. The tracking task consisted of a sum of sines with a break frequency of about 3.8 rad/sec, which appeared random to the pilots. Our preliminary work consisted mainly of closed loop analysis and showed we had selected reasonable parameters that would allow us to collect a wide range of performance information.
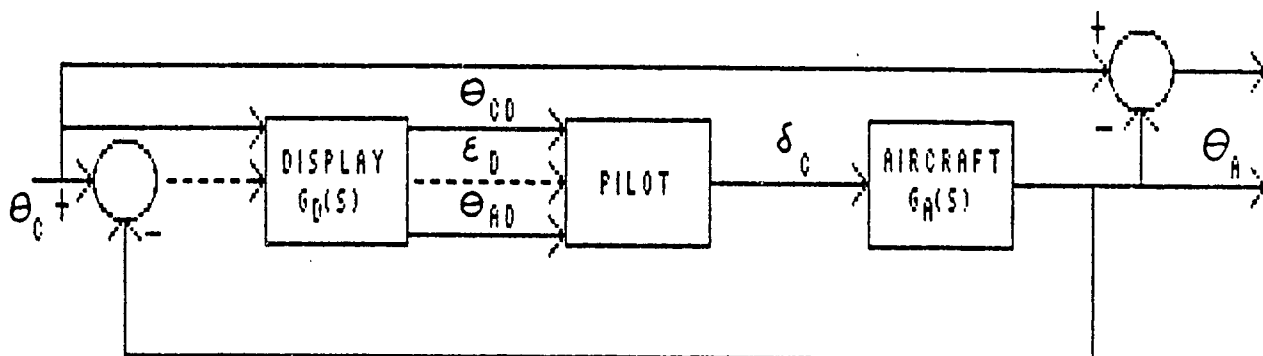
MANUAL

CONTROL LOOP

This plot shows the range of frequency response for the display
parameters varied during the simulation. We selected two values of time
delay: .0125 seconds (the baseline time delay of the simulation) and .125
seconds. We used damping ratios of .2 and .707 and bandwidths of 4, 8, and 12
rad/sec. For each aircraft the pilots flew, this allowed 12 combinations of
display characteristics. Pilots flew the display combinations in a different
random order for each aircraft.

VARIATIONS IN DISPLAY PARAMETERS
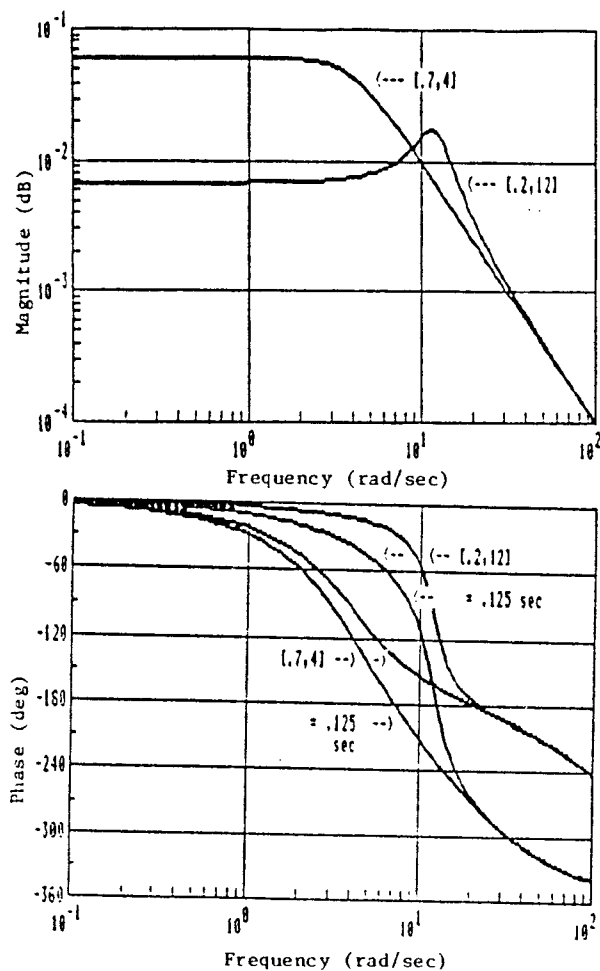
We chose three simple aircraft transfer function models for the experiment. The first is essentially a K/s, the second a K/s with a lag, and the third, a K/s^2. This allowed us to obtain a wide range of performance data and the opportunity to look at how degradations in aircraft response during a mission might affect task completion. Each pilot flew these aircraft in a different order, but they flew all the display configurations for that particular aircraft before going on to the next. In addition, we gave pilots training time on each aircraft before making recorded data runs.

AIRCRAFT PARAMETERS

$$G_A(s) = \frac{\Theta_A}{\delta_C} = \frac{K_A a_A}{s(s + b_A)}$$

	K_A	a_A	b_A
Aircraft 1	.586	40	40
Aircraft 2	2.15	1	1
Aircraft 3	1.17	1	0

We performed the simulation on the MAGIC (Microcomputer Applications of Graphics and Interactive Communications) Cockpit located in the Flight Dynamics Laboratory at Wright-Patterson AFB. The MAGIC Cockpit is a fixed-base, dynamic cockpit designed around four microcomputers. Because of the simple nature of this experiment, we used only Micro #1, which acted as the overall system executive, and Micro #4, which contained the aero model. Because of this simplicity, the simulation ran at a high frame rate of 80 Hz. We collected data at 20 Hz on stick input, tracking signal, commanded aircraft position, and error. Pilots used a Measurement Systems, Inc. sidestick with ±28.5° angular motion about neutral and a basic force gradient of about .1 lb/deg. The stick also had a ±1° deadband about neutral. Pilots performed a 2 minute pitch tracking task for each data run.

MAGIC COCKPIT
SCHEMATIC

Aero Model — Micro 4 — Gaertner Graphics — EADI

Micro 3

Micro 2

Exec — Micro 1
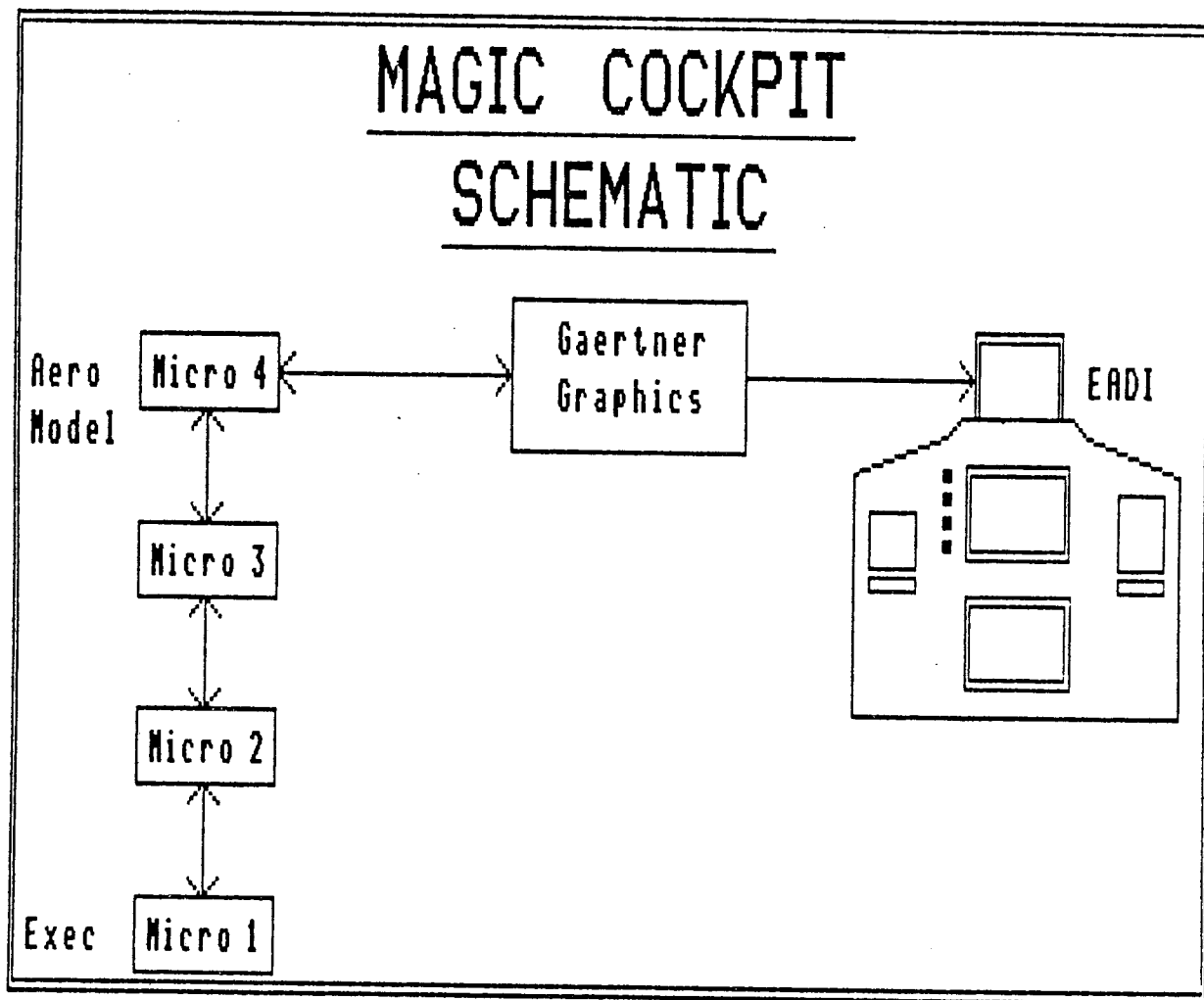
The table below gives the background of the four USAF pilots used as subjects during the experiment, which shows a wide variety of experience. We obtained some interesting results in light of these backgrounds and include some of our observations here.

Styles among pilots varied from extremely smooth, low frequency to very aggressive, wide bandwidth inputs for the same plants. However, for individual pilots, style did not change significantly with plant although inputs did. For instance, the K/s^2 plant led to more pulsing type inputs as also noted by other researchers.

Natural variation in style suggests we must use care in calling RMS stick activity a "workload measure." A naturally more aggressive pilot may expend more energy and show greater stick activity but may not perceive this as greater workload.

Finally, the "cleanest," most consistent data came from pilots who fly real aircraft regularly. Pilot 2 has flown only simulations for some time now while Pilot 3 currently works in an office environment.

PILOT BACKGROUNDS

Pilot	
1	Utility (T-39)
2	Cargo (C-141), Tankers (KC-135) Trainers (T-38), Helicopters TPS Graduate and Instructor Extensive simulation time
3	Fighters (F-4,F-15)
4	Cargo (C-141)

We noted several trends in this plot, which shows RMS tracking error against RMS stick activity for Aircraft 1 at a display bandwidth of 4 rad/sec. First, pilots had significantly higher RMS tracking errors for the lightly damped display. Second, subjects show some large differences in pilot style. For instance, Pilot 1 shows a large decrease in stick activity when we added time delay to the display while Pilot 4 shows almost no change for both the lightly damped and critically damped cases. However, they have almost identical RMS tracking errors.

EFFECT OF TIME DELAY AND DAMPING ON PERFORMANCE

Aircraft 1

$$\omega_D = 4 \text{ rad/sec}$$

RMS Stick Activity, δ_c (inches)
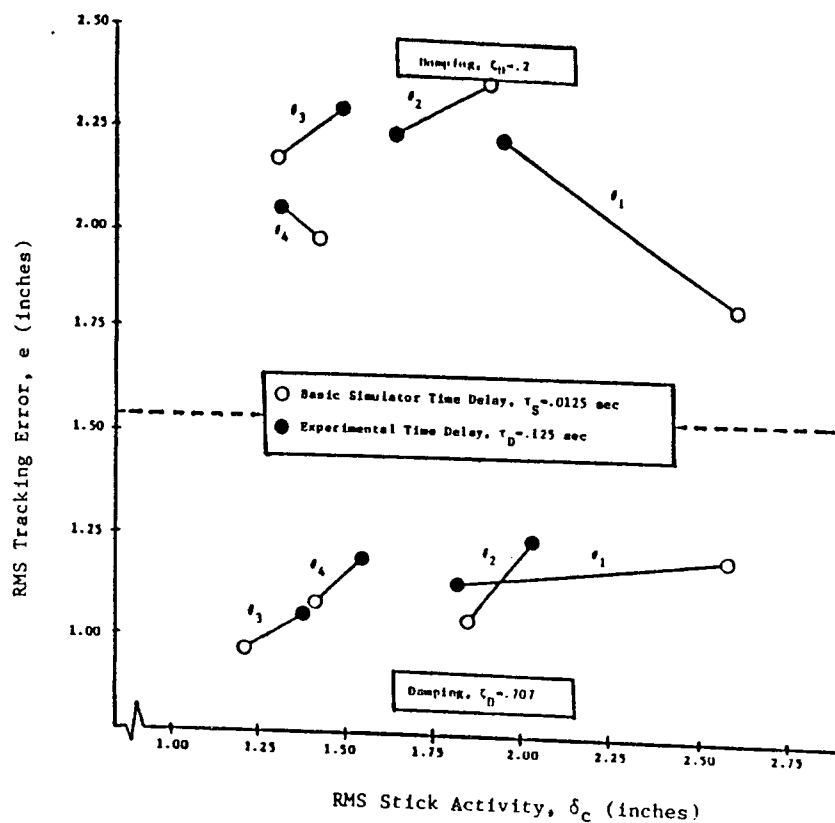
This diagram shows RMS stick activity vs. bandwidth for each of the pilots when flying Aircraft 1. Some of the pilots varied their stick activity greatly when confronted with different display configurations while others, notably Pilot 4, showed little change in stick activity.

EFFECT OF BANDWIDTH ON RMS STICK ACTIVITY

Aircraft I

Pilot 1

RMS Stick Activity, δ_c (inches)

Bandwidth, ω_D (rad/sec)

Pilot 2

RMS Stick Activity, δ_c (inches)

Bandwidth, ω_D (rad/sec)

Pilot 3

RMS Stick Activity, δ_c (inches)

Bandwidth, ω_D (rad/sec)

Pilot 4

RMS Stick Activity, δ_c (inches)

Bandwidth, ω_D (rad/sec)

196
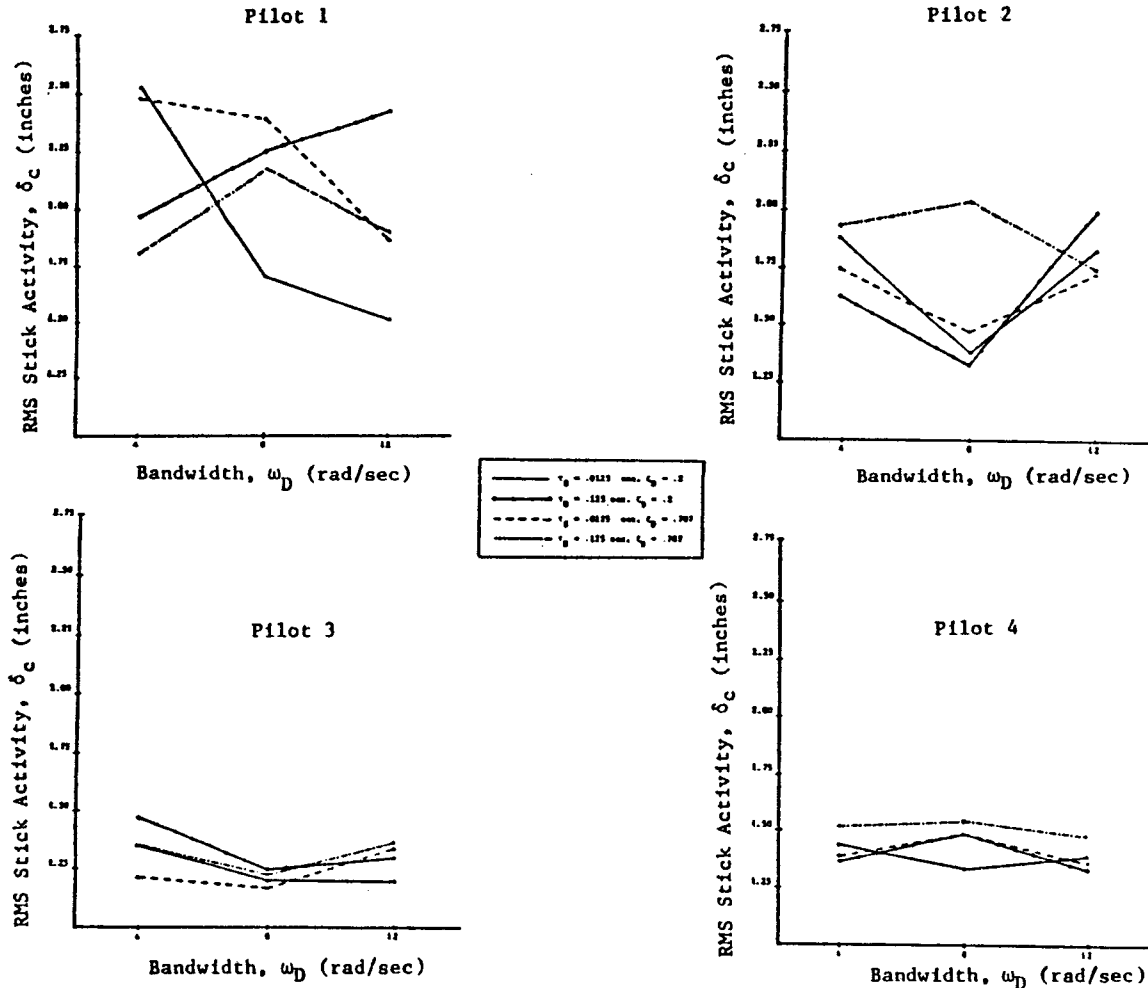
For the same conditions as the last plot, this diagram shows RMS tracking error vs display bandwidth. We noted that despite the difference in pilot style between Pilots 1 and 4 noted on the last slide, they have almost identical RMS tracking errors. Thus, although some pilots appeared to work harder than others, they achieved the same basic level of performance. We expected to see differences in style because of the differences in background shown earlier. We noted this also for the diagram showing RMS tracking error vs RMS stick activity. In addition, the added time delay had a much smaller than anticipated effect on RMS tracking error, which increased between -5% and 22%. Third, we found for Aircraft 1 and 2, when the display filter had the same or similar bandwidth as the forcing function (3.8 rad/sec), the damping ratio had a major impact on pilot performance. The lightly damped case consistently resulted in higher RMS tracking errors. Once the display bandwidth increased above the forcing function break frequency, the RMS tracking errors rapidly converged to similar values, indicating damping ratio had little effect on overall performance at higher bandwidths.

As mentioned before, we found it interesting to examine the differences in pilot style and performance. We expected some differences. For instance, we were not surprised that Pilot 4, a C-141 pilot, showed little change in stick activity while we varied the display dynamics. Pilot 1, on the other hand, flies the smaller two-engine T-39. He showed considerable change in stick activity with display configuration, probably because of his flying experience.

We did not find Pilot 3's results particularly useful. He did not identify with the task or find the simulation useful because it did not behave like a real aircraft, particularly for Plants 2 and 3. In some cases, he almost gave up the tracking task and simply kept his aircraft centered on the screen.

We expected to get consistent data from Pilot 2 because of his extensive test pilot background. However, he has flown only simulations for quite some time and this appears to contaminate his data somewhat. In addition, Pilot 2 tried to determine what we changed from one display configuration to another rather than simply flying the mission. This also appears to have contributed to scatter in his data.

EFFECT OF BANDWIDTH ON RMS TRACKING ERROR

Aircraft I
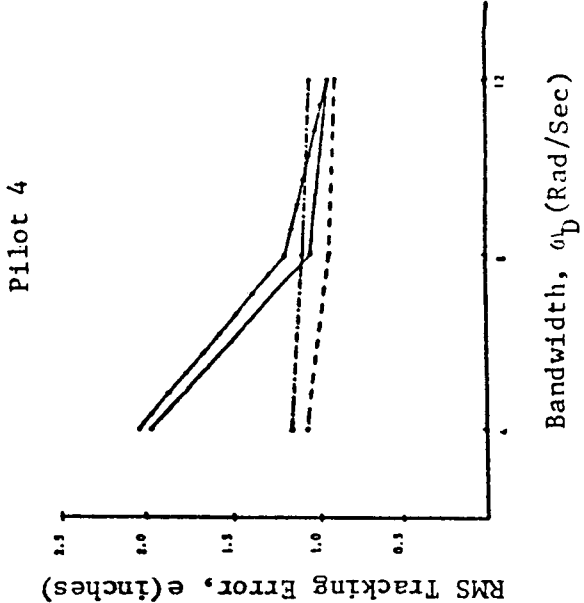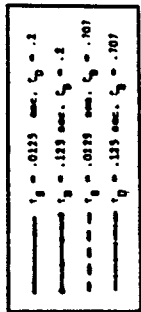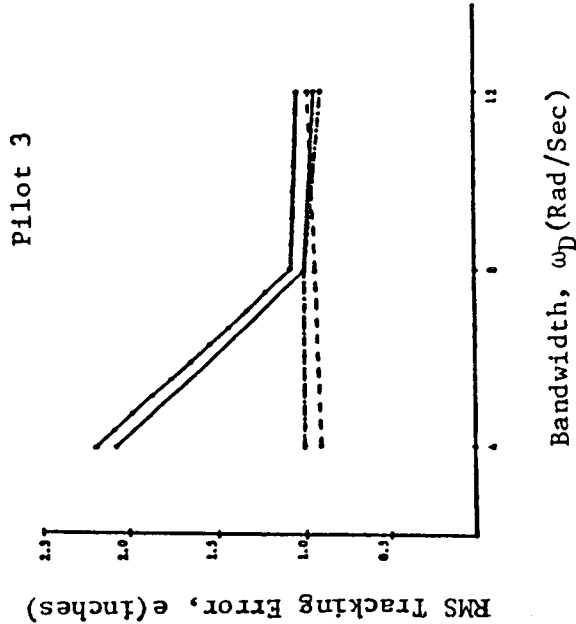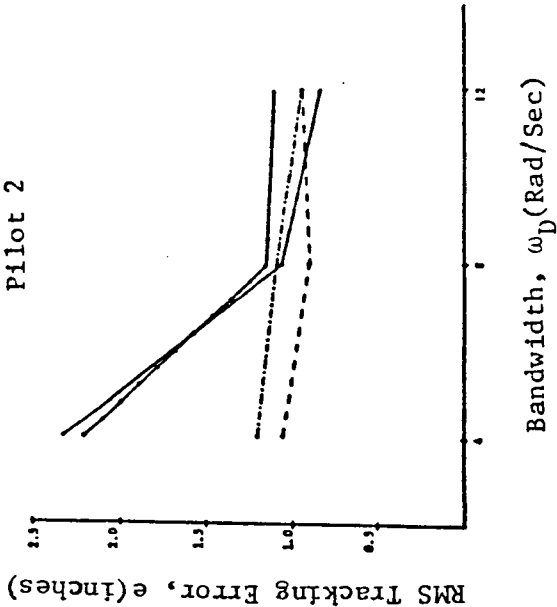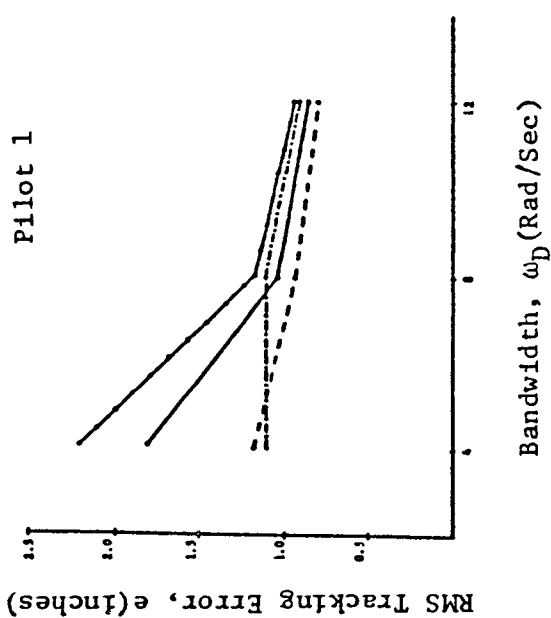
We made a number of conclusions based on this experiment. We have not solved the display dynamics problems, but we have found direction on where to go from here. We have not finished evaluating all of the data collected, and this discussion represents only a portion of the completed analysis.

We have found that for the range tested, time delay had a smaller than expected impact on performance. We would like to increase the time delay to find out when it begins to seriously affect tracking. Our data shows the significant impact display damping and bandwidth have on performance. We need to investigate in more detail what values for these parameters result in the best performance and lowest workload.

We also found pilots can tolerate degradations in aircraft response. Pilots' RMS stick activity generally increased when they flew Aircraft 2 compared to Aircraft 1, but their RMS tracking error increased very little for the same display configuration. This means pilot workload increased but not enough to significantly impact performance.

We noted the benefits of flying qualities engineers working with human factors engineers. By continuing to cooperate in future in-house efforts, we hope to eventually achieve a higher level of pilot-vehicle integration.

CONCLUSIONS

- Impact of ω_D and ζ_D on performance and workload

- Relatively small effect of τ_D for range tested

- Ability of pilots to tolerate degradations in aircraft response

- Need for human factors and flying qualities engineers to work together

We have already begun planning for future experiments. We would like to include display bandwidths which fall just on either side of the forcing function break frequency. For instance, for the same forcing function used in this first experiment, we would like to try using display bandwidths of 2, 4, and 6 rad/sec to investigate in more detail the effect this has on pilot tracking performance.

As mentioned before, we would like to increase the amount of display time delay still further to find the point where time delay begins to greatly interfere with the tracking task. We will correlate this fixed-base result with in-flight simulation results being generated by Calspan Corporation. In addition, while this experiment used the same amount of time delay for both pieces of information on the display as in an IFR task, we would like to try varying the time delay between the command and response elements of the display to simulate a VFR task.

At the suggestion of another interested party, we may try incorporating a truly random forcing function into an experiment, rather than the pseudo-random sum of sines used in this simulation, so we can attempt to use time series identification of pilot dynamics.

We designed this experiment to take a first look at the problems of pilot-display-aircraft integration. We plan on continuing our in-house efforts and augmenting them with a parallel contractual effort. We welcome any suggestions anyone has for future work in this area.

RECOMMENDATIONS

Future Research

- ω_D on either side of break frequency of the forcing function

  Ex: ω_D = 2, 4, 6 rad/sec

- Increasing time delay

- Vary time delay between command and response elements

- Incorporating a truly random forcing function

- SWAT rating scale

MODEL-BASED EVALUATION OF DISPLAY-DYNAMICS

EFFECTS IN PURSUIT TRACKING

Sanjay Garg   and   David K. Schmidt
School of Aeronautics and Astronautics
Purdue University
West Laffayette, IN 47907

Abstract

In conjunction with an experimental investigation being conducted at the Air Force Wright Aeronautical Laboratories (AFWAL), a model-based evaluation of the effects of display dynamics on human performance and workload is performed. Three different plant dynamics, ranging from K/s to K/s^2, are considered in combination with a second-order display filter, with varying display bandwidth and damping, and with/without added time delay. The task considered is that of single-axis pursuit tracking. The model-based predictions are found to be in excellent agreement with experimentally observed trends. A model-based procedure for adjusting the neuromuscular lag time constant (τ_N), a parameter used in the Optimal Control Model to more realistically model the human's performance/workload trade-off, is suggested and preliminary results using the procedure appear promising. The predicted time-delay effects are compared with the results of a previous experimental study and are found to be in agreement with those results as well.

Introduction

The Air Force Wright Aeronautical Labs (AFWAL) has initiated an experimental study to investigate the effect of display dynamics on the handling qualities of flight vehicles [7]. The specific objectives of the experimental study are to determine what display parameters affect the pilot's control task performance and to quantify the extent of these effects in order to incorporate display dynamics considerations into flying qualities criteria.

In conjunction with this experimental study, a model-based evaluation of the effects of the display dynamics on the human's performance and workload was performed, and is reported here. The human operator model considered is the Optimal Control Model (OCM) developed by Kleinman et. al. [1]. Not only is the statistical performance (e.g. rms tracking error) of interest, but also frequency-domain analysis based on the OCM results, as in Ref. [11], is of fundamental importance in understanding the pilot-vehicle interaction.

201

The overall objective of this study is to further develop model-based techniques for display analysis, and compare the results with those of the experimental investigation in an effort to further validate the modelling procedure. The OCM has previously been used for the analysis of display/control systems, see for example Ref. [2], but these studies did not take into account any display dynamics as such. Moreover, various display design methodologies based on the OCM have been suggested in the recent past [3,4,5,6]. Thus, validation of the modelling procedure will be of tremendous help in generating more confidence in the model-based design methodologies. Also, once the modelling procedure is validated, the analytical tools can be used to better understand the interaction between plant dynamics and display dynamics.

The pursuit tracking task considered in the 'AFWAL' experimental study is first discussed and some sample results are presented. A detailed description of the experimental set up and discussion of the preliminary results can be found in Ref. [7,8]. The task modelling for evaluation using the OCM is then discussed and the model-based results for the K/s plant are compared in detail with those of the experimental study. The neuromuscular lag time constant (τ_N) adjustment procedure is then presented, alongwith some preliminary results showing that such a procedure yields better agreement between model predictions and experimental results. Next, a brief summary of the comparison between analytical and experimentally observed trends for the two other plant dynamics is presented, followed by a comparison between the model-based results and Hess' findings on the effects of time delay [9].

Task Description and Sample 'AFWAL' Results

The experiment described in Ref. [7] used a single-axis pursuit tracking task with a CRT display. The block diagram for the task is shown in Fig. 1. The command (θ_C) and the plant output (θ_A) are presented to the pilot on a display with dynamics $G_D(s)$. The pilot reconstructs the error from the two observations and applies control action (δ_p) to minimize this displayed error (e_D). The three plants considered are :

$$G_A(s) = \frac{K}{s} \quad ; \quad \frac{K}{s(s+4)} \quad ; \quad \frac{K}{s^2} \tag{1}$$

The display dynamics are of the form :

$$G_D(s) = \frac{\omega_D^2}{(s^2+2\zeta_D\omega_D s+\omega_D^2)} e^{-\tau_D s} \tag{2}$$

Three values of display bandwidth, ω_D = 4, 8, 12 rads/sec, two values of display damping, ζ_D = 0.2, 0.707, and two values of display time delay,

202

τ_p = 0.012, 0.125 secs were considered. Thus for each plant (as in (1) above) twelve different cases of display dynamics were evaluated. The command θ_c was generated as a sum of five sine functions with a magnitude shelf at 0.47 rads/sec, and a maximum frequency of 3.8 rads/sec.

Four USAF pilots flew the 36 plant/display combinations in a fixed-base simulator. RMS values of the tracking performance (e_p) and control activity (δ_p) were obtained for tracking runs of two minutes each. Figs 2(a) and (b) show the variation in tracking performance and control activity with varying display dynamic parameters for the K/s plant and for pilot 4, as reported in Ref. [7]. In [7] and [8] it was reported that control activity showed large variations for different pilots while performance trends were about the same. The results presented in Figs. 2(a)-(b) are for a "more relaxed" pilot showing the most consistency in control activity.

From Fig. 2(a), the effect of display dynamic parameters on display tracking performance can be summarized as follows :

(i) Tracking performance improves with increasing display bandwidth. Also, for any given display bandwidth, the tracking performance is worse for the case of lightly damped display as compared to heavily damped display.

(ii) For low display bandwidth (ω_D = 4 rads/sec), the tracking performance is very sensitive to display damping. That is, for low display bandwidth, the tracking error increases considerably when display damping is decreased from 0.707 to 0.2.

(iii) For any given display filter, the tracking performance is uniformly worse for the case of higher time delay.

From Fig. 2(b) it is noted that for the "relaxed" pilot, the control activity is relatively constant in that it does not vary much with changes in display-dynamic parameters. One of the trends which is obvious, though, is that for the case of a heavily damped display, the control activity consistently increased with increased time delay.

As stated earlier, detailed discussion of the experimental results for the K/s plant and for the other two plants can be found in Refs. [7,8].

Model-Based Evaluation and Comparison with 'AFWAL' results

Task Modelling

For the analysis with the OCM, the command was modelled as a second order Markov process :

$$\theta_C(s) = \frac{0.8}{(s^2+2(0.7)(0.55)s+(0.55)^2)} \, w(s)$$

and

$$E(w) = 0, \quad E[w(t)w(t+\sigma)] = \delta(\sigma)$$

The damping of 0.7 was chosen for the command generator to yield a rectangular power spectra and the command bandwidth and filter gain, alongwith the intensity of the white noise, were chosen to closely match the rms values of the command and the command rate $(\dot\theta_C)$ used in the experimental study.

The block diagram corresponding to the task as modelled is shown in Fig. 3. In accordance with the task of pursuit tracking, the pilot's observations (forming the vector $\bar{y}_p$) were chosen to be the displayed error (e_D) and the displayed plant output (θ_{AD}), and the pilot.was assumed to be able to reconstruct the associated rates $\dot{e}_D$ and $\dot\theta_{AD}$ from these displayed variables. The parameters that define the human operator model in the OCM were set to the following values :

(i) Observation noise ratio of -20 dB for each observation.

(ii) Motor noise ratio of -20 d3.

(iii) Observation time delay of 0.2 secs.

(iv) Observation thresholds based on a visual arc angle of 0.05 degs and angular rate of 0.15 degs/sec at the pilot's eye.

(v) The pilot's attention allocation between e_D and θ_{AD} was optimized using the procedure in [3] and the attention allocation for the rates was set to be the same as that for the corresponding displayed variable.

The objective function was chosen to be :

$$J_p = E\{\lim_{T\to\infty} \frac{1}{T} \int_0^T (e_D^2 + g\dot\delta_p^2)dt\}$$

with 'g' selected to yield a desired neuromuscular lag time constant, τ_N. This objective function reflects the pilot's objective of minimizing the displayed error to the best of his abilities, and the choice of $\tau_N=0.1$ secs, for example, models the most aggressive human operator behavior observed in experimental studies. Such a formulation leads to a control law of the form

$$\delta_p(s) = \frac{1}{\tau_N s+1} H_p(s) \, \bar{y}_p(s)$$

K/s Plant Results

The model-based results for the K/s plant with varying display dynamic parameters are shown in Figs. 4(a) and (b). Since the values of display gain and stick gain used in the experimental study were not available, a direct comparison of numerical values was not possible. So the model-based results were normalized with respect to the predicted values for a pure K/s plant (without any added display dynamics, and K=0.13 in./sec). Fig. 4(a) shows the normalized rms tracking error as a function of the various display parameters while Fig. 4(b) shows the normalized rms control activity.

Comparing Fig. 4(a) to Fig. 2(a) we notice that the model-based prediction of the performance trends is quite similar to that observed in the 'AFWAL' study. The model correctly "predicts" that the tracking performance would improve with increasing display bandwidth and would be uniformly worse with increased time delay. Also the model-based results indicate the high sensitivity of performance to display damping for the low value of display bandwidth, but the degradation in performance predicted by the model is not quite as much as indicated by the 'AFWAL' results.

Comparing Fig. 4(b) to Fig. 2(b) we note that model-predicted control activity is also quite "flat" for higher values of display bandwidth, but model results indicate much higher control activity for low display bandwidth than that obtained in the experimental study. For the case of a heavily damped display, the trend of increased control activity for higher time delay is also borne out by the model-based results.

The disagreement between the model-based results and the experimental result in terms of control activity for the case of low display bandwidth may be due to the fact that here we are modelling the most aggressive pilot behavior with $\tau_N=0.1$ secs. From the experimental data, it seems that the pilot is willing to accept degradation in performance in order to keep his workload within acceptable limits. Such a performance/workload trade-off can be modelled using the OCM by a model-based adjustment of the neuromuscular lag time constant τ_N.

Fig. 5 shows a plot of modelled performance (rms e_p) vs. workload[*] (rms δ_p) for the case of low display damping, with low and high display bandwidth, as a function of τ_N used in the modelling procedure. Note the location of the points corresponding to $\tau_N=0.1$ secs on the two curves. For the case of $\omega_D=4$ rads/sec, the flat portion of the curve

---

[*] Wierwille et. al. [13] have shown that the pilot's perception of workload is strongly correlated with his control rate activity.

spans a large range of control rate activity which means that the pilot might increase his workload (by being more aggressive), but it will not necessarily result in improved performance. This flat portion of the curve is much smaller for the case of $\omega_D=12$ rads/sec. Thus, assume that the well-trained pilot would work just hard enough to achieve an acceptable level of performance. Then, the point on the curve at which the degradation in performance begins to be perceptible (the "knee" in the curve) can be considered to be the solution to the performance/workload trade-off made by the pilot. For both the cases shown in fig. 5, this "knee" in the curve occurs near $\tau_N=0.14$ secs. Finally, Fig. 6 compares the normalized tracking error and control activity for the two cases, for $\tau_N=0.1$ and 0.14 secs. We note that using the τ_N adjustment procedure results in "flattening" of the control activity, thus making the model results more in agreement with the experimental ones.

It should be stressed here that this τ_N adjustment procedure may be used prior to the experiment, i.e. it need not be done to match the experimental data after such data has been obtained, but rather can be used to predict the "most probable" pilot behavior.

It is also noted that for this plant, the model-based prediction for the attention allocation is that the pilot would devote about 95% attention to the displayed error and only 5% attention to the plant output. This result is in agreement with the observations in Ref. [12] (based on an extensive experimental data-base), that for a K/s plant, the pilot's behavior is mostly compensatory, even when a pursuit display is provided.

Finally, it can be shown that for the case of low display bandwidth with light damping, the magnitude cross-over frequency for the pilot-vehicle loop transfer function will be restricted to a low value to preserve an adequate gain-margin, and this results in deteriorated performance. This situation is further aggravated with time delay. Work on the details of such analysis and further frequency-domain analysis using the pilot describing functions obtained from the OCM, as in Ref. [11], is presently underway.

K/s.4/(s+4) Plant Results

Comparison between the model-based results and the experimental results for this plant is summarized as follows :

(i) Experimental results indicate that the trends in performance and control activity with changes in display dynamic parameters are similar to those for the K/s plant. The model results are in agreement with this observation.

(ii) Experimental results show little change in rms error from the K/s plant for a given display. Model results indicate an increase of 5%-20% in rms error with the increase being higher for the case of

low display bandwidth.

(iii) Experimental results show increased control activity as compared to the K/s plant. Model results are in agreement and indicate an increase of 20%-50% in rms control activity.

K/s^2 Plant Results

The tracking task with this plant was found to be considerably more difficult, and large tracking errors as well as high control activity were obtained in the experiments. The difficulty of the task was also borne out by the model results. It is stated in Ref. [7] that in some cases the pilots abandoned the task altogether. Using the model, convergence was infact difficult, and model convergence was not obtained for the cases corresponding to the combination of high display damping and high time delay. So in a sense, even the OCM abandoned the task! It is further stated in Ref. [7] that the rms error for the pilots who actively tried to track the command differed very little from those who abandoned the task. Model results, for the cases for which convergence was achieved, indicate rms tracking error values approaching the rms command value showing that the pilot's control activity is not helping much in the tracking task.

For this plant, model results predicted an attention allocation of 80% to display error and 20% to plant output for the case of high display bandwidth and this ratio changed to 50-50 as the display bandwidth was decreased. Thus the model correctly predicts an increase in pursuit behavior with increasing task difficulty [12].

Time-delay Effects

In Ref. [9], Hess has reported the results of an experimental study conducted to determine the effects of time delays in manual control systems. His key findings can be summarized as follows :

(i) Increased time delay leads to degradation in performance in that the magnitude cross-over frequency of the pilot-vehicle loop transfer function is decreased leading to increased rms error values.

(ii) Most interestingly, Hess found that with high time delay, pilot's compensation is such that the well known "cross-over" criteria [10] is violated. The pilot is forced to apply more lead, so that the magnitude is distorted, and the slope is less than -20 dB/decade at crossover.

(iii) Hess also found that a K/s^2 plant with high time delay was beyond the control capability of the human operator.

Model-based results showing uniform degradation in performance with increased time delay are then in agreement with Hess' findings. A specific comparison was made between Hess' results for a K/s plant and

model-based results for the K/s plant with large display bandwidth and low display damping (so that the controlled element is just like K/s in the frequency region of pilot's operation). For an increase in time delay from 0.012 to 0.125 secs, estimating from Hess' data [9] shows an increase of 21% in error rms value and the model results show the same percentage increase. The magnitude cross-over frequency regression from Hess' data is 3.0 to 1.5 rads/sec (estimated) while the model results show a cross-over frequency regression from 2.8 to 2.4 rads/sec. When the τ_N adjustment procedure is used, the "knee" in the curve for the case of higher time delay occurs near $\tau_N = 0.18$ secs and then the cross-over frequency regression is from 2.65 rads/sec (for $\tau_N = 0.14$ secs as before) to 2.1 rads/sec. Also, it was noted that the model predicted pilot describing function, for the case of higher time delay, is such that the pilot-vehicle loop transfer function magnitude at cross-over has a slope slightly less than -20 dB/decade.

Finally, Hess' findings that a K/s^2 plant with high time delay was "uncontrollable" by the human operator further validate the model result that convergence was not achieved for the K/s^2 plant with a large display phase loss associated with the time delay and high display damping.

Conclusions

The model-based results of the effects of display dynamics on pilot's performance and workload were found to be in excellent agreement with the experimental results of the 'AFWAL' investigation and also Hess' results, thus validating the use of the model as an analytical tool for display analysis. The τ_N adjustment procedure presents a promising technique for more realistically modelling the performance/workload trade-off characteristics of the human operator and is presently under further study. In addition, frequency-domain analysis to further understand the interaction between plant and display dynamics and its implications on the design of displays for improved handling qualities is presently being pursued.

References

[1] Kleinman, D.L., Baron, S., and Levison, W.H., "An Optimal Control Model of Human Response," Parts I and II, Automatica, Vol. 6, pp. 357-383, 1970.

[2] Baron, S., and Levison, W. H., "Display Analysis with the Optimal Control Model of the Human Operator," Human Factors, 19(5), Oct. 1977, pp. 437-457.

[3] Levison, W.H., "A Model Based Technique for the Design of Flight Directors," Proceedings of the Ninth Annual Conference on Manual Control, May 1973, pp 163-172.

[4] Hess, R.A., "Analytical Display Design for Flight Tasks conducted under Instrument Meteorological Conditions," NASA TM X-73,146, August 1976.

[5] Hoffman, W.C., Kleinman, D.L., and Young, L.R., "Display/Control Requirements for Automated VTOL Aircraft," NASA CR-158905, ASI-TR-76-39, October 1976.

[6] Garg, S., and Schmidt, D.K., "Cooperative Synthesis of Control and Display Augmentation," AIAA paper 86-2204, presented at AIAA Guidance, Navigation and Control Conference, at Williamsburg, VA., 18-20th August, 1986.

[7] McCormack, Lisa B., and George, Frank L., "Impact of Display Dynamics on Flying Qualities," NAECON 1986.

[8] McCormack, Lisa B., and George, Frank L., "Effect of Varying Cockpit Display Dynamics on Pilot Workload and Performance," 22nd Annual Conference of Manual Control, Dayton, Ohio, July 1986.

[9] Hess, R. A., "Effects of Time Delays on Systems Subject to Manual Control," Journal of Guidance, Control and Dynamics, July-August 1984, pp. 416-421.

[10] McRuer, D.T., and Jex, H.R., "A Review of Quasi-Linear Pilot Models," Transactions of Human Factors in Electronics, Vol. HFE-8, No. 3, Sept. 1967, pp. 231-249.

[11] Bacon, B.J., and Schmidt, D.K., "An Optimal Control Approach to Pilot/Vehicle Analysis and the Neal-Smith Criteria," Journal of Guidance and Control, Vol. 6, No. 5, Sept.-Oct. 1983, pp. 339-347.

[12] McRuer, D.T., and Krendel, E.S., "Mathematical Models of Human Behavior," AGARDograph No. 188, Jan. 1974.

[13] Wierwille, W.W., and Connor, S.A., "Evaluation of 20 Workload Measures Using a Psychomotor Task in a Moving-Base Aircraft Simulator," Human Factors, Vol. 25, pp. 1-16, 1983.
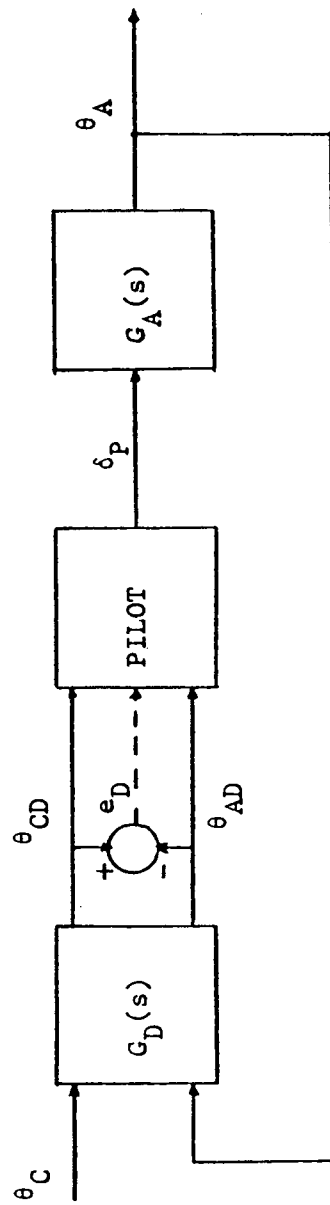
Fig. 1 Manual Control Loop Block Diagram

Legend:

$\tau_D = 0.012$ sec., $\quad G_D = 0.2$

$\tau_D = 0.125$ sec., $\quad G_D = 0.2$

$\tau_D = 0.012$ sec., $\quad G_D = 0.707$

$\tau_D = 0.125$ sec., $\quad G_D = 0.707$

(b) Control Activity, δ_P (in.) vs Display Bandwidth (rads/sec)

(a) Tracking Error, e_D (in.) vs Display Bandwidth (rads/sec)
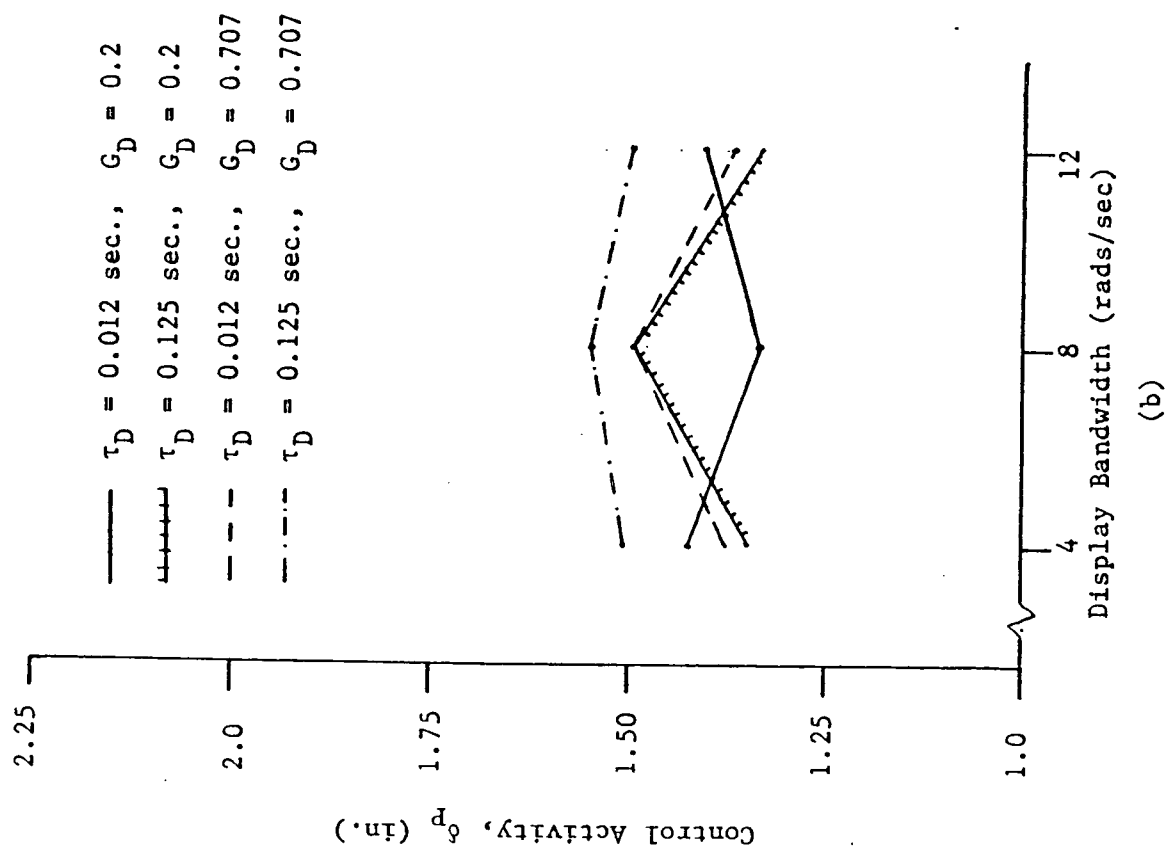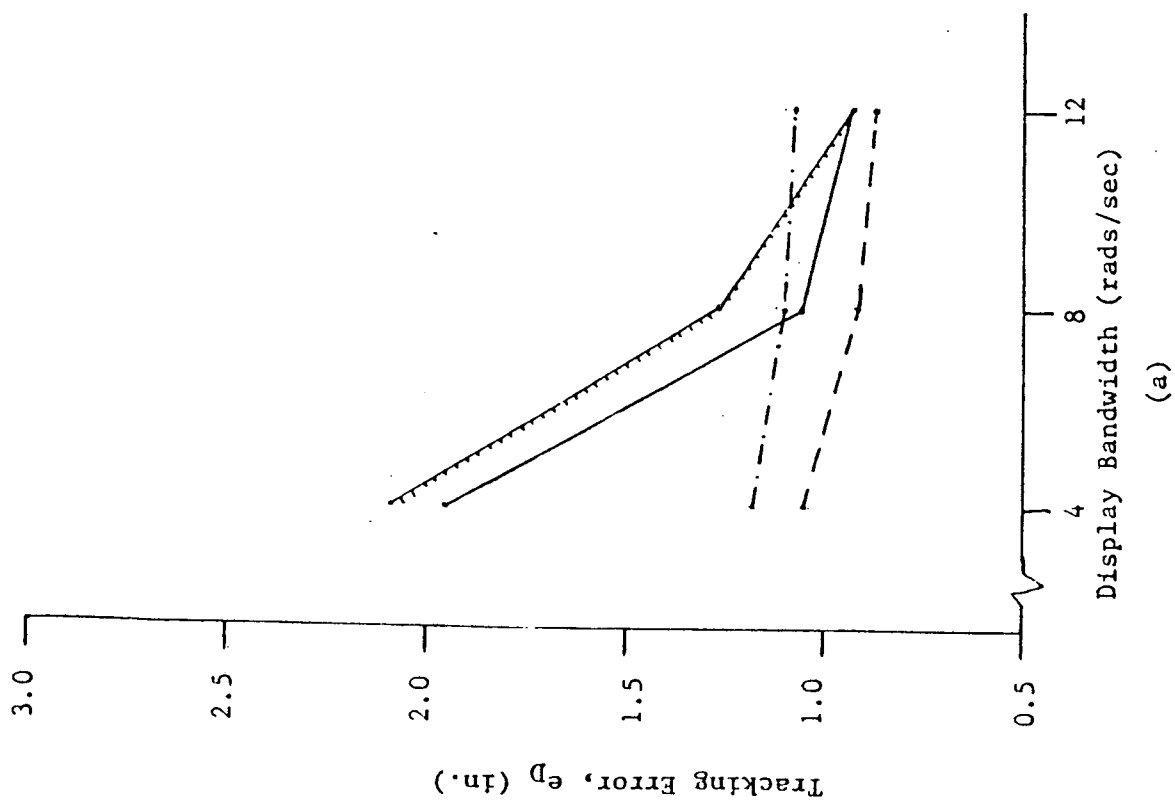
Fig. 2 'AFWAL' Results for $\frac{K}{s}$ Plant: Pilot 4
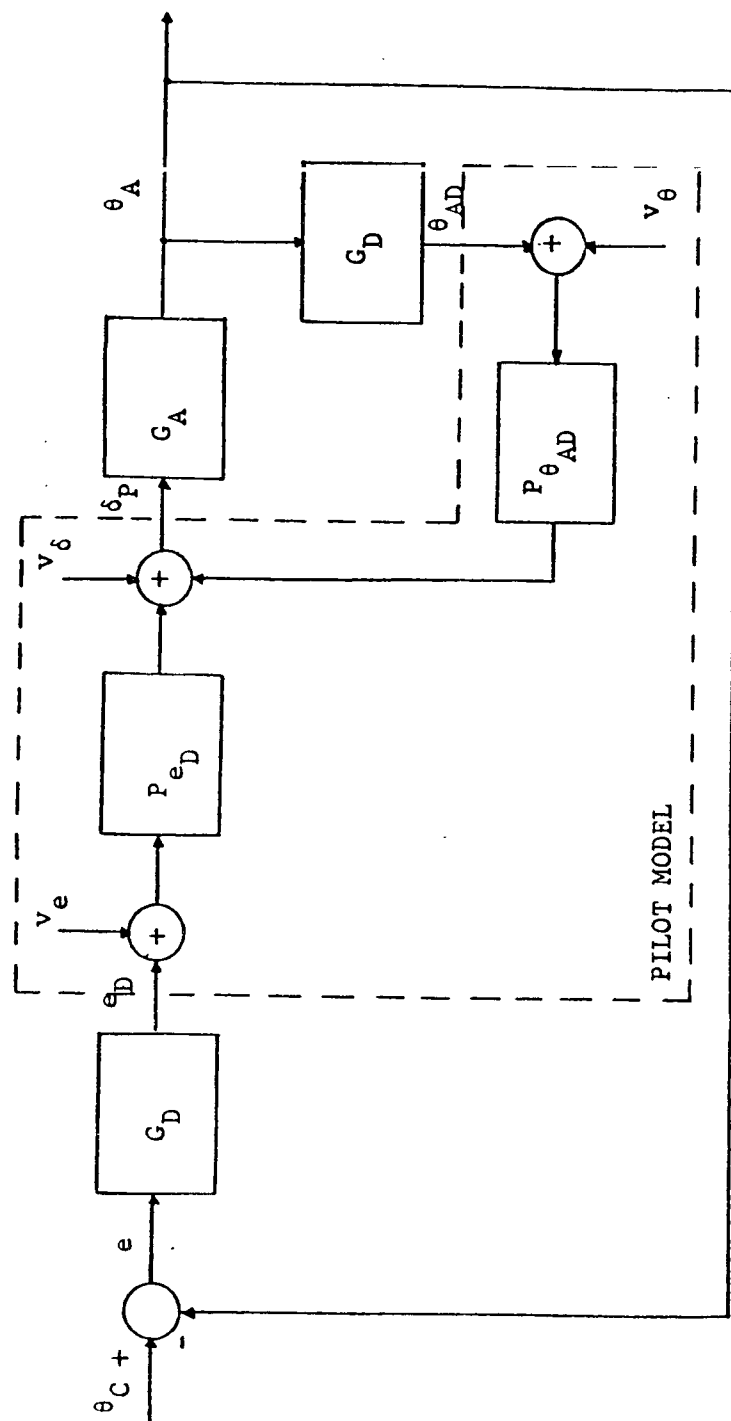
Fig. 3 Block Diagram for Task Modelling
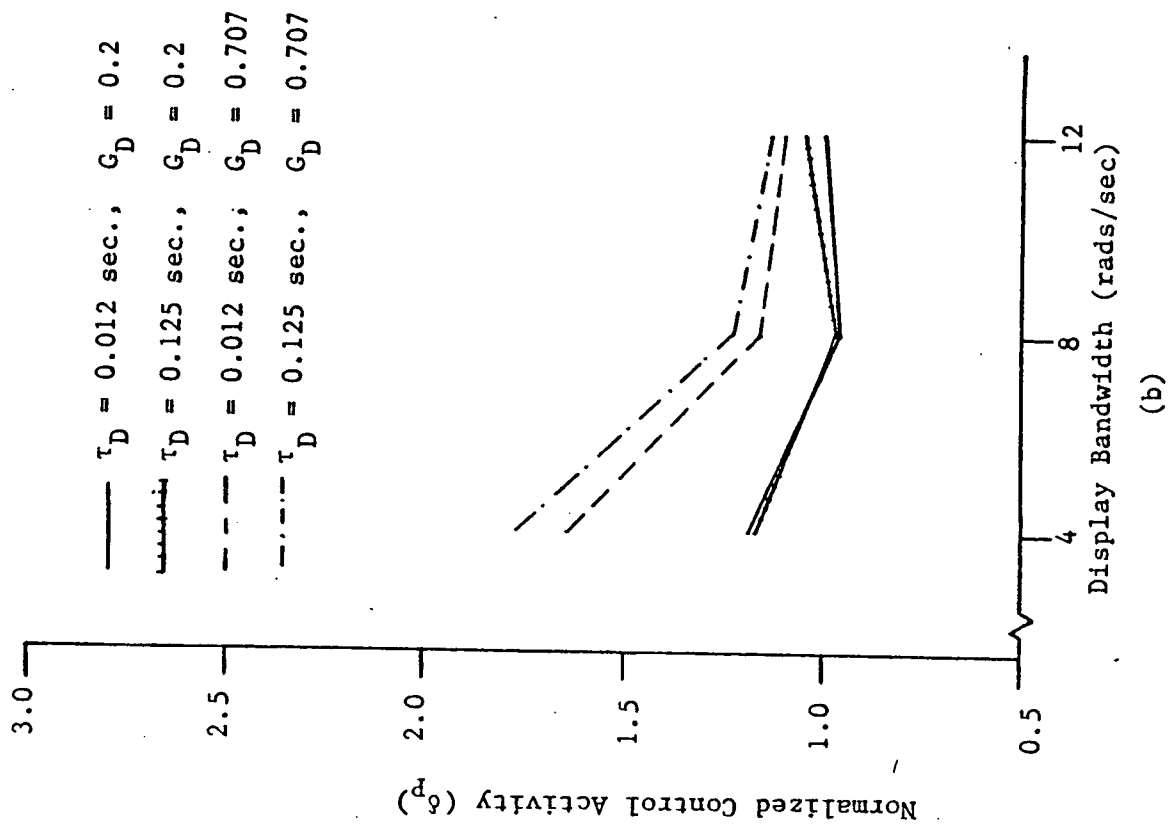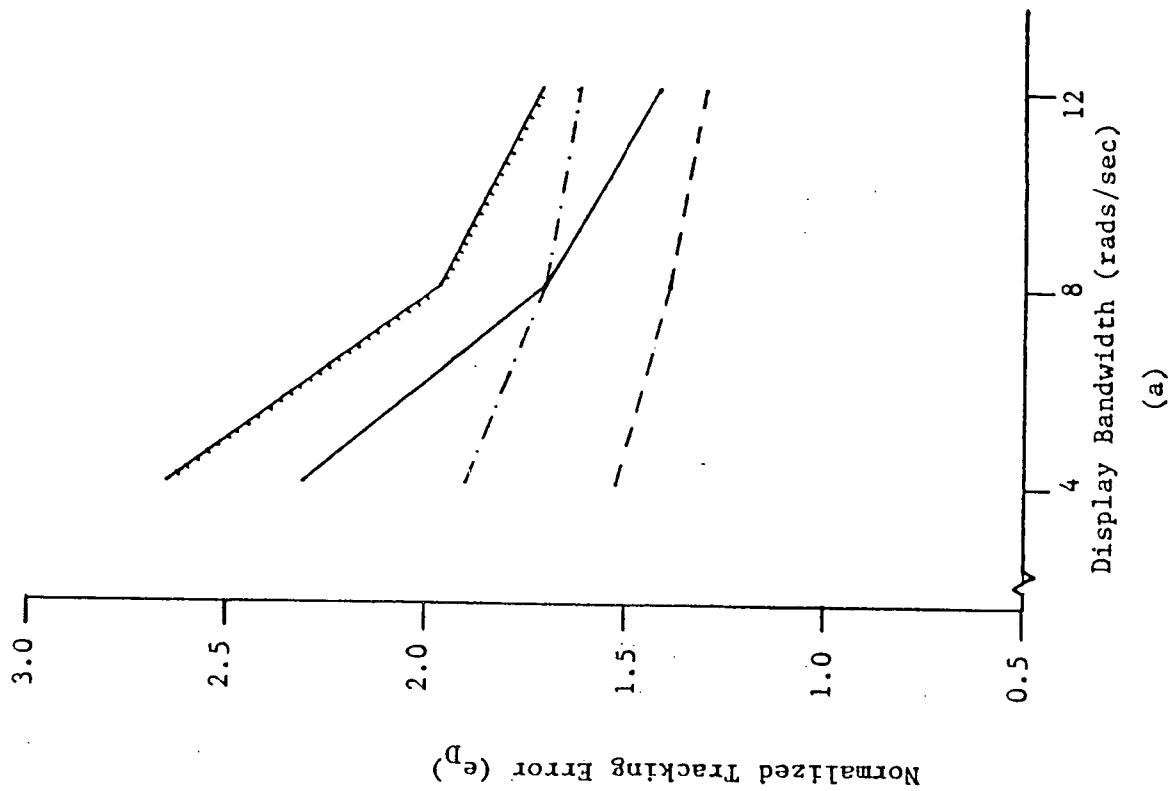
Fig. 4 Model-Based Results for $\frac{K}{s}$ Plant

$\tau_D = 0.012$ sec., $G_D = 0.2$
$\tau_D = 0.125$ sec., $G_D = 0.2$
$\tau_D = 0.012$ sec., $G_D = 0.707$
$\tau_D = 0.125$ sec., $G_D = 0.707$

Normalized Control Activity (δ_p)

Display Bandwidth (rads/sec)

(b)

Normalized Tracking Error (e_D)

Display Bandwidth (rads/sec)

(a)

213
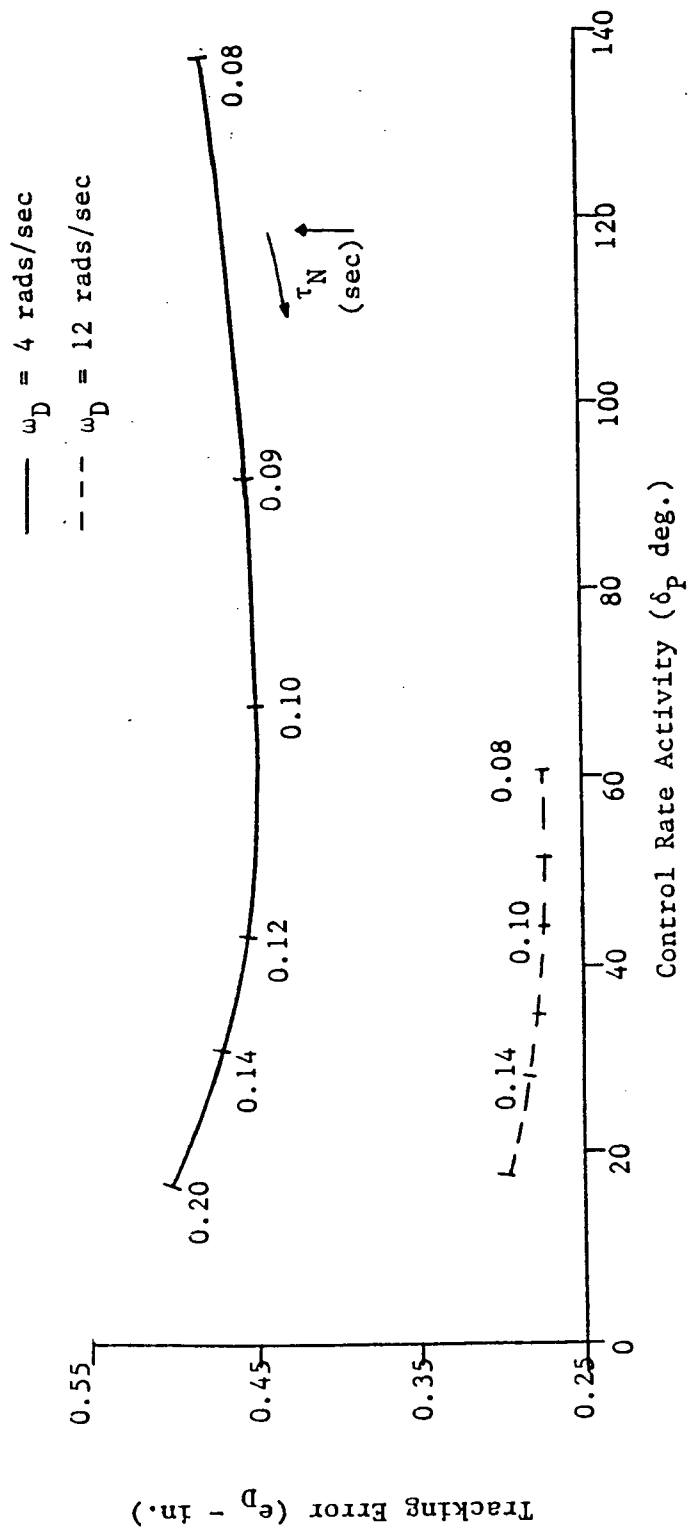
Fig. 5 Performance/Workload Trade-off by varying τ_N: $\frac{K}{s}$ Plant
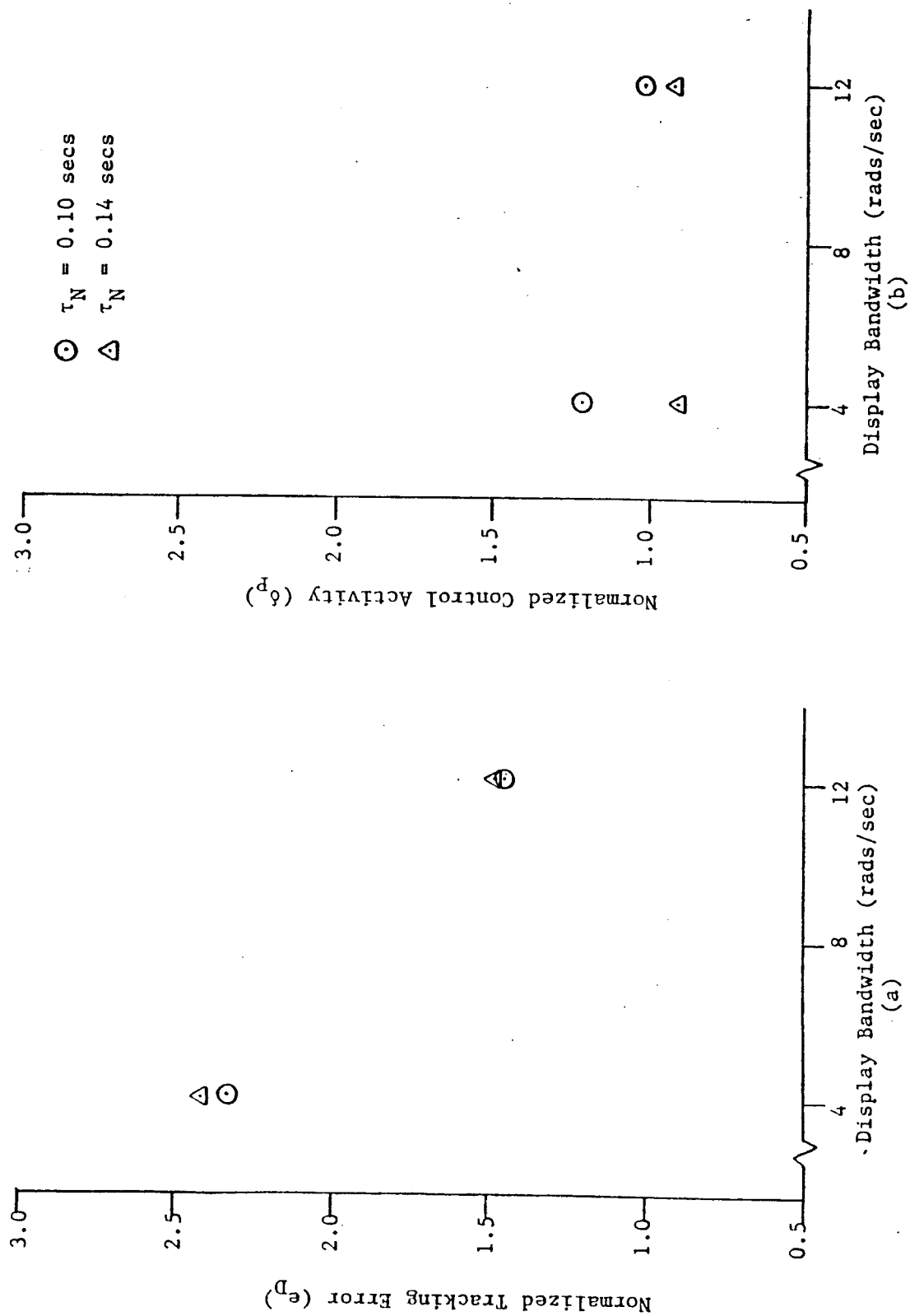
Fig. 6 'Sample' τ_N Adjustment Result: $\frac{K}{s}$ Plant

SESSION 4: PHYSIOLOGICAL MEASUREMENTS AND APPLICATIONS

Moderator: Mr. Frank L. George, AFWAL/FIGC, Wright-Patterson AFB

EFFECT OF INERTIAL LOAD ON AGONIST AND ANTAGONIST EMG PATTERNS

Daniel M. Corcos, Gerald L. Gottlieb, Gyan C. Agarwal
and Tauras J. Liubinskas

Rush Medical College
Chicago, Illinois 60612
and
University of Illinois at Chicago

Abstract.

In a previous study (Annual Manual, 1984), we showed that agonist EMG duration and quantity increase as distance moved and target size increase. This is because longer movements to larger targets are made at higher peak velocities. However, this relationship between EMG and movement velocity will only be true in cases where changes in an independent variable enable the generation of larger forces and a concomitant increase in movement velocity.

A subject made 18°, 36°, 54° and 72° elbow flexion movements to a 9° wide target with four different external loads. Constant target size leads to an increase in the Index of Difficulty ($\log_2 2A/W$) of the movement as movement distance increases. Surface EMGs were recorded from the biceps, brachioradialis, lateral head of triceps and medial head of triceps. The biceps and brachioradialis EMG quantitities increased as load and distance increased. For movements with increasing loads there was proportionately larger increases in the brachioradialis muscle activity than the biceps muscle. More significant changes occurred in the antagonist muscles. As load increased the antagonists were delayed slightly, occurred for a longer duration and with equal (or smaller) amplitude. Movement velocity increased with distance but decreased with load. Not only did peak velocity decrease as a function of load but the shape of the velocity profile changed systematically. As the load increased the acceleration time increased slightly whereas the deceleration time increased considerably.

Introduction

One frequently observed pattern of electromyographic activity (EMG) associated with rapid, self terminating movements has been described as triphasic (Wachholder and Altenburger, 1926). This refers to the observation that in the EMG there is an initial burst in the agonist muscle, followed by a burst in the antagonist muscle and then a second burst in the agonist muscle. The triphasic pattern is compatible with an impulse-timing theory of movement control in which movements are controlled by successive bursts of activity which generate forces that propel and then arrest the limb (Schmidt et al., 1979; Wallace, 1981; Wallace and Wright, 1982).

These EMG "bursts" associated with voluntary movement have been characterized by their duration, quantity (area) and amplitude (height). Some studies have provided evidence that the agonist EMG burst duration is relatively constant as movement distance and/or speed varies (Brown and Cooke, 1981; Ghez, 1979; Hallett et al., 1975; Hallett and Marsden, 1979) whereas other studies have found the duration of the initial agonist burst to lengthen with increasing distance (Benecke et al, 1985; Berardelli et al, 1984; Brown and Cooke, 1984; Cooke et al., 1985; Wadman, 1979). The activation levels of both agonist and antagonist muscles increases with inertial loads (Lestienne, 1979).

Antagonist activity has not often been quantitatively related to various movement requirements. This is due in large part to high variability in the electrical activity (Hallett and Marsden, 1979). For elbow movements, antagonist EMG duration has been reported to increase with movement distance but its amplitude remained constant (Brown and Cooke, 1981). For thumb movements, no relationship between antagonist EMG and either distance or peak velocity has been found (Hallett and Marsden, 1979). However, Marsden et al., 1983 have shown that for short distance movements the antagonist burst is large and starts soon after the agonist fires but is smaller and occurs later for for longer, slower movements. This finding is more pronounced for the elbow than the thumb.

Le Bozec, Maton and Cnockaert (1980) have shown that the agonist quantity (integrated EMG to the time of peak velocity) increases linearly with the external work (which is $1/2 * I * V^2$ where I is the inertia and V is the peak velocity).

Methods

Apparatus

The subject sat comfortably in a chair and positioned his elbow on a low inertia, almost frictionless manipulandum which required the

arm to be abducted 90°. A vertical handle was positioned at the end of the manipulandum which the subject grasped. In this position, the forearm is semi pronated and movements are made primarily but not exclusively by the biceps (BI) and triceps (TRI) muscles. When a comfortable position was established, the limb was secured by velcro straps. The subject initiated flexion movements from a resting position at approximately 135°.

A video monitor, positioned about 1.5 meters in front of the subject, continuously displayed the position of the limb, a starting reference position and a target window which defined the movement distance and a fixed target width of 9°. An IBM PC AT was used to control the experiment, digitize and record joint angle (1000 Hz) and EMGs from biceps, brachioradialis, medial and lateral heads of triceps (1000 Hz). Angle was measured by a variable capacitance transducer mounted on the shaft of the manipulandum. Velocity was calculated from digital differentiation of the angle signal (Usui and Amridor, 1982). Acceleration was measured directly by an accelerometer and inertial forces calculated by multiplying acceleration by the moment of inertia of the lever limb system. Electromyograms were recorded using Liberty Mutual (Boston) surface electrodes with built in preamplifier and band pass filter. EMGs were digitally rectified and integrated.

Procedure

The results presented in the later section are from one individual, who had considerable experience with the experimental apparatus and the logic behind the study, made elbow flexion movements over distances of 18°, 36°, 54° and 72° against inertial loads of .1818, .472, 1.1253 and 1.6813 N.m. s^2/rad. The subject performed 10 movements in each experimental condition. For any specified distance and load condition, the ten trials were presented in a block. The distance-load combinations were randomly ordered.

In all experimental conditions, the subject was instructed to make accurate, rapid movements to the target. Accuracy was mentioned first but subjects were instructed to place equal emphasis on both accuracy and speed. During the 10 experimental trials the subject was able to view the display but was not provided with feedback from the experimenter about his or her performance. Each trial was initiated by an auditory tone. No emphasis was placed on reaction time and reaction time data will not be reported. All trials in each condition were analyzed unless the onsets of the agonist and antagonist EMG bursts were unable to be identified. These trials were excluded from the analysis.

All numerical measures were derived from individual trials. The time from 5% of peak velocity to 5% of peak velocity served to define movement time. The EMG measures calculated were: 1) the EMG area from the onset of the EMG until 50 ms before the the time when the velocity of the movement fell below 5% of its peak (termed the EMG quantity Q_V) and 2) the latency of the antagonist EMG onset with respect to the agonist (ANTLAG). The EMG onset of both the agonist and the antagonist muscles was the first time the rectified EMG signal exceeded and did not rapidly return to baseline level. This criterion gives the earliest onset of activation, a factor which needs to be considered when making temporal comparisons between this and other studies. The reason for our criterion for calculating Q_V was our estimate of about 50 ms delay between the appearance of an EMG signal and the consequent motion that muscle activation would produce. The interval is intended to encompass the EMG activity associated with forward motion towards the target. We end at 5% of peak velocity instead of zero velocity to avoid excessively long intervals which might be produced by exponential-like approaches.

Averaged trajectories and EMGs shown in the figures were computed by aligning records with respect to the onset of agonist (biceps) activity as determined by computer assisted visual measurements. This point is taken as time 0 on all the Figures.

Results

Distance and Inertial Load Effects on Movement Kinematics

Figure 1 (part a) depicts a subject making 18° and 72° movements to a 9° target against a light load (I = .1818 N.m. s²/rad.) and (part b)   against a heavier load (1.6813 N.m. s²/rad.) In Figure 2 the same data are replotted to show the effect of inertial load for 18° and 72° movement. Some important points to note are: 1) the peak velocity increased as movement distance increased but decreased as inertial load increased, 2) the acceleration and deceleration phases of the movement are asymmetrical and the duration of both phases increased as movement distance increased 3) as inertial load increased the acceleration time increased slightly whereas the deceleration time increased considerably and 4) the movement time increases with distance and with load.

An alternative way to present these observations is to define a new index of difficulty (following Fitts' Law) which is based on movement distance and inertial load. Since movement time increased as both distance and load increased, an initial choice for such an index is a product of these two independent variables, i. e.

ID = Distance * Moment of Inertia

Figure 3 shows the movement time as a function of distance multiplied by moment of inertia. These data are for four distances (18°, 36°, 54° and 72°) and four inertial loads (0.1818, 0.472, 1.1253 and 1.6813 N.m. s²/rad.).

Figure 4 shows the peak movement velocity as a function of distance times moment of inertia. The peak movement velocity increases with distance for a given load but decreases with load for a given distance.

Distance and Load Effects on EMG Activities

As distance increases the agonist burst in both flexors (biceps and brachioradialis) increases in duration as well as amplitude. The same observation is also valid with increasing inertia. Figure 5 depicts the Q_v quantity for the agonist as a function of distance times moment of inertia. Figure 6 shows the antagonist data. Although Figure 6 shows more antagonist EMG for a short movement than for a long one in the lightest load condition but this total activity is nearly constant. For the next two load conditions, increased distance leads to increased antagonist EMG. At the heaviest load there is less of an effect which may be because the maximum EMG signal has been reached.

With respect to the onset of the agonist EMG, distance and load both were related to the initiation delay in the antagonist EMG as shown in Figure 7. Since movement time increased as distance and load increased, the delay of the antagonist EMG is also proportional to the movement time.

Discussion

Several studies have reported a linear relationship between movement velocity and agonist EMG. This finding, however, will only be true for experiments in which changes in the manipulated variables (e. g. movement distance and target width) lead to increases in movement velocity. In cases when the independent variable leads to decreases in movement velocity (e.g. inertial load and we suspect any other type of load) this will not be the case. This supports the assertion that the relationship beteen the EMG and any kinematically derived variable can only be understood in the

context of the relationship between EMG, force and work. Any variable which allows greater forces to be used in generating movements should be associated with increases in agonist EMG. The time course and function of this relationship will be contigent on the types of forces and movement velocities involved.

Le Bozec, Maton and Cnockaert (1980) have shown a linear relationship between EMG quantity and the external work. There are, however, some significant differences between their study and the present work. Their study emphasized velocity and no target width was present. They defined the EMG quantity as integrated EMG to the first peak velocity point i. e. maximum kinetic energy of the limb and not over the total movement.

Our finding that the antagonist EMG is delayed for longer movements agrees with that of Marsden, Obeso and Rothwell (1983) who report earlier antagonist onset for fast, short movements than slow, long movements. We find that as distance increases, the antagonist is delayed. However, in our experiments, there is a concomitant increase in movement velocity as distance increases (Figure 1). The antagonist is also delayed for larger inertial loads. This observation is entirely reasonable on physical grounds and can be explained in terms of movement time. If distance is held constant, faster movements (those made against lower inertial loads) are completed sooner and involve smaller inertial forces. This requires earlier application of braking forces to arrest the movement at the appropriate time. As load increases, the braking force needs to be applied later but also more antagonist EMG is required to decelerate the larger load.

In many studies cited which involve movement, force has not been reported and may often not have been measured. This is because of major technical obstacles in obtaining such information and/or because the experimental design deprives it of significance. For example, in these experiments, the net external force measured was that required to accelerate and decelerate the manipulandum and is exactly computable from knowledge of the manipulandum moment of inertia (including the subject's limb) and the acceleration. This net force, which is plotted in Figures 1 and 2 is certainly only a part of the actual forces produced by the muscles. The interrelationship between the instructed task, the EMG and the kinematics will not be well described unless the forces produced by the individual muscles can be measured or estimated. Further efforts in this direction are in order.

REFERENCES

Benecke, R., Meinck, H. M. , & Conrad, B. (1985). Rapid goal-directed elbow flexion movements: limitations of the speed control system due to neural constraints. Experimental Brain Research, 59, 470-477.

Berardelli, A., Rothwell, J. C., Day, B. L., Kachi, T., & Marsden, C. D. (1984). Duration of the first agonist burst in ballistic arm movements. Brain Research, 304,183-187.

Brown, S. H. C. , & Cooke, J. D. (1981). Amplitude and instruction-dependent modulation of movement-related electromyogram activity in humans. Journal of Physiology, 316, 97-107.

Brown, S. H. C. , & Cooke, J. D. (1984). Initial agonist burst amplitude depends on movement amplitude. Experimental Brain Research, 55, 523-527.

Cooke, J. D., Brown, S., Forget, R. , & Lamarre, Y. (1985). Initial agonist burst duration changes with movement amplitude in a deafferented patient. Experimental Brain Research, 60,184-187.

Corcos, D. M., Gottlieb, G. L. , & Agarwal, G. C. (1984). Electromyographic patterns associated with discrete limb movements. Twentieth Annual Conference on Manual Control, NASA-Ames, NASA Conf. Publ. 2341, (2), 157-173.

Fitts, P. M. (1954). The information capacity of the human motor system in controlling the amplitude of movement. Journal of Experimental Psychology, 47, 381-391.

Ghez, C. (1979). Contribution to rapid limb movement in the cat. In: Integration in the Nervous System (edited by H. Asanuma and V. J. Wilson) (pp. 305-319). Tokyo: Igaku-Shoin.

Hallett, M., Shahani, B.T. , & Young, R. R. (1975). EMG analysis of voluntary stereotyped movements in man. Journal of Neurological Neurosurgical Psychiatry, 38, 1154-1162.

Hallett, M. , & Marsden, C. D. (1979). Ballistic flexion movements of the human thumb. Journal of Physioliogy, 294, 33-50.

Le Bozec, S., Maton, B. , & Cnockaert, J. C. (1980). The synergy of elbow extensor muscles during dynamic work in man. I. Elbow extension. European Journal of Applied Physiology, 44, 255-269.

Lestienne, F. (1979). Effects of inertial load and velocity on the braking process of voluntary movements. Experimental Brain Research, 35, 407- 418.

Marsden, C. D., Obeso, J. A. and Rothwell, J. C. (1983). The function of the antagonist muscle during fast limb movements in man. _Journal of Physiliogy_, 335, 1-13.

Schmidt, R.A., Zelaznik, H., Hawkins, B., Frank, J.S. , & Quinn, J. T. (1979). Motor-output variability: a theory for the accuracy of rapid motor acts. _Psychological Review_, 86, 415-451.

Usui, S. , & Amridor, I. (1982.). Digital low-pass differentiation for biological signal processing. _IEEE Transactions Biomedical Engineering_, BME 29, 686-693.

Wachholder, K. , & Altenburger, H. (1926). Beitrage zur physiologie der willkurlichen bewegung. X. Einzelbewegungen. _Pfl Arch Ges Physiol_, 214, 642-661.

Wadman, W. J., Denier Van Der Gon, J. J., Geuze, R. H., & Mol, C.R. (1979). Control of fast goal-directed arm movements. _Journal of Human Movement Studies_, 135, 3-17.

Wallace, S. A. (1981). An impulse-timing theory for reciprocal control of muscular activity in rapid, discrete movements. _Journal of Motor Behavior_, 13, 144-160.

Wallace, S. A. , & Wright, L. (1982). Distance and movement effects on the timing of agonist and antagonist muscles: a test of the impulse-timing theory. _Journal of Motor Behavior_, 14, 341-352.
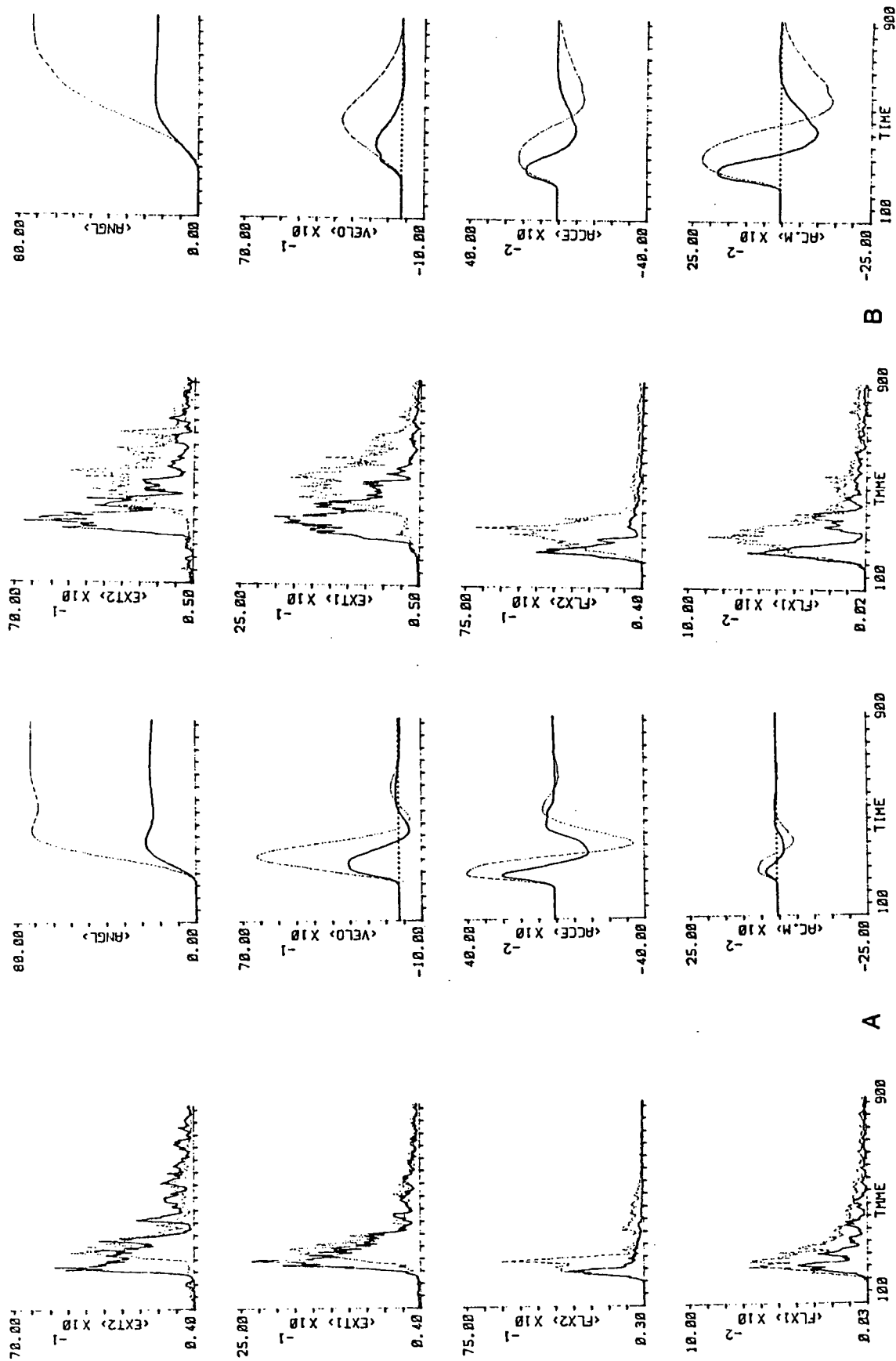
Figure 1A 18° and 72° movements to a a 9° target against a light load (Moment of inertia of manipulandum and forearm = .1818 Nm/s2 per deg). **Figure 1B** shows a heavier load (1.6813 Nm/s2 per deg). FL1 = biceps, FL2 = brachioradialis, EXT1 = lateral head of triceps and EXT2 = medial head of triceps.

227
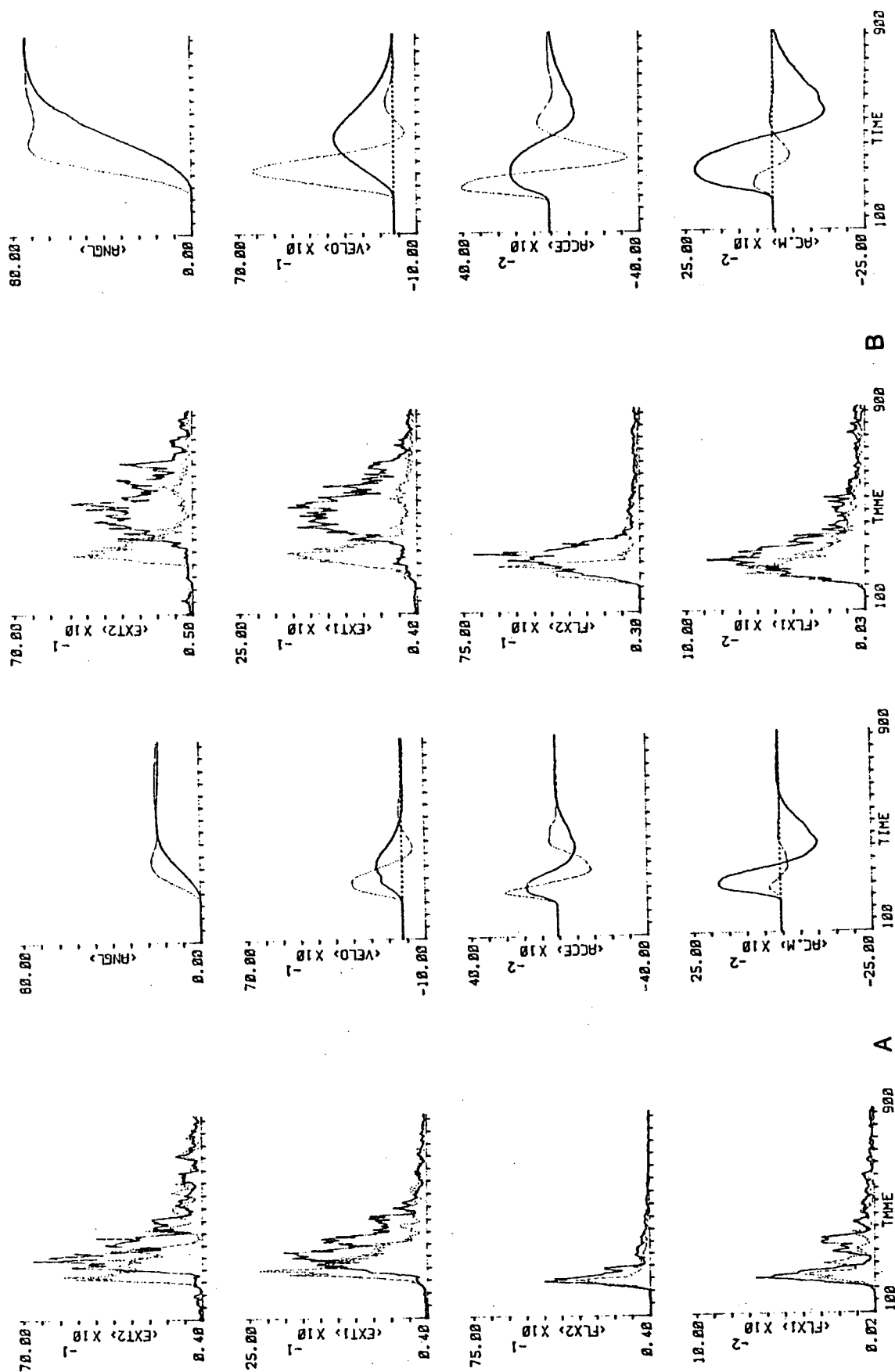
Figure 2A an 18° movement to a 9° target against two loads (.1818, 1.6813 nm/s2 per deg). **Figure 2B** depicts 72 degree movements to a 9° target. FL1 = biceps, FL2 = brachioradialis, EXT1 = lateral head of triceps and EXT2 = medial head of triceps.

228
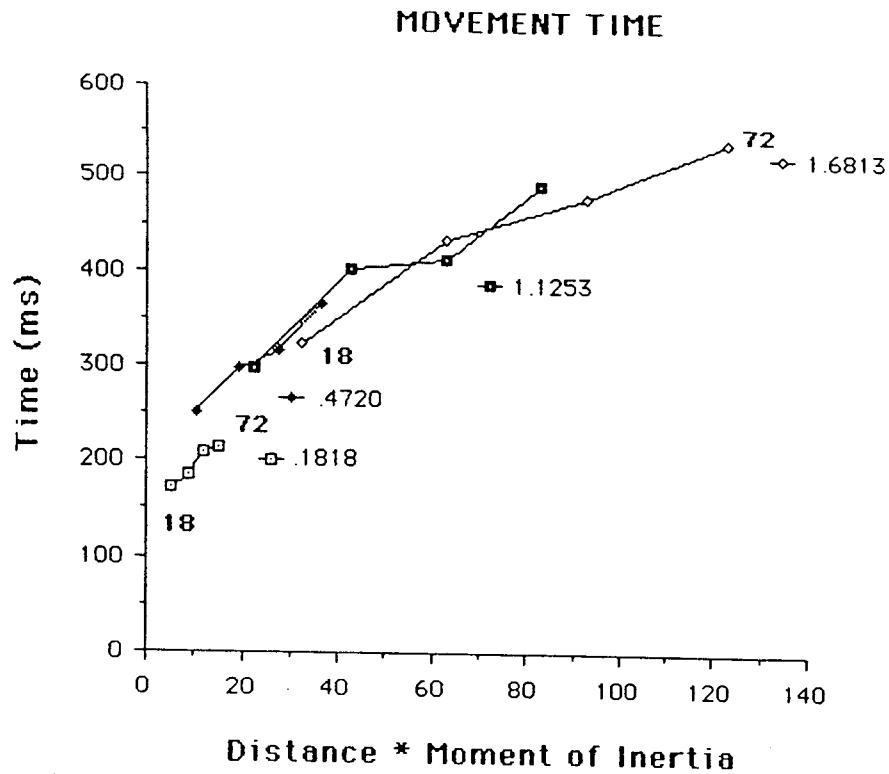
MOVEMENT TIME

Figure 3. Movement time plotted as a function
of distance * moment of inertia. In figures 3, 4,
5, 6 and 7, four distances are plotted with joined
lines for movements against four inertial loads.

PEAK MOVEMENT VELOCITY
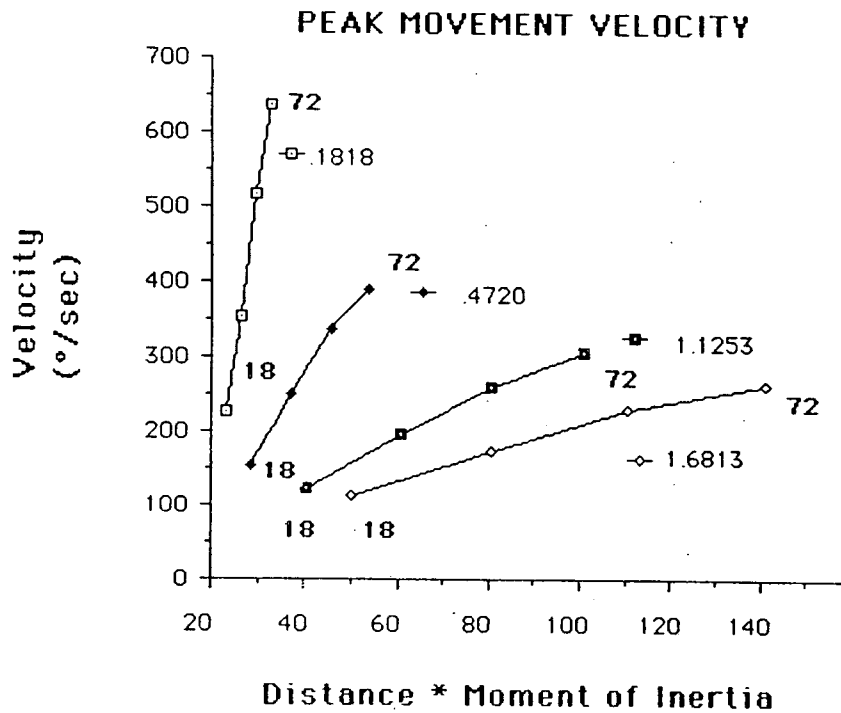
Figure 4. Peak movement velocity plotted as
a function of distance * momenmt of inertia.
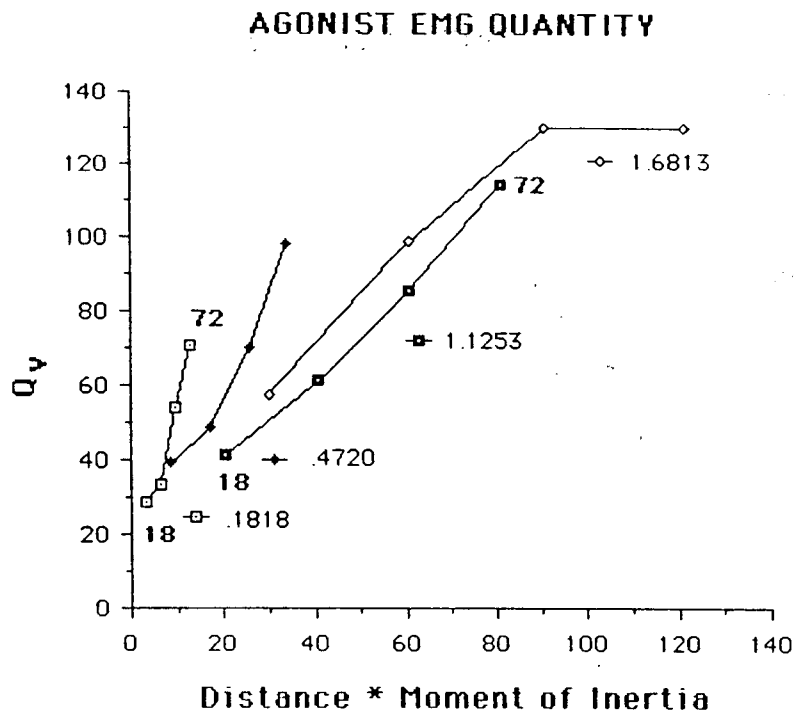
AGONIST EMG QUANTITY

Figure 5. Agonist EMG Q_v plotted as a function
of distance * moment of inertia.

ANTAGONIST EMG QUANTITY
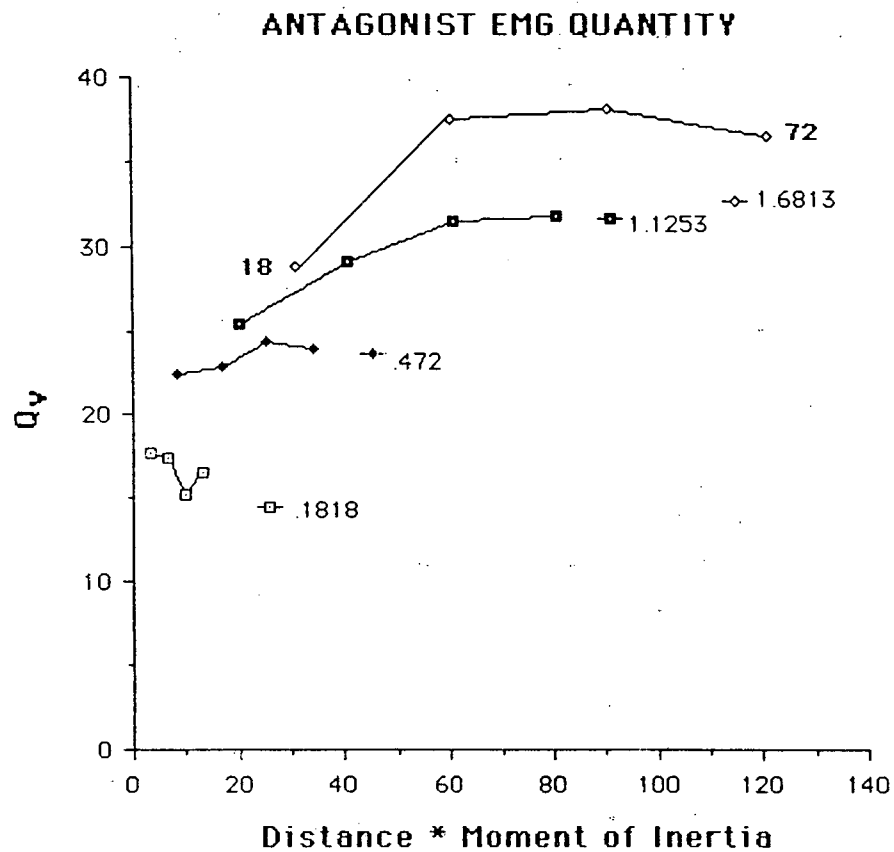
Figure 6. Antagonist EMG Q_v plotted as a function
of distance * moment of inertia.
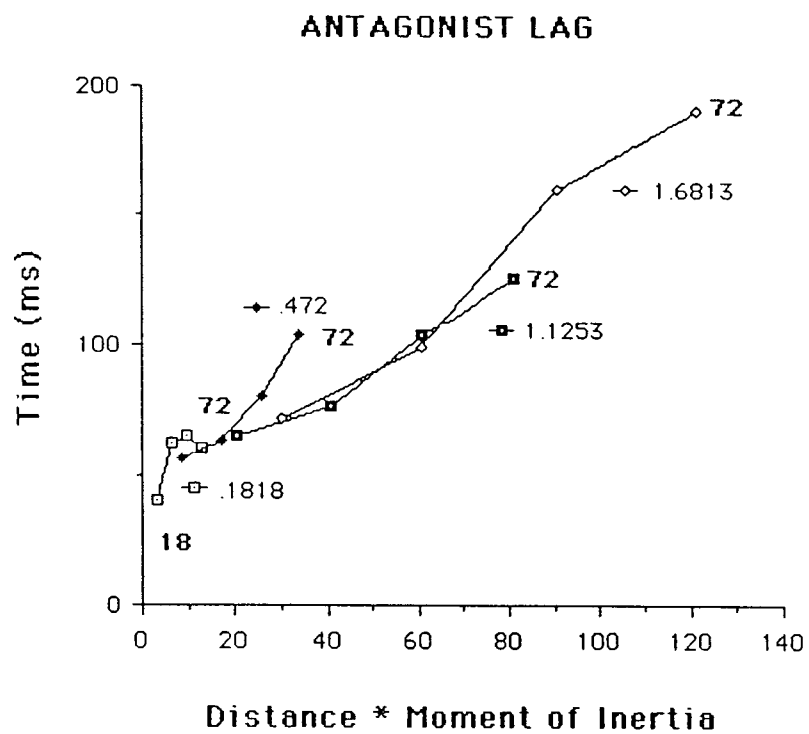
ANTAGONIST LAG

Figure 7. Antagonist onset delay plotted as a
function of distance * moment of inertia.

A NEW FREQUENCY ANALYSIS TECHNIQUE
FOR
BRAIN ACTUATED CONTROL SYSTEMS

John H. Schnurer
Systems Research Laboratories, Inc., Dayton, Ohio

Andrew M. Junker
AAMRL/HEG, Wright-Patterson AFB, Ohio

Kevin M. Kenner
Systems Research Laboratories, Inc., Dayton, Ohio

Evoked EEG response research indicates the potential for a Usable Brain Actuated Control System (UBACS). This work has demonstrated several key elements that are necessary for the development of UBACS. When visually stimulated by sinusoidally modulated light a subject produces a corresponding increase in EEG activity at the frequency of stimulation, called a Visual Evoked Response (VER). Appropriate signal processing techniques, utilizing selective filtration, amplification, and analysis permit the VER to be detected and recorded. The input/output nature of the VER may provide the beginnings of a subject controllable feedback loop.

Present analysis involves discrete Fourier transformation for signal improvement and frequency domain measures. To achieve frequency sensitivity this analysis produces a time lag between signal acquisition and output of 'useful' data. Reduction of this time lag is essential for the development of a subject training system, which is the next phase of UBACS research. We are presently investigating a Lock-In Amplifier System (LAS) to overcome these limitations.

Frequency and phase facile system capabilities are being developed for the LAS. Improved LAS response time is projected. This powerful tool should enable effective training by continuously supplying subjects with an indication of their EEG output at a reference frequency. Such training techniques, when realized, should lead directly to a usable brain actuated control system. The experimental/prototype system will be discussed and initial data will be presented.

EFFECTS OF DECISION MAKING TASK DIFFICULTY ON THE STEADY STATE VISUAL EVOKED RESPONSE

Andrew M. Junker
AAMRL/HEG, Wright-Patterson AFB, Ohio

Kevin M. Kenner
Human Factors Div., SRL Inc., Dayton, Ohio

Elizabeth J. Casey,
Univ. of Illinois

Earlier work has shown the value of the steady state Visual Evoked Response (VER) as a potential workload metric. Previous work delineated a technique for using Sum-of-Sines modulated light, as an evoking stimulus, with an apparatus that allowed for simultaneous task presentation. This project utilized the same stimulation technique and presentation apparatus while presenting a Dynamic Decision Making (Supervisory Control) task. The Decision Making task was chosen because it utilizes the same neuromuscular response across conditions of varying degrees of task-processing difficulty. Transfer function for EEG (output) and photocell (input) channels were computed using Systems Engineering based analyses. Results indicate that the gain is attenuated and there is a consistent phase shift with increased task difficulty. Results support the continuation of this approach for the development of an objective workload metric.

Manual Control of a Peripheral Vision
Light Bar in Sustained Acceleration Research

by
William B. Albery
Acceleration Effects Branch
Biodynamics & Bioengineering Division
Harry G. Armstrong Aerospace Medical Research Laboratory
Wright-Patterson AFB, Ohio 45433-6573

Abstract

A semi-circular light bar device used to determine human G tolerance on a centrifuge is described. This device uses manual control by the centrifuge subject to keep bilateral pairs of LEDs (light emitting diodes) lit at the edge of the subject's peripheral vision during acceleration exposure. The light bar provides a simple and adequate indication of a subject's loss of peripheral vision – a precursor to blackout and loss of consciousness (LOC).

The 180° of arc semi-circular light bar with 60 pairs of LEDs is located 40" away from the seated subject and is at eye level. Subjects control the lighting of opposing LEDs through a pressure sensitive force stick. Increasing forward pressure progressively illuminates pairs of lights from the periphery towards the center. Increasing aft pressure moves the lights from the center back toward the periphery. When the lights are moved into the central 60° of included arc the computer senses this and brings the centrifuge to a stop. In this way G tolerance is determined at a definite point short of visual blackout or LOC.

Introduction

Measuring one's tolerance to sustained acceleration has been an elusive parameter for many years. The most direct method is to allow the subject to incur accelerative forces until he or she is unconscious. These types of G tolerances have been obtained (Stoll, 1956). A safer method, developed in 1981 (Cohen, 1981) provides a means for determining an end point in acceleration research. The light bar, as it is called, allows the subject to actively track the extent of his/her peripheral visual field. Peripheral light loss (PLL) is a precursor to loss of central vision, or blackout, and loss of consciousness (LOC). The light bar allows the subject to monitor his peripheral visual field while performing another task, such as evaluating an anti G-suit. G tolerance is defined, then, in terms of PLL into a 60° cone of vision; once the subject has run the LEDs into this 60° cone, the computer returns the centrifuge to a baseline (1.4 Gz) condition. Although the light bar has been demonstrated to provide a subjective measure of G tolerance, it does have its limitations.

Using the Light Bar in Acceleration Research

The Cohen light bar was first used at the AAMRL, Wright-Patterson AFB in 1983. The AAMRL light bar (Fig. 1) is similar to that developed by Cohen but differs in that a pair of flickering LEDs on opposite sides of the bar are used to indicate the extremities of the subject's peripheral vision, rather

than just one LED on each side (Albery, et al., 1985). A side-arm controller/stick is used by the subject to control the location of these LEDs. The light bar has been a valuable tool in anti G-valve evaluations. Using the technique of Crosbie (1982, 1984), subjects progress from a lower G level to a higher G level at 0.5G increments. When they near their G tolerance, PLL is observed and the subjects move the LEDs into the 60° cone of the light bar. A typical strip chart of this event is shown in Fig. 2. As shown in Fig. 2, the subject actively tracks the edge of his/her peripheral field (middle trace) and as the Gz acceleration increases (second trace) the light bar half visual angle decreases from approximately 70° to 0° in about 5 seconds. When the LEDs cross into the 60° (30° half visual angle) imaginary cone of the light bar, the computer senses this and returns the centrifuge to a baseline (1.4 Gz) condition.

Other measures used to determine the condition of the subject include a color, closed circuit TV system for observing the subject's face and a Doppler temporal artery flow meter device for monitoring blood flow velocity through the temporal artery (Fig. 2, fourth trace).

Measuring G Tolerance

+Gz tolerance is defined as the +Gz level the subject successfully completes (15 secs plus 3 sec rise time, for example) plus that fraction of the next higher Gz level during which the subject lost his peripheral vision (Crosbie, 1982).

where G_{TL} = Subject's G tolerance limit
G_{TL1} = Highest G level tolerated for complete G profile
T^{TL1} = Time of G profile, rise plus plateau time (18 secs)
ΔT = Time from start of G before PLL occurs
ΔG = Incremental G above G_{TL1}, 0.5 G in this experiment

$$G_{TL} = G_{TL1} + \Delta T/T \ (\Delta G)$$

Thus, if a subject sustained a 4.5 G run and experienced PLL after 7 seconds at the 5 G level, his tolerance was calculated to be,

$$G_{TL} = 4.5 + (10/18) \ (0.5) = 4.78 \ G$$

This method of determing a number for an individual's G tolerance to a particular anti G-valve, G-suit or other G protection device has been successful. Coupled with the Doppler temporal artery flow data, the light bar signal provides a good estimate of a subject's G tolerance.

Future Considerations

Although the light bar provides a good estimate of subject tolerance it does have its limitations. First of all, it is a subjective measure of a physiological limit. Subjectivity introduces error into the data. The light bar can be "cheated" if the subject does not faithfully track the observed peripheral field. Another drawback is that when a subject uses the light bar, no other visual task such as tracking or performing can take place. The subject is instructed to attend to a central LED and to simultaneously monitor his/her peripheral vision.

A new development in measuring the steady-state visual evoked response (Kenner, et al., 1987) may provide an objective measure of PLL. This technique takes advantage of the fact that a peripherally stimulated light source can produce a measurable visual evoked response (VER). When vision is impaired, as in acceleration, this VER disappears. Research with such a technique is currently underway at AAMRL.

Summary

A manually-controlled semi-circular light bar is currently being used by the Air Force to measure G tolerance in acceleration research. The device allows for a fairly accurate measurement of one's G tolerance. Two drawbacks of this technique for monitoring PLL are its subjectivity and lack of flexibility, as only light bar tracking and no CRT monitor tracking (performance task) can take place. A technique for monitoring the peripheral visual evoked response is currently being developed which may enhance if not replace the current light bar technique of measuring G tolerance.

References

Albery, W.B., Jennings, T., Frazier, J., Roark, M., Ratino, D. Simulation of High +Gz Onset in the Dynamic Environment Simulator, AFAMRL-TR-85-030, Apr 85.

Cohen, M. Visual Field Perimeter and Psychomotor Tracking Performance Measuring Apparatus, DTIC ADD010248, Apr 1981

Crosbie, R.J. A Servo Controlled Rapid Response Anti-G-Valve, NADC, Warminster, PA, Proceedings of the 1983 SAFE Annual Symposium, Las Vegas, NV, 6-8 Dec 82.

Crosbie, R.J. Analysis of the Transient Response of Temporal Artery Blood Flow Data Relative to Various Anti-G-Suit Pressure Schedules, NADC, Warminster, PA, Presented at AGARD meeting on Human Factors Considerations in High Performance Aircraft, 4 May 84.

Kenner, Junker, Albery, Gill. Frequency Domain Analysis of Peripheral (Steady State) Visual Stimulation as a Physiological Metric for Gz Stress, 22nd Annual Conference on Manual Control, Proceedings, 1987.

Stoll, A. Human Tolerance to Positive G as Determined by the Physiological end points, J. Aviat. Med. 27:356, 1956.

LIGHT BAR

LIGHT BAR
CONTROL STICK
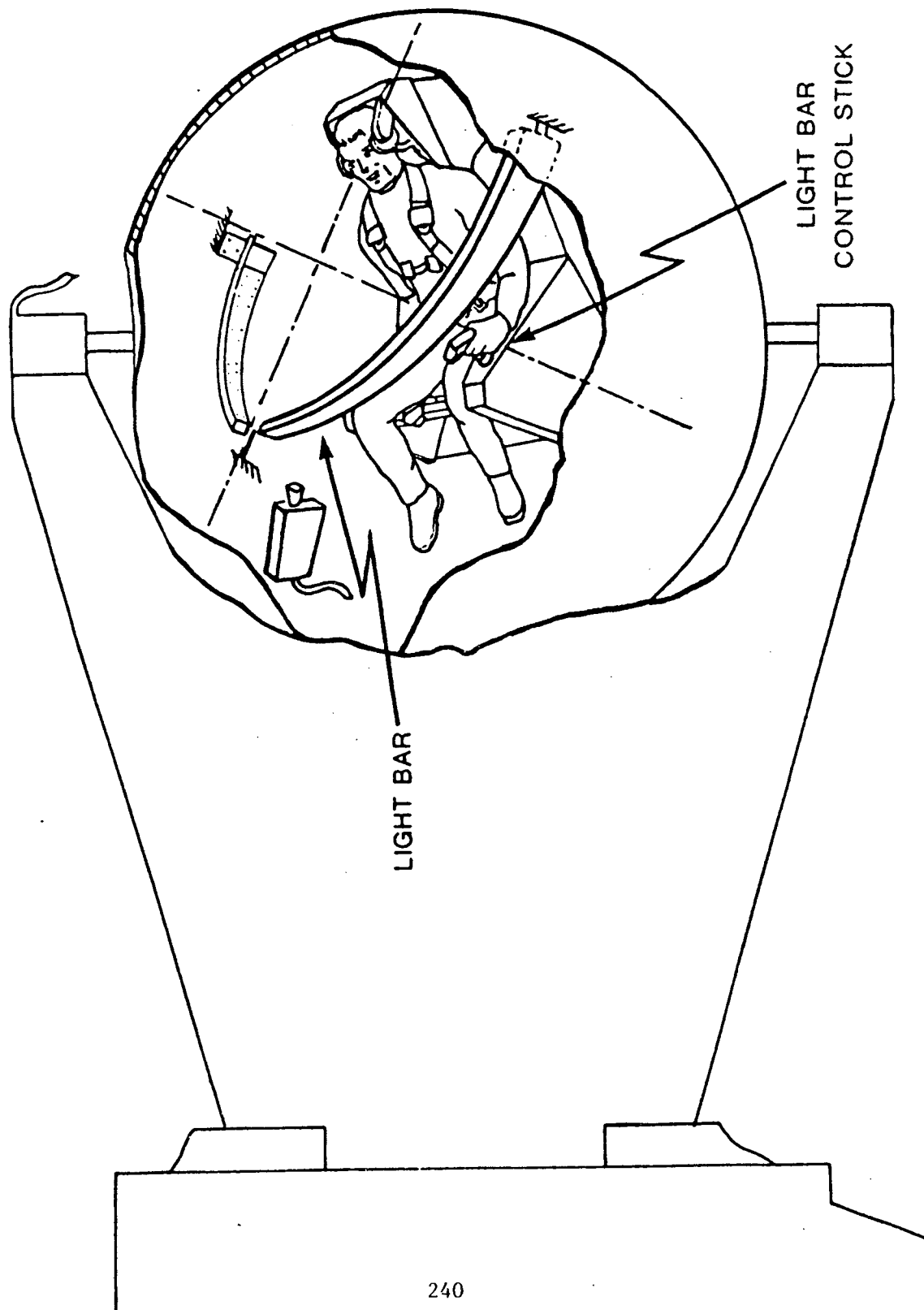
Figure 1   THE REPPERGER LIGHT BAR SHOWN IN RELATION TO THE SUBJECT AND DES GONDOLA.
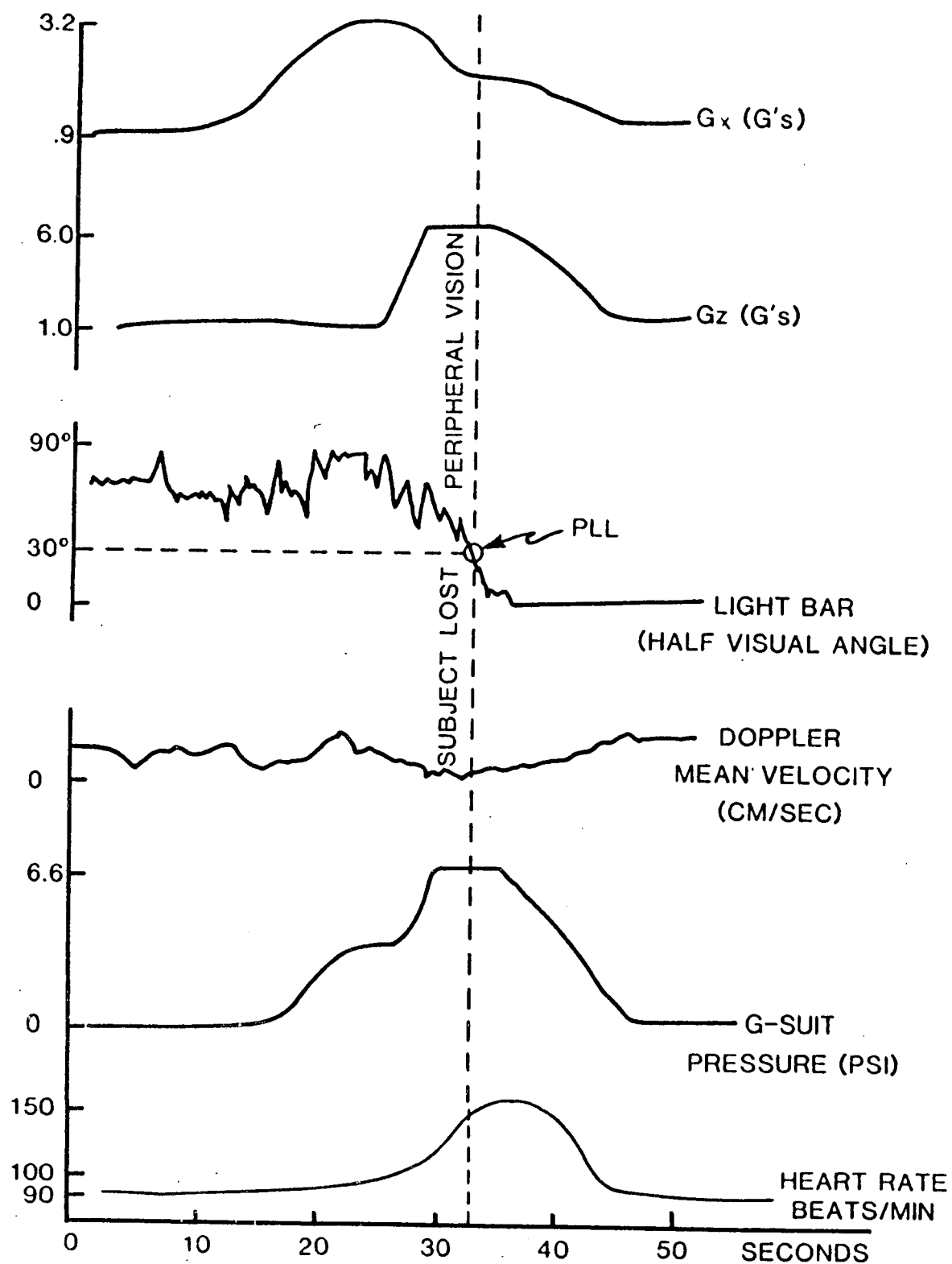
Figure 2   TYPICAL STRIP CHART RECORDING FROM EXPERIMENT

241/242

FREQUENCY DOMAIN ANALYSIS OF
PERIPHERAL (STEADY-STATE) VISUAL STIMULATION
AS A PHYSIOLOGICAL METRIC FOR Gz-STRESS

Kevin M. Kenner
Human Factors Division, SRL Inc. Dayton, Ohio

Andrew M. Junker
AAMRL/HEG, Wright-Patterson, AFB

William B. Albery
AAMRL/BBS, Wright-Patterson, AFB

Richard T. Gill
Univ. of Idaho, Moscow Id.

High levels of Gz stress causes aircrew performance degradation, and has been implicated in the loss of life and equipment with high performance aircraft. The danger in head-to-foot (Gz) acceleration is the loss of cranial blood supply; the first visual symptom is Peripheral Light Loss (PLL), leading to black-out (loss of central vision) and eventually to Loss Of Consciousness (LOC). Because PLL is currently measured subjectively in centrifuges, it would be desirable to have an objective, physiologically based, methodology for determining the onset of PLL.

A technique has been developed to stimulate the periphery of the visual field with sinusoidally modulated light and to detect a Visual Evoked Response (VER) as measured with the EEG. The VER is at the same frequency as the stimulus. The first phase of this experiment was conducted in a static, laboratory, environment. The Fast Fourier Transform (FFT) was applied to the two channels (Photocell and EEG) of data, RMS POWER and COHERENCE were recorded. Results have shown Coherence (a ratio that indicates linear cause/effect relationships for sinusoidally stimulated systems) to be a sensitive measure of peripheral stimulation. The sensitivity of this measure indicates the potential for the development of an objective measure of Gz induced stress. Analytic techniques and initial static, and dynamic, data will be presented.

SESSION 5: HUMAN-MACHINE SYSTEMS AND CONTROL

Moderator: 1Lt. Lisa B. McCormack, AFWAL/FIGC
            Wright-Patterson AFB

CRITICAL TASK PERFORMANCE AND WORKLOAD CHARTING

by
Robert K. Heffley
Manudyne Systems, Inc.
349 First Street
Los Altos, CA 94022

ABSTRACT

A test procedure for evaluating flying qualities is offered which is useful in portraying a clear picture of the trades among workload, task performance, and aircraft characteristics. This procedure therefore adds another dimension to the evaluation procedure typically used in assessing aircraft flying qualities. Furthermore, it is possible to obtain a far more direct correlation between pilot rating and causal vehicle characteristics than is usually found. To illustrate this technique, results from recent flying qualities evaluations are presented. These include both low-level helicopter hover tasks as well as aggressive up-and-away flight. In one example it is demonstrated how to measure the benefit a simulator digital delay compensator as a tradeoff between task performance and pilot workload. The ultimate reward of the charting method is believed to be a means for expressing the cost benefit of flying qualities in terms of mission performance.

INTRODUCTION

The purpose of aircraft flying qualities evaluations is generally to establish a clear relationship among "task performance," "pilot workload," and "aircraft characteristics." The correlations found are usually based on pilot-determined levels of performance, and often these are only qualitatively defined. As a result it is possible for the pilot to vary task performance subtly when the vehicle configuration is changed. The consequence can be to obtain false or misleading indications of pilot opinion rating versus configuration variation. Equally important, the effect of vehicle response on mission performance might be missed entirely.

An evaluation procedure has been developed for mapping both pilot opinion and task performance for crucial short-term flight tasks and maneuvers. It has been found necessary to systematically "force" the evaluation pilot to perform given tasks in ways which precipitate performance and workload limits.

Results are presented from various evaluations of fixed-wing and helicopter aircraft flying qualities. For example, the

effect of roll response bandwidth is shown for the helicopter air combat task in terms of how close the attacking aircraft can move in on the target.

Figure 1 diagrams the components of flying qualities to be discussed and indicates the relationships found by the charting procedure described here. The paper concludes that far more attention must be paid to task definition and performance measurement in the process of evaluating flying qualities and establishing criteria. Significant deficiencies can exist in current approaches to criteria specification.
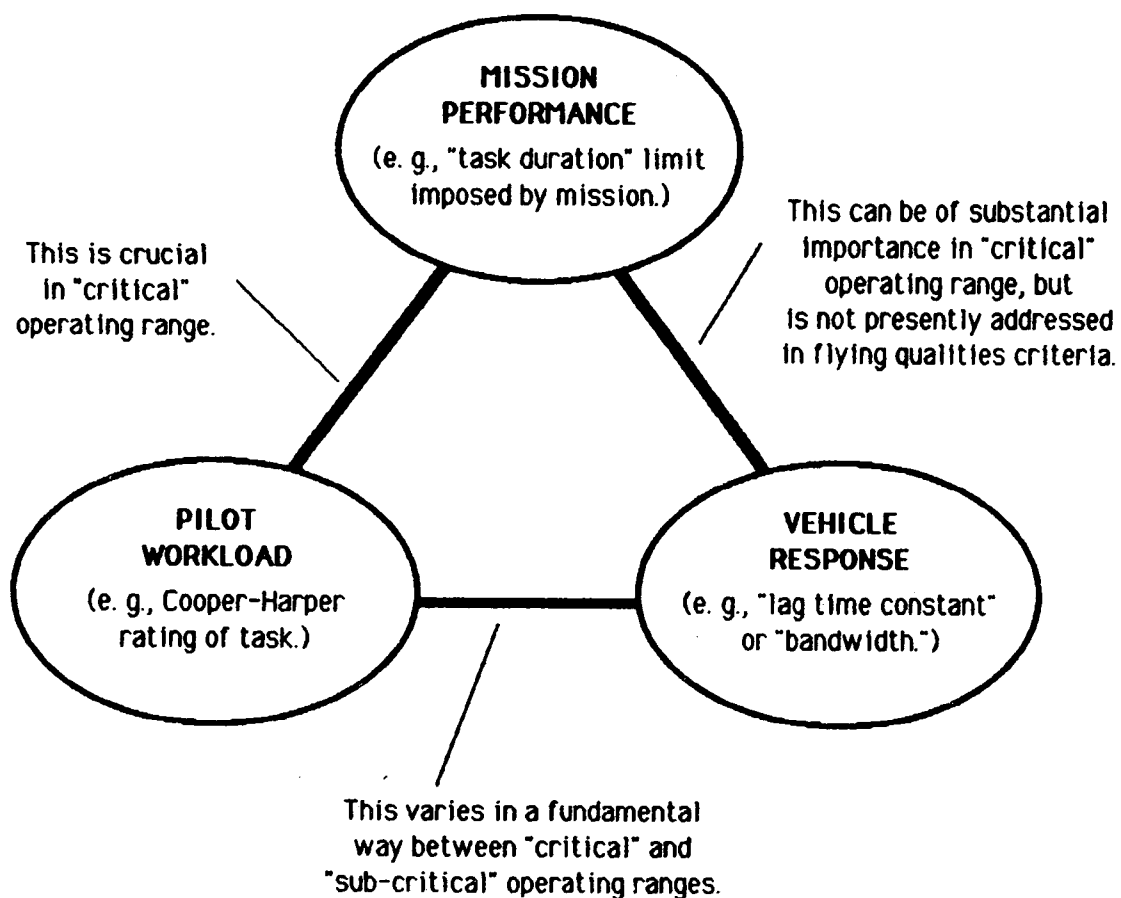
Figure 1. Components of Flying Qualities and their Interrelationships—the Objective of "Critical Task Performance and Workload Charting."

TECHNICAL APPROACH

The basis of the technical approach is to distinguish carefully among "pilot workload," "task performance," and "aircraft response." Hence quantitative metrics are needed for each. It is convenient to use the Cooper-Harper rating procedure (Reference 1) for the first of these. Task performance must be a set of goals or standards clearly visible to the pilot and reasonable with regard to accomplishment of a given task. One crucial dimension of task performance can be the time requirement for successfully completing task objectives, but there can be other task performance metrics too. Finally, it is adequate to quantify vehicle response in common flying-qualities terms such as "control power," "lag," or "sensitivity." All the above metrics ought to be generally compatible to a given situation or task scenario.

Consider as an example a helicopter hover sidestep maneuver. (This will be the basis of some of the data to be presented shortly.) The task is described in Figure 2. Note that the pilot translates to each tree in succession upon an external pacing command. Given that there is sufficient time, the pilot must hold lateral position within 10 ft and stabilize roll attitude.
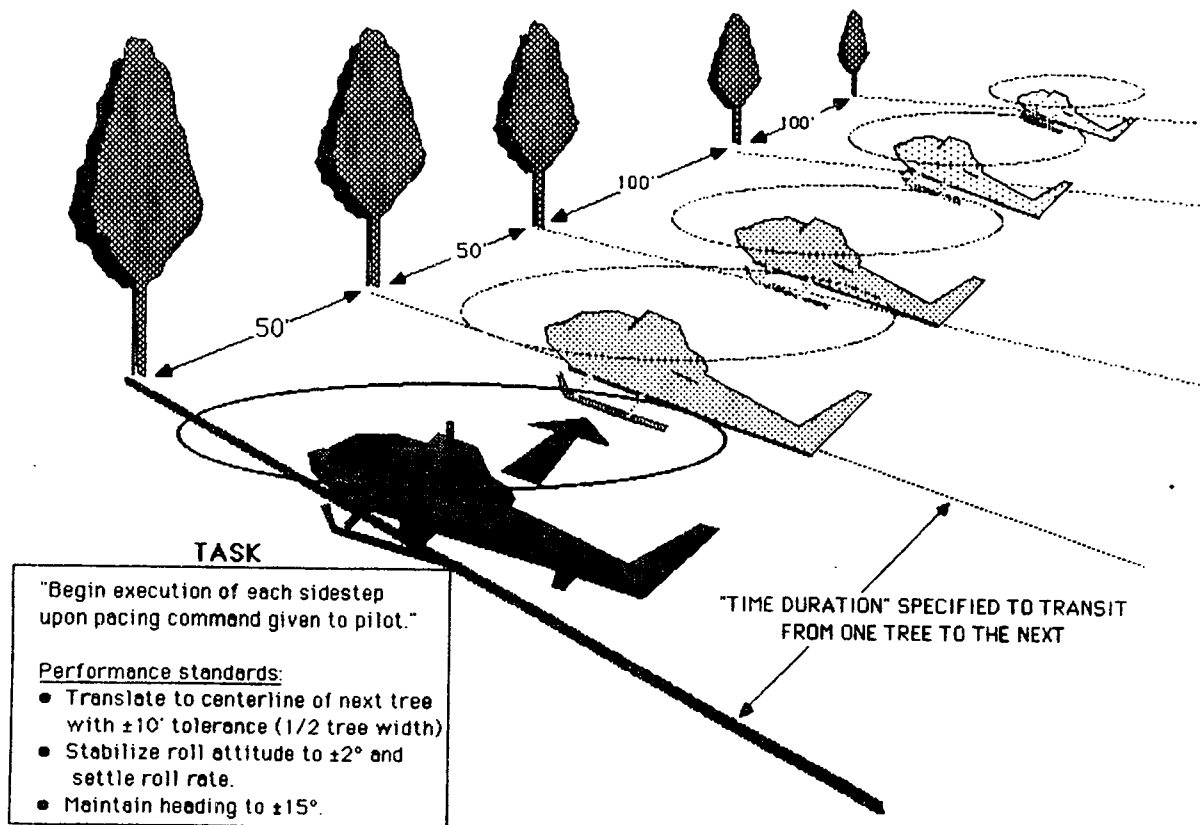
Figure 2. Sketch of Timed Sidestep Maneuver

In exploring helicopter roll response requirments for this task, it was found, not suprisingly, that the aggressiveness of the pilot affected pilot ratings. Thus by systematically varying aggressiveness through setting task duration limits, it was possible to track pilot rating. Ultimately task duration should be made so short that the pilot can no longer do the task to prescribed performance standards. This same procedure can then be repeated with a different vehicle response in order to explore effects on ratings for a range of maneuver aggressiveness.

The approach described in the above example can be applied to any combinations of features characterizing "task performance," "workload," or "vehicle response." Table 1 suggests some possibilities.

To summarize then, the procedure is to rig the task scenario in order to apply a variable time pressure or other mission-related feature, then to chart workload as the task feature is varied.

Table 1. Examples of Features which Describe Componments of Flying Qualities.

Component	Feature
Mission performance (or task performance)	task duration precision amplitude aggressiveness settling cognitive activity
Pilot workload	Cooper-Harper rating Hart-Bortolussi scale rating (Ref 2) SWAT rating (Ref 3) secondary critical task score (Ref 4) etc.
Vehicle response (motion, displays, etc.)	control sensitivity control power short-term response } for each cross coupling control axis nonlinearity

250

EXPERIMENTAL RESULTS

A number of flight simulator experiments have been run which illustrate the use of critical task performance and workload charting. These include both helicopter and fixed-wing aircraft applications involving several tactical maneuvers and flight tasks. In each case it has been shown that pilot rating (workload) can depend upon task performance standards as well as the aircraft characteristics. The following discusses primarily helicopter simulation results.

Effects of short-term roll response for a hover sidestep are shown in the first set of data. The performance of an aggressive hover sidestep would be likely in quickly moving from behind one cover to another while avoiding hostile fire or radar detection. This is also know as a "lateral unmask/remask maneuver." (Recall that this maneuver was described earlier in Figure 1.) There is some motivation for examining the sensitivity to more or less aggressive maneuvering because of the cost tradeoff between survival against given anti-helicopter weapons and the cost of enhancing roll control via flight control augmentation or rotor system design.

Short-term roll control was varied in terms of the "flapping stiffness" of a basic, unaugmented helicopter. This can be expressed in several ways, including roll time constant, rigid-body roll damping, and bandwidth for a net roll attitude phase margin of 45 deg. The bandwidth metric is used in the data presented here. A bandwidth of 0.8 rad/sec is relatively sluggish, 2.6 rad/sec moderate, and 4.1 rad/sec rather quick.

Figure 3 shows the effect of task duration on pilot opinion for the above three roll response bandwidths. Clearly there is improvement as bandwidth is increased, but it is a strong function of how aggressively the pilot was performing the task. Several features are worth noting.

First, for somewhat unaggressive sidesteps (12 sec or longer) the pilot ratings do not vary much and are in an acceptable range. However, as the sidestep duration is shortened the ratings degrade quickly beyond a certain point. Furthermore, that point is a function of the roll bandwidth. Thus, the amount of improvement must be expressed in terms of task performance as well as the usual Cooper-Harper rating or workload metric.

Other notable features of Figure 3 are the limiting of pilot rating for excessively quick maneuvering and the slight worsening for very slow sidesteps. The ultimate Cooper-Harper rating limit of "7" is because controllability is not in question even though the pilot cannot obtain adequate performance. (See the copy of the Cooper-Harper rating scale in Figure 4.) For other tasks greater hazards might be present for extremes in task performance

251
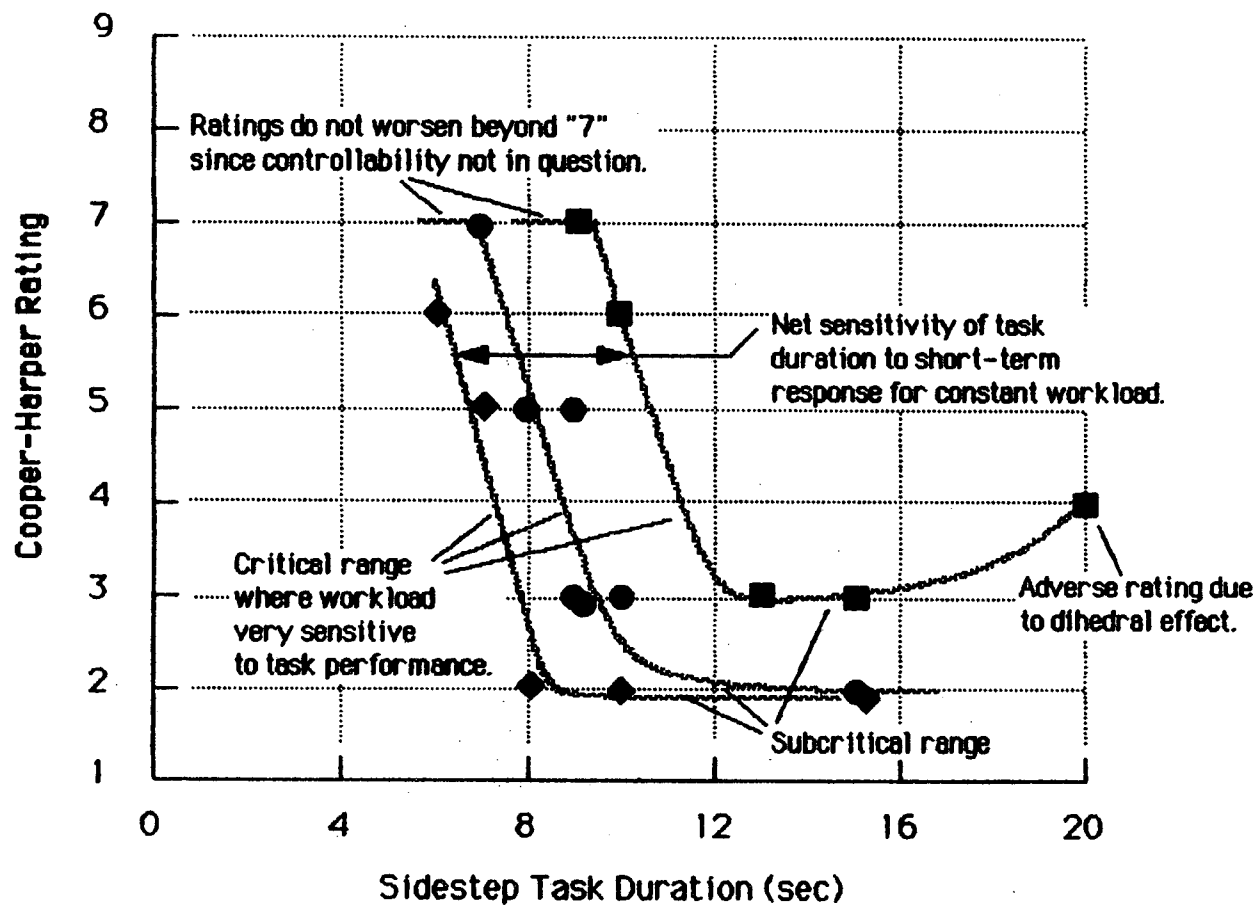
Figure 3. Effect of Short-Term Roll Response as a Function of Sidestep Duration (Raw Data).

ADEQUACY FOR SELECTED TASK OR REQUIRED OPERATION*	AIRCRAFT CHARACTERISTICS	DEMANDS ON THE PILOT IN SELECTED TASK OR REQUIRED OPERATION*	PILOT RATING
	Excellent Highly desirable	Pilot compensation not a factor for desired performance	1
	Good Negligible deficiencies	Pilot compensation not a factor for desired performance	2
	Fair — Some mildly unpleasant deficiencies	Minimal pilot compensation required for desired performance	3
Is it satisfactory without improvement? — No → Deficiencies warrant improvement	Minor but annoying deficiencies	Desired performance requires moderate pilot compensation	4
	Moderately objectionable deficiencies	Adequate performance requires considerable pilot compensation	5
	Very objectionable but tolerable deficiencies	Adequate performance requires extensive pilot compensation	6
Is adequate performance attainable with a tolerable pilot workload? — No → Deficiencies require improvement	Major deficiencies	Adequate performance not attainable with maximum tolerable pilot compensation. Controllability not in question	7
	Major deficiencies	Considerable pilot compensation is required for control	8
	Major deficiencies	Intense pilot compensation is required to retain control	9
Is it controllable? — No → Improvement mandatory	Major deficiencies	Control will be lost during some portion of required operation	10

Yes (loops from "Is it satisfactory without improvement?")
Yes (loops from "Is adequate performance attainable with a tolerable pilot workload?")
Yes (loops)

Pilot decisions

Cooper-Harper   Ref NASA TND-5153

* Definition of required operation involves designation of flight phase and/or subphases with accompanying conditions

Figure 4. Cooper-Harper Rating Scale.
(Reproduced from Reference 1.)

The worsening of pilot rating for a 20 sec sidestep was due to the washout of roll attitude as a result of dihedral effect and the necessity to continue applying lateral control trim. This corresponds to the very low frequency "hover cubic" response mode which would not be visible to the pilot during quicker, higher frequency maneuvering. This particular effect is significant, however, because of its implication on control trim characteristics as a function of task performance.

One observation that was made was that without specification of a task duration, a pilot typically operates just short of the abrupt upward break in ratings. Hence maneuver performance appears to be set more to optimize workload than to maximize performance, a phenomenon has also seen in other tasks.

253

The data shown previously in Figure 3 are replotted in Figure 5 in order to present a more familiar form for flying qualities data, i. e., rating versus aircraft response. This, however, clearly varies greatly over the 6 to 15 sec span in task duration. Further, just a difference between 6 sec and 8 sec produces a dramatic change in rating trends. Finally, these plots can be merged in order to map fully the task performance effect. The mapping on the far right of Figure 5 will be further analyzed shortly.
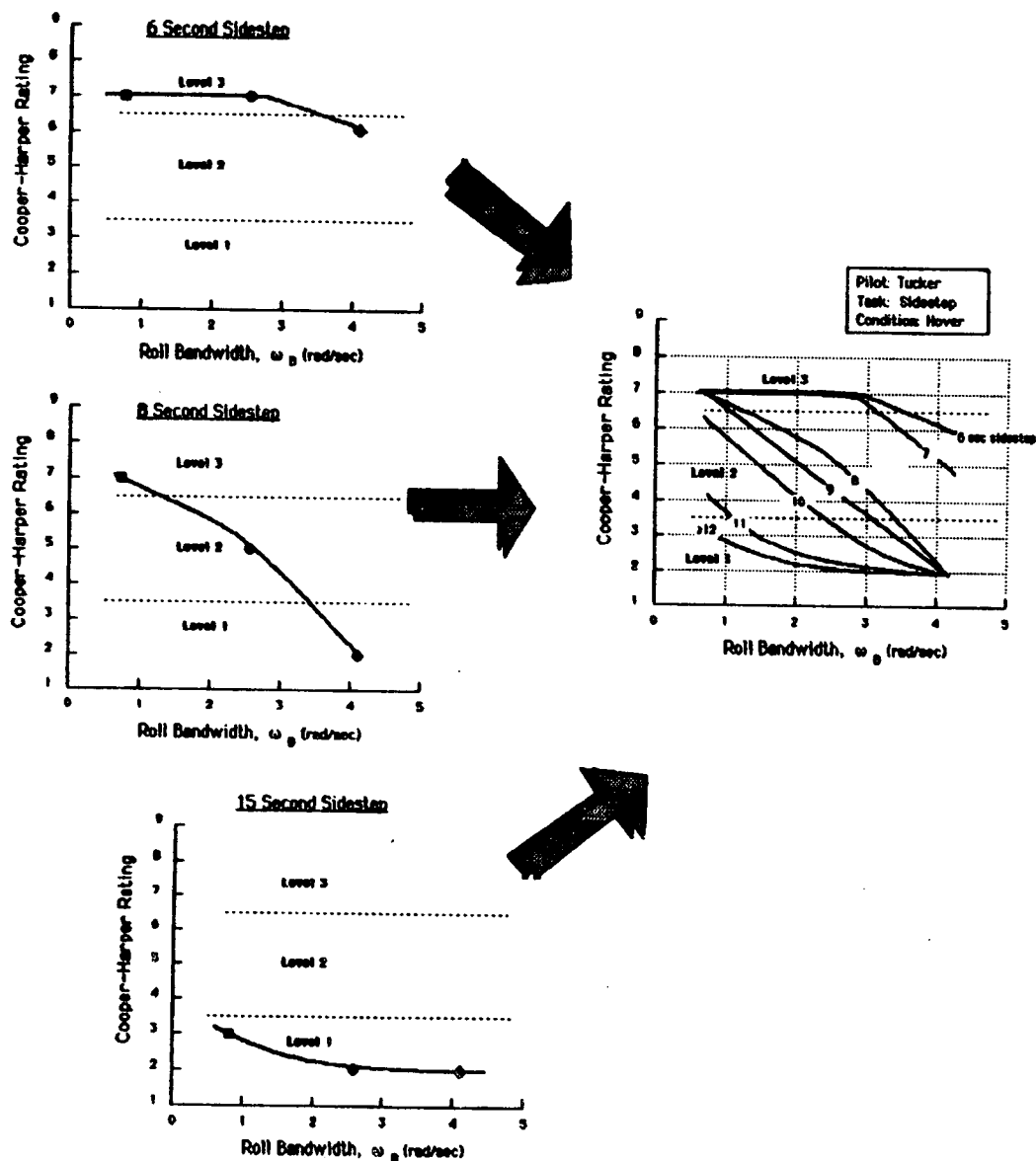
Figure 5. Pilot Rating Data Replotted for Sidestep Task.

Air combat tracking of a target is another task where the critical task performance and workload charting procedure was applied. Here another task performance metric was used, namely distance to the target. Vehicle characteristics included not only short-term response bandwidth, but also the type of response furnished by augmented flight control systems.

In this task the attacking pilot attempted to hold a fixed gunsight on the target while it flew a pseudo-random series of level heading reversals. Range to the target was not held precisely and typically varied 200 ft about the mean. Mean range was varied simply by requesting the pilot to fly the task "in-close" or "loose" on the target. The task is described in greater detail in Reference 5.

Figure 6 shows the experimental results of the ACM task in terms of pilot rating versus the mean range to the target during a run of about 90 sec. The general trend line is established by the baseline case having a "rate" response type and a bandwidth of 2.6 rad/sec. Note that as the pilot closes with the target the workload increases greatly.

Increasing the roll response bandwidth to 4.1 rad/sec allows the pilot to move in about 100 ft closer without a change in pilot rating. However, changing to a rate-command/attitude-hold flight control system architecture degrades task performance by about 150 ft. Use of an attitude-command/attitude-hold system worsens pilot rating even at longer ranges, but surpasses performance of the other response types as range is decreased. Unfortunately the critical break point was not established for this last configuration.

Example of "critical task performance
and workload charting" method:
Short-term roll response must
be examined as a function of range
from target otherwise workload
will appear to vary randomly.

Pilot: Parlier
Task: Helo ACM Tracking
Condition: Varying range to target.
Configurations:
  Rate type, 4.1 rad/sec ◆
  Rate type, 2.6 ●
  Rate command/att hold type, 2.6 ▲
  Attitude comm/att hold type, 2.6 ■

baseline

Attitude loops in augmented
configurations degrade
performance for this task.

Net improvement
due to increased
roll bandwidth.

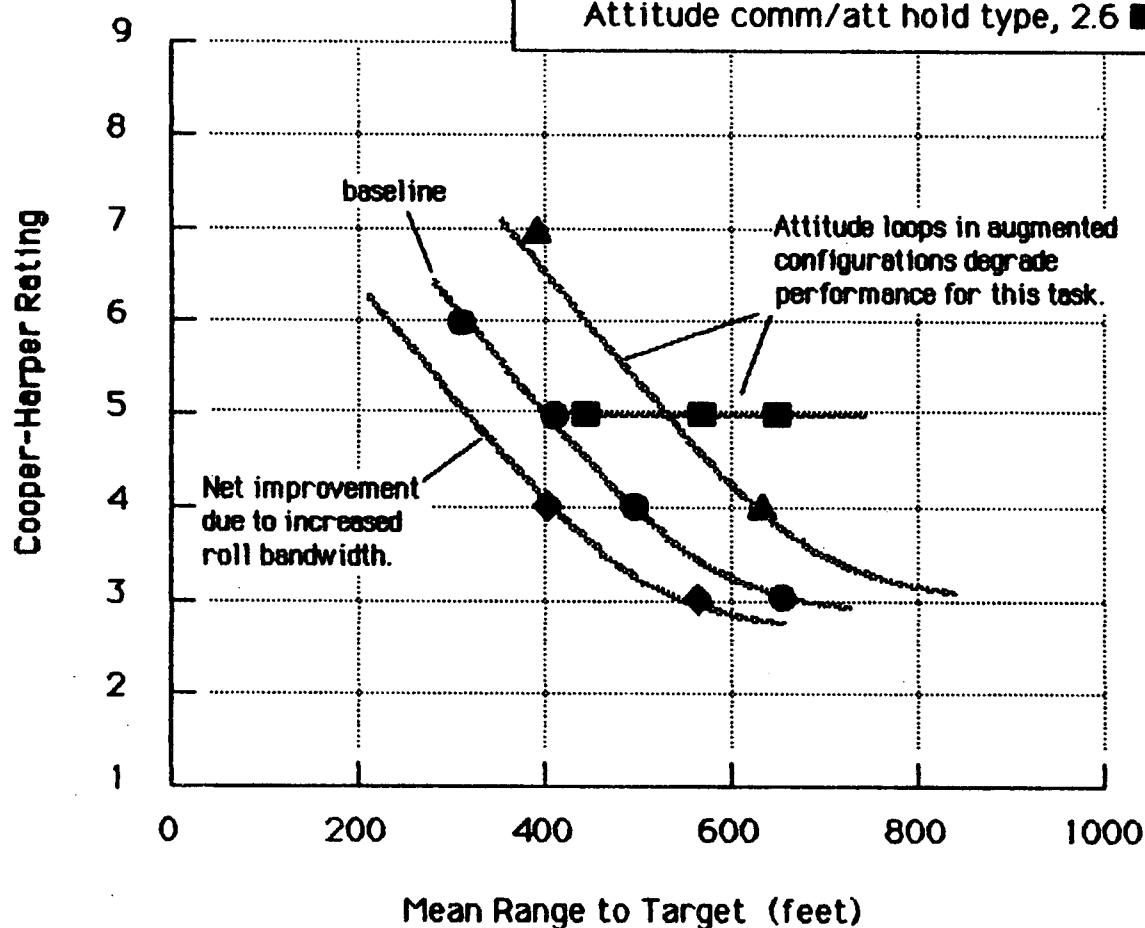**Figure 6. Effect of Short-Term Response
as a Function of Range from Target in Helo ACM.**

The effect of a simulator delay compensator was also documented through use of this technique. Prior simulator experience with helicopter lateral maneuvers from hover had suggested that system delays may have badly affected the validity of ratings. As a result, McFarland at NASA Ames developed a digital delay compensation scheme (Reference 6). The implementation of this compensator on the Ames Vertical Motion Simulator was examined using the charting technique both to plan the experiment and to conduct it.

It was believed crucial to evaluate the compensator under favorable conditions in order to maximize what could be subtle or changeable effects. First the sidestep task was chosen because it had been established to be an aggressive, demanding lateral task in flight as well as in the simulator (Reference 5). Next a high-bandwidth roll response configuration (4.1 rad/sec) was used to minimize vehicle response effects and accentuate those of simulator delay. Finally, for the nominal condition a task duration of 8 sec was picked because it appeared to be the most aggressive maneuver possible while still obtaining the very good "sub-critical" pilot rating of "2."

The experimental data are shown in Figure 7 for a net compensation of 100 msec. As with other data, the effect of the delay compensator can be expressed both in terms of task performance or in terms of workload (pilot rating). For a sidestep duration of 8 sec, removal of the delay compensator degraded the Cooper-Harper rating from a "2" to a "6." Or, alternatively, for a constant pilot rating of "6," the 100 msec compensator permitted the pilot to perform the maneuver 2 sec faster.

Other experimental data have been obtained with the critical task performance and workload charting procedure. One such set of data describes the effects of flight path and airspeed lag on the Navy carrier landing task. These data are presented in Reference 7 and show how the task parameters involving limited time or space impact basic airframe design parameters, including approach speed, wing loading, drag, and engine lag.

Vertical-axis helicopter response characteristics have also been examined experimentally and results are currently being analyzed by Blanken and Whalley of the U. S. Army Aeroflight-dynamics Directorate at Ames research center. Pilot rating data have been obtained which show how heave damping and thrust margin requirments depend upon the specific level of maneuver aggressiveness.

NOTE

A delay compensator can profoundly enhance workload or performance but that tradeoff must be carefully tracked in order to measure the effect.

Pilot: Tucker
Task: Sidestep--Hi Precision
Condition: Hover, calm winds.
Configurations:
Roll response 4.1 rad/sec
◇ delay compensator off
◆ 100 msec compensator on

For this task performance 100 msec compensation improves rating from "6" to "2."

100 msec delay compensation improves task performance by 2 sec.

Subcritical range where compensator expected to have no effect.
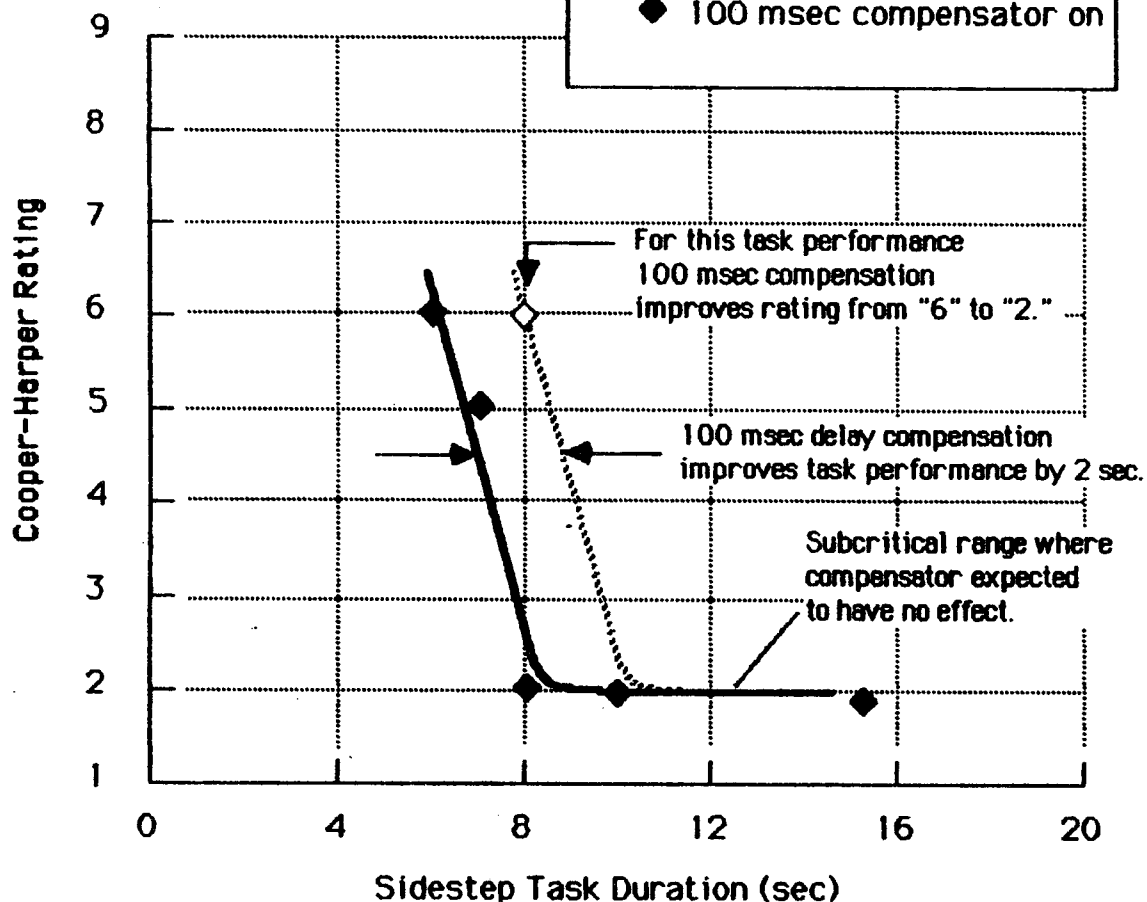
Fig 7. Effect of CGI Delay Compensator on CHR as a Function of Sidestep Task Duration.

258

ANALYSIS OF RESULTS

The above experimental results provide a number of new ideas about the formulation of flying qualities criteria and requirements. The following is a brief analysis of those data in terms of how they impact flying qualities and, moreover, how flying qualities are affected by mission performance.

Figure 8 is a "cleaned up" version of the Figure 3 raw data plot. For the lateral unmask/remask manever (sidestep) it represents the specific tradeoff between roll response and task duration. In addition, task performance limits were estimated to indicate the contributions of other vehicle features and the pilot.
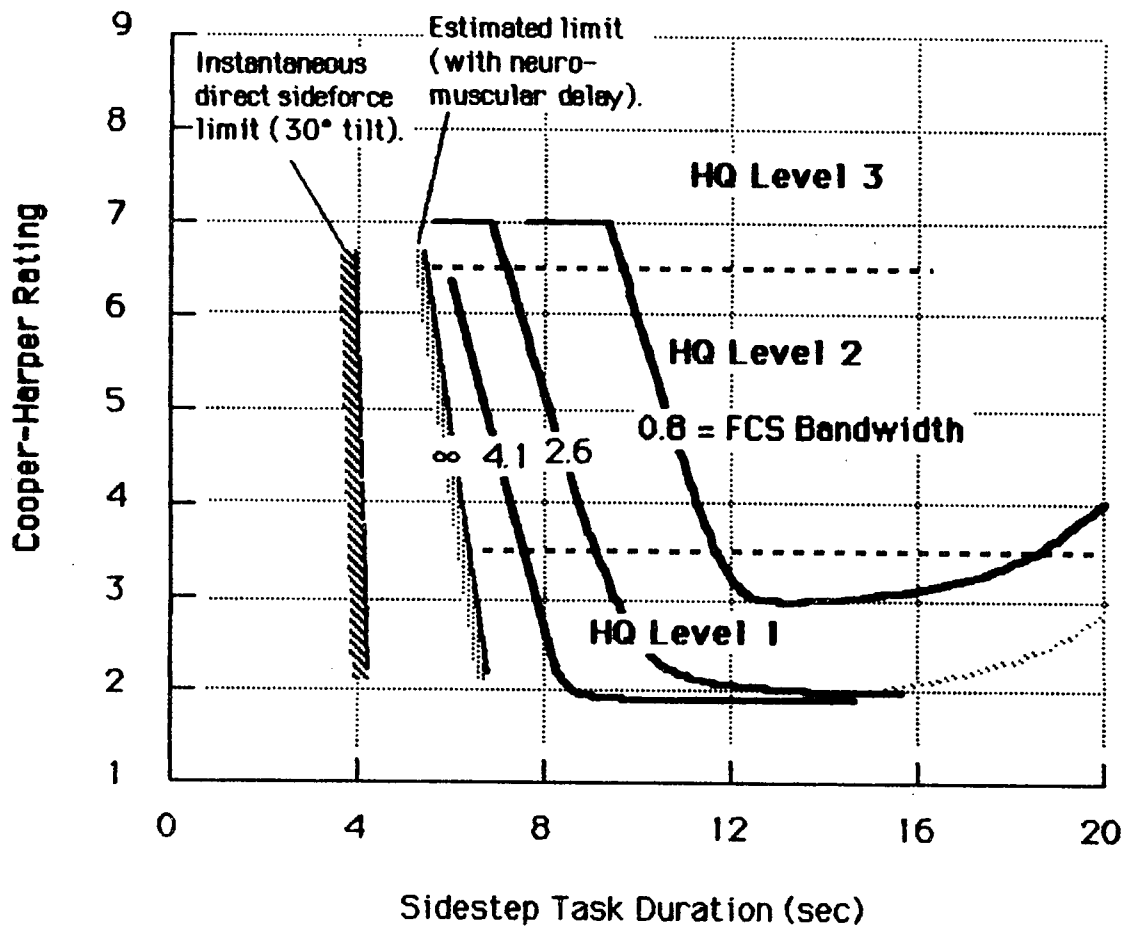
Fig 8. General Effect of Roll Response Bandwidth on Rating as a Function of Sidestep Task Performance.

Based on simulator observations, present bandwidth require-
ments would likely be set according to the pilot opinion given to
the right of the upward break for each configuration in Figure 8.
Hence for this task even the 0.8 rad/sec case might be judged
suitable for Level 1 handling qualities unless the pilot insisted
on performing the sidestep in less than 12 sec.

With the addition of a mission performance time requirement,
e. g., based on avoiding radar lock-on, the bandwidth requirment
could then be set as a rational function of that time. For
example, referring to Figure 9 (a cross plot of the same data),
an 8 sec maneuver would require a bandwidth of about 3.5 rad/sec
for Level 1 operation (Cooper-Harper < 3.5) and about 1.3 rad/sec
for Level 2 (Cooper-Harper < 6.5).
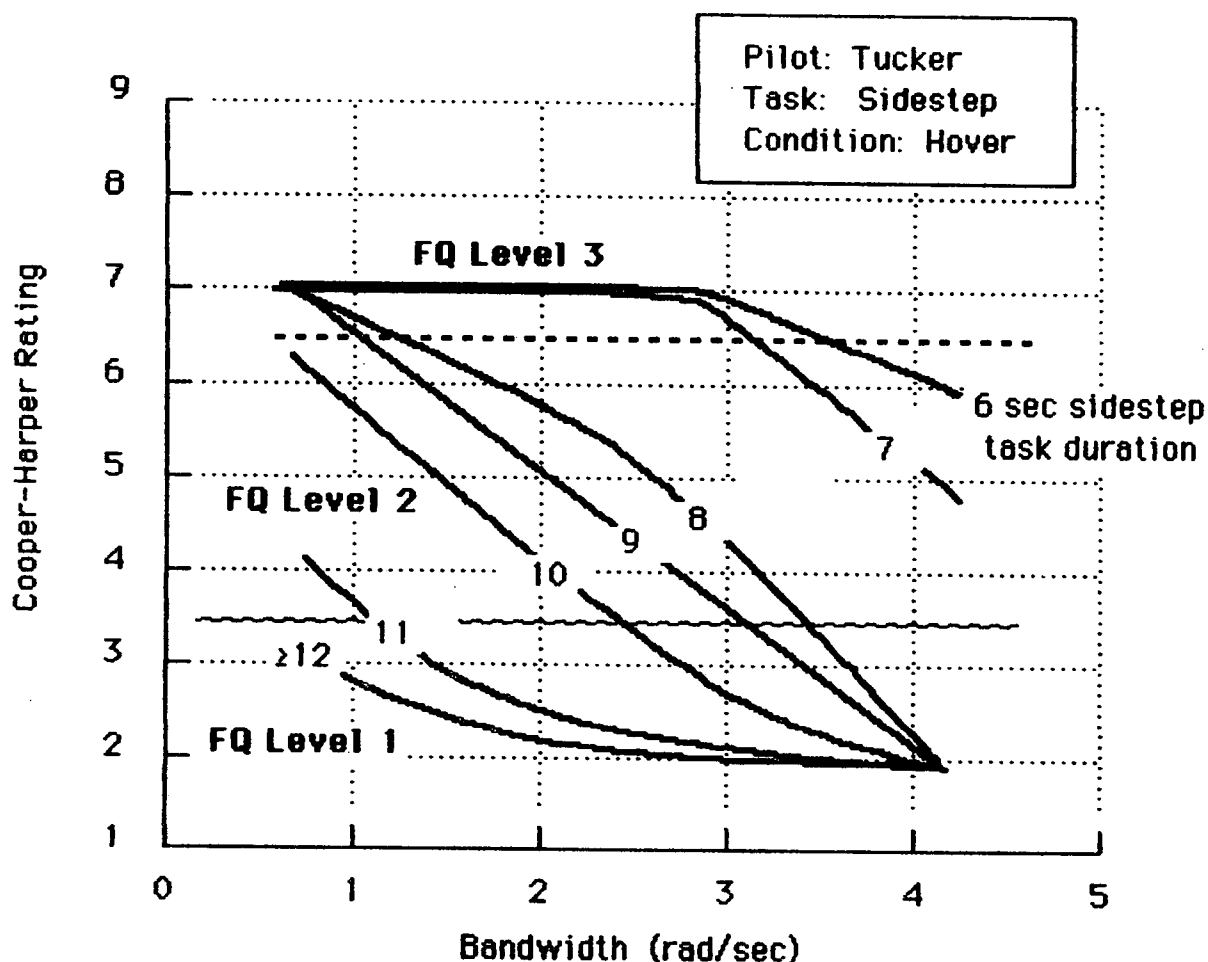
**Fig 9. Effect of Vehicle Response on
Pilot Rating as a Function of Task Performance**

According to the estimates made, however, there is a physical limit to the task duration time. At least four seconds are needed just to accelerate and stop even if there are no pilot or control delays. Another 2 sec can be added to account for neuromuscular lag of about 6 rad/sec. Figure 10, also based on the above curves, shows this asymptotic performance performance extratpolation more clearly. Its importance is in establishing where an enhancement in airframe and flight control response no longer improves performance or flying qualities.
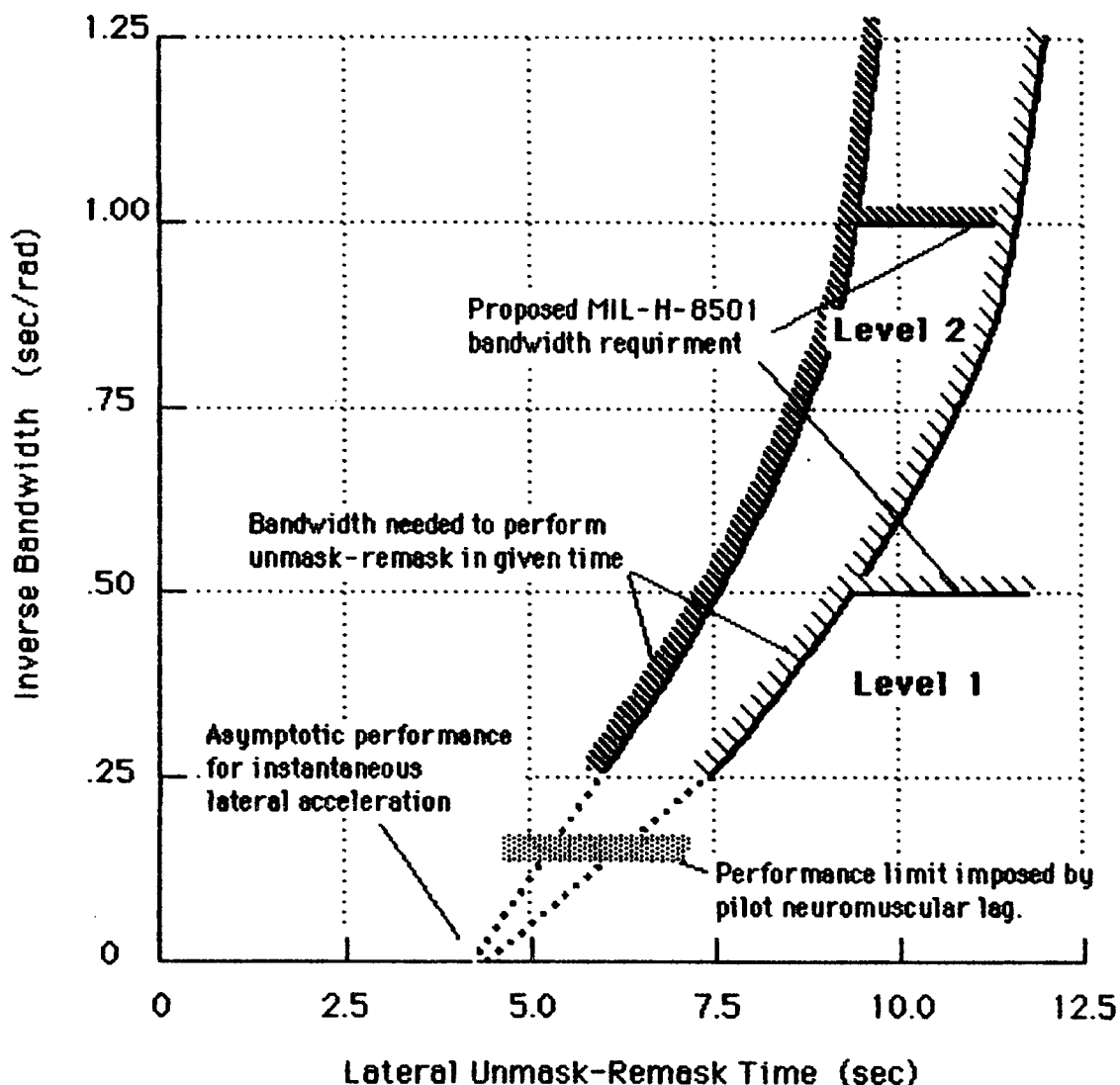
Figure 10. HQ Level Boundaries for Short-Term Response vs Lateral Unmask/Remask (Sidestep) Task Performance

261

Another feature of Figure 10 is comparison of Level 1 and Level 2 boundaries set by this experiment with those currently proposed for the MIL-H-8501 Mil Spec update (Reference 8). The latter were based on "aggressive maneuvering" but without quantitative tracking of task performance. They provide for a sidestep of about 9 to 10 sec.

Figures 11 and 12 are fairings of the ACM task results. Both are restatements of the fact that flying qualities depend upon task performance standards. Figure 11 shows how roll response bandwidth and flight control architecture both contribute to how closely a pilot can approach a target. Also for distances beyond the sub-critical range of 600 to 800 ft, there may be no particular effect of roll response, per se. Thus if offensive weapons were effective at, say, 1000 ft, then roll response could be considered relatively unimportant to mission effectiveness. On the other hand, the use of guns might require very close, precise tracking thus heavy emphasis on roll-axis flying qualities.
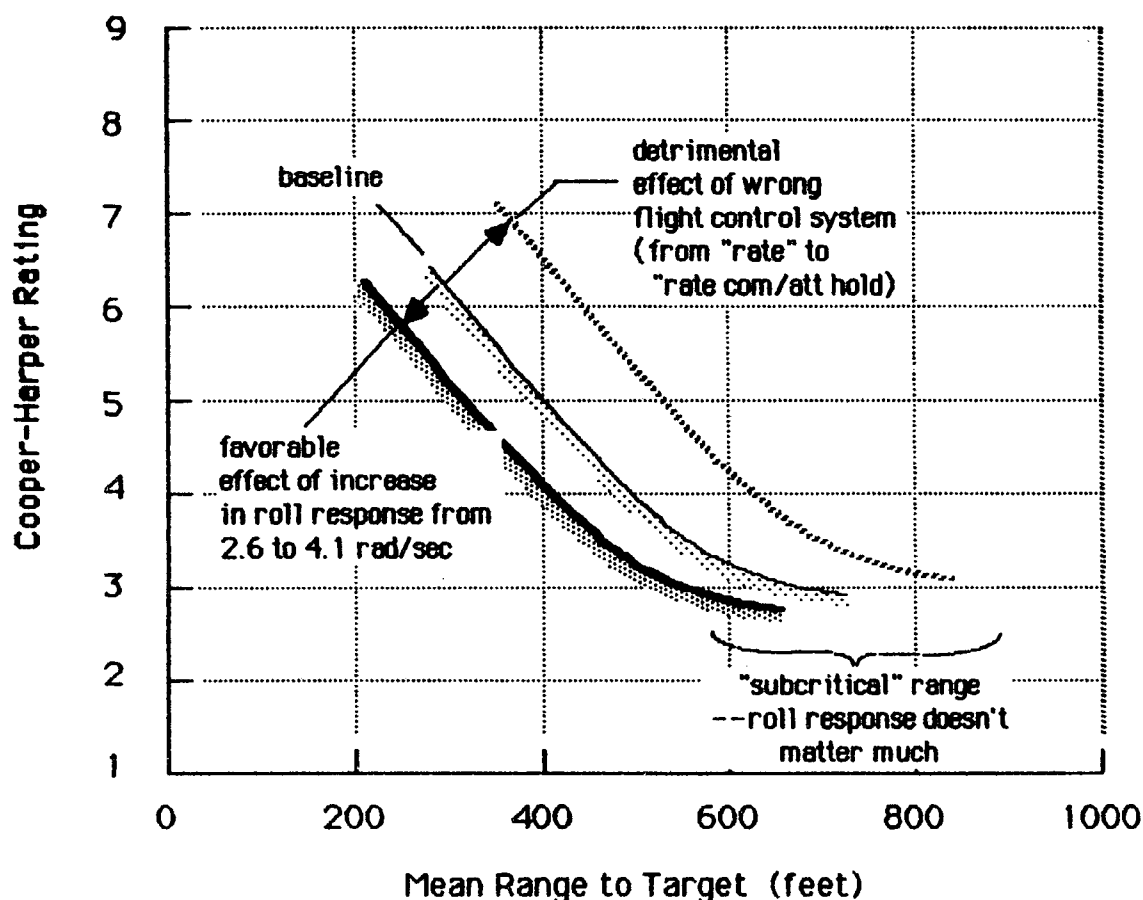
Figure 11. Effect of Short-Term Response Characteristics on Rating as a Function of ACM Target Range.

Figure 12 is analogous to Figure 10 but applies to the ACM task as opposed to the lateral unmask/remask. Ultimate closure performance is estimated based on pilot neuromuscular lag of about 6 rad/sec. Also, the proposed MIL-H-8501 bound is indicated. Note that enhancement of roll response could permit ACM ranges of about 200 ft closer than proposed bandwidth requirments.
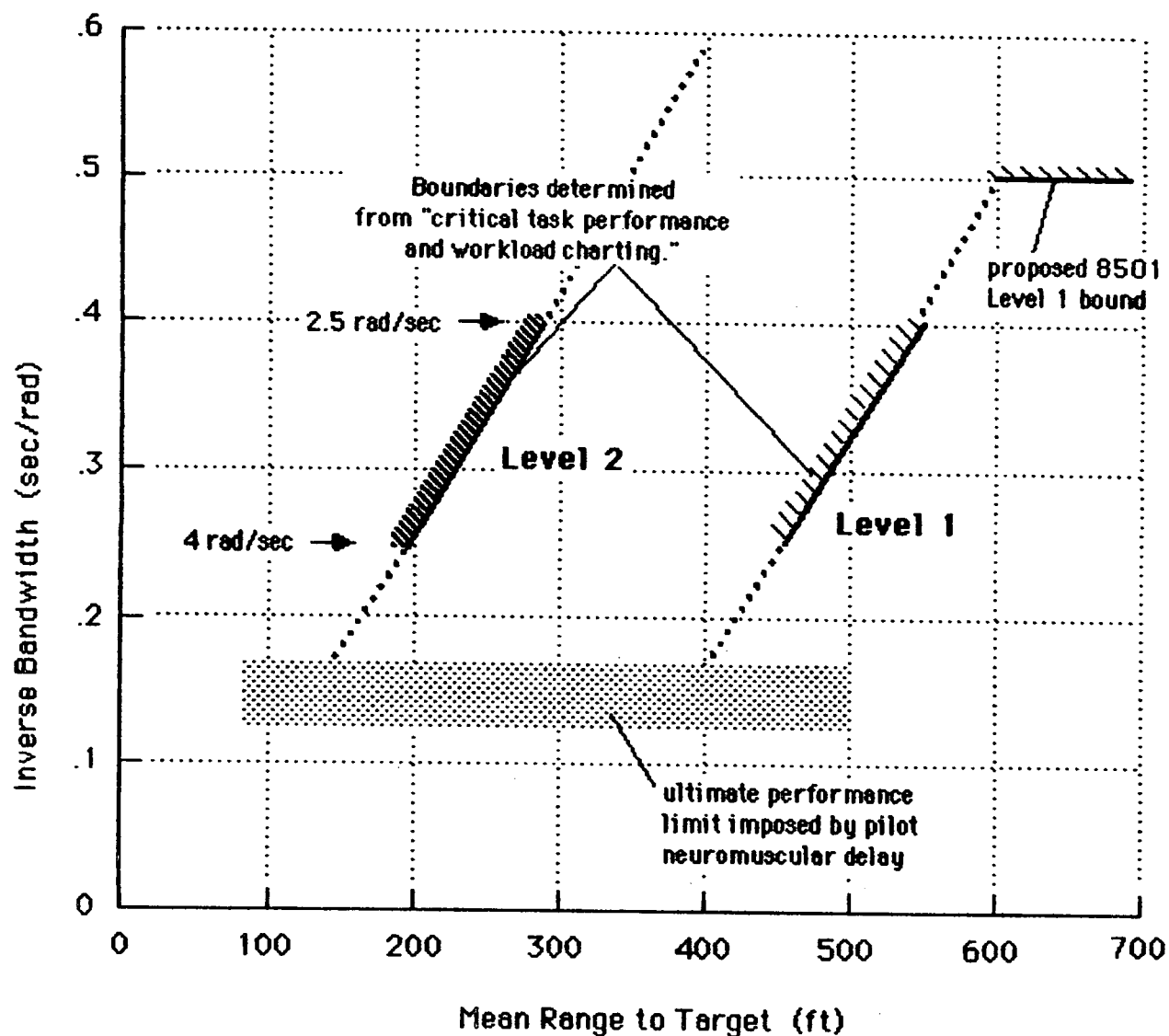
Figure 12. HQ Level Boundaries for Short-Term Response vs Helo Air Combat Task Performance.

Figure 13 is a generalized example of trends which might be found by critical task performance and workload charting. (Specific examples were presented in Figures 3, 6, and 7.) In general, with the variation of an appropriate mission performance parameter one finds a "sub-critical" range where there is little effect on workload and a "critical" range where mission performance is traded off with increased workload. A variation in some vehicle response parameter may alter the workload-performance relationship favorable to design objectives.

In addition, Figure 13 indicates that the pilot is likely to gravitate toward operation at some point still in the "sub-critical" range. Thus when comparing competing configurations, pilot ratings might be based on different levels of task performance. For example, Configurations A and B would receive about the same rating although B is inferior in terms of performance potential. An even more unfortunate oversight might be made between A and C. Configuration C could be judged worse than A even though the performance, both demonstrated and potential, was better with A.
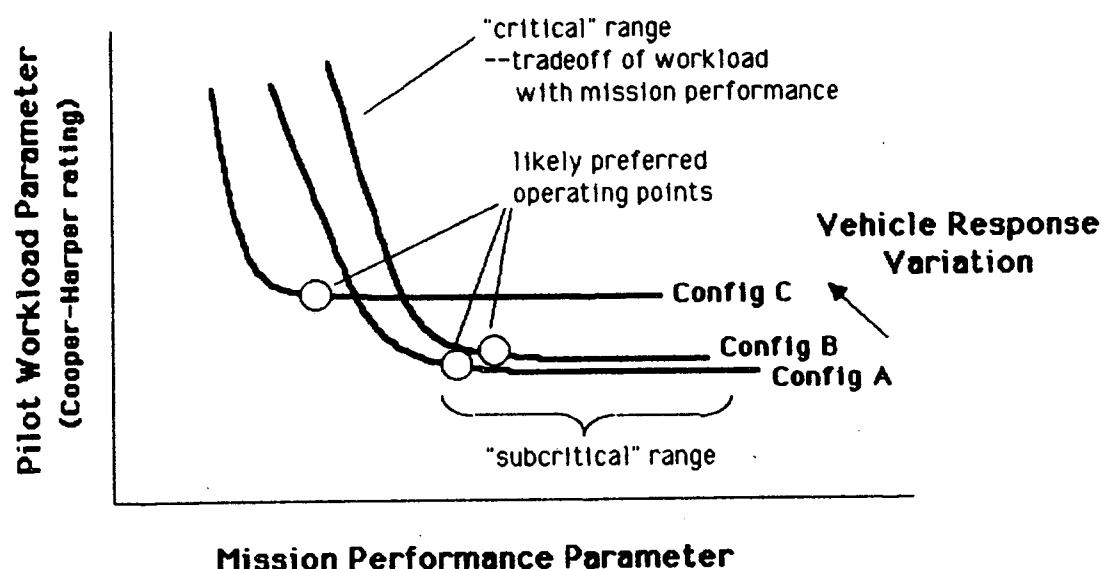
Figure 13. A Generalized Example of Trends Which Might be Found by "Critical Task Performance and Workload Charting."

CONCLUSIONS

The "critical task performance and workload charting" technique can provide an added dimension to assessment of flying qualities. Not only is the dependence between pilot rating and vehicle response defined, but also the tradeoff with mission or task performance.

If an evaluation pilot is allowed to choose certain task performance variables there can be a subtle variation in performance from one configuration to another. That is, two experimental variables can, in fact, be changing at once. Hence false or misleading conclusions could be made regarding the relation between workload and vehicle characteristics.

Data obtained for the helicopter sidestep (lateral unmask/remask maneuver) showed that the benefit of enhanced short-term roll response (bandwidth) varies substantially with the time available to do the maneuver. For task duration times of 12 sec or more, the Level 1 roll bandwidth boundary is below 1 rad/sec. As the time available is shrunk to 8 sec, the bandwidth requirement increases to 3.5 rad/sec. Thus flying qualities criteria need some mission performance basis. Further this basis must be appropriately quantified and not simply labeled "aggressive" or associated with an insufficiently defined task.

The effect of a digital delay compensator was measured for the sidestep task. This also demonstrated that benefits must be assessed in terms of task performance and pilot rating. For a particularly critical sidestep task duration the 100 msec compensation was responsible for changing the Cooper-Harper rating from a "6" to a "2." Alternatively for a constant pilot rating of "6", the compensator permitted the task to be done 33 percent faster. Little or no effect was noted when pilots were allowed to examine the compensator without sufficiently rigid task performance standards.

Roll response affects offensive helicopter air combat maneuvering workload and performance. In particular, the roll response bandwidth and flight control architecture permit the pilot to achieve a closer range from the target with a given level of workload. Increasing bandwidth from 2.6 to 4.1 rad/sec allows the attacker to approach 100 ft closer while, for the same range, the pilot opinion difference is only 1 rating point. The introduction of attitude loops in the flight control system generally degrades the task.

Based on the above results and other helicopter and fixed-wing simulator data now being analyzed, one concludes that careful tracking of workload and task performance must be made. The approach demonstrated here is a simple, effective one which adds a needed dimension to flying qualities assessment.

265

REFERENCES

1 Cooper, G. E. and R. P. Harper, The Use of Pilot Rating in the Evaluation of Aircraft Handling Qualities, NASA TN D-5153, April 1969.

2 Hart, S. G. and M. R. Bortolussi, "Pilot Errors as a Source of Workload," Journal of the Human Factors Society, Vol. 26, No. 5, October 1984.

3 Reid, G. B. and C. A. Shingledecker, "Application of Conjoint Measurement to Workload Scale Development," Proceedings of the Human Factors Society--25th Annual Meeting, October 1981, pp 522-526.

4 Schiflett, S. G., Evaluation of a Pilot Workload Assessment Device to Test Alternate Display Formats and Control Stability Variations, NATC SY-33R-80, February 1980.

5 Heffley, R. K., S. M. Bourne, H. C. Curtiss, Jr., W. S. Hindson, and R. A. Hess, Study of Helicopter Roll Control Effectiveness Criteria, NASA CR 177404 (USAAVSCOM TR-85-A-5), April 1986.

6 McFarland, R. E., CGI Delay Compensation, NASA TM-84281, January 1986.

7 Heffley, R. K., Terminal Control Factors for the Carrier Landing Task, AIAA Paper 86-2251-CP, August 1986.

8 Hoh, R. H., D. G. Mitchell, et al, Proposed Airworthiness Design Standard: Handling Qualities Requirements for Military Rotorcraft, STI TR 1194-2, December 1985.

AN EXPERIMENTAL PROTOCOL FOR THE EVALUATION
OF GRAPHIC INPUT DEVICES IN MICROGRAVITY

Steven R. Bussolari[*], Jess E. Fordyce[*], and Byron K. Lichtenberg[**]

[*]Man-Vehicle Laboratory, Massachusetts Institute of Technology
Cambridge, MA, 02139

[**]Payload Systems, Inc., PO Box 758, Wellesley, MA, 02181

An experimental protocol was developed to evaluate human operator performance using three graphic input devices in the microgravity environment of low earth orbit. The experiment is controlled by a GRiD Compass microcomputer that accepts cursor positioning commands from a joystick, cursor movement keys, or a trackball. The goal of the experiment is to evaluate the performance and operator workload associated with the use of each of the devices in weightlessness. The experiment will be performed by four crewmembers during the EOM 1/2 Spacelab mission.

Ground tests were conducted to validate the experimental technique and to establish a data baseline. Results of the ground-based experiments showed significant differences in performance and workload among the graphic input devices. For the cursor positioning task utilized, the trackball facilitated the best operator performance, followed by the joystick and the keyboard, respectively.

TEST PILOT EVALUATION OF THE

CLOSED-LOOP "GRATE" FLIGHT TEST TECHNIQUE

Daniel J. Biezad, Lt Col, USAF
Assistant Professor
Air Force Institute of Technology
Wright-Patterson AFB, OH 45433

Steven R. Sturmer, 1Lt, USAF
Flying Qualities Engineer
Air Force Wright Aeronautical Laboratories
Wright-Patterson AFB, OH 45433

Abstract

A flight test method called the Ground Attack Target Equipment (GRATE) technique has been developed by DFVLR, the research center for the Federal Republic of Germany. This technique is a relatively precise and repeatable method for exposing poor handling qualities, should any exist, of modern fighter/bomber aircraft. GRATE was applied to low-order dynamic models of a ground attack and a fighter aircraft in the Large Amplitude Multi-Mode Research Simulator (LAMARS) at the Air Force Flight Dynamics Laboratory as part of a joint AFWAL/DFVLR program. The technique was evaluated while simultaneously investigating the effects on flying qualities of varying time delay and turbulence intensity. Results showed that GRATE was effective, and easy to both learn and use. It was as effective as simulated turbulence in unmasking poor flying qualities, and the concept may easily be extended to other flying tasks such as air-to-air tracking.

Introduction

In order to evaluate or identify aircraft handling qualities from closed-loop tests, sufficient excitation or disturbance must exist over a reasonably wide bandwidth (Ref.1). The turbulence models commonly used to accomplish this verify the precision of flight path control and test the ability of a pilot to recover from certain environmental conditions (Ref.2). This is especially important during operations, such as precision landing, where flying qualities "cliffs" may exist which seriously degrade performance at critical times during the flight (Ref. 3).

It is very difficult to simulate realistic turbulence during in-flight evaluations, and in many instances an offset or repositioning is accomplished instead. These maneuvers are difficult to model for spectral content, and are technique dependent, so it is possible that poor flying qualities may remain masked even in an otherwise rigorous test program.

The GRATE technique was developed by DFVLR to accomplish required closed-loop excitation in a mathematically precise way during actual air-to-ground flight tests (Ref. 4). This technique was implemented and evaluated by applying it to a generic low-order transfer function representation of a ground attack and a fighter aircraft at the LAMARS facility of the AFWAL Flight Dynamics Laboratory.

The purpose of the simulation was to evaluate the GRATE technique by varying flight configurations with known handling qualities in a precise and repeatable manner. Different levels of time delay and turbulence intensity were investigated relative to the baseline configurations.

In the next section, the experiment is described, followed by results in the form of Cooper-Harper pilot ratings and pilot comments. The results presented are preliminary and qualitative, but are useful in determining the value and potential of the GRATE technique.

Simulation Conduct

The GRATE technique is fully explained in Reference 4. For the LAMARS simulation, a set of lamps were arranged in an eight-pin pattern shown in Figure 1 and mounted on the terrain board along the ground track of the aircraft. An input signal switched one lamp on at a time for a 2.55 second interval. The pilot flew a 10 degree dive angle at 390 knots starting at an altitude of 600 meters (range of about 3300 meters). Data was taken for about 10 seconds as the pilot attempted to align and fine track the lamps as they switched on.

The lamp switching was set to present a random yet mathematically precise input spectrum to the pilot. In this way, the closed-loop bandwidth was sufficient in both the longitudinal and lateral axes to excite all the modes and cross couplings likely to be encountered in the air-to-ground mission. Lamp switching was accomplished so that the angular changes were less than one degree and the pilot was required to pull-up at the end of the run, for safety considerations.

Three time delays (TAU1, TAU2, TAU3) were investigated relative to the baseline configurations by adding a first-order Pade approximation to the model transfer functions in the longitudinal and the lateral/directional axes. Additionally, each time delay was flown in three different levels of turbulence (ATM1, ATM2, ATM3). The basic test matrix is shown in Figure 2.

In addition to the basic tests, approaches were flown with and without turbulence with all the lamps on to suppress the GRATE technique. At approximately 250 meters AGL, the pilot switched from aiming at the closest lamp to the farthest lamp to simulate an offset maneuver. In this way, it could be determined

whether the offset maneuver was as effective as the GRATE technique in unmasking poor handling qualities. Due to time constraints, only a small portion of the test matrix could be flown for these investigations.

The transfer functions for the low-order simulations of the baseline aircraft are provided in the Appendix. These were implemented with simple, linear equations of motion on the LAMARS simulator. The visual scene was provided by a terrain board projection along with a sky/earth projection and a ground attack HUD overlaid in the simulator cockpit. The cockpit was representative of a single-seat, high-performance aircraft with a center stick controller. Motion cues were provided to the pilot in all axes.

Recorded results included pipper error plots in both the longitudinal and the lateral directions. Cooper-Harper pilot ratings and comments were annotated, and a large set of digitally recorded parameters were stored for future analysis. Performance time-histories were also made. Video recordings on three-quarter inch tape were taken. The pilot ratings and comments were for each set of four data runs (two runs each with two different lamp sequences). Approximately 60 runs were accomplished per simulation period. Following each period, comprehensive evaluation forms were accomplished, including those for the test technique itself.

The pilot (first author) accomplishing these tests has an extensive background in flight test with over 4000 hours of total flight time in a wide variety of aircraft. The test engineer (second author) supervising these tests has three years of experience with handling qualities testing.

Results and Evaluation

The test technique was intuitive and natural, but the closed-loop bandwidth required by GRATE forced the pilot to use the rudders for tracking. Using ailerons to roll onto the target lamp simply took too much time. Therefore, harmony between roll and yaw, a problem in previous simulations (Ref. 5), was not evaluated. Lamp switching patterns were adjusted to keep visual steps less than one degree, but the task seemed more demanding below about 300 meters AGL than when starting the dive pass. Results were obtained using aggressive pitch and rudder inputs which were blended while keeping bank angle near zero.

Results for the baseline ground attack and fighter aircraft with no added time delay or turbulence are shown in Table 1. Each pilot rating applies to a set of four data runs and includes an assessment of alignment and final tracking in the pitch and yaw axes.

271

Table 1. Baseline Configuration Pilot Ratings Using GRATE
No Turbulence - ATM0, No Time Delay - TAU0
==

Configuration	Pilot Rating*	Comments
Ground Attack	3	"solid Level 1 aircraft"
Fighter	2	"slight pitch bobble"

==
* Overall ratings include assessment of alignment and final tracking in pitch and yaw axes

The effect of three turbulence intensities (Dryden form) on the baseline configurations is shown in Table 2. The application of turbulence to the GRATE technique did not significantly affect the flying qualities evaluation. The turbulence affected performance slightly, but making the small changes necessary to track the target lamps was relatively easy with or without turbulence.

Table 2. Turbulence Influence on Baseline Pilot Ratings
No Time Delay - TAU0
==

Configuration	ATM0	ATM2	ATM3
Ground Attack	3	3	-
Fighter	2	3	4*

==
* "literally driving task with turbulence - too high for flight test"

Table 3 summarizes the results of varying time delay and turbulence levels for the ground attack configuration. Predictably, the effect of increasing time delay was to induce closed-loop oscillations in both pitch and yaw axes. By reading the ratings horizontally, it is concluded that the GRATE technique for no turbulence is as effective as the application of turbulence in identifying degradations in handling qualities caused by increasing time delays. There is no tendency for increasing turbulence intensity to make ratings worse, at least in terms of the Level rating. The pilot, therefore, apparently rated a qualitative degradation in flying qualities due to time delay which was not significantly affected by turbulence.

Table 3. Turbulence and Time Delay Influence on the Ground
Attack Configuration Pilot Ratings

Time Delay	ATM0	ATM1	ATM2
TAU0	3	3	3
TAU1	3/3*	3	–
TAU2	4/6	4	5
TAU3	7/9**	8**	8**

* "slight pitch bobble for tracking"
** "could not perform task within reasonable tolerance"

Results for the fighter configuration using the GRATE
technique were similar to those for the ground attack
configuration and are shown in Table 4. Except for the pilot
rating of 6 for the large time delay (TAU3), once again there are
no variations in the ratings which depend on turbulence. Figures
3 and 4 show the quantitative difference in performance between
the zero and 300 millisecond time delays for the fighter
configuration. Note that the technique exposes the poor flying
qualities without added turbulence.

Table 4. Turbulence and Time Delay Influence on the Fighter
Configuration Pilot Ratings

Time Delay	ATM0	ATM1	ATM2
TAU0	2	2	3
TAU1	5	5	5
TAU2	7	7	7
TAU3	8	6*	8

* "not really able to do the task, but a little better than
with higher turbulence level [ATM2]"

To check that the GRATE technique was truly effective in
unmasking poor handling qualities, GRATE was suppressed by flying
with all the lamps on. An offset was simulated by transitioning
from the closest to the farthest lamp at about 250 meters AGL.
The results are shown in Table 5. Note that with no turbulence,
the offset simulation failed to unmask the degradation in rating
due to TAU1. For TAU2, the offset resulted in a degradation in

flying qualities, but not to the same extent as with the GRATE technique. The optimistic ratings for the offset are due to the pilot compensating for time delay and/or turbulence by flying very smoothly, an option which is not available with the high-bandwidth input excitation of the GRATE technique. It is apparent from the last row of Table 5 that the offset maneuver, even with turbulence, did not consistently unmask flying qualities deficiencies.

Table 5. Fighter Configuration Pilot Ratings Comparison

Time Delay	GRATE Technique		Offset Maneuver	
	ATM0	ATM1	ATM0	ATM1
TAU1	5	5	2	5
TAU2	7	7	4	3

Note: Offset ratings based on two data runs

Conclusions

The GRATE method of evaluating closed-loop handling qualities shows much promise. It effectively portrays degradations due to poor system dynamics or excessive time delay due to the high-bandwidth input excitation of the GRATE technique. It is superior to the lower-bandwidth offset maneuver in this regard, and effectively substitutes for turbulence as a technique to generate higher closed-loop bandwidth. The GRATE concept should be extended to other closed-loop tasks.

References

1. McRuer, D.R., "Human Dynamics in Man-Machine Systems", Automatica, Vol. 16, May 1980, pp. 237-253.

2. "Military Specification - Flying Qualities of Piloted Airplanes", MIL-F-8785C, Nov 1980.

3. Berry, D.T., B.G. Powers, K.J. Szalai, and R.J. Wilson, "In-Flight Evaluation of Control System Pure Time Delay", Journal of Aircraft, Vol. 19, No. 4, Apr 1982, pp. 318.

4. Koehler, R., and E. Buchacker, "A Flight Test Method for Pilot/Aircraft Analysis", 21st Annual Conference on Manual Control, Ohio State University, Jun 1985.

5. Biezad, D.J., and D.K. Schmidt, "Normalizes Predictive Deconvolution: A Time Series Algorithm for Modeling Human Operator Dynamics", AIAA Journal of Guidance, Control, and Dynamics, Vol. 8, No. 6, Nov-Dec 1985, pp. 768-776.

- Angular changes less than 1 deg
- Lamp switching interval = 2.55 sec
- Dive pass lasts 10 sec

Start dive pass
390 kts

600 m

Pull-up point

Target lamps

10 deg

3300 m

470 m
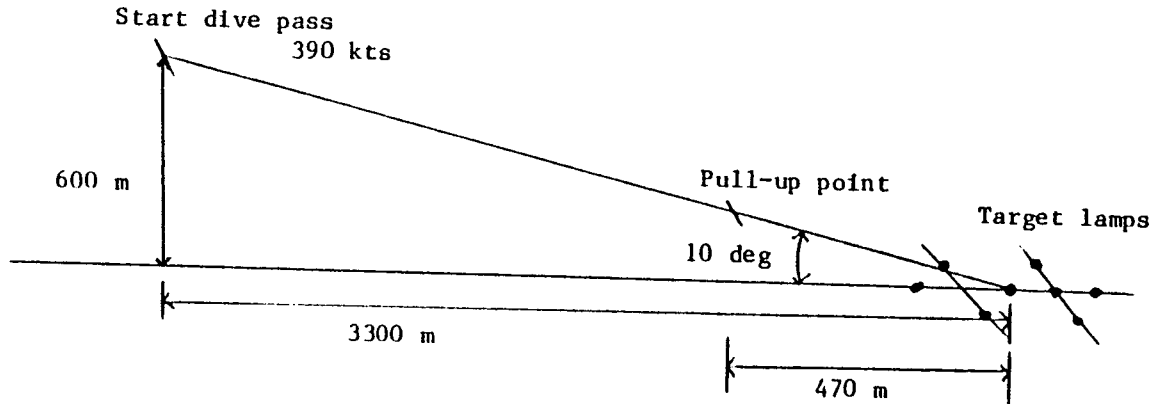
Figure 1. Light Pattern for LAMARS Simulation.

Time Delay (x/δ_c)	Turbulence Intensity (fps rms)			
	ATM0 (none)	ATM1 (light-1.5)	ATM2 (mod-3.0)	ATM3 (heavy-5.0)
TAU0 (0.0 sec)	X	X	X	X*
TAU1 (0.1 sec)	X	X	X	—
TAU2 (0.2 sec)	X	X	X	—
TAU3 (0.3 sec)	X	X	X	—

* ATM3 unrealistically severe

Figure 2. Test Matrix for LAMARS Simulation.
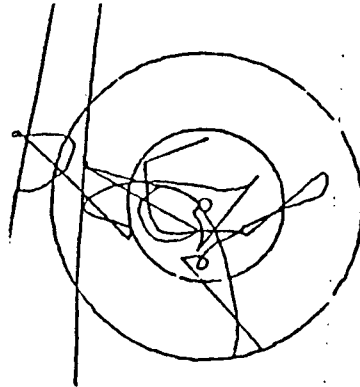
Figure 3. Pipper Error Plot (TAU0, ATM0).
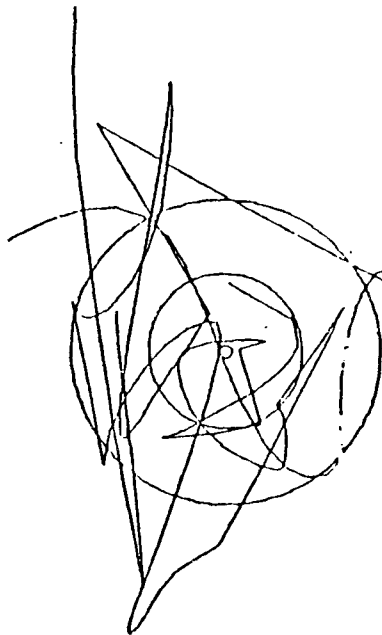
Figure 4. Pipper Error Plot (TAU3, ATM0).

Appendix

Ground Attack Configuration:

	s^0	s^1	s^2	s^3	s^4	
$\alpha/\delta es$	-.0086	-1.5	-.019			deg/mm
$\Theta/\delta es$	-2.38	-1.406				deg/mm
$\Delta long$	.0985	23.5	5.67	1.0		
$\beta/\delta as$	-2.15	-21.8	.275	.0143		deg/mm
$p/\delta as$	-.592	-125	-49.3	-5.64		deg/sec/mm
$r/\delta as$	-.4	2.09	2.2	-.0327		deg/sec/mm
$\phi/\delta as$	-128	-52.5	-5.59			deg/mm
$\beta/\delta rp$	1.07	33.9	4.89	.114		deg/mm
$p/\delta rp$	-.749	-135	15.6	1.27		deg/sec/mm
$r/\delta rp$	-4.245	-1.86	-23.9	-2.53		deg/sec/mm
$\phi/\delta rp$	-135	19.8	1.71			deg/mm
Δlat	13.9	262	49.5	12.5	1.0	

Fighter Configuration:

	s^0	s^1	s^2	s^3	s^4	
$\alpha/\delta es$	0.0	-.89	-.0198			deg/mm
$\Theta/\delta es$	-1.137	-.948				deg/mm
$\Delta long$	0.0	9.0	4.2	1.0		
$\beta/\delta as$	0.0	-.3863	-.1385	-.0507		deg/mm
$p/\delta as$	0.0	-134.8	-29.72	-10.05		deg/sec/mm
$r/\delta as$	0.0	-.3115	-1.56	-.369		deg/sec/mm
$\phi/\delta as$	-134.8	-29.72	-10.05			deg/mm
$\beta/\delta rp$	0.0	5.746	1.5	.0179		deg/mm
$p/\delta rp$	0.0	-29.26	.449	.8638		deg/sec/mm
$r/\delta rp$	0.0	-1.33	-5.43	-1.27		deg/sec/mm
$\phi/\delta rp$	-29.26	.449	.8638			deg/mm
Δlat	0.0	49.0	26.25	7.5	1.0	

AIRCRAFT "PILOT INDUCED OSCILLATION" TENDENCY EVALUATION—

A COMPARISON OF RESULTS FROM IN-FLIGHT AND GROUND BASED SIMULATORS

D. Francis Crane
Aerospace Engineer

Gordon H. Hardy
Aerospace Engineer and Pilot

NASA Ames Research Center, Moffett Field, CA 94035

SUMMARY

Military flying qualities (FQ) specifications[1] are incomplete due to a lack of data to substantiate various specification requirements.[2] One consequence of the lack of generic data to guide aircraft development is that initial models of numerous aircraft have exhibited pilot-induced-oscillation (PIO) and other FQ deficiencies which required considerable effort to correct.[3] Progress in generating the required FQ data has been slowed by the widespread opinion that FQ ratings of aircraft PIO tendencies obtained in ground-based simulators (GBS) are unreliable.[2,3]

In the study reviewed here, research test pilots evaluated aircraft approach and landing FQ in both the Air Force NT-33 in-flight simulator (IFS) and in the NASA Ames Research Center Vertical Motion Simulator (VMS). The various aircraft configurations evaluated were selected to exhibit a range of (longitudinal axis) PIO tendencies. Aircraft lateral characteristics, pilot task and training, and evaluation procedures were chosen to minimize rating variability.

Preliminary evaluation of the data and pilot commentary indicate that:

- Ratings of "PIO-prone" configurations are extremely sensitive to task and to pilot control technique (aggressiveness).

- In both the IFS and the VMS (for the standard lateral-offset approach, precision-landing task)

  some pilots observed serious PIO tendencies

  some pilots did not observe serious PIO tendencies

- Tasks which require urgent or aggressive closed-loop pilot control more effectively expose latent FQ deficiencies.

There is a continuing need for a national program to acquire generic data to support military FQ specification requirements. The observed sensitivity of pilot ratings to pilot control technique and task supports Twisdale's[4] assertion that thorough evaluation of aircraft approach and landing FQ requires pilot evaluation of a variety of challenging test maneuvers. Flight safety and efficiency considerations dictate that the bulk of this data should be obtained in research-quality, ground-based simulators with selected data confirmed by flight-test evaluations.

REFERENCES

1. Hoh, R. H. et al., "Proposed MIL Standard and Handbook--Flying Qualities of Air Vehicles," AFWAL TR 82-3081.

2. Hoh, R. H., "Bring Cohesion to Handling-Qualities Engineering," Astronaut. Aeronaut., June 1983.

3. Berry, D. T., "Flying Qualities: A Costly Lapse in Flight-Control Design?" Astronaut. Aeronaut., April 1982.

4. Twisdale, T. and Schofield, B. L., "Test Maneuvers for Approach and Landing Handling Qualities Evaluation." Flight Test Technology Branch Memo 1983 available from T. Twisdale at 6520 TG/ENFJ, Edwards AFB, CA 93523.

The following reports are referenced in the slides (copies attached) used in presenting this informal paper.

Chung, W. W. and Barkley, W. C., "VMS Performance-Simtech Configuration," SYRE report CM 6445, April 1986.

Jones, A. David, "Operations Manual: Vertical Motion Simulator," NASA TM 81180, May 1980.

Knotts, L. H. and Smith, R. E., "The Role of In-Flight Simulation in Aircraft Test and Evaluation," NATC Conference on Simulation, Aircraft Test and Evaluation, March 1982.

McFarland, R. E., "CGI Delay Compensation," NASA TM 86703, 1986.

Smith, R. E., "Effects of Control System Dynamics on Fighter Approach and Landing Longitudinal Flying Qualities," AFFDL TR 78-122, 1978.

AIRCRAFT "PILOT-INDUCED-OSCILLATION" TENDENCY EVALUATION — A COMPARISON OF RESULTS FROM IN-FLIGHT AND GROUND BASED SIMULATORS

Sponsored by

NASA-Ames Research Center
Naval Air Development Center
Air Force Flight Dynamics Laboratory

Fig. 1

OUTLINE

- BACKGROUND
- OBJECTIVES
- EXPERIMENT DESIGN
- DATA
- CONCLUDING REMARKS

Fig. 2

PILOT-INDUCED-OSCILLATION DEFINITION

- OSCILLATION WHICH DEVELOPS WHEN PILOT INITIATES URGENT MANEUVER OR ATTEMPTS TIGHT CONTROL. PILOT MUST REDUCE GAIN OR ABANDON TASK TO RECOVER

Fig. 3

BACKGROUND (I)

MILITARY FLYING QUALITIES (FQ) SPECIFICATIONS ARE INCOMPLETE DUE TO LACK OF DATA TO SUBSTANTIATE SPECIFICATION REQUIREMENTS

"AGARD FQ MEETING ATTENDEES AGREED UNANIMOUSLY THAT THE FIELD NEEDS MORE EXPERIMENTAL DATA TO REPLACE THE EXISTING DATA BASE WHICH INCLUDES INAPPROPRIATE TASKS AND FOR THE MOST PART CLASSICAL UNAUGMENTED AIRPLANES."

HOH (1983)

Fig. 4

BACKGROUND (II)

INITIAL MODELS OF NUMEROUS NEW AIRCRAFT (F-16, F-18, SPACE SHUTTLE) HAVE HAD SERIOUS FLYING QUALITIES DEFICIENCIES. DEFICIENT DESIGNS OFTEN ATTRIBUTED TO 'UNRELIABLE' FQ PREDICTIONS FROM FLIGHT SIMULATORS

"... THE VERY POOR LONGITUDINAL FLYING QUALITIES IN THE LANDING APPROACH WERE NOT OBSERVED DURING GROUND SIMULATION STUDIES ON A VERY SOPHISTICATED SIMULATOR: HOWEVER, THE DEFICIENCIES WERE DRAMATICALLY EXPOSED DURING THE INITIAL IN-FLIGHT SIMULATION SORTIES."

SMITH (1978)

"... ONE OF THE MOST NOTABLE RECENT FLYING QUALITY DESIGN DEFICIENCIES OCCURRED WITH THE YF-16. THIS AIRCRAFT WAS ESSENTIALLY DESIGNED ON A GROUND SIMULATOR SINCE DATA FOR THE NEW SIDE STICK CONTROLLER DID NOT EXIST. THE RESULT WAS A NEAR DISASTROUS LATERAL PIO ON THE FIRST INADVERTENT FLIGHT."

KNOTTS (1982)

Fig. 5

BACKGROUND (III)

REPORTS OF PARTICULAR (POORLY DOCUMENTED) INCIDENTS HAVE LED MANY TO CONCLUDE THAT GROUND-BASED-SIMULATOR PREDICTIONS OF FQ OF 'PIO PRONE' AIRCRAFT ARE INHERENTLY UNRELIABLE

"... GROUND SIMULATORS DO NOT SUIT CERTAIN CLASSES OF TASKS — NOTABLY THOSE ASSOCIATED WITH PIO TENDENCIES, CONTROL RESPONSE AND SENSITIVITY, TIGHT-CLOSED-LOOP TASKS, HIGH-STRESS SHORT-TERM PILOTING, AND CONTROL NEAR THE GROUND DURING LANDING."

FLYING QUALITIES MEETING CONSENSUS
REPORTED BY BERRY (1982)

Fig. 6

OBJECTIVES

- INVESTIGATE THE CORRELATION BETWEEN PILOT RATINGS OF AIRCRAFT FLYING QUALITIES OBTAINED IN FLIGHT AND IN A GROUND BASED SIMULATOR

- INVESTIGATE THE SENSITIVITY OF FLYING QUALITIES RATINGS TO GROUND BASED SIMULATOR VISUAL AND MOTION SYSTEM LIMITATIONS

Fig. 7

EXPERIMENT DESIGN FEATURES

- GUIDE — LAHOS STUDY (AFFDL TR 78-122)
  - FLARE IS CRITICAL TASK
  - FQ 'CLIFFS' EXIST

- CONFIGURATIONS — VARY LONGITUDINAL AXIS
  FIX LATERAL AXIS – LEVEL 1

- TASK — LATERAL OFFSET APPROACH, PRECISION LANDING

- PERFORMANCE STANDARDS — APPROACH AIRSPEED VARIATION
  DESIRED +5 knots, ADEQUATE +10, -5 knots

TOUCHDOWN	POSITION	SINK RATE
DESIRED	$|X_{TD} - X_{AIM}|$ 250 ft	$\dot{h}$ 60 fpm
ADEQUATE	$|X_{TD} - X_{AIM}|$ 500 ft	$\dot{h}$ 120 fpm

- INSTRUCTIONS — CONTROL AGGRESSIVELY BUT REALISTICALLY CONSISTENCY EMPHASIZED, FQ CLIFFS NOTED

- IN-FLIGHT SIMULATOR — NT-33

- GROUND-BASED SIMULATOR — AMES VMS (NASA TM 81180)
  CGI VISUAL (NASA TM 86703)

- AIRCRAFT MODEL — CALSPAN SUPPLIED (TR 7205-5)

- PILOTS — AMES TEST PILOTS (3)

- TRAINING — IFS ORIENTATION FLIGHT
  VMS 3 hr

- TIMING — VMS 11/25 - 12/19
  IFS 12/3 - 12/12

- LANDINGS/EVAL. — IFS 2-3 ; VMS 3-6

- RECALIBRATION — SHOWN BASELINE BETWEEN EVALS.

- REPLICATE — ALL EVALUATIONS

- SESSIONS — SHORT (1.25 hr) TO MINIMIZE FATIGUE

- DATA
  - 'COOPER-HARPER' RATINGS
  - PIO RATINGS
  - TIME HISTORIES

Fig. 8

LONGITUDINAL CONFIGURATIONS

1. LAHOS 2-1 (LEVEL 1)

2. " " + 108 ms CONTROL SYSTEM DELAY

3. " " + 144 ms CONTROL SYSTEM DELAY

4. " " + (.7, 12) PREFILTER; Δt_{EQ} 120 msec

5. LAHOS 6-1 (ORIGINAL YF-17, Δt_{EQ} 250 msec)

Fig. 9

EVALUATION TASK 1 SCHEMATIC
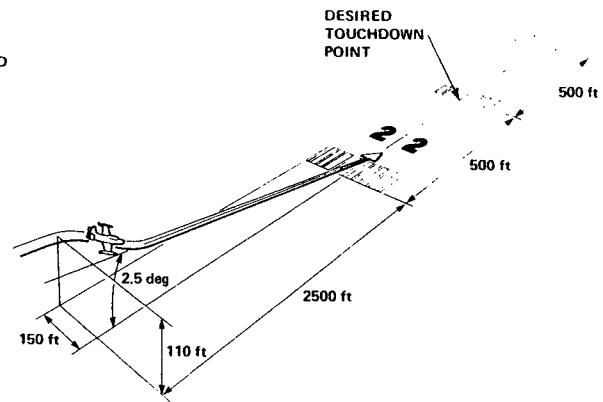(LATERAL OFFSET APPROACH, PRECISION LANDING)

Fig. 10

COMPARISON OF PILOT RATINGS FROM IFS AND VMS
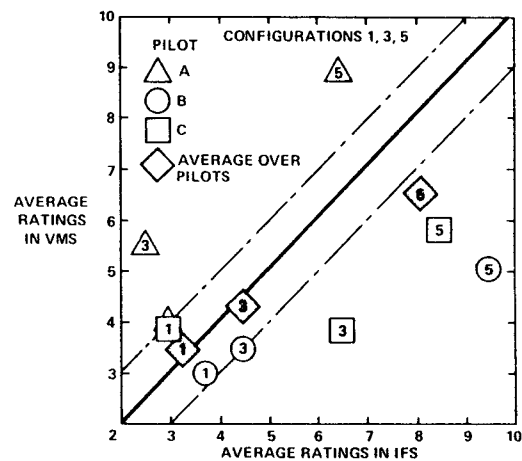COOPER-HARPER SCALE, TASK1

Fig. 11

282

EVALUATION TASK 2 SCHEMATIC
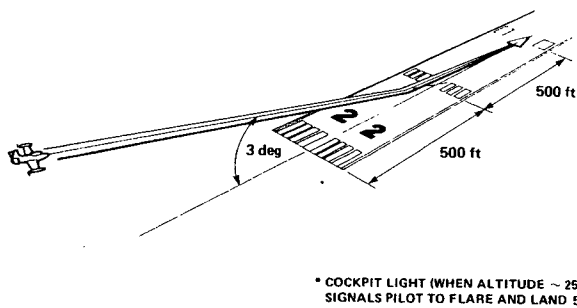### PRECISION LANDING AT 'EXTENDED' TOUCHDOWN POINT *

500 ft

3 deg

500 ft

* COCKPIT LIGHT (WHEN ALTITUDE ~ 25 ft)
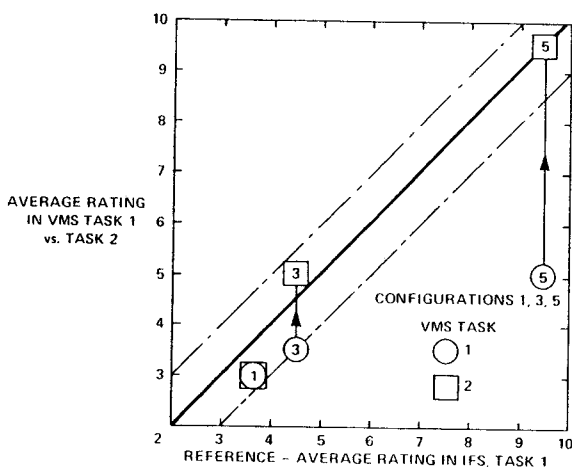SIGNALS PILOT TO FLARE AND LAND 500 ft 'LONG'

Fig. 12

SUMMARY OF RESULTS

- PILOT RATINGS OF "PIO PRONE" CONFIGURATIONS ARE EXTREMELY SENSITIVE TO TASK AND TO PILOT CONTROL TECHNIQUE (AGGRESSIVENESS)

- IN BOTH THE IFS AND THE VMS
  (FOR THE LATERAL-OFFSET APPROACH, PRECISION LANDING TASK)

  - SOME PILOTS OBSERVED SERIOUS PIO TENDENCIES

  - SOME PILOTS DID NOT OBSERVE SERIOUS PIO TENDENCIES

- TASKS WHICH REQUIRE URGENT OR AGGRESSIVE PILOT CONTROL INPUTS MORE EFFECTIVELY EXPOSE LATENT FQ DEFICIENCIES

Fig. 14

COMPARISON OF PILOT 'B' RATINGS FROM VMS FOR TASK 1 AND TASK 2
COOPER-HARPER SCALE

AVERAGE RATING IN VMS TASK 1 vs. TASK 2

REFERENCE – AVERAGE RATING IN IFS, TASK 1

CONFIGURATIONS 1, 3, 5

VMS TASK
○ 1
☐ 2

Fig. 13

CONCLUDING REMARKS

- THOROUGH EVALUATION OF AIRCRAFT APPROACH AND LANDING FQ REQUIRES PILOT EVALUATION OF A VARIETY OF CHALLENGING TASKS

- THERE IS A NEED FOR A NATIONAL PROGRAM TO ACQUIRE GENERIC DATA TO SUPPORT MIL SPEC FQ REQUIREMENTS. FLIGHT SAFETY AND EFFICIENCY DICTATE THAT THE BULK OF THIS DATA SHOULD BE OBTAINED IN RESEARCH-QUALITY GBS, WITH SELECTED DATA CONFIRMED BY FLIGHT TEST EVALUATIONS

Fig. 15

PILOT RATING SUMMARY
COOPER HARPER SCALE

AIRCRAFT CONFIGURATION	PILOT A			PILOT B			PILOT C	
	IFS	VMS TASK 1	VMS TASK 2	IFS	VMS TASK 1	VMS TASK 2	IFS	VMS TASK 1
1	4, 2*	4, 4	4, 3	3, 5, 3	3, 3	3	4, 2, 3	3.5, 4
2	3, 2, 2	5, 6	5, 5	3, 4	3, 4	3	5, 3	4, 5
3	2, 3	7, 4	5, 7	6, 3	3, 4	5	6, 7	3.5, 4
4	2, 2	5, 6	6, 4	3, 3	4	2, 5	5, 2	4.5, 3
5	6, 7	7.5, 10	9, 10	10, 9	5, 5	10, 9	9, 8	6, 5.5

* REPEATED RATINGS ARE SEPARATED BY COMMAS

Fig. 16

MICROCOMPUTER PROGRAMS FOR THE DYNAMIC ANALYSIS OF

MANUAL VEHICLE CONTROL

by
R. Wade Allen
Theodore J. Rosenthal
Raymond E. Magdaleno
Systems Technology, Inc.
13766 S. Hawthorne Blvd.
Hawthorne, CA 90250
(213) 679-2281

ABSTRACT

Various analysis methodologies and analytical procedures have been developed over the years for studying manual vehicle control problems. Most of the analysis techniques have evolved into computer programs, and the evolution of microcomputer capability has reached a point that now permits the analysis of complex systems in a desk top computing environment. Although significant advances in microcomputer computational and memory capability have made their application practical for complex dynamic systems analysis, it is the convenient graphics interface that has permitted the development of efficient user interactive programs.

The purpose of this paper is to describe the microcomputer implementation of two manual control system analysis programs. The first program is setup to permit the analysis of pilot/vehicle systems, and includes a general modeling module, a specific longitudinal control model, and an expert system help feature. The second program implements a specific driver/vehicle directional control (steering) model, and permits specifying vehicle dynamics at operating conditions out to limit cornering and braking conditions. Both programs allow transfer functions and transient responses to be conveniently specified and displayed. The pilot/vehicle analysis program also contains a convenient interface to a more general purpose control systems analysis package that allows for classical, state space and optimal control analysis options. This paper describes the purpose and capability of each program, and comments on the future application of microcomputers to dynamic systems analysis.

INTRODUCTION

This paper describes two microcomputer program packages that have been developed to assist in the analysis of manual control systems generally defined by the generic block diagram of Fig. 1. One program addresses pilot/vehicle analysis problems, including basic vehicle dynamics, stability augmentation system design, and dynamic modes introduced by the nature of the piloting task (e.g., target tracking, IFR landing approach, etc.) and display system. The basic approach and capabilities of this program have been described previously (Ref. 1). The second program is setup to permit
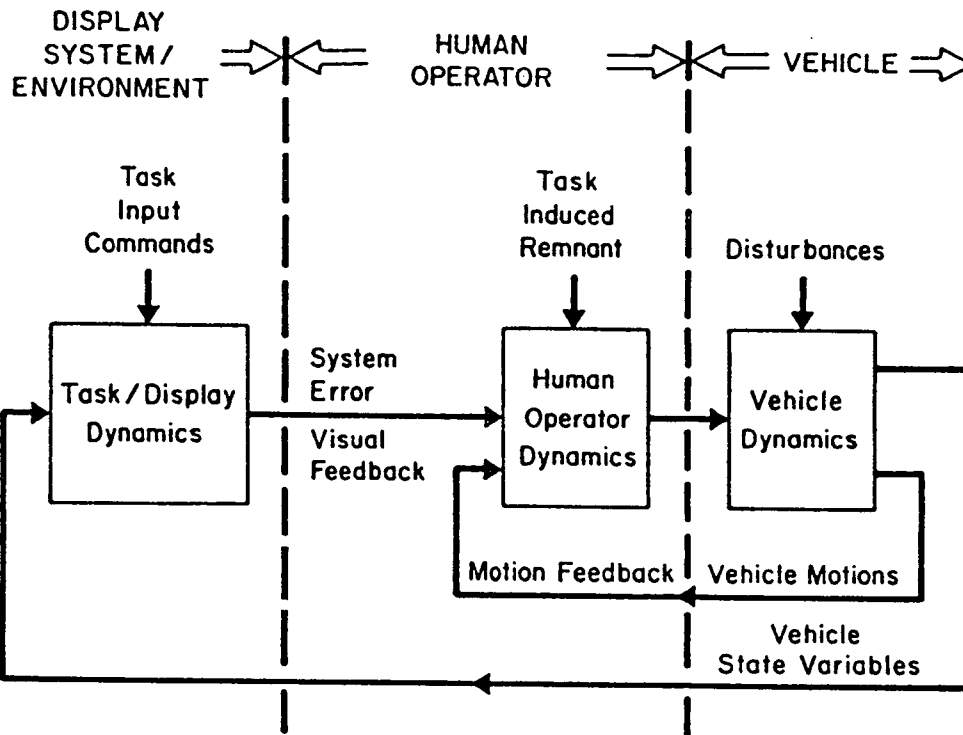
Figure 1. Generic Manual Control System

analysis of automobile dynamics and driver/vehicle control over the complete maneuvering range from straight running to limit lateral and longitudinal acceleration conditions, where the vehicle dynamics depart radically from what would be considered conventional acceptable handling qualities. The basic analysis approach employed in this second program has recently been described elsewhere (Refs. 2, 3).

Both of the above microcomputer programs incorporate linear systems analysis procedures and algorithms, which permit the user to evaluate a variety of system transfer functions and transient time responses for relatively complex model structures. The programs assist the user in defining model parameters, and provide a variety of CRT screen output formats for displaying transfer functions (Laplace tranforms in factored pole/zero format with a literal description), transfer function Bode plots, and transient time traces of up to ten variables in response to an arbitrary input waveform (up to four per plot). The pilot/vehicle analysis program permits the development of new models with arbitrary dynamic structure, and also incorporates a relatively complete longitudinal pilot/vehicle control model. The driver/vehicle program contains a relatively fixed dynamic model structure, but contains algorithms for determining quasilinear vehicle dynamics model parameters over the complete range of tire nonlinear operating conditions deriving from cornering and/or braking conditions.

286

Paper No. 391

MICROCOMPUTER PROGRAMS FOR THE DYNAMIC ANALYSIS OF MANUAL VEHICLE CONTROL

R. Wade Allen
Theodore J. Rosenthal
Raymond E. Magdaleno

Presented at the

22 Annual Conference on Manual Control
Belton Inn
Dayton, Ohio
15-16 July 1986

287

A major emphasis in the development of these programs was to setup a simple and efficient user/computer interface, which would minimize the user's effort in learning and using the system. Major program modules are accessed through menu selections. Transfer functions and transient responses are presented as CRT screen outputs, and hard copy can easily be obtained through printer graphics dumps. The computer I/O is setup so that the analyst can easily carry out fairly complex dynamic analyses, and obtain hard copy documentation as required. Provisions are also made in the pilot/vehicle analysis program for linking to a control system analysis package, which allows for a wide range of classical and modern control theory procedures.

In the remainder of the paper, we will separately describe the pilot/vehicle and driver/vehicle analysis programs, including the objectives, approach, and analysis capability of each package. The paper concludes with some comments on the potential future for microcomputer based dynamic systems analysis programs.

PILOT/VEHICLE ANALYSIS PROGRAM

This program is designed to provide the user with a practical systematic approach for the design and analysis of dynamic systems. As suggested in Fig. 2, procedures within the program allow for model specification, and the calculation and display of transfer functions and transient time responses. As noted in Fig. 2, the different program modules are linked by data files so that modeling development and computation can be saved at each stage for use at a later time, or in a production mode several cases can be computed and stored before final output is generated.

Dynamic models can be specified in several ways as indicated in Fig. 2. Specific model structures for a pilot/vehicle longitudinal control problem have been setup, and all the user need define is parameter values. The longitudinal pilot/vehicle module then generates an equations of motion (EOM) file that can be further processed by the general modeling program to generate transfer function (T/F) files. In selecting longitudinal pilot model parameters, the user can also get some help from an expert system guide as noted in Fig. 2. An example has been previously published for the pilot/vehicle longitudinal control model (Ref. 1).

If the user has developed a new set of equations for a dynamic model, then the general modeling module can be used in an interactive mode to create a matrix structure for an equations of motion model. As a simple example, consider the Table 1 mechanical system whose motions can be described in a straightforward manner using Newton's law. Acceleration equations for each mass are given in Table 1 along with two auxiliary equations defining the mass velocities. These equations can then be rearranged with dependent variables on the left hand side (LHS), and independent or forcing function variables on the right hand side (RHS).

The key to the modeling and analysis of manual and other dynamic control systems is the specification of feedback equations. As an example, consider feedbacks specified for the Table 1 mechanical model example to control

288

TABLE 1.   MECHANICAL SYSTEM MODELING EXAMPLE
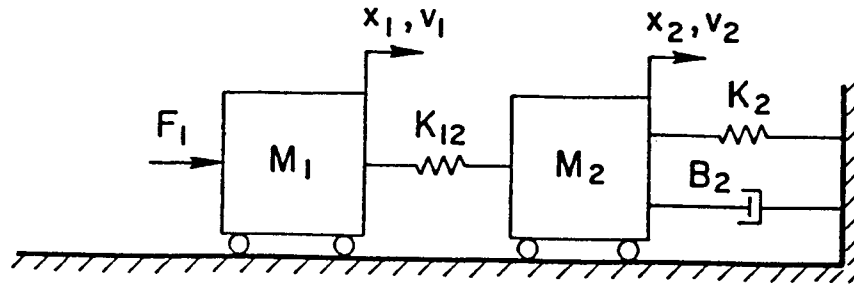
SYSTEM EQUATIONS $(ma = \Sigma\, F)$

$$M_1\, \ddot{x}_1 = F_1 + (x_2 - x_1)\, K_{12}$$

$$M_2\, \ddot{x}_2 = (x_1 - x_2)\, K_{12} - x_2 K_2 - \dot{x}_2 B_2$$

$$\dot{x}_1 - v_1 = 0$$

$$\dot{x}_2 - v_2 = 0$$

SYSTEM MATRIX EQUATIONS (Laplace Transform)

$$[L(s)]\,[Y] = [R(s)]\,[X]$$

$$
\begin{array}{cccc}
\text{XX1} & \text{XX2} & \text{VV1} & \text{VV2}
\end{array}
$$

$$
\begin{bmatrix}
M_1 s^2 + K_{12} & -K_{12} & & \\
-K_{12} & M_2 s^2 + B_2 s + (K_2 + K_{12}) & & \\
s & 0 & -1 & 0 \\
0 & s & 0 & -1
\end{bmatrix}
\begin{bmatrix}
XX1 \\ XX2 \\ VV1 \\ VV2
\end{bmatrix}
=
\begin{bmatrix}
1 \\ 0 \\ 0 \\ 0
\end{bmatrix}
FF1
$$

TEST CASE

$M_1 = 10$ lbs $\qquad\qquad K_{12} = 3$ lb/ft

$M_2 = 1$ lb $\qquad B_2 = 1$ lb/ft/sec $\qquad K_2 = 1$ lb/ft
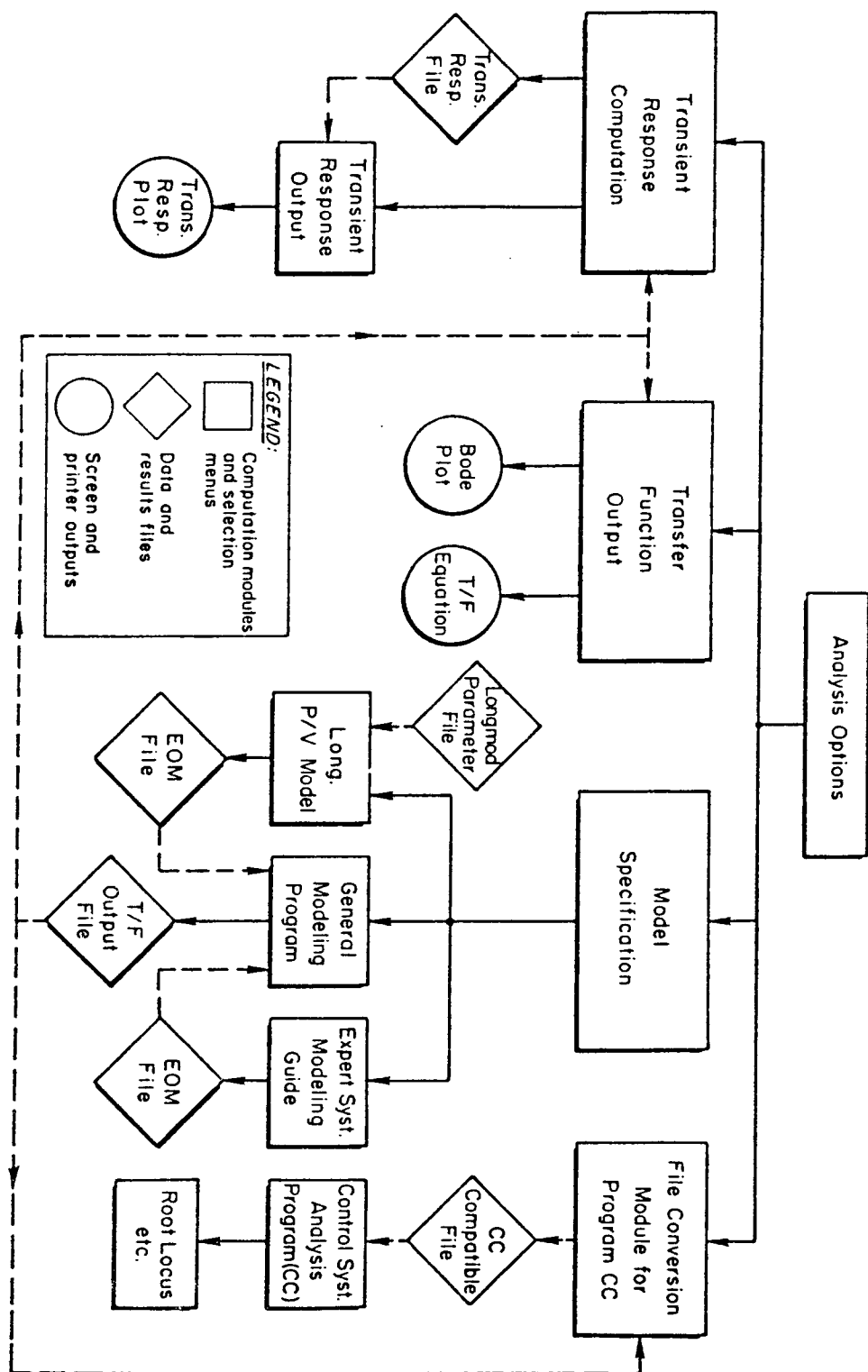
Figure 2. General Structure for Pilot/Vehicle Analysis Microcomputer Program

LEGEND:

□ Computation modules and selection menus

◇ Data and results files

○ Screen and printer outputs

mass 1 to a set point x_o. The model for this control structure is summarized in Table 2, where both velocity and acceleration terms are combined with position feedback in order to properly compensate for the motions of the second mass. The user now augments the Table 1 matrix with the feedback and error equations shown in Table 2.

The model LHS and RHS matrices for Laplace transform of the example mechanical model can be entered into the general model program using commands that define the matrix elements. As noted in Table 1, each matrix element can contain up to a second-order system, e.g.,

$$M_2 s^2 + B_2 s + (K_2 + K_{12})$$

with numerical values entered for each of the coefficients. The user can easily request a screen display and hard copy of the matrix form of a defined model. Table 3 gives the screen displayed matrix for the Table 1 and Table 2 mechanical model, where the s^2 coefficient appears at the top of each matrix cell, and the constant term appears at the bottom. This matrix format allows equations to be directly coded into the computer in the same form in which they were derived, which simplifies model verification, and leads to a compact matrix structure. Modern state space approaches require much more algebraic manipulation to suit analytic forms, and result in much less compact matrix structures.

Given entry and confirmation of the model, the user can then select the transfer function output module to display transfer functions in factored form and as Bode plots. For the mechanical model, the display for the factored transfer function between the feedback variable (CX1) and the error signal (XXE) is given in Table 4. (The literal description explains the shorthand notation used.)

Although a satisfactory value for the mechanical system feedback gain K_f could be found from a Bode plot, it is helpful to analyze the effect of this parameter on the closed-loop dynamics by computing a root locus. This can be accomplished by a subsidiary path as indicated in Fig. 3, where the model feed forward plus feedback transfer function is analyzed in a subsidiary control systems analysis program (Ref. 4). A module in the pilot/vehicle analysis program is set up to conveniently convert transfer function files for use in this second program. Using the root locus option in this second program, we then can easily get a display of a closed-loop root survey as a function of K_f as shown in Fig. 3. Finally, the user can obtain a step input transient response plot as shown in Fig. 4 to confirm that reasonable system performance has been achieved with the feedback compensation.

The modeling and analysis process can give the analyst insight into parameter variation sensitivities in a system. This process has been illustrated elsewhere in more detail for the longitudinal pilot/vehicle model (Ref. 3). This approach is to be contrasted with single design point approaches such as optimal control procedures, which result in an optimal set of feedback control parameters, but do not directly yield any insight into system dynamics and sensitivity to parameter variations.

291
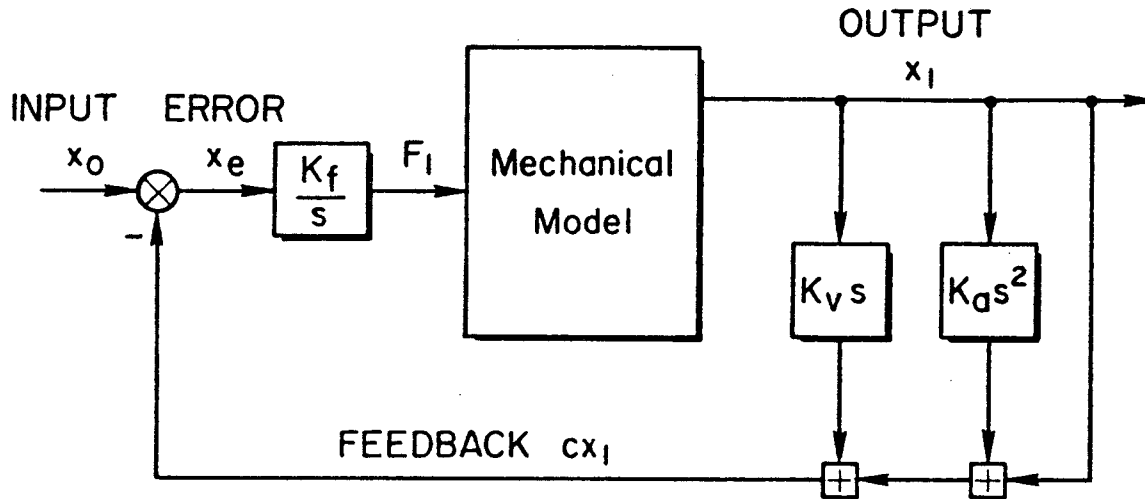
$$K_a = 12.2 \, sec^2 \quad ; \quad K_v = .73 \, sec \quad ; \quad K_f = 4000 \, lbs/ft$$

$$cx_1 = x_1 (1 + K_v s + K_a s^2)$$

$$x_e = x_0 - cx_1$$

$$F_1 = \frac{K_f}{s} x_e$$

Rearrange for matrix:

$$cx_1 - x_1 (1 + K_v s + K_a s^2) = 0$$

$$x_e + cx_1 = x_0$$

$$K_f x_e - F_1 s = 0$$

	1 XX1	2 XX2	3 VV1	4 VV2	5 CX1	6 XXE	7 FF1			1 XX0
	$\widehat{10.0}$ M_1	0					0	!! !	!	!! !
1	0	0	0	0	0	0	0	!!XX1! 1 !	0	!!XX0!
	$\widehat{3.00}$ K_{12}	-3.00					-1.0	!! !	!	!! !
	0	$\widehat{1.0}$ M_2						!! !	!	
2	0	$\widehat{1.0}$ B_2	0	0	0	0	0	!!XX2! 2 !	0	
	-3.00	$\widehat{4.00}$ $K_2 + K_{12}$						!! !	!	
	0	0						!! !	!	
3	1.0	0	0	0	0	0	0	!!VV1! 3 !	0	
	0	-1.0						!! !	!	
	0	0						!! !	!	
4	0	1.0	0	0	0	0	0	!!VV2! = !	0	
	0	0	-1.0					!! !	!	
	.400E-01				0			!! !	!	
5	.200	0	0	0	0	0	0	!!CX1! 5 !	0	
	1.0				-1.0			!! !	!	
					0	0		!! !	0	
6	0	0	0	0	0	0	0	!!XXE! 6 !	0	
					1.0	1.0		!! !	1.0	
					0	0		!! !	!	
7	0	0	0	0	0	0	-1.0	!!FF1! 7 !	0	
					.400E+04	0		!! !	!	

293

TABLE 4.   SCREEN DISPLAY FOR THE FACTORED TRANSFER FUNCTION OF THE
FEEDBACK TO ERROR SIGNAL RATIO FROM THE MECHANICAL SYSTEM
EXAMPLE (WITH LITERAL DESCRIPTIONS OF THE
SHORTHAND NOTATION)

```
TRANSFER FUNCTION FORM :

              K (S+Z)i (S² + 2 Zz Wz + Wz²)j     K (Z)i [Zz,Wz]j
     T.F. = ─────────────────────────────────── = ───────────────
              (S+P)k (S² + 2 Zp Wp + Wp²)l         (P)k [Zp,Wp]l


YOUR TRANSFER FUNCTION IS :

              16 [ .25, 2 ] [ .5, 5 ]
     CX1/XXE = ─────────────────────────────────────────────────────
               ( 0 ) [ .103709, .268039 ] [ .231082, 2.04344 ]
```

DRIVER/VEHICLE ANALYSIS PROGRAM

The approach taken in this program is somewhat different from the pilot/ vehicle program, in that the driver and vehicle models have a fairly general but nonetheless fixed structure. The basic objective of this program is to allow the user to assess the effect of fairly radical changes in vehicle dynamics on driver capability and overall driver/vehicle performance. The force output characteristics of rolling pneumatic tires are quite nonlinear, and can cause significant changes in vehicle directional control (steering) dynamics under hard maneuvering conditions. The driver/vehicle program is setup to permit the user to assess the dynamic consequences of nonlinear tire dynamics, and a range of other vehicle inertial and kinematic parameters on the driver's directional control ability under conditions ranging from straight running to high-g braking and cornering, as might occur under radical accident avoidance maneuvering conditions.

The basic driver/vehicle directional control model structure setup in this program is shown in Fig. 5 as adapted from Ref. 5. The driver model includes analyst adaptive driver characteristics consisting of a lead time constant which is set to compensate for vehicle steering response lags, a trim function which is set to reduce low frequency tracking errors, and a visual loop gain, K_ψ, which is adjusted to achieve stable closed-loop directional control and maximize control bandwidth. The requirements placed on the driver's parameter adjustments to optimize closed-loop system performance are dictated by the vehicle dynamics, which therefore receive a significant emphasis in the driver/vehicle program. Let us first consider the approximate nature of the vehicle dynamics, then review the analysis capability of the driver/vehicle program.

The yaw rate to steering input transfer function is the basic vehicle response function to which the driver responds. As noted last year
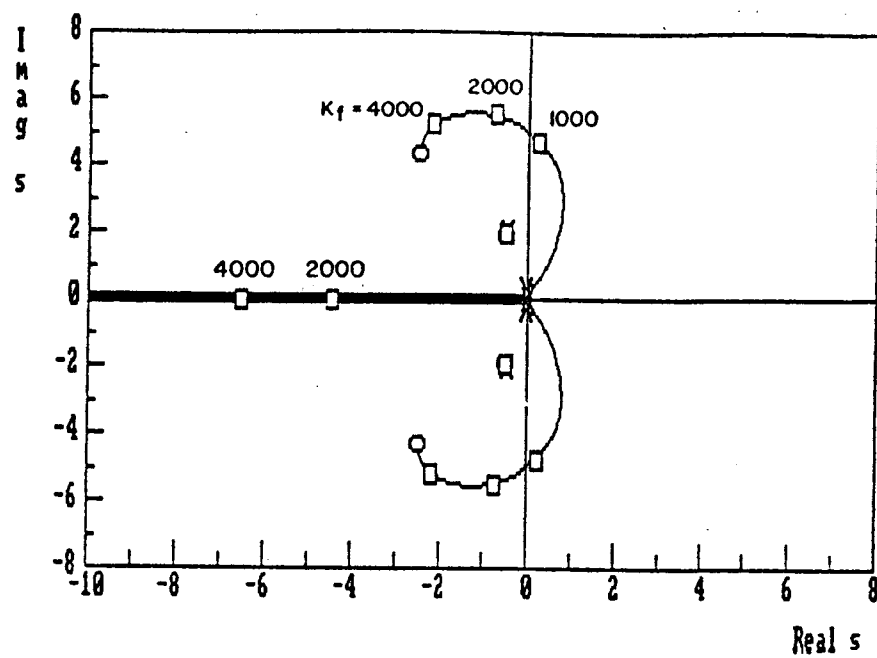
Figure 3. Root Locus for Feedback Gain (K_f) Variation
in the Mechanical System Model of Tables 1 and 2
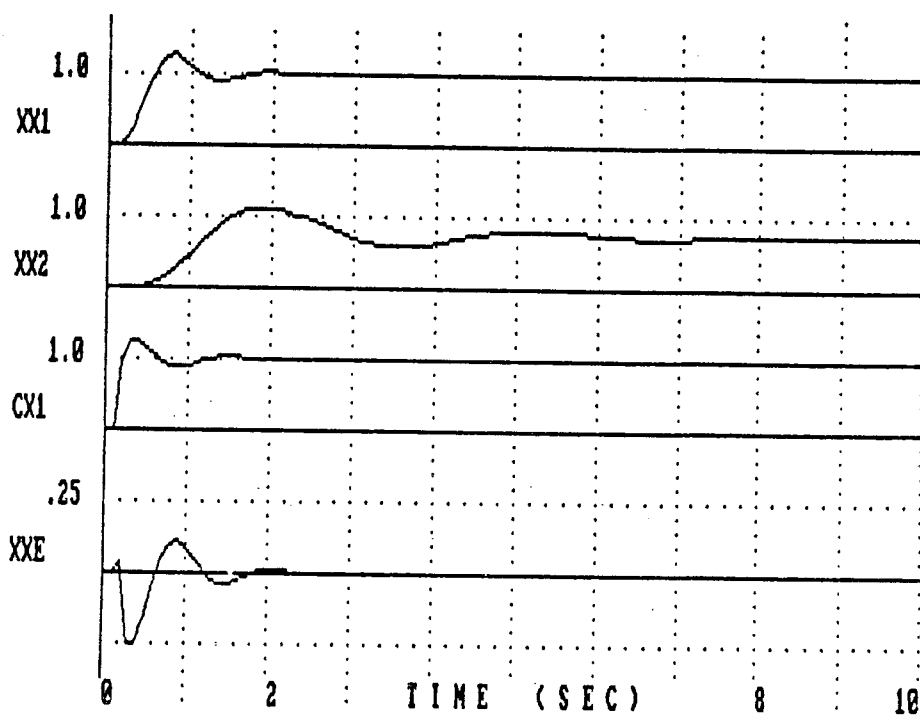
Figure 4. Transient Response of Mechanical System Variables
to a Step Change in Set Point (X_o)

295

Figure 5. Driver/Vehicle Stability Analysis Model
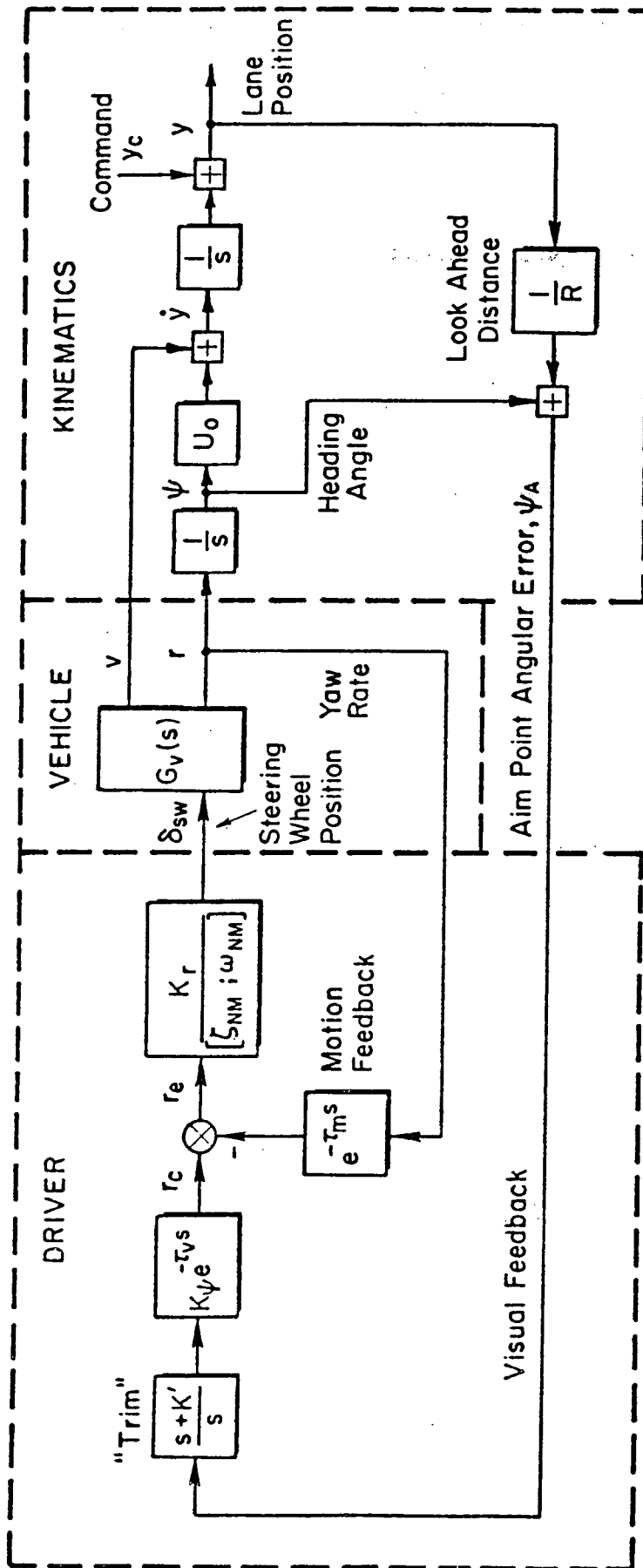
K' = trimming gain, K_ψ = visual feedback gain, K_r = motion feedback loop gain

ζ_{NM} ; ω_{NM} = neuromuscular damping and natural frequency, $G_v(s)$ = vehicle transfer function

τ_v ; τ_m = visual and motion feedback time delay, U_o = vehicle speed, R = aim point (look ahead) distance

296

(Ref. 6), the transfer function can be derived from a simple two degrees-of-freedom vehicle model in terms of vehicle parameters as summarized in Table 5. As noted last year (Ref. 6), the transfer function is dominated by the front and rear axle side force coefficients ($Y_{\alpha 1}$, $Y_{\alpha 2}$ respectively). These coefficients can be given as a function of the vehicle maneuvering conditions given by lateral (cornering or steering induced) acceleration (a_y) and longitudinal (braking) acceleration (a_x). Basically the side force coefficients decrease as maneuvering acceleration increases, because of the nonlinear force saturation characteristics of the tires.

A trimming program has been developed to compute per axle side force coefficients as a function of maneuvering acceleration operating points (e.g., Refs. 2, 3), and Fig. 6 shows a computer generated plot of these relationships. Because the tire characteristics are such a critical part of the vehicle dynamics specification, a single point trim module is included in the driver/vehicle program. This then allows the user to specify a given maneuvering operating point at which analysis is desired along with other physical parameters from which the program then computes the complete vehicle dynamics equations of motion. Given this capability, the driver/vehicle program then permits meeting the objective of allowing the user to analyze driver/vehicle interactions over the full range of vehicle dynamics induced by cornering and braking maneuvers.

A block diagram showing the various program options is given in Fig. 7. While the model dynamic structure is fixed, the ability to compute and display transfer functions and transient responses is similar to the pilot/vehicle program. The vehicle dynamics trim point calculations are unique to the driver/vehicle program. Vehicle dynamics computed over the full maneuvering range for two example vehicles have previously been published (Ref. 3). As an example here, we will consider vehicle dynamics characteristics under hard braking and hard cornering conditions to demonstrate the dramatic effect of tire nonlinearities.

The user first defines vehicle parameters via screen menus as shown in Table 6. The operating point parameters can either be specified by the user, or obtained by running the operating point trim module. The trim module requires tire model data which is contained in a file generated with the aid of another program (Ref. 7). For the example here, the trim module was run for several maneuvering conditions (as discussed in Refs. 2, 3) and two conditions selected for illustration here.

Given parameter files for various operating conditions, the user can then run modules for generating transfer function Bode plots and transient response time traces. In Fig. 8, the vehicle yaw to steering wheel transfer function is shown for hard braking conditions, which cause the vehicle to oversteer (increased apparent steering sensitivity), and for hard cornering conditions, which cause the vehicle to understeer (decreased apparent steering sensitivity).

Transient response plots can also be obtained for up to ten variables, and up to four variables can be selected for each plot. Examples for the hard braking and hard cornering operating conditions are shown in Fig. 9.

297

TABLE 5. VEHICLE DIRECTIONAL DYNAMICS TRANSFER FUNCTIONS

Complete Transfer Function :

$$\frac{r}{\delta_w} = \frac{\left(\dfrac{Y_{a1} - F_{T1}}{Y_{a1}}\right) \bullet \left(\dfrac{m\,a\,U_0}{\ell Y_{a2}}\,s + 1\right)}{\dfrac{m\,U_0\,I}{\ell Y_{a1}\,Y_{a2}}\,s^2 + \left[\dfrac{m}{\ell}\left(\dfrac{a^2}{Y_{a2}} + \dfrac{b^2}{Y_{a1}}\right) + \dfrac{I}{\ell}\left(\dfrac{1}{Y_{a1}} + \dfrac{1}{Y_{a2}}\right)\right]s + \dfrac{\ell}{U_0} + \dfrac{m\,U_0}{\ell}\left(\dfrac{b}{Y_{a1}} - \dfrac{a}{Y_{a2}}\right)}$$

where ℓ = wheelbase = a + b

s	= Laplace transform variable
m	= mass
U_0	= longitudinal speed
Y_{a1}	= front axle side force coeff. (left + right)
Y_{a2}	= rear axle side force coeff. (left + right)
F_{T1}	= front axle traction force
a	= distance from front axle to c.g.
b	= distance from real axle to c.g.
r	= yaw rate
I	= moment of inertia

Yalpha (FRONT AXLE) VS LATERAL ACCELERATION
FOR CONSTANT VALUES OF Ax   03-05-1986

Yalpha (REAR AXLE) VS LATERAL ACCELERATION
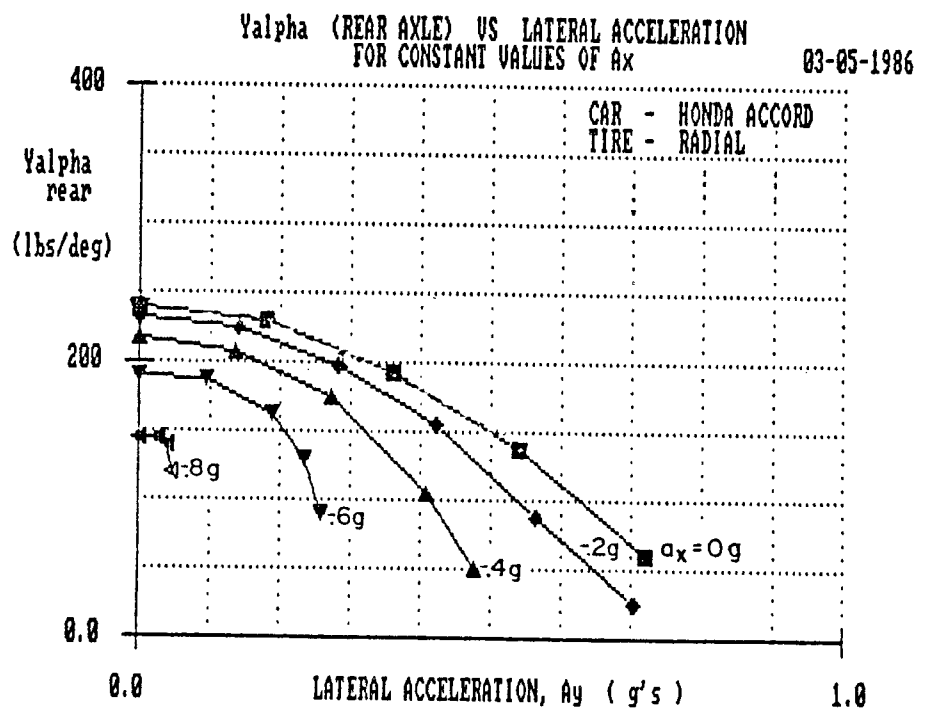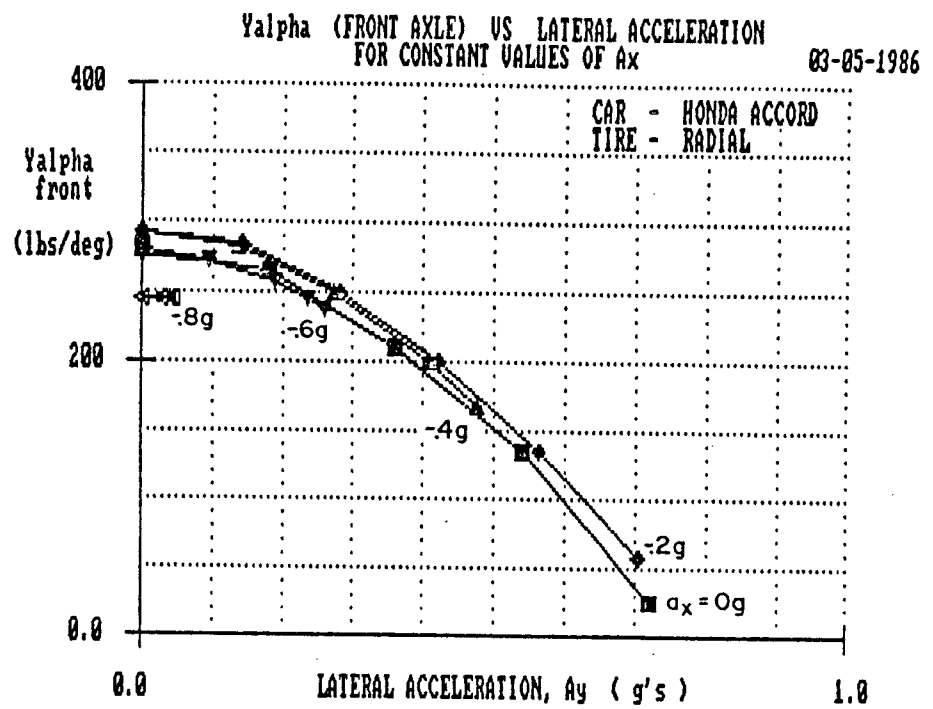FOR CONSTANT VALUES OF Ax   03-05-1986

Figure 6.   Per Axle Side Force Coefficients for a Small
Front Wheel Drive Vehicle Under Various
Maneuvering Accelerations
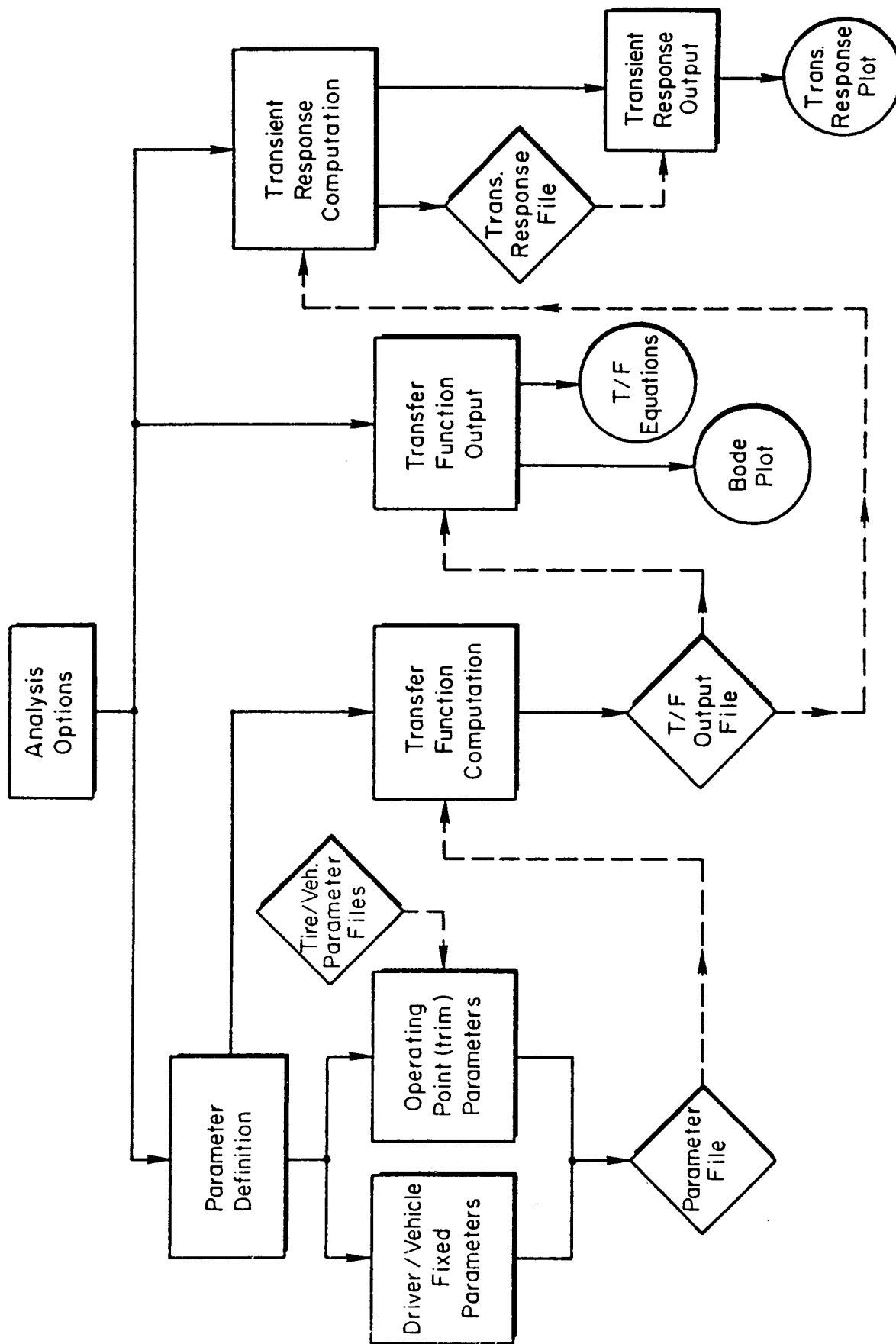
Figure 7. General Structure for Driver/Vehicle Analysis Microcomputer Program

300

TABLE 6.   SCREEN MENUS FOR ENTERING PROGRAM PARAMETERS

Vehicle Parameters

⇒ M   = 89   Ksr   = 16.3
  Ms   = 80   Kscf   = 0
  a   = 3.28   Kscr   = 0
  b   = 4.77   Kcf   = 0
  Ixx   = 368   Kcr   = 0
  Izz   = 1200   e   = 1.5
  Ixz   = 0   Ktor   = -50000
  Ef   = .2 $\mathcal{E}L/\mathcal{E}P$ = -2590
  Er   = -.2

RETURN TO THE MAIN MENU

| M   = |

Aerodynamic Parameters

⇒ $\mathcal{E}La/\mathcal{E}v$ = 0

  $\mathcal{E}Ya/\mathcal{E}v$ = 0

  $\mathcal{E}Na/\mathcal{E}v$ = 0

RETURN TO THE MAIN MENU

| $\mathcal{E}La/\mathcal{E}v$ = |

Operating Point Parameters

⇒ Yαf   = 4923.729   Lptr = -7.351727E-02

  Yαr   = 5820.787   TLf   = .039

  Uo   = 48.4   TLr   = .031

  Lptf = -.1166534

RETURN TO THE MAIN MENU

| Yαf   = |

301
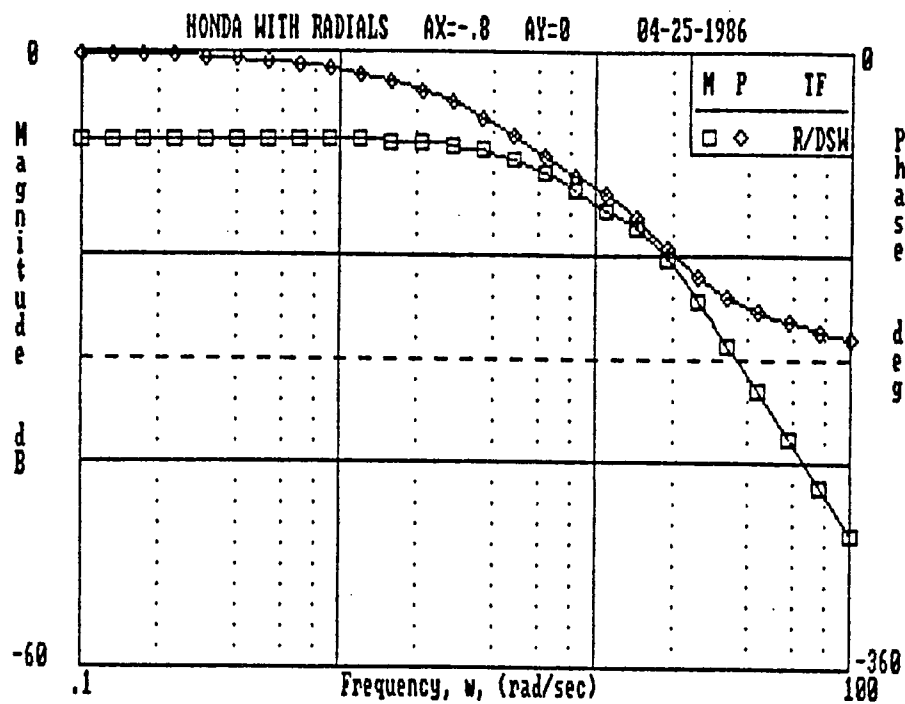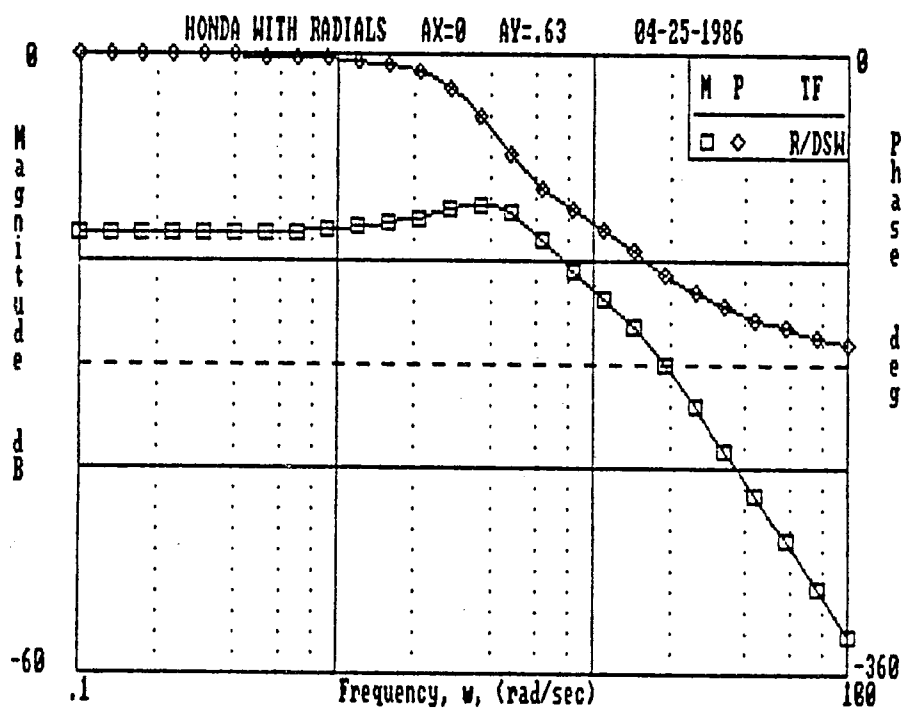
a) Hard Braking

b) Hard Cornering

Figure 8. Yaw Rate to Steering Wheel Transfer Functions
for a Small Front Wheel Drive Car Under
Two Maneuvering Conditions

HONDA WITH RADIALS   AX=-.8   AY=0   04-25-1986

Steering Wheel, δ_{sw}(rad)

Yaw Rate, r (rad/sec)

Lateral Acceleration, a_y (ft/sec^2)

Roll Angle, ϕ(rad)

a) Hard Braking

HONDA WITH RADIALS   AX=0   AY=.63   04-25-1986

Steering Wheel, δ_{sw}(rad)

Yaw Rate, r (rad/sec)

Lateral Acceleration, a (ft/sec^2)

Roll Angle, ϕ(rad)
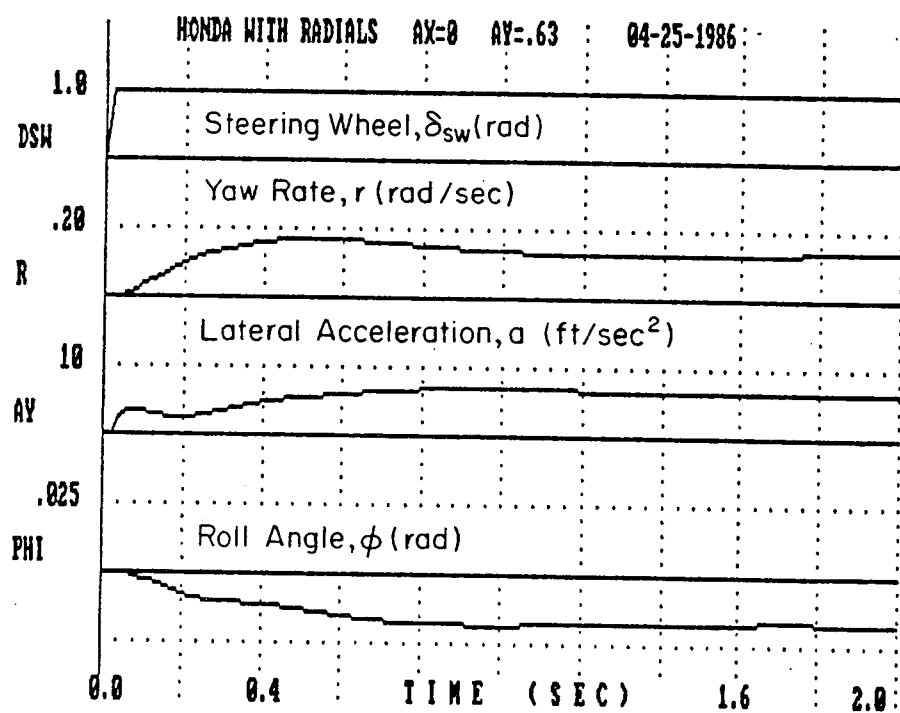
b) Hard Cornering

Figure 9.   Step Steer Response of a Small Front Wheel Drive
Car Under Two Maneuvering Conditions

303

Here, the consequences of under and oversteer are quite apparent. Also, note that the vehicle response is somewhat oscillatory under hard braking (understeering) conditions.

CONCLUDING REMARKS

The detailed dynamic analysis of manual vehicle control systems generally requires significant digital computer computation. The efficiency of analysis procedures is directly related to the amount of interaction afforded the analyst. The extensive CRT screen based hardware and software routinely provided in microcomputers is ideal for preparing user interfaces. Two microcomputer applications which attempt to exploit this interactive environment have been cited herein. Some of the core algorithms for carrying out the dynamic computations were taken from older mainframe and minicomputer Fortran programs. However, a significant effort was specifically devoted to developing the microcomputer CRT user interface.

As evidenced at past manual control conferences, a great deal of effort has been devoted to improving the man/machine interface in manual/supervisory control systems. The objective is to allow human operators to more effectively carry out their jobs and achieve maximum system performance while minimizing resources and operational costs. We have sought similar objectives in providing the manual control systems analyst with microcomputer based analysis tools. The objectives in future microcomputer software development should be to make problem setup and computation as efficient as possible, and to provide sufficient user interaction so that the analyst can guide the computer aided analysis as effectively as possible.

ACKNOWLEDGEMENTS

REFERENCES

1. Allen, R. Wade, D. T. McRuer, R. E. Magdaleno, et al., "Computer-Aided Procedures for Analyzing Pilot/Vehicle/System Interactions," Systems Technology, Inc., P-385, presented at NAECON '86, Dayton, Ohio, 19-23 May 1986.

2. Allen, R. Wade, W. A. Johnson, T. J. Rosenthal, et al., "Quasilinear Analysis of Nonlinear Dynamic Simulation," Systems Technology, Inc., P-386, presented at the 1986 Summer Computer Simulation Conference, Reno, Nevada, 28-30 July 1986.

3. Allen, R. Wade, H. T. Szostak, T. J. Rosenthal, et al., "Test Methods and Computer Modeling for the Analysis of Ground Vehicle Handling," Systems Technology, Inc., P-388, presented at the 1986 West Coast International Meeting, Society of Automotive Engineers, Universal City, CA, 4-7 Aug. 1986.

4. Thompson, Peter M., Program CC User's Guide, Version 3.0, Systems Technology, Inc., May 1985.

5. Allen, R. Wade, "Stability and Performance Analysis of Automobile Driver Steering Control," Systems Technology, Inc., P-310, presented at the 1982 SAE International Annual Congress & Exposition, Detroit, MI, 22-26 Feb. 1981.

6. Allen, R. Wade, J. R. Hogue, and Z. Parseghian, "Manual Control of Unstable Systems," Systems Technology, Inc., P-373, presented at the 21st Annual Conference on Manual Control, Ohio State U., Columbus, OH, 17-19 June 1985.

7. Szostak, Henry T., Walter A. Johnson, R. W. Allen, et al., "A Microcomputer Program for Analyzing a Tire Model to be Used in Vehicle Dynamics Simulations," Systems Technology, Inc., P-381, presented at the 1986 SCS MultiConference, San Diego, CA, 23-25 Jan. 1986.

8. Szostak, Henry T., R. Wade Allen, and Theodore J. Rosenthal, An Interactive Tire Model for Driver/Vehicle Simulation, Systems Technology, Inc., TM-1227-1, March 1986.

Describing Functions of the Man-Machine
with an Active Controller

A. Morris   D.W. Repperger*

Systems Research Laboratories, Inc., Dayton, Ohio 45440-3696
*AAMRL, Wright-Patterson Air Force Base, Ohio 45433-6573

ABSTRACT

It is of interest in the study of active (or assistive) controllers to investigate how the active device may modify describing functions of the human operator or the overall man-machine system. The term "active controller" refers to a controller which can produce both force and position changes on the human's arm as a function of the human's output commands and an algorithm on a computer which may be based on an empirical rule. The total interaction of the human and the active controller can be modelled as a force summer combining the human's output with a force signal generated from another part of the man-machine system.

To better understand this interaction, three plants (Gain = 1, 1/S, and $1/S^2$) were run in combination with four possible force loops (zero force = passive stick, a gain 1 multiplying the plant output, S' multiplying the plant output, and 1/S multiplying the plant output). This is equivalent to no feedback, position feedback, velocity feedback, and integrated position feedback from the plant, respectively. The experiment consisted of a 12 x 12 Latin square design which involved 12 subjects. The subjects tracked a compensatory tracking task consisting of a sum of sine waves disturbance input signal. Analysis of the transfer functions of the human operator were obtained. Finally, based on the describing function data and performance scores, a recommendation for the best (in terms of man-machine interaction) type of active controller was obtained.

INTRODUCTION

The interaction of man with machines takes on a new role when the stick controller is allowed to be active. This area of research appeared to be first investigated by Herzog [1,2] using a "matched manipulator" technique. In Herzog's work he found that if the dynamics of the stick controller were made equal to the dynamics of the plant being controlled, the tracking error would be the lowest value he observed when several different configurations were tested. The physical explanation of why this type of controller aids tracking is that the subject (when tracking with the matched manipulator) senses both position and force cues when he moves the stick. This is because the output of the displacement stick follows in a similar manner to the response of the plant. Thus if the subject observes the output of the stick, he senses the plant position output from stick commands. The subject also senses the control force or input to the plant from the reaction force of the stick. The net result is that the subject senses force feedback from his feel of the stick and position feedback of the plant by observing the output of the stick. This provides more information to the human operator as compared to the case of just a normal passive stick being used. It should be emphasized that the stick used in Herzog's work was a passive stick (it applied no

307

external forces to the human hand), but its transfer function dynamics could be changed.

In 1976, Merhav and Ya'Acov [3] devised an active stick in which the stick was driven by a torque motor with transfer function characteristics type 1, 3rd order. By wrapping a loop around the stick controller and inserting in this loop the output of the plant, the stick is then driven by information from the plant. Implicit in this variable (the plant) is knowledge of the disturbance input forcing function. Thus the human operator now has implicit information on the forcing function and this adds more knowledge to the human in his tracking scenario. The control augmentation device developed by Merhav and Ya'Acov showed tracking performance improvement as well as workload reduction. However, they considered only one special loop configuration involving the plant with a disturbance input.

More recently work [4,5,6,7] has been done using an assistive aid (termed the "smart stick") which consists of a hydraulic device. This device has an overall transfer function type zero, 2nd order for the combined arm-stick-hydraulic system. It is active in the sense that external forces can be added to the hand as a function of the stick output, plant output, or any variable desired. Since the plant output feeds back through the force loop, this device allows implicit information on the forcing function disturbance input to become a proprioceptive input to the human. This device differs from the one discussed in [3] in three ways: (1) In [3] the dynamics of the torque motor were type 1, third order; in the smart stick study, the dynamics of the stick-hydraulic system were type zero, 2nd order. (2) the plant and feedback loops to the torque motor were constrained to a fixed structure in [3]. For the smart stick study both the plant's characteristics and the force loop characteristics were varied to obtain 12 different combinations of the basic structures (Gain = 1, 1/S, 1/S^2, or S). (3) In [3], the torque motor can only be driven by θ (the plant output) through a compensating network. The smart stick allows stick error (and consequently the disturbance input forcing function) as well as θ and its derivatives to drive the current pressure transducer valves to produce forces on the human's hand.

The Experimental Apparatus

Figures 1-2 illustrate an assistive device developed at Wright-Patterson Air Force Base to help pilots improve tracking as measured by a compensatory tracking task.

In Figure 1 the actual mechanical device is illustrated [4]. It works in principal as shown in Figure 2. The control stick moves laterally (side to side) under commands of the human subject. As the stick is moved, the output of the stick is sensed and acts as an input to a computer algorithm. The "smart" computer algorithm was developed based on empirical evidence [7] that represents a special type of man-machine interaction which is known to improve tracking performance. The output of the smart algorithm drives a pair of pressure-current transducers that regulate gas pressure in a specially constructed cylinder which moves the stick in a prescribed manner. The human operator can override the force commands from the transducers but he must exert a greater force to overcome the original stick force. The net interaction of the human operator commands and the force signal generated via the computer-force transducer combination is what ultimately drives the

system. It is the goal of the designer to somehow improve this interaction in such a way as to obtain better tracking performance. The key element in these studies is to find a "smart algorithm" which will alter the muscle function in such a way as to improve the tracking performance of the task at hand. In [7] such an empirical relationship was found and this procedure provides a basis for the design of such assistive devices.

Experimental Design

Twelve male subjects participated in this experiment. They were involved in 3 days of training on the performance tasks and on the fourth day data were collected. Each day of the experiment required 12 tracking runs of 85 seconds duration with a 2 minute rest between tasks. The RMS (Root Mean Square) error scores of the tracking error were plotted each day for this compensatory tracking task with sum of sine wave inputs. The tracking error was the lateral distance seen on a display and consisted of the output of a plant being controlled about a zero position (three plant dynamics were used) when forced with a stick error signal consisting of stick output summed with a disturbance input forcing function. The real time system was sampled and updated at the rate of 25 Hz. The criterion used to establish that training was completed was the rule that a subject had to demonstrate less than 5% change in his performance score over three successive replications. Figure 3 illustrates the experimental design chosen for the three different conditions of plant = 1, $1/S$, and $1/S^2$. The loop conditions (loop = passive (gain = 0), $1/S$, 1, and s) were also selected. Figure 4 illustrates the system block diagram in which the plants and the loops were changed independently. Each day a subject tracked 12 conditions of plants and loops which were determined in a random manner. A Latin square design was used for the training data as well as the selection of the sequence of plants and loops on the data day.

Performance Results

Table I illustrates entries of Root Mean Square tracking error when averaged across all 12 subjects. The lower the score values, the better the performance. It is obvious that the plant $1/S$ with loop s is the optimal man-machine combination in the sense of best tracking performance.

Table I - RMS Tracking Error Values (Across 12 Subjects)

		Plant		
		1	1/S	1/S²
	P	21.0 ± 1.7	9.1 ± 1.9	15.3 ± 6.4
Loop	1	19.7 ± 2.2	8.2 ± 1.4	15.0 ± 5.5
	S	19.6 ± 1.8	6.9 ± 1.3	13.4 ± 4.7
	1/S	21.1 ± 3.6	9.6 ± 2.9	17.9 ± 7.0

Statistical tests were performed across subjects and loops, holding plant constant. These results are displayed in Table II.

Table II - Plant Fixed, Averaged Across Subjects and Loops

	Plant		
	1/S	1/S²	1
Mean Score ± Std of Subjects	8.5 ± 1.7	15.4 ± 5.2	20.3 ± 1.9

The scores displayed in Table II were significantly different at a .05 level. It is observed in Table II, the profound influence of plant dynamics on tracking performance.

If an analysis is conducted across plants and subjects (for loop fixed), the results appear in Table III.

Table III - Loop Fixed, ERMS Error Scores Averaged Across Subjects and Plants

| | Loop | | | |
	S	1	P	1/S
Mean Score ± Std of Subjects	13.3 ± 1.9	14.3 ± 2.5	15.1 ± 3.0	16.2 ± 3.9

The score values underlined indicate those experimental conditions not significantly different at a .05 level. There is a hierarchy of performance effects as the loops decrease in order from S' to 1/S. In addition to the above analyses, the ANOVA showed no significant interactions between plant and loop.

Transfer Function Results

In discussing human operator transfer functions it is necessary to refer to the measured signals in Figure 5 to describe the different types of transfer functions that can be obtained with this assistive device. Typically in the man-machine area, the human operator transfer function is usually written:

$$HOTF_2 = \text{Human Operator Transfer Function}_2 = \text{stick output/display error} \quad (1)$$

With the assistive device described herein, it is now possible to measure human force output and to develop another type of transfer function:

$$HOTF_1 = \text{Human Operator Transfer Function}_1 = \text{human force output/display error} \quad (2)$$

These types of transfer functions will be compared for the case (plant = 1/S) and the conditions loop = passive, 1, and S'. This was the case where the best tracking performance being best occurred.

Before the transfer functions are given, it is of interest in Figure 5 to examine the stick's mechanical impedance through the signals: stick output (a position signal) and the resulting force signal (which can be determined in units of force). Figure 6 illustrates a Bode plot of the stick's mechanical impedance. A rough Bode plot gives a type zero system, second order of the form:

$$\text{stick mechanical impedance} = 15.8/(1 + S/0.6)(1 + S/4.0) \quad (3)$$

Thus in controlling a 1/S plant, normally the human operator would act as a gain. Since the stick's mechanical impedance has second order characteristics as given in equation (3), we should expect the transfer

function of type $HOTF_1$ to have lead terms so that the transfer function $HOTF_2$ would appear as a gain.

Table IV presents all the frequency data averaged across 8 of the 12 subjects using the two tranfer functions $HOTF_1$ and $HOTF_2$ for passive loop vs S' loop and also for the S' loop vs loop = 1. T-tests were conducted at each frequency of the pairwise comparisons and P-values were calculated.

Table IV - Significant Results (Plant = 1/S) - P Values

ω	Human Force/Display Error				Stick Output/Display Error			
	Passive Loop Vs. S' Loop		S' Loop Vs. Loop = 1		Passive Loop Vs. S' Loop		S' Loop Vs. Loop = 1	
Rad/Sec	Gain	Phase	Gain	Phase	Gain	Phase	Gain	Phase
.230	.129	.546	.016*	.040*	.382	1.00	.691	.742
.537	.0008*	.742	.016*	.312	.008*	.460	.040*	.312
.999	.250	.024*	.008*	.148	.008*	.742	.078	.844
1.457	.016*	.016*	.016*	.148	.008*	.312	.040*	.281
2.224	.148	.008*	.016*	.148	.008*	.016*	.110	.016*
2.838	.040*	.016*	.008*	.148	.032*	.946	.016*	.148
4.065	.196	.016*	.047*	.148	.016*	.054	.691	.110
6.059	.008*	.016*	.008*	.148	.840	.129	.187*	.110
8.207	.032*	.016*	.016*	.148	.008*	.640	.008*	.946
10.661	.250	.040*	.054	.640	.016*	.546	.016*	.844
16.184	.546	.078	.546	1.00	.250	.460	.460	.742
21.706	.546	.312	.546	.460	.024*	.250	.040*	.382
32.137	.008	.844	.008*	.546	.844	.844	1.00	.844
45.022	.054	1.0	.024*	.312	.312	.742	.110	.844
64.351	.008	1.0	.008*	.546	.312	.546	.110	.460

* means significantly different at a P $<$ .05 level

The results of Table IV are more easily seen in the overlaid Bode plots of the respective transfer functions. Figure 7 illustrates the transfer function human force/display error for the passive loop versus the S' loop. It is seen that the S' loop gives rise to higher gain but the phase looks about the same although it is significantly different at some frequencies. In Figure 8 it is seen that for the transfer function stick out/display error for the two experimental conditions passive loop versus loop = S', the human operator shows the tendency to act like a gain in both cases. Thus the crossover model seems to hold here when we have active loops. In Figure 8, similar to Figure 7, we observe the gain slightly higher for the S' loop but the phase seems to be the same across these experimental conditions.

Figure 9 illustrates the transfer function human force/display error when the comparison is made between loop = 1 and loop = S' (for the case plant = 1/S). It is noted that for the S' loop, the gain is higher but the phase angles are slightly more negative for lower frequencies but not significantly different. From Table IV we see many asterisks for the gain differences, but few for phase. Figure 10 illustrates the transfer function stick out/display error between the two loop conditions loop = 1 and loop = S'. Again the human tends to act like a gain (somewhat independent of the loop characteristics) and the crossover model seems to hold for these two active loops. In Figure 10, similar to Figure 9, the gain for the S' loop case is higher for the loop

= 1 case. The phase seems to be the same across these two experimental conditions.

DISCUSSION

The human operator tends to prefer the experimental condition plant = 1/S and loop = S'. In terms of tracking performance this is where the best achievement occurs. In terms of human operator transfer functions, the loop condition S' gives rise to higher gain values but with little change in phase. This agrees with better tracking performance because the higher human operator gain (with the same phase) will more tightly close the man-machine loop and result in better tracking performance. Finally, the crossover model seems to hold for the four loop conditions (passive, S', 1, and 1/S). The shape of the traditional human operator transfer function (HOTF$_2$) seemed to remain the same across all the loop conditions. The small increase in gain simply means (in terms of the man-machine transfer function) a small increase in crossover frequency.

SUMMARY AND CONCLUSIONS

A study on the three different plants (1, 1/S, and $1/S^2$) and the four force loops (1, 1/S, passive, and S') indicated that the best performance combination was plant = 1/S and loop = S'. This combination had the highest gain for all the human operator transfer functions considered. The phase information for these transfer functions seemed to be about the same. The transfer functions chosen were the traditional stick output/display error for the human operator and the new representation obtained here: human force output/display error. Finally, the crossover model seemed to hold for all the loops examined. The only impact of the smart loop S' was to slightly increase the crossover frequency.

REFERENCES

[1] Herzog, J.H. "Proprioceptive Cues and Their Influence on Operator Performance in Manual Control," NASA CR-1248, January 1969.

[2] Herzog, J.H. "Manual Control Using the Matched Manipulator Control Technique," IEEE Transactions on Man-Machine Systems, Vol. MMS-9, No. 3, pp 56-60, September 1968.

[3] Merhav, S.J. and Ya'Acov, O.B. "Control Augmentation and Workload Reduction by Kinesthetic Information from the Manipulator," IEEE Transactions on Systems, Man, and Cybernetics, Vol. SMC-6, No. 12, pp 825-835, December 1976.

[4] Repperger, D.W., Frazier, J.W., and Van Patten, R.E. "A Smart Stick Controller Design Based on a Static Equilibrium Model," Proceedings of the 1984 NAECON Conference, pp 810-817, May 1984.

[5] Repperger, D.W., and Goodyear, C. "Active Controllers and the Time Duration to Learn a Task," Proceedings of the 21st Annual Conference on Manual Control, pp 18.1-18.12, June 1985.

[6] Morris, A., and Repperger, D.W. "Adaptability of Muscle Function with the Use of Computer Aided Assistive Devices," Proceedings of the 1986 NAECON Conference, Dayton, Ohio, pp 738-745, May 1986.

[7] Repperger, D.W., Frazier, J.W., and Van Patten, R.E. "Results from a Biomechanical Stick Study," Proceedings of the 1983 Aerospace Medical Association Meeting, Houston, Texas, pp 192-193, May 1983.
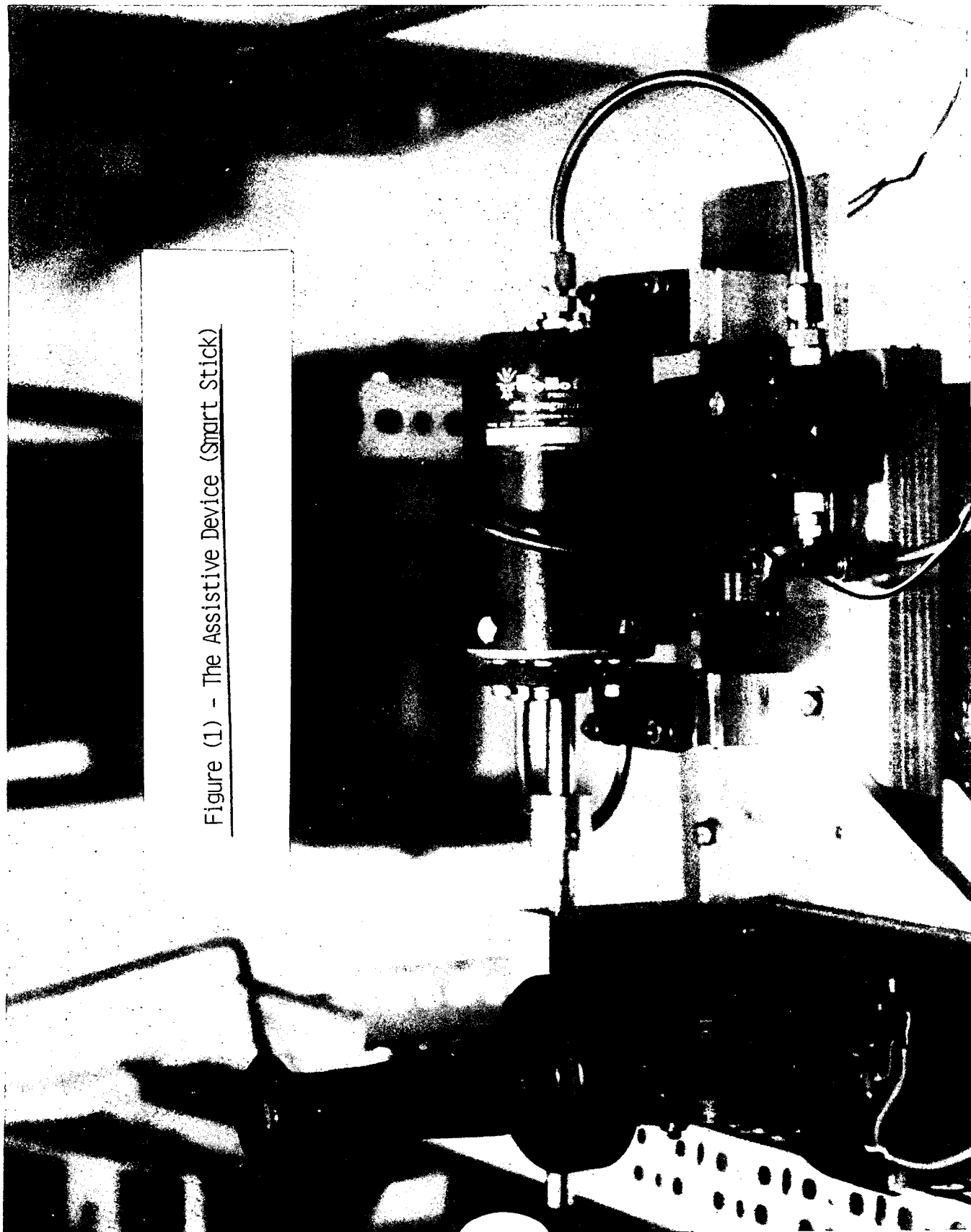
Figure (1) – The Assistive Device (Smart Stick)
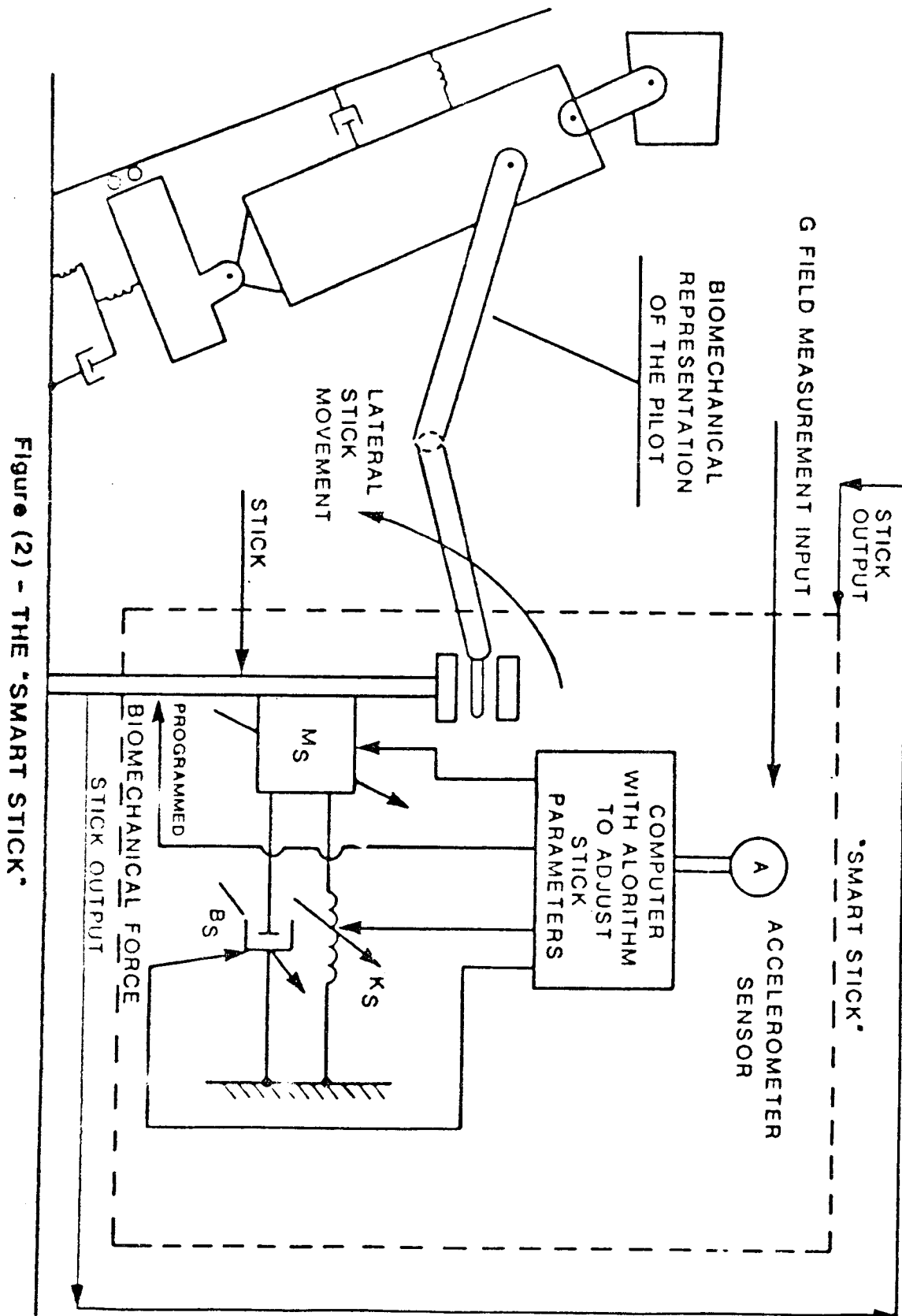
Figure (2) — THE "SMART STICK"

315

LOOPS
LOOP = PASSIVE
1/S
1
S

1   1/S   1/S²

PLANTS

12 SUBJECTS

Figure (3) — The Experimental Design

DISTURBANCE INPUT
FORCING FUNCTION

STICK ERROR

PLANT

PLANT OUTPUT

STICK IMPEDANCE

LOOP

HUMAN OPERATOR

-1

STICK OUTPUT
(DISPLACEMENT)

FORCE SUMMER   FORCE OUTPUT   DISPLAY ERROR
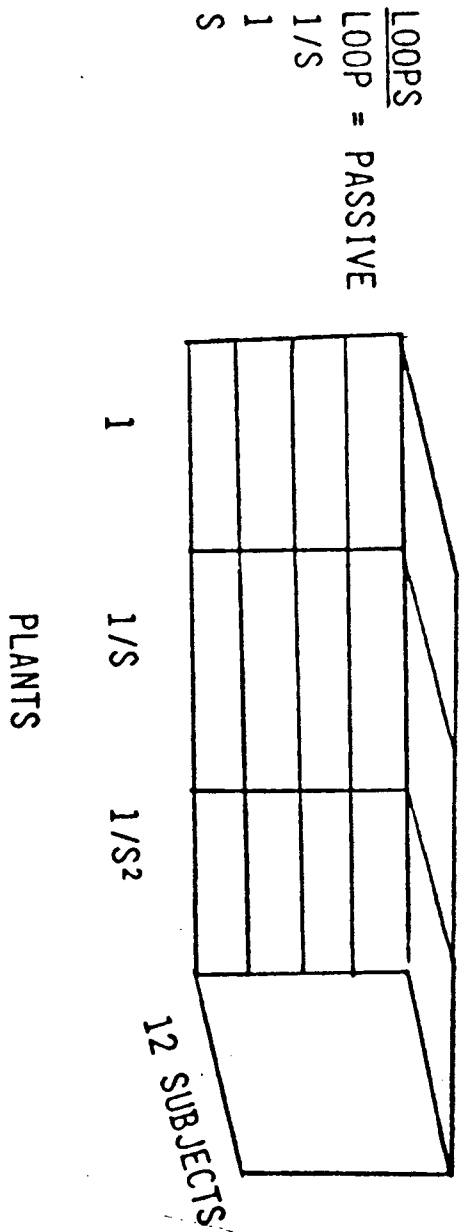
Figure (4) — The System Block Diagram

316
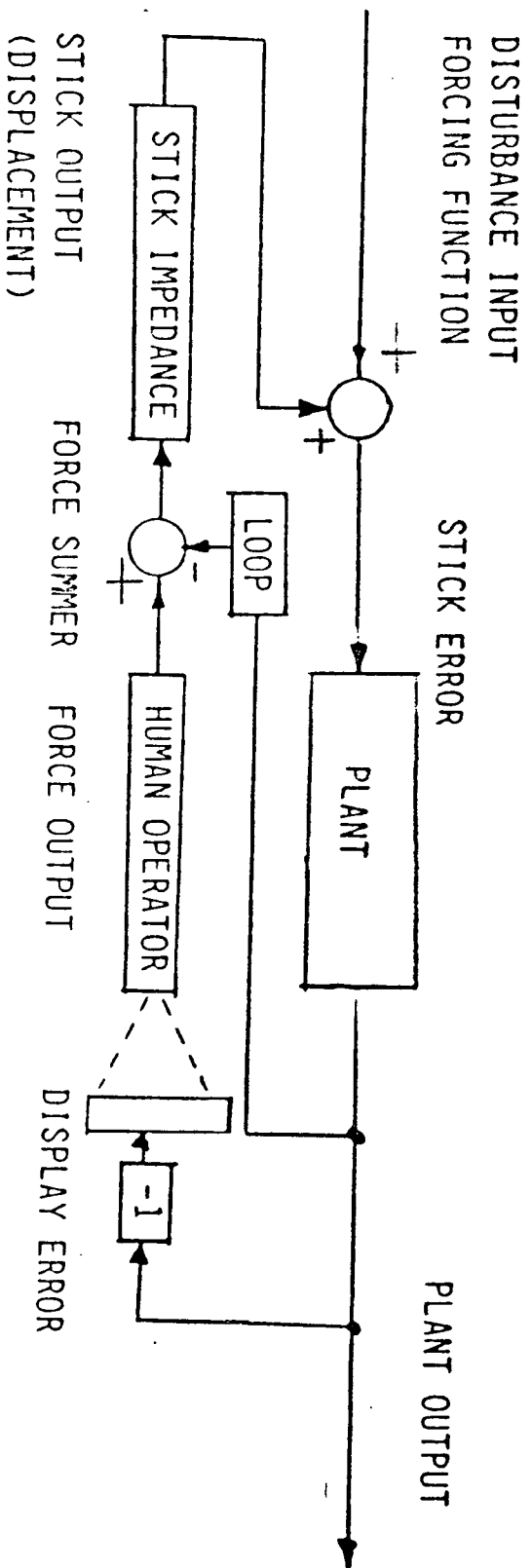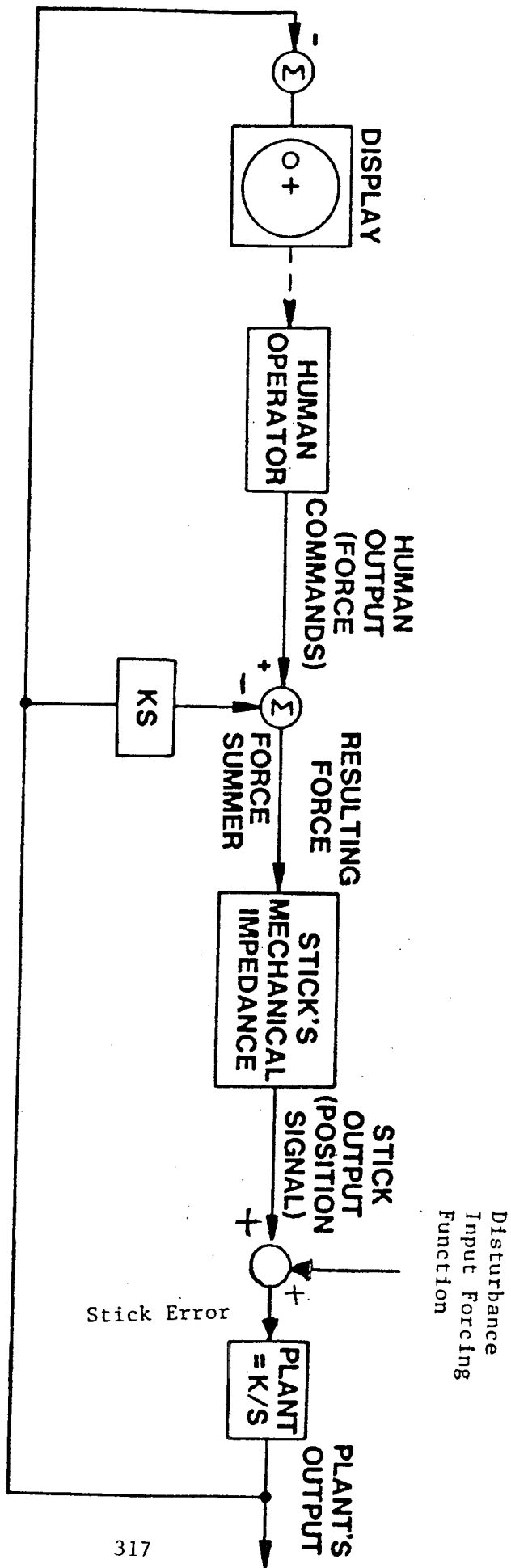
Figure (5) THE MAN–MACHINE SYSTEM

317

Figure (6) – Stick Impedance = $\dfrac{\text{Stick Output}}{\text{Resultant Force}}$

$$= \frac{15.8}{(1 + \frac{s}{0.6})(1 + \frac{s}{4.0})}$$

O – Phase

X – Gain

Figure (7) – Human Operator Transfer Function

$$HOTF_1 = \frac{\text{Human Force}}{\text{Display Error}}$$

Loop = s¹ compared to passive loop

X = Gain, O = Phase (Plant = 1/s)

319

Figure (8) — Human Operator Transfer Function

$$HOTF_2 = \frac{Stick\ Out}{Display\ Error}$$

Loop = s^1 compared to passive loop

X = Gain, O = Phase   (Plant = 1/s)

320

Figure (9) - Human Operator Transfer Function

$$HOTF_1 = \frac{\text{Human Force}}{\text{Display Error}}$$

Loop = s¹ compared to Loop = 1

X = Gain, 0 = Phase

(Plant = 1/s)

Figure (10) — Human Operator Transfer Function

$$HOTF_2 = \frac{Stick\ Output}{Display\ Error}$$

Loop = s^1 compared to Loop = 1

X = Gain, O = Phase   (Plant = 1/s)

ARTIFICIAL INTELLIGENCE IN THE COCKPIT

BY

Dominick Andrisani

School of Aeronautics and Astronautics

Purdue University

West Lafayette, IN

"ARTIFICIAL INTELLIGENCE IS THE STUDY OF HOW TO

MAKE COMPUTERS DO THINGS AT WHICH, AT THE MOMENT, PEOPLE

DO BETTER."

ELAINE RICH, ARTIFICIAL INTELLIGENCE
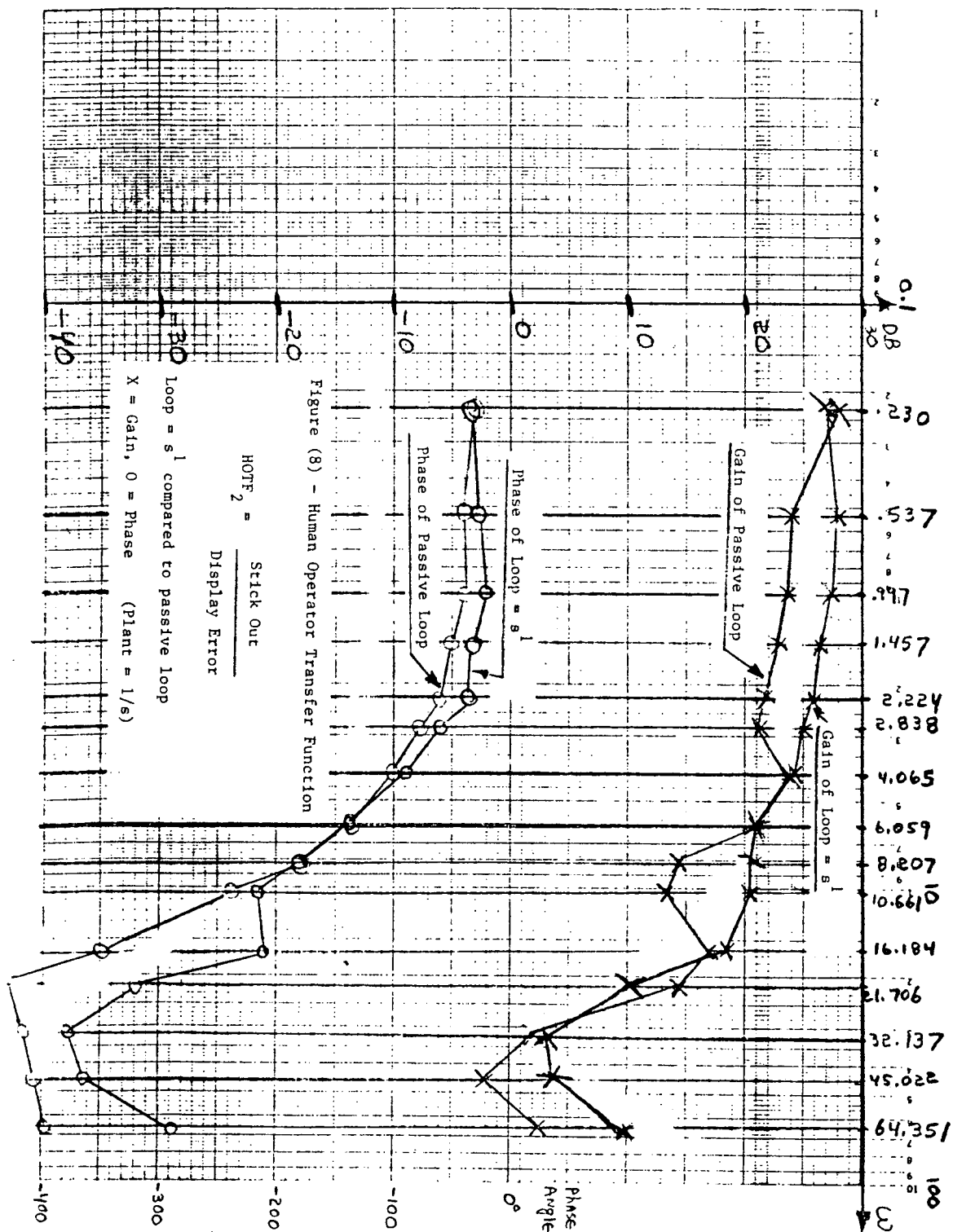
NOTE: PEOPLE MUST ALREADY KNOW HOW TO DO IT.

WHAT IS AI?

VERY SIMPLY, AI IS AN INTERDISCIPLINARY POLYPHASIC
CONUNDRUM OF EMBRANGLED ATTEMPTS AT HUMAN COGNITIVE
EMULATION THROUGH THE ITERATIVE APPLICATION OF MULTI-
PARADIGM SOFTWARE CONFIGURATIONS, VIZ., A SYNERGISTIC
FUSION OF APPLIED EPISTEMOLOGICAL RESEARCH PROBING THE
ONTOLOGICAL NATURE OF KNOWLEDGE REPRESENTATIONS EMBODIED
IN NON-STANDARD COMPUTATIONAL MODELS, FORMULATED IN
NEOLOGISMS.

THREE POSSIBILITIES FOR AI
IN THE COCKPIT

- INTEGRATION OF INFORMATION
  (MULTI-SENSOR FUSION)

- ANALYSIS OF INFORMATION
  (SITUATION OR THREAT ASSESSMENT)

- PLANNING BASED ON INFORMATION
  (DYNAMIC MISSION PLANNING)

NOTE: DURING A MISSION THESE MUST BE DONE IN
REAL-TIME.

FEATURES OF REAL-TIME
AI SYSTEMS

- EXTENSIVE ON-LINE DATABASE

    * ALL THE KNOWLEDGE OF AN EXPERT IN A
      PARTICULAR DOMAIN OF KNOWLEDGE

    * FACTS AND RULES FOR EXAMPLE

- THE ABILITY TO GATHER TIME VARYING DATA FROM THE
  CHANGING ENVIRONMENT

- THE ABILITY TO DRAW CONCLUSIONS FROM THE AVAILABLE DATA

    * INTEGRATE

    * ANALYZE

    * PLAN

- THE ABILITY TO EXPLAIN ITS ACTION

AN EXAMPLE

- REAL-TIME FACT:

    THE BATTLEFIELD CONTAINS A MIG-21 AND A MIG-25

- STATIC FACT:

    A MIG-25 IS MORE LETHAL THAN A MIG-21

- RULE:

    ALWAYS ENGAGE THE MOST LETHAL TARGET <u>FIRST</u>.

* CONCLUSION:

    ENGAGE THE MIG-25 FIRST

MULTI-SENSOR FUSION
(INTELLIGENT DISPLAYS)

- COMBINE A PRIORI INFORMATION WITH REAL TIME INFORMATION FROM MANY SENSORS

- ANALYZE AND PRIORITIZE THE INFORMATION TO BE PRESENTED

- PROBLEMS
    - EFFICIENT KNOWLEDGE REPRESENTATION
    - DEALING WITH UNCERTAINTY
    - COUPLING TO THE DYNAMIC PLANNER
    - DISPLAY FORMAT FOR PILOT

F-15 Engagement Display

23:16:12z

FRIEND

HOSTILE

BIT

40

28/10

30

13

12

F/20

2F/20

NET
SNET
ID
MSAM

RELN
COR
ROUTE

MENU

2 M-23
HOSTILE
20K
510KTS

M3
62

MODE

SELF

EXP

AI and Control Systems

MISSION OBJECTIVE ~ EXTERNAL SITUATION

AIRCRAFT

ATTITUDE LOOPS
3-5 R/S

FLIGHT PATH LOOPS
1-2 R/S

NAVIGATION LOOPS
.5-1 R/S
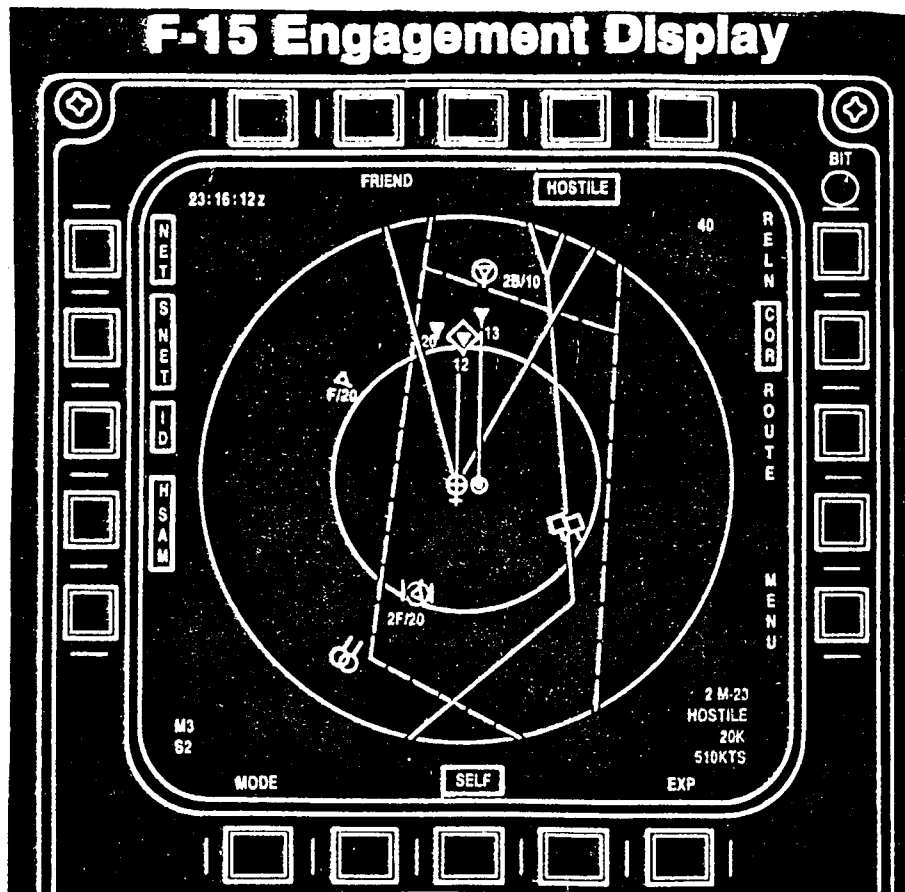
MISSION PLANNING LOOPS
.1-.5 R/S
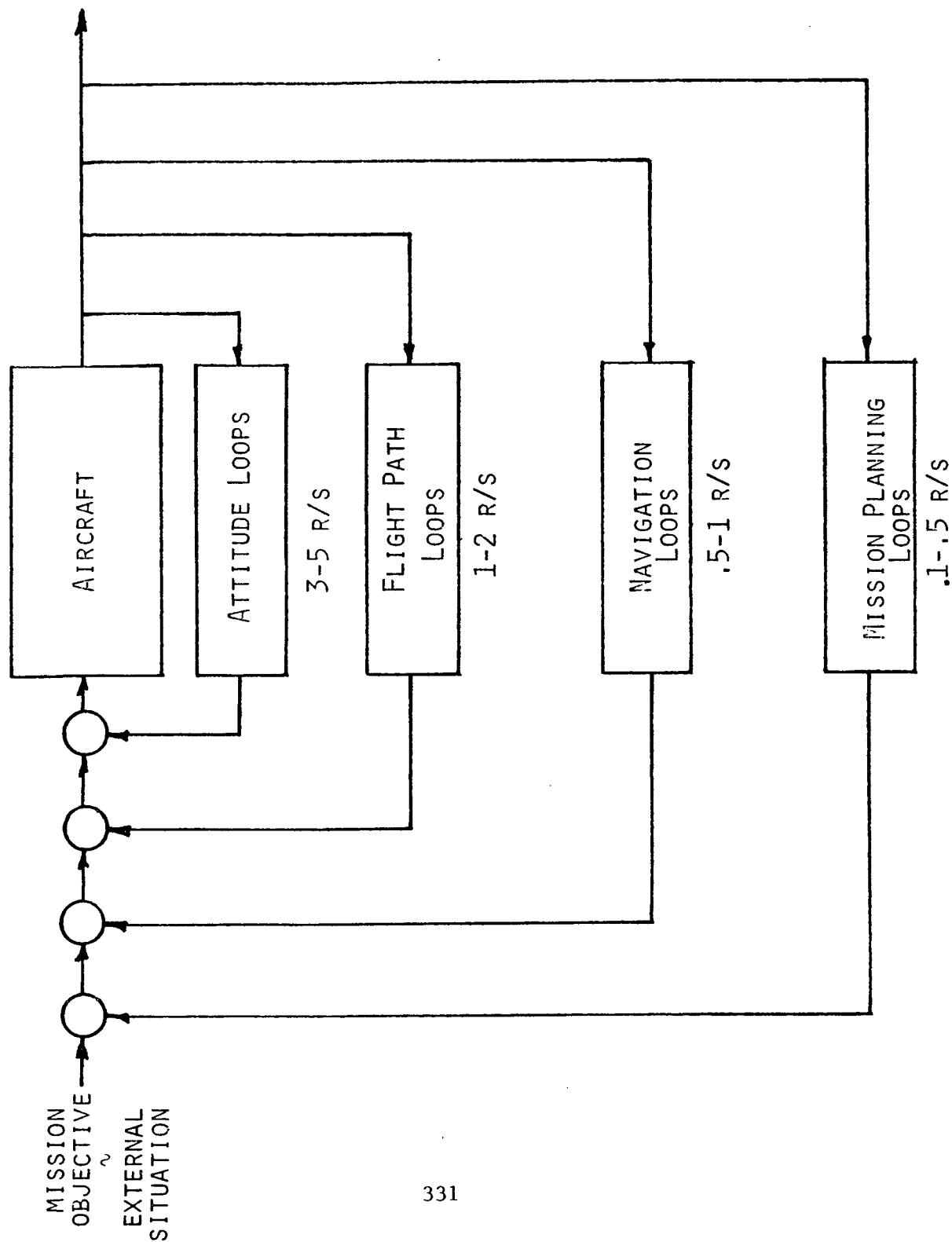
WHERE DOES THE PILOT BELONG?
WHAT SHOULD BE DISPLAYED TO THE PILOT?

Control Loop Characteristics

Inner Loops

- Governed by Newtonian calculus

- The time dependence of the problem is explicitly stated

- Algorithmic solutions exist, $U = KX$

- Analysis and synthesis methods are mature

- Stability and robustness measures exist

- Short time constants

Planning Loops May Involve

- Predicate calculus (the calculus of logic)

- The time varying nature of the process may not be stated

- Heuristic solution (rule based, or search strategy)

- Analysis and synthesis methods are immature

- Stability and robustness measures don't exist

- Longer time constants

COMBAT ENVIRONMENT

EXTERNAL SYSTEMS

JTIDS

OWNSHIP SENSORS
THREAT
TERRAIN

MISSION BRIEFED DATA

CONTROL SYSTEM
MANEUVER
CM
WEAPONS

AIRCRAFT SYSTEMS

CONTROLLER
AUTOMATIC MODE PILOT OVERRIDE
ADVISE ONLY PILOT CONTROL
PILOT ONLY

EXPERT SYSTEMS INTEGRATOR "BLACKBOARD CONTROL"

PILOT/SYSTEMS MANAGER

PILOT

OWNSHIP & TERRAIN STATE EXPERT

THREAT ASSESSMENT EXPERT

GLOBAL PLANNING EXPERT

LOCAL PLANNING EXPERT

EXPERT SYSTEMS

GRAPHICS DISPLAYS & AUDIO

EXPLICATOR

PILOT VEHICLE INTERFACE (PVI)

333

Why Go This Way?

- The AI deduction process is closer to the thought procedure followed by the pilot.

- The pilots' procedure may well be non-algorithmic or rule-based.

- Display generation requires the manipulation of large databases.

Difficulties with the Real-Time Expert Systems Approach

- Heuristic reasoning can be incomplete

- Incomplete or inaccurate knowledge can only be corrected by extensive simulation and testing

- Experts must know how to solve the problem

- Computation time can be excessive relative to "time constants" of a tactical situation

- Computer generated plans are predictable

CLOSING REMARKS

CONTROL/DISPLAY DESIGNERS SHOULD BE

- UNEASY ABOUT THE LIKELIHOOD OF FLAWS IN HEURISTIC REASONING

- CONCERNED ABOUT THE LACK OF METHODS FOR VALIDATION OF HEURISTIC REASONING

- INTRIGUED ABOUT THE POTENTIAL PAYOFF IN INCREASED MISSION EFFECTIVENESS IN CERTAIN MISSIONS

AI RESEARCHERS SHOULD IMPROVE METHODS FOR DEALING WITH

- THE REAL TIME ENVIRONMENT

- UNCERTAINTY

- EFFICIENT KNOWLEDGE REPRESENTATION

LIST OF AUTHORS

22ND ANNUAL CONFERENCE ON MANUAL CONTROL

AUTHORS

APPENDIX - Late Papers

STEREO DEPTH DISTORTIONS IN TELEOPERATION

Daniel B. Diner, Ph.D.
Marika von Sydow, M.S.
Mail Stop 23
Jet Propulsion Laboratory
California Institute of Technology
4800 Oak Grove Drive
Pasadena, California 91109

ABSTRACT

In teleoperation, a typical application of stereo vision is to view a work space located short distances (1 to 3 meters) in front of the cameras. The work reported in this paper treats converged camera placement and studies the effects of intercamera distance, camera-to-object viewing distance, and focal length of the camera lenses on both stereo depth resolution and stereo depth distortion. While viewing the fronto-parallel plane 1.3 meters in front of the cameras, we have measured depth errors on the order of 2 centimeters.

A geometric analysis was made of the distortion of the fronto-parallel plane of convergence for stereo TV viewing. The results of the analysis were then verified experimentally. The objective was to determine the optimal camera configuration which gave high stereo depth resolution while minimizing stereo depth distortion.

We find that for a fixed camera-to-object viewing distance, larger intercamera distances allow higher depth resolutions, but cause greater depth distortions. Thus with larger intercamera distances, operators will make greater depth errors (because of the greater distortions), but also be more certain that they are not errors (because of the higher resolution).

The analysis predicts camera configurations and a camera motion strategy that minimize stereo depth distortion without sacrificing stereo depth resolution.

LIST OF SYMBOLS

ALIGN   horizontal distance between the camera convergence point and the center point between two test bars

C   camera convergence point

D   camera-to-object viewing distance

dL   distance between the camera Vieth-Mueller circle and the left test bar

dR   distance between the camera Vieth-Mueller circle and the right test bar

f   focal length of the TV camera lenses

FPP   fronto-parallel plane including the camera convergence point

ICD   intercamera distance

ITD   intertarget distance

k   horizontal distance from the camera convergence point to a point in the fronto-parallel plane

L   distance from first nodal point of the TV camera lens to the camera convergence point

Lf'   projection of distance k on line of equidistant projection for far left camera

Ln'   projection of distance k on line of equidistant projection for near left camera

MTERM   multiplicative product of ICD and ALIGN

Pl'   projection of distance k on the line of equidistant projection for the left camera

Pr'   projection of distance k on the line of equidistant projection for the right camera

Rf'   projection of distance k on line of equidistant projection for far right camera

Rn'   projection of distance k on line of equidistant projection for near right camera

w   one-half of the intercamera distance

WP   width per pixel at the CCD camera

344

1. INTRODUCTION

In teleoperation, one typical application of stereo vision is the viewing of a work space located 1 to 3 meters away from the cameras. We have investigated such close stereo viewing and, over the range of parameters tested, we have explored the trade-off between stereo depth resolution and stereo depth distortion as a function of camera configuration.

When selecting a stereo camera configuration, it is necessary to choose between parallel and converged camera configurations. Parallel configurations, which may have certain advantages for far stereo viewing, have inherent undesirable aspects for near stereo viewing. First of all, the two views of the cameras do not overlap entirely in the work space. Thus some of the image on the monitor screen will not be presented in stereo. Second, an object located exactly in front of the stereo camera system will be seen to the left of center by the right camera, and to the right of center by the left camera. This may force uncomfortable viewing conditions upon the observer, and may reduce performance drastically.

For this reason, we have focused our attention on converged camera configurations. Properly converged camera configurations do not suffer either of the undesirable aspects mentioned above.

However, converged camera configurations can induce stereo depth distortion. For example, with widely converged cameras, an observer stereoscopically viewing a meter stick (located in the fronto-parallel plane including the camera convergence point) reports that the meter stick appears to be curved away from the observer. As the intercamera distance is decreased, and thus the camera convergence angle is decreased, the apparent curvature of the meter stick decreases, but with a loss of stereo depth resolution. This distortion/resolution trade-off is the subject of this paper.

This distortion changes with intercamera distance, viewing distance, and focal length of the camera lenses. Unfortunately, widely converged camera configurations, which yield higher stereo depth resolution, also yield larger stereo depth distortions.

Camera configurations which are similar to natural human viewing conditions are called orthostereoscopic; unnaturally wide camera separation configurations are called hyperstereoscopic. In the literature on stereo imaging, some researchers advocate orthostereoscopic camera alignments, and other researchers advocate hyperstereoscopic camera alignments.

Shields, Kirkpatrick, Malone and Huggins (1) found no gain in performance with hyperstereopsis on a stereo depth comparison task, and recommended orthostereopsis. This does not surprise us, as the depth distortion of hyperstereopsis may well have overridden the advantage of the increased depth resolution.

Grant, Meirick, Polhemus, Spencer, Swain, and Tewell (2) found no gain in performance with hyperstereopsis on a peg-in-hole task, and recommended orthostereopsis. This result does surprise us, in that a peg-in-hole task requires high depth precision only in a small region of the work space. The depth distortion of hyperstereopsis only becomes significant for objects which are separated horizontally. Thus the performance of the insertion of the peg into the hole should increase with the increased depth resolution of hyperstereopsis. Perhaps the depth distortions hurt the performance of the long range motions (such as moving towards the peg and moving the peg towards the hole) enough to overshadow the increase in performance of the insertions.

Upton and Strother (3) reported that hyperstereopsis greatly enhanced depth detection of camouflaged buildings from helicopter mounted stereo cameras. This result is expected. The critical point here is that the accurate detection of depth is a different phenomenon than the accurate estimate of the magnitude of a true depth. Hyperstereopsis artificially magnifies the perceived magnitude of a true depth difference, making that depth difference easier to detect, but much harder to perform accurate teleoperation upon. For example, hyperstereopsis might make a one-story camouflaged building appear to be four stories tall.

Zamarian (4) reported that hyperstereopsis improved performance over orthostereopsis on a three-bar depth adjustment task. He used converged cameras. The three bar depth adjustment task insures that the depth distortions will play a role in his experiment. He states, "...it was found that performance improved with increasing [camera] separation but at a decreasing rate of improvement." We suspect that he was experiencing the trade-off between increased resolution and distortion.

Pepper, Cole, and Spain (5) reported that hyperstereopsis improved performance on a two-bar depth adjustment task. They used parallel camera configurations, and therefore introduced no stereo depth distortions. These results, therefore, should not apply directly to our work.

Spain (6) reported that hyperstereopsis improved performance on a two-bar depth adjustment task. He converged the cameras so that the camera convergence point was half-way between the two bars when the bars were located at equal depth. We feel that each bar experienced the same depth distortion. The net effect then would have been that the relative distortion between the two bars cancelled out. In that case, the increased stereo depth resolution of hyperstereopsis would have improved performance.

Bejczy (7) reported surprisingly poor performance with a stereo TV viewing system of a task which required the positioning and orienting of an end-effector in an almost static visual scene. Operators were required to pick up one block and place it upon another block. Although the thrust of this work was to evaluate the effect of short-range proximity sensors in conjunction with mono and stereo camera systems on the performance of this task, the surprisingly poor performance with stereo viewing must be noted.

In reviewing the literature, we noticed that most analyses of stereo TV viewing use small angle approximations. However, the actual stereo distortions of the fronto-parallel plane of convergence are such that small angle approximations obscure the relationship between the key parameters of the camera configurations.

To investigate this question more rigorously, we have used a geometric analysis of the distortion of the fronto-parallel plane of convergence (FPP) for stereo TV viewing, without any small angle approximations, and have used this analysis in our experimental program.

This paper explores the following question. Will human observers' responses follow the predictions of our geometric analysis, despite internal perceptual corrections and/or distortions? If so, we may use our geometric analysis to predict optimal camera configurations, which can then be tested and verified. We wish to find camera configurations which give high stereo depth resolution without large stereo depth distortions.

This is not a trivial question. We humans surely have perceptual corrections and distortions. Each time we converge our eyes on a flat wall, for example, we experience similar distortions to those described above for converged cameras. We should therefore perceive flat walls as curved away from us. The fact that, in general, we do not, indicates the existence of these corrections and distortions. However, the distortions and corrections may not be so powerful as to negate the predictions of our geometric analysis.

Our ultimate goal is to determine the best trade-off between stereo resolution and distortion per performance task, for work spaces limited to 3 meters depth. A necessary first step is to minimize all non-stereo depth cues. Then we can measure how the observers react to the stereo depth distortion cues in the absence of other possible interfering cues. Once we understand the factors determining the optimal stereo camera configuration for each specific task, we plan to integrate this understanding into experimentation involving visual scenes rich in the other depth cues.

2. GEOMETRIC ANALYSIS

Most geometric analyses of the stereo camera system use small angle approximations, which, as previously noted, obscure the relationship between the key parameters of the camera configuration. Therefore, we have made a geometric analysis of the distortion of the fronto-parallel plane of convergence (FPP), without using small angle approximations. For the derivation, see Appendix 1.

This analysis predicts distortions for converged camera configurations, but not for parallel camera configurations. Figure 1 shows that parallel cameras, when viewing two objects separated by a horizontal distance, k, will see the same distance between the objects. That is, Pl' = Pr'. Therefore, no stereo depth distortion will be produced by the camera geometry.

In contrast, consider the converged camera configuration in Figure 1, viewing the same two objects where one object is now located at the camera convergence point. The left camera will see a greater distance between the two objects than the right camera. Therefore the two cameras will present different distances between the two objects to the monitor. We call the difference between the distances on the monitor the spatial monitor disparity between the two camera images. The stereo system presents the left camera image to the left eye, and the right camera image to the right eye. Figure 2 shows that if the eyes see different distances between two objects, the objects will be perceived at different depths.

Static Depth Distortions

Figure 3 shows the nature of the static stereo depth distortions. By static, we mean the distortion that is present when we do not move the cameras. It stems from the camera alignment geometry.

In a quantized TV system, the spatial monitor disparity can be analyzed as the number of pixels difference between the two camera images. The quantized TV system separates space into regions within which motion is invisible. Figure 3 represents two CCD cameras converged and viewing a work-space. Each diamond-like shape, which we shall call a lozenge, represents the region in space that is seen by a pair of pixels, one on each camera. If a point source of light is moved within a lozenge, no change will be registered by the TV cameras. The stereo depth resolution will be defined by the lozenge size. Specifically, an object must move at least half a lozenge length in depth for any change to be registered. The stereo depth distortion of the FPP can be understood as the difference in spatial monitor disparity of the various points on the plane. The camera convergence point, which is on the FPP, has zero spatial monitor
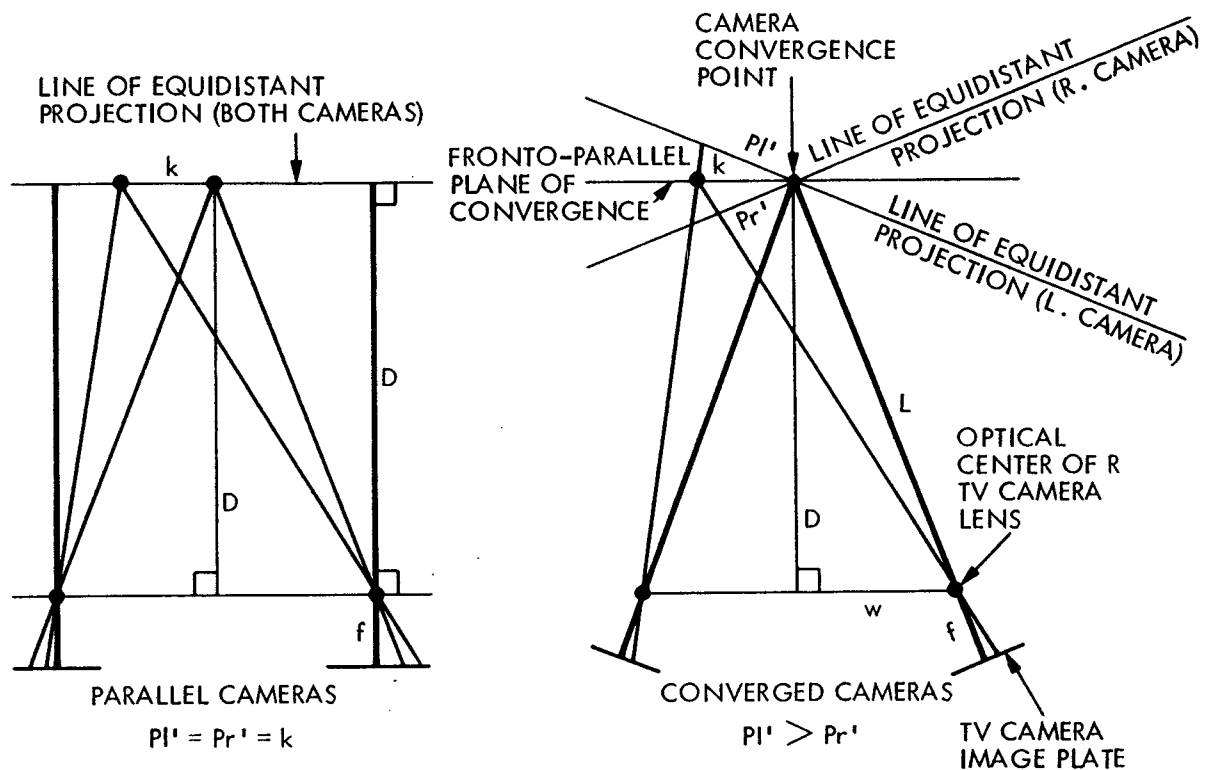
Figure 1. The geometry of parallel and converged CCD camera
configurations. On the lines of equidistant projection, every
pixel sees a unit length segment. This segment length is
(D/f) * (width/pixel at CCD) for the parallel cameras, and
(L/f) * (width/pixel at CCD) for the converged cameras. The
pixels difference presented to the monitor by the two
cameras will be proportional to (Pl' - Pr'). Consider an
object located a horizontal distance k from the camera
convergence point. For converged cameras, Pl' > Pr', while
for parallel camera configurations, Pl' = Pr'.
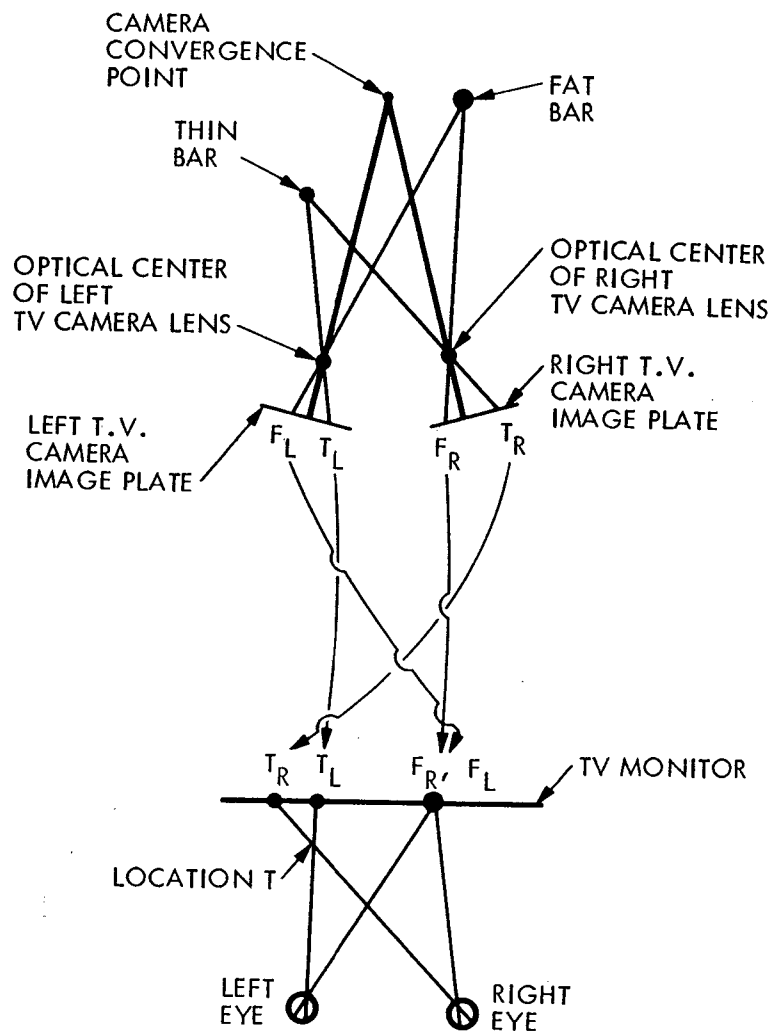
Figure 2. The stereo depth cues. The right camera records a greater # pixels between the thin and fat bars than the left camera, and displays them on the TV Monitor. The observer's right eye sees only the right camera image on the TV monitor, and the observer's left eye sees only the left camera image. Location T is the intersection of the left and right eyes' lines of sight for the thin bar. This is the only place in space that the thin bar could be, and still be seen by the two eyes on those particular lines of sight. The pixel information (# pixels difference between the two camera views as presented on the TV monitor) that determines this location includes both the true stereo depth cues and the stereo depth distortion cues Note: we did not use bars of different thickness in our experiments.

350

Figure 3. The geometry of the work space as viewed by converged stereo cameras. Shaded lozenges all present the same number of pixels difference to the monitor screen.

Labels in figure: C, A, B, OPTICAL CENTER OF T.V. CAMERA LENS, T.V. CAMERA IMAGE PLATE

disparity. Therefore, the depth distortion of any point on the FPP can be reduced to its spatial monitor disparity.

For two points on the FPP, one located at the convergence point, and the other a horizontal distance, k, from the convergence point, spatial monitor disparity, expressed as a number of pixels, will be:
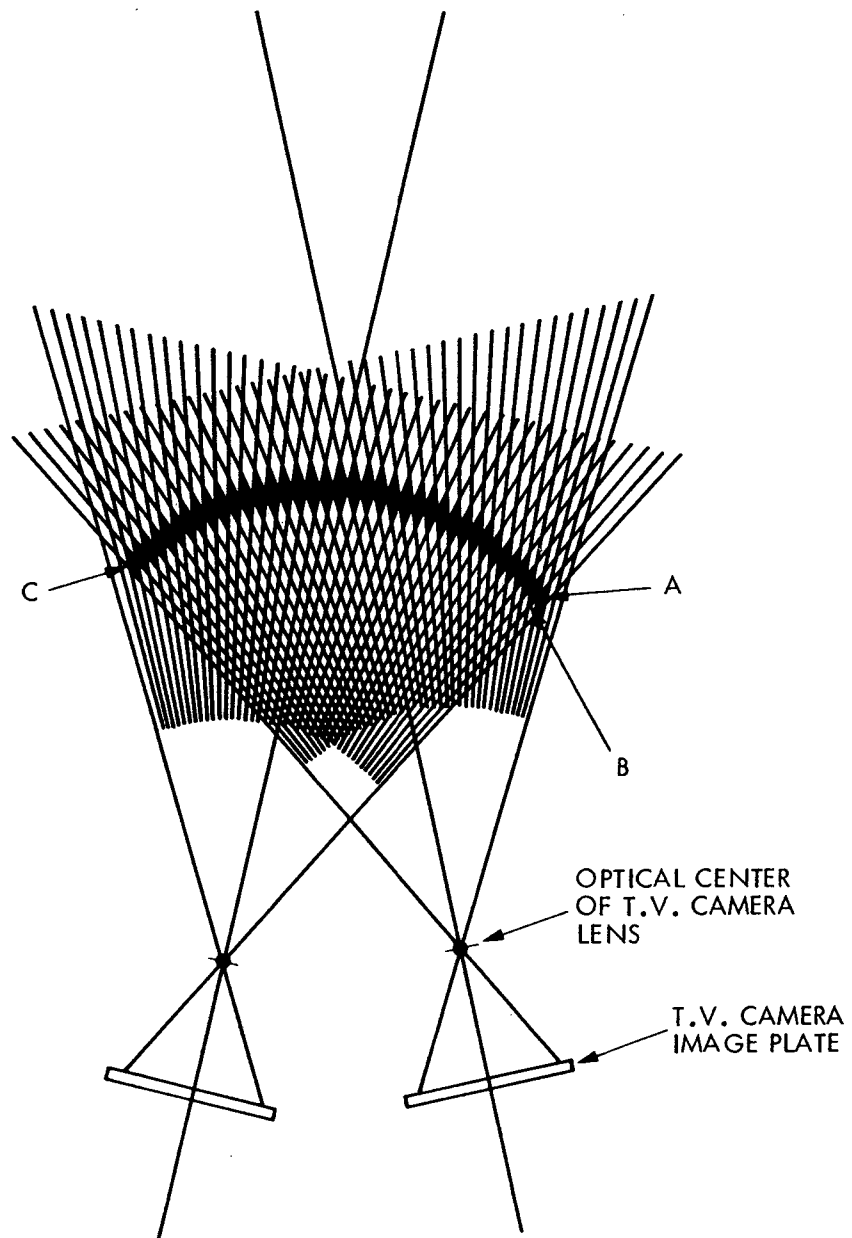
$$\text{number of pixels} = \frac{2*k^2*D*f*w}{(D^4 + w^4 + 2*D^2*w^2 - k^2*w^2) * (WP)} \quad (1)$$

where D = camera viewing distance (from the convergence point to the point equidistant between the first nodal points of the camera lenses)

    f = focal length of the lenses (equal for both cameras)
    w = ICD/2
    WP = the width/pixel at CCD

For the ranges we are interested in, k^2*w^2 can always be restricted to less than $D^4/1000$, and thus can be ignored.

Formula (1) can be generalized for two points located anywhere in the FPP at arbitrary distances from the camera convergence point. Consider two vertical bars held a fixed distance apart. Let us call the horizontal distance between the camera convergence point and the center point between the two bars ALIGN, and the distance between the bars the inter-target distance (ITD). The values of k in Formula (1) will then be ITD/2 + ALIGN and ITD/2 - ALIGN. The number of pixels difference we expect is the difference between these squared values which equals 2*ITD*ALIGN. Therefore,

$$\text{number of pixels diff (2 bars)} = \frac{2*D*f*ITD*ALIGN*ICD}{(D^2 + (ICD/2)^2)^2 * (WP)} \quad (2)$$

Here we have replaced w with ICD/2.

. By moving the bars horizontally in the FPP, and measuring observers' perceptions of relative depth between the bars, the apparent shape of the FPP can be determined. For example, if an object in space is located within a lozenge with three pixels difference between camera views, the three pixel difference presented on the monitor will be the stereo depth cue the observer will see. If the object happens to be in the FPP, then the perceived depth associated with the three pixel difference will be purely distortion. In Figure 3, lozenges A and B have the same number of pixels difference. That is because lozenge A

is seen by a pair of pixels which is one pixel to the left (on each camera) of the pair of pixels which sees lozenge B. In fact, all the shaded lozenges in Figure 3 have the same number of pixels difference. Therefore objects located within these lozenges will appear in the same plane when viewed on the stereo monitor. This is because all such objects will have the same angular disparity when viewed by the human eyes, and angular disparity is the human stereo depth cue. Equal disparity leads to equal depth, which we interpret as flatness. If this curve in space appears flat, the FPP will appear convexly curved.

For the ranges we are interested in, ICD/2 never exceeds D/4 and the denominator will never be larger than $1.2*D^4$. Thus Formula (2) can be approximated by a $1/D^3$ relation. This will lead to a camera configuration technique which significantly reduces the stereo depth distortion without reducing the stereo depth resolution, and will be discussed later.

The results of this analysis may be surprising at first. It is well known that when the two eyes converge on a point, the points in space that are at equal angles to both eyes lie on a circle. This circle passes through the convergence point and the first nodal points of the two eyes. This circle is known as the Vieth-Mueller circle. Analagously, a Vieth-Mueller circle can be defined for two converged TV cameras. The circle will pass through the convergence point and the first nodal points of the two lenses. See Figure 4. The equal angles imply that the number of pixels difference between the left and right images will be zero for all points on the camera Vieth-Mueller circle.

For a fixed viewing distance D, a smaller ICD yields a Vieth-Mueller circle with smaller radius, that is sharper curvature.

$$\text{Radius (V.-M. circle)} = \frac{D^2 + (ICD/2)^2}{2*D} \quad (3)$$

Thus, less spatial distortion could be expected for the larger ICD, because a bar need move less distance from the FPP to the location of 0 pixel difference. However, with the larger ICD, formula (2) predicts a larger number of pixels difference, and thus, a larger stereo depth distortion.

The solution is as follows:

A larger ICD enhances the stereo monitor disparity, and hence the stereo percept of depth for a given physical separation of two objects in space. Thus the depth difference between the FPP and the Vieth-Mueller circle is enhanced. Calculations for two bars 15 cm apart in the FPP, aligned off-center by 5.5 cm, and for three typical ICDs are presented in Table 1.

353

Table 1

Pixel Characteristics of Depth Distortion of Converged Cameras at Three Intercamera Distances

ICD	Depth (FPP to V.-M. C.)	Depth / pixel diff	# pixels
16 cm	1.277 cm	0.515 cm	< 2.5
38 cm	1.255 cm	0.219 cm	> 5.7
60 cm	1.217 cm	0.141 cm	> 8.6

Table 1 shows that by increasing the ICD by a factor of 3.75, (i.e., 60cm/16cm), we enhance the depth signal (number of pixels difference) by a factor of more than 3.4, (i.e., 8.6/2.5), even though the actual distance a bar would have to move from the FPP to reach a location of 0 disparity would be smaller.

The detection of a depth difference is a threshold phenomenon. The number of pixels difference must exceed the threshold, or no depth difference will be perceived. For the purposes of this discussion, let us assume a threshold of two pixels difference. Table 1 shows that for the 16 cm ICD, two pixels difference would represent 1.030 cm of depth. For the 60 cm ICD, two pixels would represent only 0.242 cm of depth.

If one bar were located in the FPP and a horizontal distance, k, from the camera convergence point, and a second bar were located at the camera convergence point, then the distance the first bar would have to be moved foward in order to lose the percept that it is behind the second bar is a measure of the depth distortion of the FPP.

For the 16 cm ICD, the first bar need only be moved 0.247 cm, (i.e., 1.030 cm behind the Vieth-Mueller circle,) and the observers would not see it as behind the second bar. However, for the 60 cm ICD, the first bar would have to be moved foward 0.933 cm (i.e., 0.284 cm behind the Vieth-Mueller circle,) before the observers would no longer see it behind the second bar. Clearly, the 60 cm ICD camera configuration will suffer more distortion than the 16 cm ICD configuration.

The stereo depth resolution for the 60 cm ICD configuration will be higher than for the 16 cm ICD configuration. This is because, with the 60 cm ICD, the first bar need be moved a shorter depth distance before the number of pixels difference changes, than with the 16 cm ICD. For example, with the 60 cm ICD, the first bar would be perceived at equal depth with the second bar when it is anywhere between 0.284 cm behind and 0.284 cm in front of the Vieth-Mueller circle. With the 16 cm

ICD, the first bar would be perceived at equal depth with the
second bar when it is anywhere between 1.030 cm behind and
1.030 cm in front of the Vieth-Mueller circle. Thus when
attempting to measure the perceived depth distortions, observers
would be expected to be more certain of their perceptions of
depth with the 60 cm ICD.

The conclusion here should be stressed. The larger ICDs
produce higher depth resolutions, but at the expense of
producing greater depth distortions. Thus with larger ICDs,
we expect the operator to make larger depth errors (because of
the greater distortions), and to be more certain that they are
not errors (because of the higher resolution).

Dynamic Depth Distortions
- -

In order to inspect the work space horizontally by
moving the cameras, one can either translate (as shown in Figure
4) or pan (as shown in Figure 5) the cameras. Any other
horizontal motion can be described as a combination of these two
Motion of either type will cause additional distortion, which we
shall call dynamic depth distortion. By comparing Figure 4 with
Figure 5, it can be seen that the depth difference, dL-dR, is
smaller in Figure 5. This is because the rotated Vieth-Mueller
circle is closer to the left bar and further from the right bar,
than the translated Vieth-Mueller circle. The camera
configurations are otherwise identical, and therefore the depth
per pixel difference (and stereo depth enhancement) will be the
same in both configurations. We therefore expect that panning
the cameras will produce less depth distortion than horizontally
translating the cameras.

All of the above predictions of the geometric analysis were
tested with four human observers under controlled laboratory
conditions.

Figure 4. Depth distortion between 2 bars as stereo camera pair is translated to the right. The left bar must be moved distance dL - dR to be equidistant behind the Vieth-Mueller circle, with the right bar. Those points on the Vieth-Mueller circle which are visible to the cameras present 0 pixels difference to the monitor screen.

Figure 5. Depth distortion between 2 bars as stereo camera pair is panned to the right. Note: dL - dR is smaller here than in Figure 4.

356

3. THE EXPERIMENTS

EQUIPMENT

Two black vertical rods (0.9 cm diameter) were viewed at 1.3 meters distance by a stereo pair of RCA TC1004 videcon cameras with Vicon V17-102M auto-iris, zoom lenses. A plain white background was located about 2 meters behind these test bars. The background gave no depth cues. All non-stereo depth cues were minimized. For example, the size cue (closer bars appear larger) was minimized by adjusting the cameras and bar motions so that the tops of the bars always appeared at the same height on the monitor. The bottoms of the bars were not visible on the monitor. Thus closer bars did not appear taller. The focus cue (sharply focused bars appear closer) was minimized by limiting bar motions so that no bar ever appeared out of focus.

Stereo images were presented via a Honeywell field-sequential PLZT Stereo Viewing System, through a Dynair series 10 video switcher, to a 19" Toshiba 'Blackstripe' color shadow-mask monitor. The monitor has 600 horizontal pixels (triads) per line, and was the limiting factor in horizontal resolution. The shadow mask monitor breaks the screen into 600 discrete image windows. Thus, our system optically and mathematically emulates a system with CCD cameras.

The right bar was mounted on a tripod, and did not move during the experiment. The left bar was mounted on a Unimate Puma 560 robot arm. An IBM/AT Personal Computer was used to control the experiment and collect the data. Parallel ports and co-axial switches were used to enable the computer to turn on and off the information flow to the viewing monitor. When the co-axial switches were turned off, the viewing monitor appeared blank. The monitor was blanked to prevent the observers from seeing any motion of the test bars.

The two TV cameras were mounted on a precision-machined, stereo-camera mounting apparatus which could be manually adjusted to move both cameras symmetrically about the viewing axis. The stereo pair of cameras could be manually translated horizontally, precisely perpendicular to the viewing axis, or they could be panned (rotated) about a point between the cameras. See Figure 6

A computer keyboard was masked off so that only the top row keys 1, 2, 3, 4, and 5 could be depressed. The computer read this keyboard through a serial port. This keyboard and the stereo monitor were set up in a control room where the experimental observers sat. Observers sat with their eyes about 75 cm from the stereo TV monitor. They could not see the experimental bars directly from the control room. See Figure 7.

A 20-line/inch removable transparent plastic grid was fitted to the monitor screen to aid in the precision alignment of the cameras. The grid was not present during experimentation.
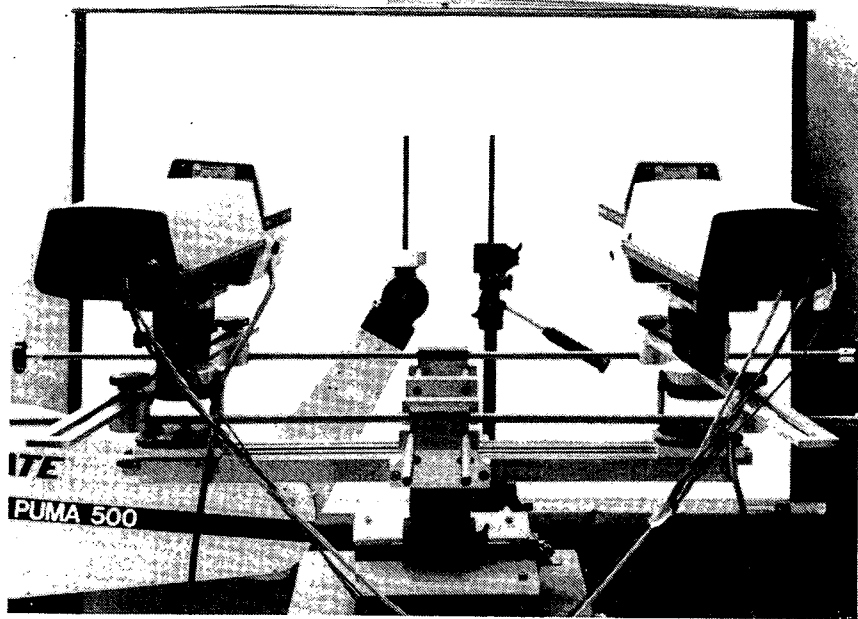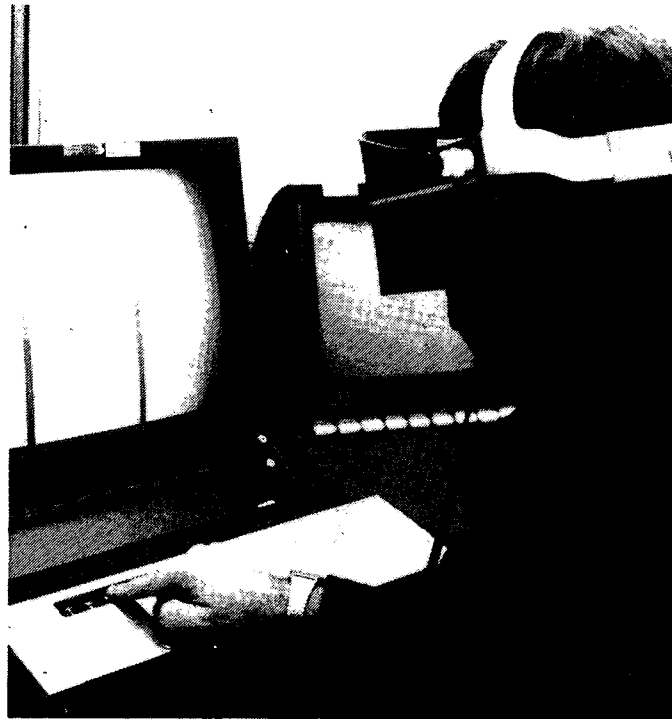
Figure 6. Experimental workspace.

Figure 7. Experimental control room.

PROCEDURE

In experiment 1,we tested three ICD's of 16, 38 and 60 cm, and five locations of the camera convergence point in the FPP, for each ICD. The two test bars were separated horizontally by 15 cm, and presented in the FPP.

The curvature of the apparent fronto-parallel plane (AFPP) can be measured by placing the right test bar in several locations of the FPP, maintaining a fixed horizontal ITD, and determining the location of the left test bar that appears equal in depth. To do this, the left bar was moved by the robot arm to one of 19 test locations located on a line perpendicular to the plane of convergence, and parallel to the axis of symmetry between the cameras. See Figure 8. These locations were numbered 0 to 18, with location 9 in the plane of convergence. Locations 0 to 18 were -6.0, -5.0, -4.0, -3.0, -2.5, -2.0, -1.5, -1.0, -0.5, 0.0, 0.5, 1.0, 1.5, 2.0, 2.5, 3.0, 4.0, 5.0, and 6.0 cm from the plane of convergence, where negative values are behind the plane of convergence and positive values are in front of the plane of convergence. By "in front", we mean closer to the cameras.

The left bar was presented at each of these 19 locations five times in random order.

The experimental observers were instructed to report their perceptions of relative depth as follows:

"1" if the left bar is surely in front of the right bar
"2" if the left bar is probably in front of the right bar
"3" if the the observer is not sure which bar is closer
"4" if the left bar is probably behind the right bar
"5" if the left bar is surely behind the right bar.

In addition, if the observer perceived the bars at equal depth, he/she was instructed to report "3".

We actually moved the cameras horizontally, instead of moving the bars horizontally. These two procedures are optically and mathematically identical. The five horizontal camera alignments tested for each ICD were, in this order, 0.0, 5.5, -5.5, -3.0, and 3.0 cm. Positive numbersmeanthe cameras were movedtotheleft. Thus positive numbers mean the images were moved to the right on the monitor.
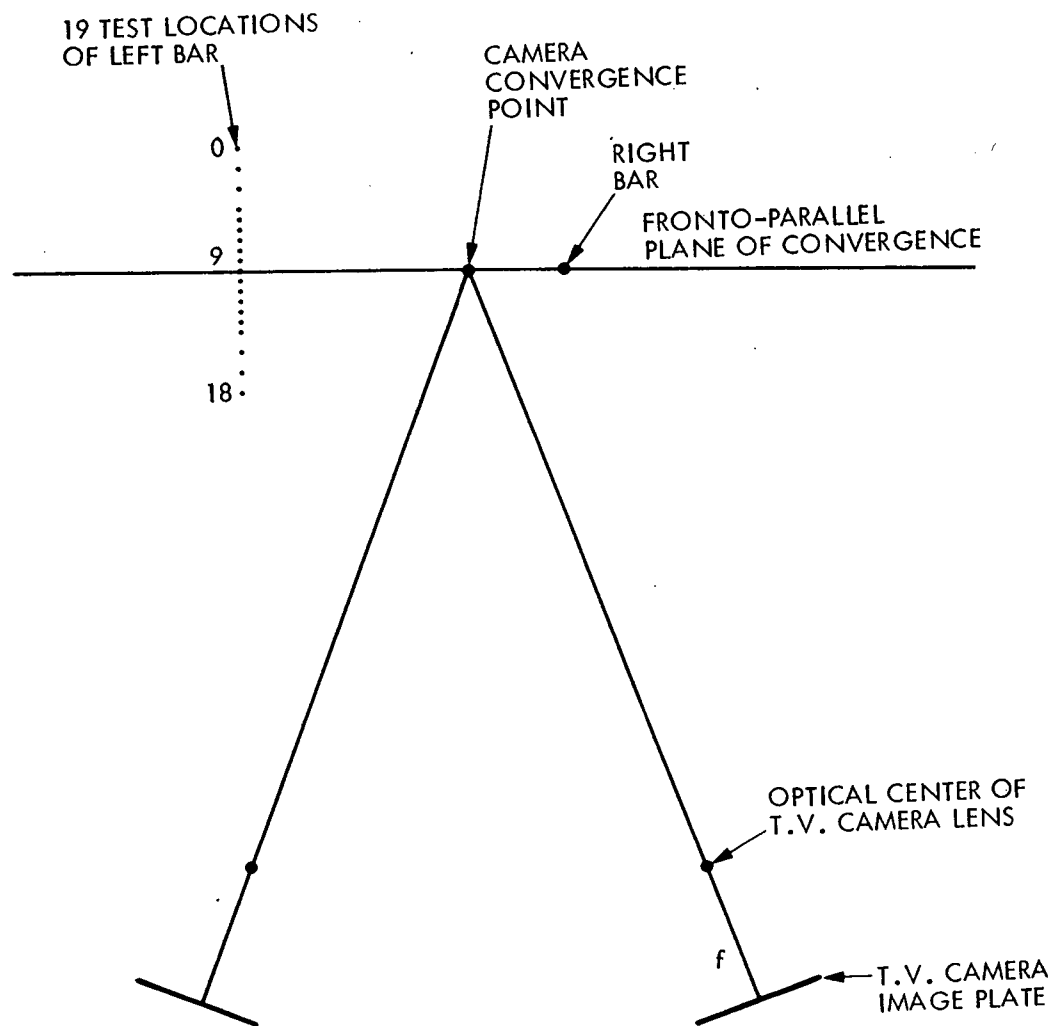
The experiment proceeded as follows.

Figure 8. Experimental set-up showing the fixed right bar and the 19 possible test locations of the movable left bar.

The cameras were adjusted to the first ICD, and aligned at
0.0 cm. This proved to be a delicate task. We therefore
normalized our data to control for possible adjustment
inaccuracies. This is discussed below. The bars were placed in
the plane of convergence (i.e., the right bar in its place, and
the left bar at position 9). The alignment grid was placed on
the monitor screen to measure the distance between the images of
the two bars. The cameras were aligned so that each camera
presented the same distance between the images of the two bars to
the monitor. The adjustment grid was then removed.

The observer was seated in the control room and was asked to
don the stereo visor. The experimental run then started.

The computer blanked the monitor screen. The robot moved
the left bar to a randomly selected test location. After 2
seconds, the computer presented the stereo image to the monitor
screen and then waited for the response from the keyboard.

The observer viewed the monitor screen until reporting a
response by pressing a key ("1" to "5").

The computer recorded the response, blanked the screen, and
selected the next test location. The experiment continued until
all 19 locations had been presented 5 times each.

At this point, the screen was blanked for 9 seconds, the
left bar was moved to position 9, the data was printed out
(see Figure 9), and the experimenter was informed that the run
had been completed.

The observer left the room without seeing the experimental
setup. The experimenter moved the cameras horizontally to the
next alignment, and the observer re-entered the control room.

After the 5 alignments had been tested, the observer rested
for 15 minutes while the experimenter adjusted the cameras to
the next ICD. A maximum of 10 experimental runs (2 ICDs with 5
alignments) was run each day on any one observer. Usually, only
5 experimental runs (1 ICD) were run per observer per day. The
total time for 5 runs, including adjusting time, was about 25-40
minutes per observer.

As discussed later, each ICD was tested twice, in the
following counterbalanced order:

16, 38, 60, 60, 38, 16 cm.

EXPERIMENT 2

In experiment 2, the stereo cameras were rotated about a
point between the cameras, instead of translated, as in
experiment 1. Otherwise, experiments 1 and 2 were identical.

361

4. DATA ANALYSIS

For each experimental run, we computed an observed depth distortion and a measure of the observer's uncertainty of that distortion. The calculation procedures are detailed in Figures 9 and 10 and Appendix 2.

Tables 2 and 3 show the computed distortions and uncertainties for experiments 1 and 2 respectively.

Next, we normalized the computed distortions and uncertainties to the 0.0 cm camera alignment value. This controlled for initial adjustment inaccuracies and enabled us to better see the effects of the camera alignments at each ICD. In other words, the data were shifted to the 0.0 cm aligned position as origin. Quite simply, for each experimental run, we subtracted the measured depth distortion of the 0.0 cm aligned position from all the measured depth distortions of that run. We adjusted the uncertainty values accordingly. These shifted data are presented in Tables 4 and 5 for experiments 1 and 2 respectively.

Our geometric analysis predicts the main independent variable to be the product of ICD and image alignment, which we shall call MTERM. In order to test if our observers' responses followed the predictions of the geometric analysis, an analysis of variance of the data in Tables 2 through 5 (both shifted and non-shifted data) was performed using the Statistical Package for the Social Sciences (SPSS) Regression program. This analysis was performed with the following 4 combinations of independent variables:

ICD and image alignment (ALIGNMENT)
ICD, ALIGNMENT and observer (OBSERVER)
MTERM, ICD, and ALIGNMENT
MTERM, ICD, ALIGNMENT and OBSERVER.

STEREO VISION IN TELEOPERATION

EXPERIMENT 1

Measured Distortion & Corresponding Uncertainty
for
Intercamera Distances of 16cm, 38cm, and 40cm. Alignments A=aligned, B=far right, C=far left, D & E=midpoints left and right resp.

OBSERVER	1		2		3		4	
16cm RUN	1	4	1	4	1	4	1	4
C	.10 +- .322	-1.10 +- .169	-.50 +- .325	-1.05 +- .135	1.45 +- .177	.35 +- .205	1.25 +- .122	.65 +- .071
D	.05 +- .351	-1.45 +- .164	-.20 +- .336	-.95 +- .160	1.15 +- .168	.15 +- .168	.90 +- .124	.90 +- .119
A	-.36 +- .267	-1.35 +- .170	.75 +- .384	-1.35 +- .148	.20 +- .153	-.10 +- .167	.35 +- .164	-.25 +- .075
E	-.60 +- .402	-.45 +- .200	-.65 +- .233	-1.30 +- .205	.25 +- .190	-.35 +- .184	.65 +- .120	.05 +- .087
B	.36 +- .292	-.65 +- .232	1.35 +- .312	-1.05 +- .238	-.15 +- .156	-1.00 +- .174	.60 +- .081	.15 +- .122

38cm	2	1	5	2	1	5	2	1	5	2	1	5
C	.70 +- .249	.25 +- .180	.15 +- .191	.30 +- .133	2.15 +- .135	1.00 +- .153	2.30 +- .108	.85 +- .071
D	1.15 +- .198	-.60 +- .210	-.20 +- .245	-.30 +- .170	1.95 +- .167	.70 +- .155	1.80 +- .053	.75 +- .000
A	-.05 +- .266	-.85 +- .168	-1.20 +- .237	-.70 +- .119	.95 +- .139	.00 +- .088	.80 +- .053	-.05 +- .087
E	.35 +- .264	-1.10 +- .210	-1.73 +- .213	-1.45 +- .148	.50 +- .151	-.95 +- .189	.60 +- .053	-.30 +- .053
B	.15 +- .247	-.95 +- .190	-1.75 +- .254	-1.30 +- .141	.25 +- .125	-1.00 +- .088	.60 +- .113	-.55 +- .125

60cm	3	1	4	3	1	4	3	1	4	3	1	4
C	1.00 +- .234	.30 +- .217	.60 +- .323	1.70 +- .286	1.45 +- .120	1.00 +- .088	1.05 +- .087	1.25 +- .010
D	1.05 +- .218	.13 +- .210	.25 +- .232	-.65 +- .233	1.65 +- .120	.55 +- .103	1.00 +- .088	.75 +- .000
A	.85 +- .205	-.05 +- .194	-.25 +- .211	-.25 +- .164	.95 +- .103	1.00 +- .088	1.25 +- .000	.35 +- .071
E	.20 +- .188	-.70 +- .198	-.35 +- .181	-.70 +- .179	.00 +- .088	-.85 +- .120	-.05 +- .088	-.30 +- .088
B	-.05 +- .212	-.90 +- .191	-1.10 +- .256	-.95 +- .177	-.45 +- .103	-1.00 +- .088	.05 +- .100	-.35 +- .071

Table 2. Measured distortions and corresponding uncertainties of experiment 1 for four observers. Note the counterbalanced order of presentation. For example, the first two columns are data for Observer 1. Runs 1, 2, and 3 (down the first column) were followed by runs 4, 5, and 6 (up the second column).

STEREO VISION IN TELEOPERATION

EXPERIMENT 2

Measured Distortion & Corresponding Uncertainty
for
Intercamera Distances of 16cm, 38cm, and 40cm. Alignments A=aligned, B=far right, C=far left, D & E=midpoints left and right resp

OBSERVER	1		2		3		4	
16cm RUN	1	4	1	4	1	4	1	4
C	-1.40 +- .174	-.16 +- .166	-1.58 +- .194	-1.40 +- .151	-.25 +- .170	-.70 +- .201	.30 +- .119	.20 +- .108
D	-1.15 +- .192	-.70 +- .129	-1.65 +- .223	-1.60 +- .149	-.35 +- .197	-.15 +- .190	.55 +- .007	.25 +- .100
A	-.95 +- .144	-1.05 +- .112	-1.70 +- .108	-1.75 +- .194	-.35 +- .173	-.35 +- .184	.15 +- .112	.20 +- .053
E	.30 +- .155	-.75 +- .141	-.55 +- .200	-1.05 +- .156	-.40 +- .161	-.05 +- .211	.50 +- .086	.75 +- .075
B	.05 +- .226	.15 +- .158	-.30 +- .163	-1.22 +- .220	-.65 +- .200	-.15 +- .217	.60 +- .081	1.10 +- .081

38cm	2	1	5	2	1	5	2	1	5	2	1	5
C	.15 +- .112	-.45 +- .087	-.35 +- .244	-.35 +- .135	.50 +- .145	.10 +- .113	.45 +- .007	.55 +- .087
D	-.05 +- .087	-.30 +- .119	.25 +- .123	-.95 +- .152	.25 +- .125	-.05 +- .103	.25 +- .000	.60 +- .081
A	-.60 +- .143	-.50 +- .088	.05 +- .107	-.65 +- .071	.05 +- .125	-.25 +- .125	.10 +- .081	.20 +- .053
E	.15 +- .146	.00 +- .108	-.10 +- .081	-.90 +- .129	-.05 +- .148	-.25 +- .135	.10 +- .081	.50 +- .088
B	.70 +- .130	-.55 +- .132	.25 +- .214	-1.15 +- .103	-.25 +- .125	-.50 +- .116	-.25 +- .000	.10 +- .102

60cm	3	1	4	3	1	4	3	1	4	3	1	4
C	.35 +- .112	-.10 +- .124	-.05 +- .113	.05 +- .097	.45 +- .125	-.50 +- .124	.95 +- .087	.75 +- .000
D	.15 +- .071	-.25 +- .141	-.25 +- .120	-.40 +- .088	.20 +- .124	.35 +- .112	.45 +- .087	.80 +- .088
A	.30 +- .131	-.35 +- .112	-.50 +- .108	-.40 +- .088	.05 +- .103	.05 +- .103	.20 +- .053	.20 +- .053
E	-.20 +- .088	-.25 +- .156	-.65 +- .171	-.35 +- .139	-.45 +- .125	-.20 +- .124	.45 +- .087	.55 +- .071
B	.40 +- .113	.35 +- .112	-.85 +- .075	-.70 +- .053	-.55 +- .138	-.35 +- .120	.05 +- .087	-.05 +- .087

Table 3. Measured distortions and corresponding uncertainties of experiment 2 for four observers.

EXPERIMENT 1

Measured Distortion & Corresponding Uncertainty
for
Intercamera Distances of 16cm, 38cm, and 60cm. Alignments A=aligned, B=far right, C=far left, D & E=midpoints left and right resp.

SHIFTED TO ALIGNED POSITION AS ORIGIN

OBSERVER	1		2		3		4	
16cm RUN	1	6	1	6	1	6	1	6
C	.40 +- .418	.25 +- .240	-1.25 +- .503	.30 +- .200	1.25 +- .234	.45 +- .266	.90 +- .204	.90 +- .103
D	.43 +- .441	-.10 +- .236	-.95 +- .510	.40 +- .216	.95 +- .227	.25 +- .237	.55 +- .206	1.15 +- .141
A	.00 +- .000	.00 +- .000	.00 +- .000	.00 +- .000	.00 +- .000	.00 +- .000	.00 +- .000	.00 +- .000
E	-.22 +- .463	.90 +- .262	-1.40 +- .449	.05 +- .233	.05 +- .244	-.45 +- .248	.30 +- .203	.30 +- .115
B	.74 +- .396	.70 +- .288	.60 +- .495	-.50 +- .280	-.55 +- .219	-.90 +- .241	.25 +- .163	.40 +- .143

38cm	2	1	2	1	2	1	2	1
C	.75 +- .366	1.10 +- .246	1.35 +- .304	1.00 +- .178	1.20 +- .194	1.00 +- .159	1.50 +- .120	.90 +- .112
D	1.20 +- .332	.25 +- .269	1.00 +- .341	.40 +- .208	1.00 +- .233	.70 +- .178	1.00 +- .075	.80 +- .087
A	.00 +- .000	.00 +- .000	.00 +- .000	.00 +- .000	.00 +- .000	.00 +- .000	.00 +- .000	.00 +- .000
E	.40 +- .389	-.25 +- .269	-.53 +- .391	-.75 +- .190	-.45 +- .205	-.95 +- .208	.00 +- .075	-.25 +- .102
B	.20 +- .365	-.10 +- .254	-.55 +- .347	-.64 +- .185	-.70 +- .167	-1.00 +- .124	-.20 +- .125	-.50 +- .152

60cm	3	4	3	4	3	4	3	4
C	.15 +- .311	-.35 +- .291	.85 +- .386	1.95 +- .331	.70 +- .158	.00 +- .124	-.20 +- .087	.90 +- .072
D	.20 +- .299	.18 +- .286	.50 +- .314	-.38 +- .285	.70 +- .158	-.45 +- .135	-.25 +- .088	.40 +- .071
A	.00 +- .000	.00 +- .000	.00 +- .000	.00 +- .000	.00 +- .000	.00 +- .000	.00 +- .000	.00 +- .000
E	-.65 +- .278	-.65 +- .277	-.10 +- .278	-.45 +- .243	-.95 +- .135	-1.85 +- .149	-1.30 +- .088	-.85 +- .113
B	-.90 +- .295	-.85 +- .272	-.95 +- .333	-.68 +- .241	-1.40 +- .146	-2.00 +- .124	-1.20 +- .100	-.70 +- .100

Table 4. Measured distortions and corresponding uncertainties shifted to the 0.0 cm aligned position as origin. Data from experiment 1.

EXPERIMENT 2

Measured Distortion & Corresponding Uncertainty
for
Intercamera Distances of 16cm, 38cm, and 60cm. Alignments A=aligned, B=far right, C=far left, D & E=midpoints left and right resp

SHIFTED TO ALIGNED POSITION AS ORIGIN

OBSERVER	1		2		3		4	
16cm RUN	1	6	1	6	1	6	1	6
C	-.45 +- .226	.89 +- .212	.12 +- .224	.35 +- .246	.10 +- .243	-.35 +- .273	.15 +- .163	.00 +- .120
D	-.20 +- .240	.35 +- .185	.05 +- .248	.15 +- .245	.00 +- .262	.20 +- .264	.40 +- .142	.05 +- .113
A	.00 +- .000	.00 +- .000	.00 +- .000	.00 +- .000	.00 +- .000	.00 +- .000	.00 +- .000	.00 +- .000
E	1.25 +- .212	.30 +- .193	1.15 +- .227	.70 +- .246	-.05 +- .236	.30 +- .280	.35 +- .142	.55 +- .092
B	1.00 +- .268	1.20 +- .206	1.40 +- .196	.53 +- .293	-.30 +- .264	.20 +- .285	.45 +- .138	.90 +- .097

38cm	2	1	2	1	2	1	2	1
C	.75 +- .182	.05 +- .124	.30 +- .307	-.30 +- .153	.45 +- .191	.55 +- .169	.35 +- .119	.35 +- .102
D	.55 +- .167	.20 +- .148	.20 +- .225	-.30 +- .168	.20 +- .177	.20 +- .162	.15 +- .081	.40 +- .097
A	.00 +- .000	.00 +- .000	.00 +- .000	.00 +- .000	.00 +- .000	.00 +- .000	.00 +- .000	.00 +- .000
E	.75 +- .204	.50 +- .139	-.15 +- .204	-.25 +- .147	-.10 +- .194	.00 +- .184	.00 +- .115	.30 +- .103
B	1.30 +- .199	-.05 +- .159	.20 +- .284	-.50 +- .125	-.30 +- .177	-.25 +- .171	-.35 +- .081	-.10 +- .115

60cm	3	4	3	4	3	4	3	4
C	.05 +- .174	.25 +- .181	.45 +- .158	.45 +- .151	.40 +- .162	-.35 +- .161	.75 +- .102	.55 +- .053
D	-.15 +- .151	.10 +- .193	.25 +- .161	.00 +- .124	.15 +- .161	.30 +- .152	.25 +- .102	.60 +- .103
A	.00 +- .000	.00 +- .000	.00 +- .000	.00 +- .000	.00 +- .000	.00 +- .000	.00 +- .000	.00 +- .000
E	-.50 +- .159	.10 +- .206	-.15 +- .202	.05 +- .165	-.50 +- .162	-.25 +- .161	.25 +- .102	.15 +- .089
B	-.10 +- .175	.70 +- .173	-.35 +- .131	-.30 +- .103	-.60 +- .172	-.40 +- .158	-.15 +- .102	-.25 +- .102

Table 5. Measured distortions and corresponding uncertainties shifted to the 0.0 cm aligned position as origin. Data from experiment 2.
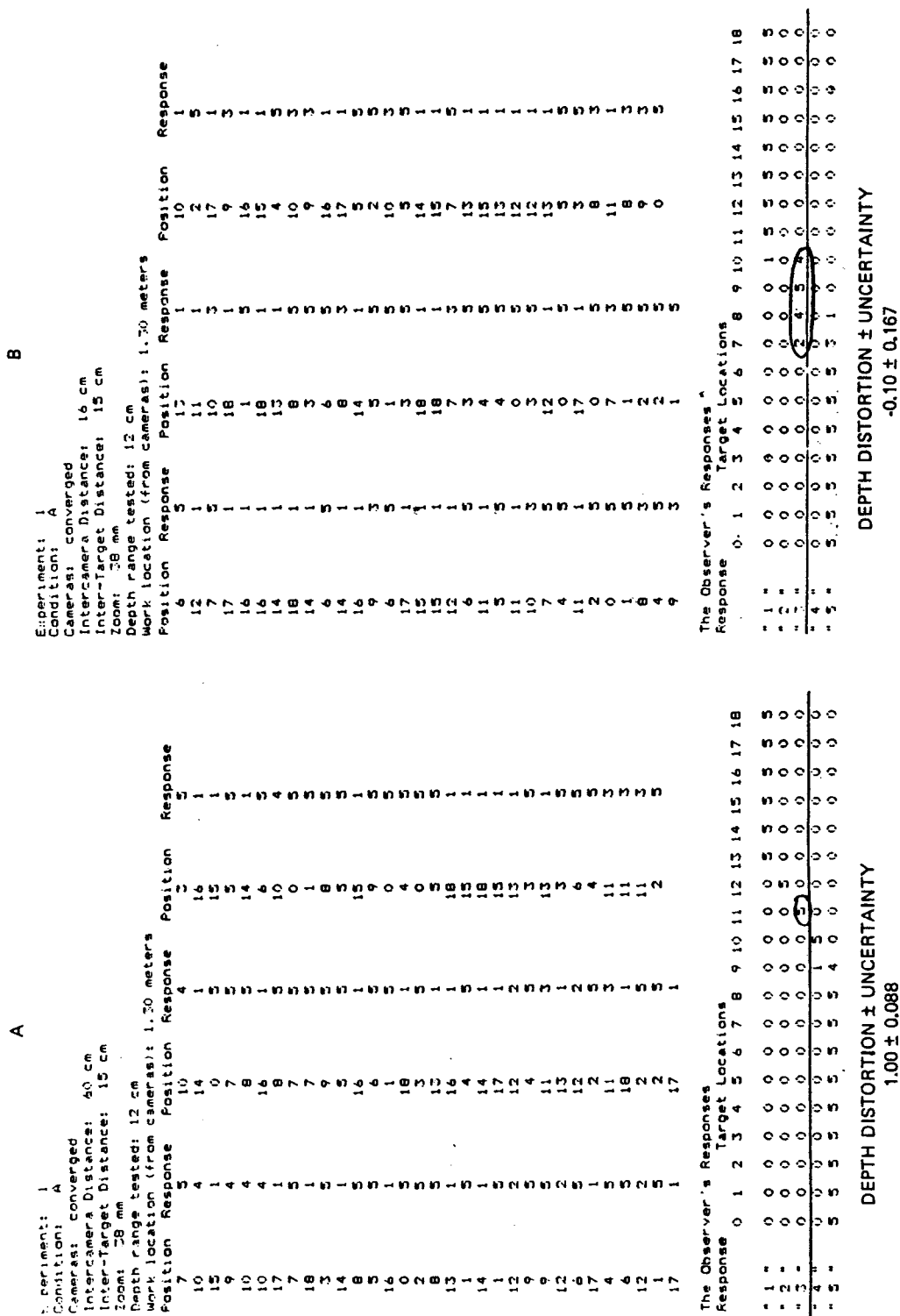
Figure 9. Actual data for two experimental runs of one observer. Data for 60 cm ICD in A. Data for 16 cm ICD in B. Note wider spread of "3" responses (circled) in B, yielding greater estimate of uncertainty.
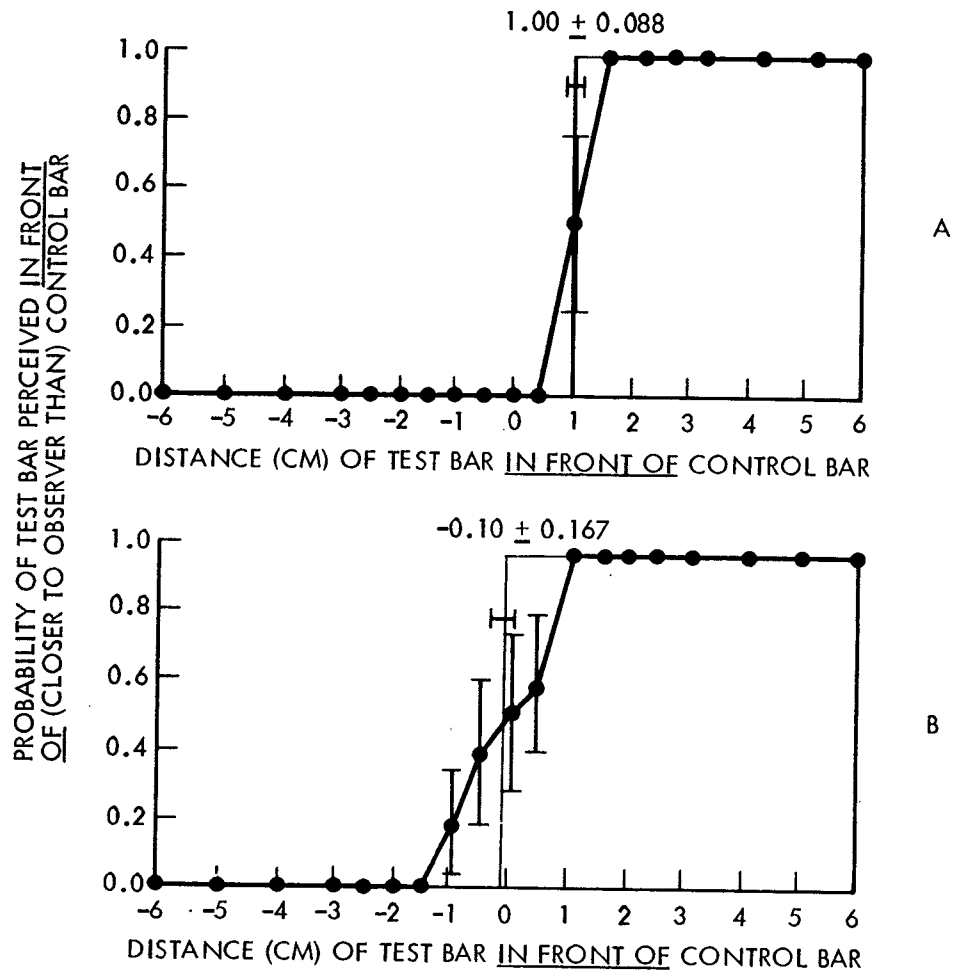
Figure 10. Probability right bar is perceived in front of left bar as a function of distance of right bar in front of left bar. Heavy line shows rectangles of equal area. Measured distortions and corresponding uncertainties were computed from the left edges of the rectangles of equal area. Data from Figure 9.

Table 6

F and p values from Regression Analysis.
Experiment 1, Non-shifted and Shifted Data.

A. Non-shifted					
Independent Variables	Depth Distortions			Uncertainties	
	F	p		F	p
ICD	3.803	<0.05		7.665	<0.001
ALIGNMENT	40.042	<0.001		0.001	NS
ICD	4.716	<0.01		17.975	<0.001
ALIGNMENT	49.649	<0.001		0.002	NS
OBSERVER	29.072	<0.001		158.364	<0.001
MTERM	7.668	<0.001		0.368	NS
ICD	4.020	<0.05		7.624	<0.001
ALIGNMENT	0.077	NS		0.314	NS
MTERM	9.667	<0.001		0.866	NS
ICD	5.068	<0.01		17.954	<0.001
ALIGNMENT	0.097	NS		0.740	NS
OBSERVER	31.244	<0.001		158.181	<0.001
B. Shifted					
Independent Variables	Depth Distortions			Uncertainties	
	F	p		F	p
ICD	11.446	<0.001		3.830	<0.05
ALIGNMENT	83.666	<0.001		0.001	NS
ICD	11.350	<0.001		4.955	<0.01
ALIGNMENT	82.964	<0.001		0.001	NS
OBSERVER	0.018	NS		35.355	<0.001
MTERM	17.265	<0.001		0.116	NS
ICD	13.037	<0.001		3.802	<0.05
ALIGNMENT	0.173	NS		0.092	NS
MTERM	17.119	<0.001		0.150	NS
ICD	12.927	<0.001		4.919	<0.01
ALIGNMENT	0.171	NS		0.119	NS
OBSERVER	0.021	NS		35.096	<0.001

NOTE: p values > 0.05 are reported as NS.

Table 7

F and p values from Regression Analysis.
Experiment 2, Non-shifted and Shifted Data.

A. Non-shifted

Independent Variables	Depth Distortions		Uncertainties	
	F	p	F	p
ICD	11.261	<0.001	28.768	<0.001
ALIGNMENT	0.168	NS	0.051	NS
ICD	14.251	<0.001	35.373	<0.001
ALIGNMENT	0.212	NS	0.063	NS
OBSERVER	32.075	<0.001	27.864	<0.001
MTERM	10.994	<0.001	0.041	NS
ICD	12.223	<0.001	28.532	<0.001
ALIGNMENT	7.927	<0.001	0.007	NS
MTERM	14.288	<0.001	0.050	NS
ICD	15.884	<0.001	35.083	<0.001
ALIGNMENT	10.301	<0.001	0.009	NS
OBSERVER	35.749	<0.001	27.635	<0.001

B. Shifted

Independent Variables	Depth Distortions		Uncertainties	
	F	p	F	p
ICD	8.381	<0.001	8.308	<0.001
ALIGNMENT	0.374	NS	0.006	NS
ICD	8.477	<0.001	8.800	<0.001
ALIGNMENT	2.335	NS	0.006	NS
OBSERVER	0.379	NS	7.937	<0.001
MTERM	27.810	<0.001	0.007	NS
ICD	10.302	<0.001	8.237	<0.001
ALIGNMENT	20.051	<0.001	0.002	NS
MTERM	28.261	<0.001	0.008	NS
ICD	10.489	<0.001	8.725	<0.001
ALIGNMENT	20.376	<0.001	0.002	NS
OBSERVER	2.883	<0.05	7.869	<0.001

NOTE: p values > 0.05 are reported as NS.

368

5. RESULTS

The Depth Distortions

Tables 6 and 7 show the effects of the independent variables on the observers' responses.

In experiment 1 (Table 6), for the non-shifted data, the depth distortions are significantly influenced by the ALIGNMENT, the OBSERVER, and the ICD. When we include MTERM as the first independent variable, the residual effects of ICD and OBSERVER are seen to be significant, although the residual effects of the ALIGNMENT are not. These results agree with Formula (2), which has the term ALIGN*ICD in the numerator and an ICD term in the denominator.

Shifting the data greatly reduces the significance of the effect of OBSERVER and increases the significance of the effect of the other independent variables. This suggests that much of the variability in our unshifted data stems from inaccuracies in our initial adjustments. We repeated the initial adjustment each run so that each observer, each day, may have seen a different initial adjustment. Had the variability in our unshifted data stemmed mostly from the effect of OBSERVER, the significance of the OBSERVER effect would not have been reduced so drastically by shifting the data. All the statements in the above paragraph about MTERM, ALIGN and ICD remain true for the shifted data.

In experiment 2 (Table 7), for the non-shifted data, the depth distortions are significantly influenced by the OBSERVER and the ICD, but not by the ALIGNMENT. When we include MTERM as the first independent variable, the residual effects of ICD, OBSERVER, and also ALIGNMENT, are seen to be significant. Note that the effect of ALIGNMENT is not seen to be significant until MTERM is introduced as the first independent variable. This occurs in both the shifted and non-shifted data, and stands in marked contrast to the results of the same test in experiment 1.

Perhaps image alignment has two cancelling effects in experiment 2. One is an MTERM effect, and one is not an MTERM effect. This makes sense logically, as image alignment here is the result of panning the cameras, thus causing both the MTERM effect of experiment 1 and the cancelling effect of rotating the fronto-parallel plane of convergence. See Figures 4 and 5.

Shifting the data in experiment 2 reduces the significance of the effect of OBSERVER and ICD and increases the significance of the effect of MTERM and ALIGNMENT. This once again suggests that much of the variability in our unshifted data stems from inaccuracies in our initial adjustments.

The depth distortions in experiment 1 were significantly greater than the depth distortions in experiment 2. This can be shown in two ways.

The first way is to simply compare the depth distortions of experiment 1 with those of experiment 2. The SPSS analysis showed the depth distortions to be larger in experiment 1 than in experiment 2 (p < 0.001).

The second way to study the magnitudes of the distortions of experiments 1 and 2 is to compare the difference in observed distortions between the negative and positive 5.5 cm camera alignment test conditions. This data is presented in Table 8, and graphed in Figures 11 and 12, for experiments 1 and 2 respectively.

The SPSS analysis of variance was run on this data, and once again, ICD was found to be a significant factor (p < 0.002 and p < 0.001 for experiments 1 and 2 respectively). The values for experiment 1 were significantly greater than the values for experiment 2, (p < 0.001). Neither ALIGNMENT nor ALIGNMENT*ICD could be tested here as we chose the two most extreme alignments to compare, thus eliminating ALIGNMENT as a variable.

TABLE 8

Statistics of Differences in Perceived Depth Distortions
of the -5.5 cm and 5.5 cm Camera Alignment Test Conditions

Experiment Number	ICD	Group Mean Distortion Difference	Standard Error of the Mean	Regression Co-efficient	F	p
	16	0.29	0.395			
1	38	1.54	0.171	0.5892	12.65	<0.002
	60	1.67	0.202			
	16	-0.57	0.202			
2	38	0.37	0.163	0.6178	14.91	<0.001
	60	0.48	0.168			
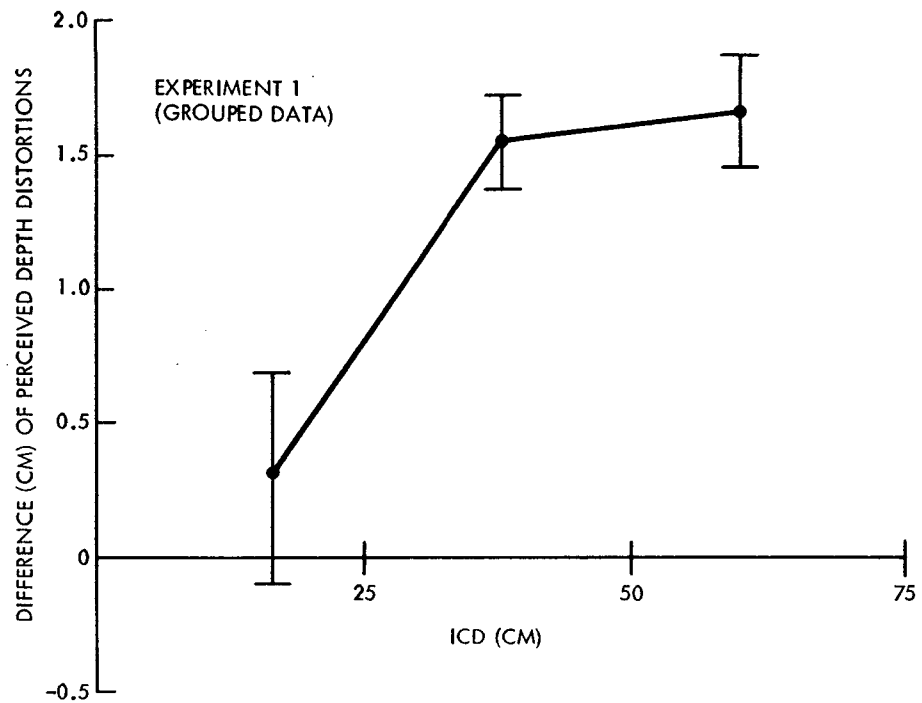
Figure 11. Difference in perceived depth distortion of the
-5.5 cm and 5.5 cm camera alignment test conditions as a
function of intercamera distance for experiment 1, grouped data.
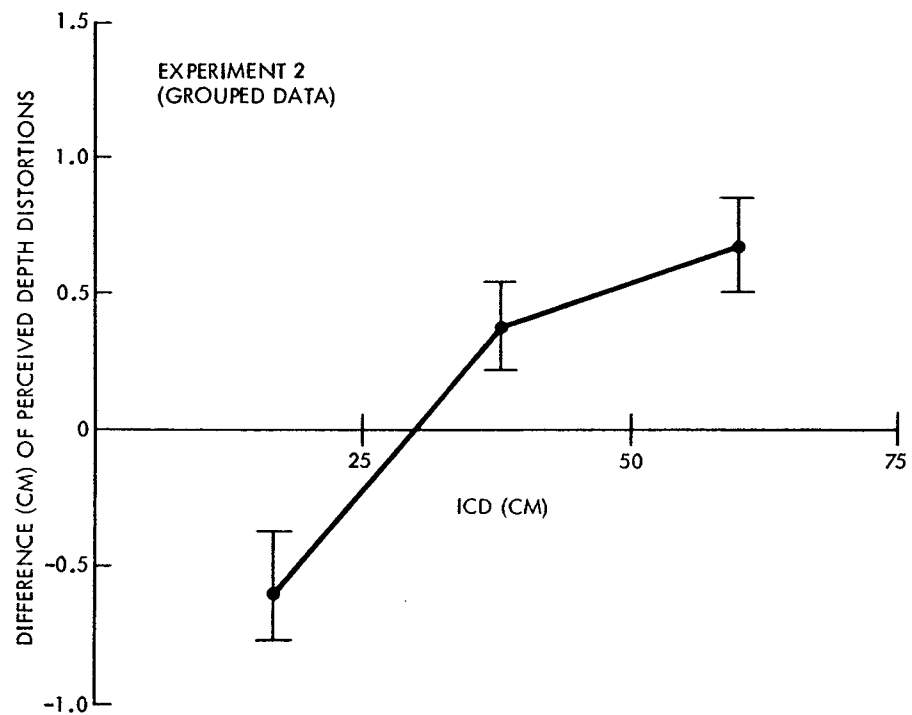
Figure 12. Difference in perceived depth distortion of the
-5.5 cm and 5.5 cm camera alignment test conditions as a
function of intercamera distance for experiment 2, grouped data.

371

The Uncertainties

The computed uncertainties in Tables 2 through 5 relate theoretically to the size of the lozenges in Figure 3, and the depth/pixel difference in Table 1. In Tables 6 and 7, in all cases, ICD and OBSERVER are the only independent variables with significant effects on the uncertainties. Specifically, uncertainty decreases with increasing ICD ($p < 0.007$ and $p < 0.0001$ for experiments 1 and 2 respectively). This agrees with expectation. However, the effect is much smaller than expected.

Table 1 predicts that the measured uncertainty of the 60 cm ICD would be less than 30% of the measured uncertainty of the 16 cm ICD. However, we found the 60 cm ICD uncertainty to be about 70% of the 16 cm ICD uncertainty. This could be due to the double meaning of the response "3", which always contributes to the calculation of the uncertainty, although it is only an uncertain answer some of the time. Specifically, when the bars are truly at the same depth, and the observer so perceives them with absolute certainty, he/she responds "3"; but, our uncertainty statistic computes this as an uncertain response. This artificially increases all the estimates of uncertainty, thus adding a roughly constant amount to all conditions. This may well explain the difference between the expected 30% and the observed 70%.

This problem arose during the actual data collection. The observers asked what response to give when they were sure the bars were at equal depth. We decided they should respond "3" as that would yield an accurate value for the perceived depth distortion. The proper reaction should have been to redesign the response keyboard to allow a separate response button to be pressed. Then both our perceived depth distortions and our uncertainty measures would have been accurate. This shall be done in all future work. Nevertheless, despite this bias against us in our measurement, we have successfully measured a significant drop in uncertainty with increasing ICD.

Time-order effects, including practice, must be considered in experiments of this type. We were able to tease out the time-order effects from the effects of the ICD by counterbalancing the presentation of the ICD tests, (16, 38, 60, 60, 38, 16 cm).

We have plotted the uncertainty values in Figures 13 and 14 for experiments 1 and 2 respectively. An SPSS linear regression analysis was run with time as the only independent variable, and then with ICD as the only independent variable. In experiment 1, time was a factor ($p < 0.0007$) and ICD was a factor ($p < 0.007$). In experiment 2, time was not a factor ($p > 0.40$) but ICD was a factor ($p < 0.0001$). We therefore estimate that the time-order effects, including practice, were completed during experiment 1.

This was not expected, as we allowed our observers to practice for about one hour per day, five days a week, for one month, prior to the start of experiment 1.

In summary, one result of this work is that the criterion of certainty varies between our observers, although the actual depth distortions they perceive do not.

The main result of this work is that the observers' responses follow the geometric predictions of the stereo information (number of pixels difference) on the TV monitor. Thus, the observers' internal corrections and/or distortions do not invalidate the usefulness of our geometric analysis to predict optimal camera configurations.
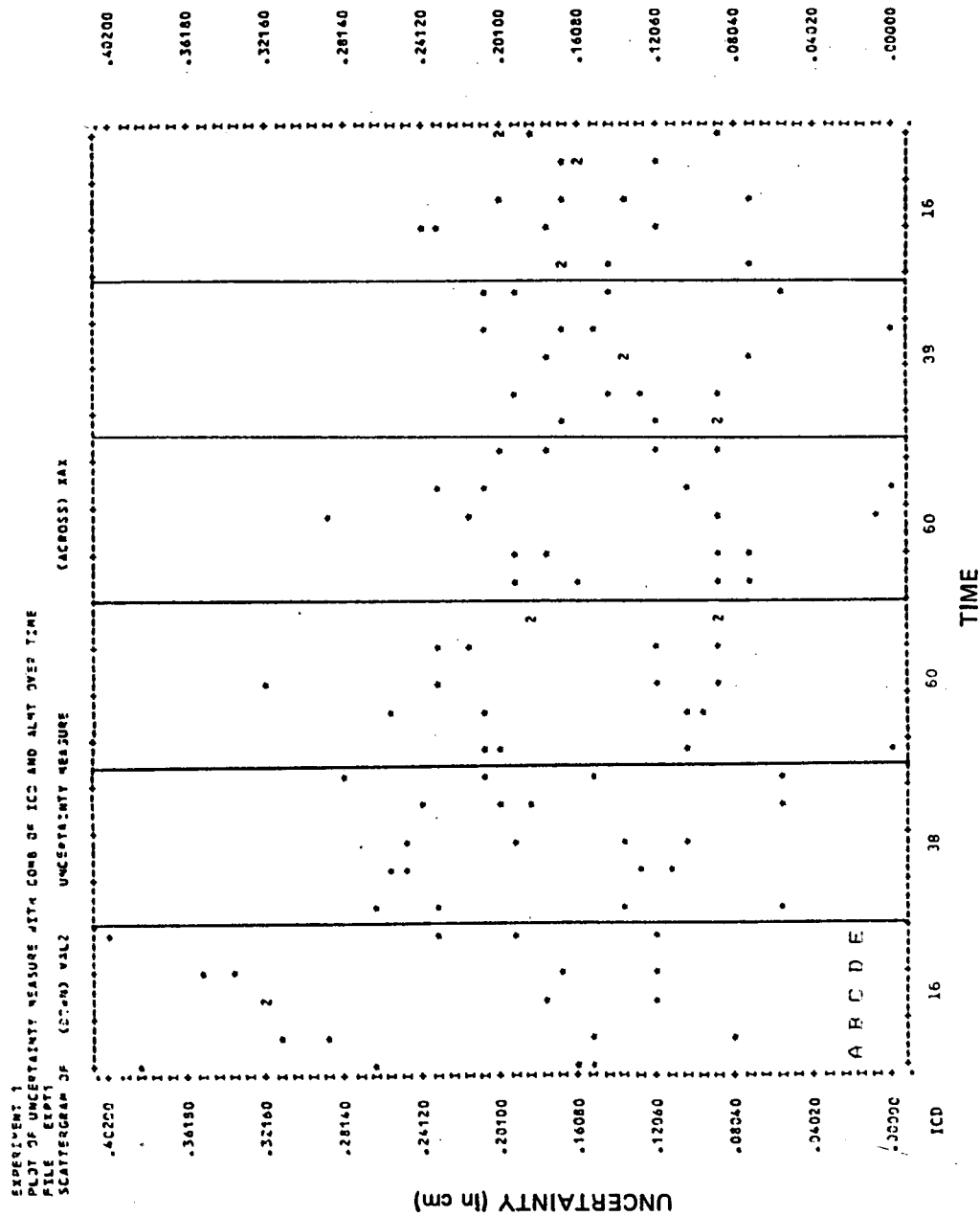
Figure 13. Uncertainty measurements as a function of order of presentation of ICD for experiment 1. Each of the 6 main columns includes 5 minor columns of camera alignments (A = 0.0, B = 5.5, C = -5.5, D = -3.0, and E = 3.0 cm.) Each camera alignment column contains four points, one for each subject's uncertainty measurement. A "2" represents 2 data points at that location.

374
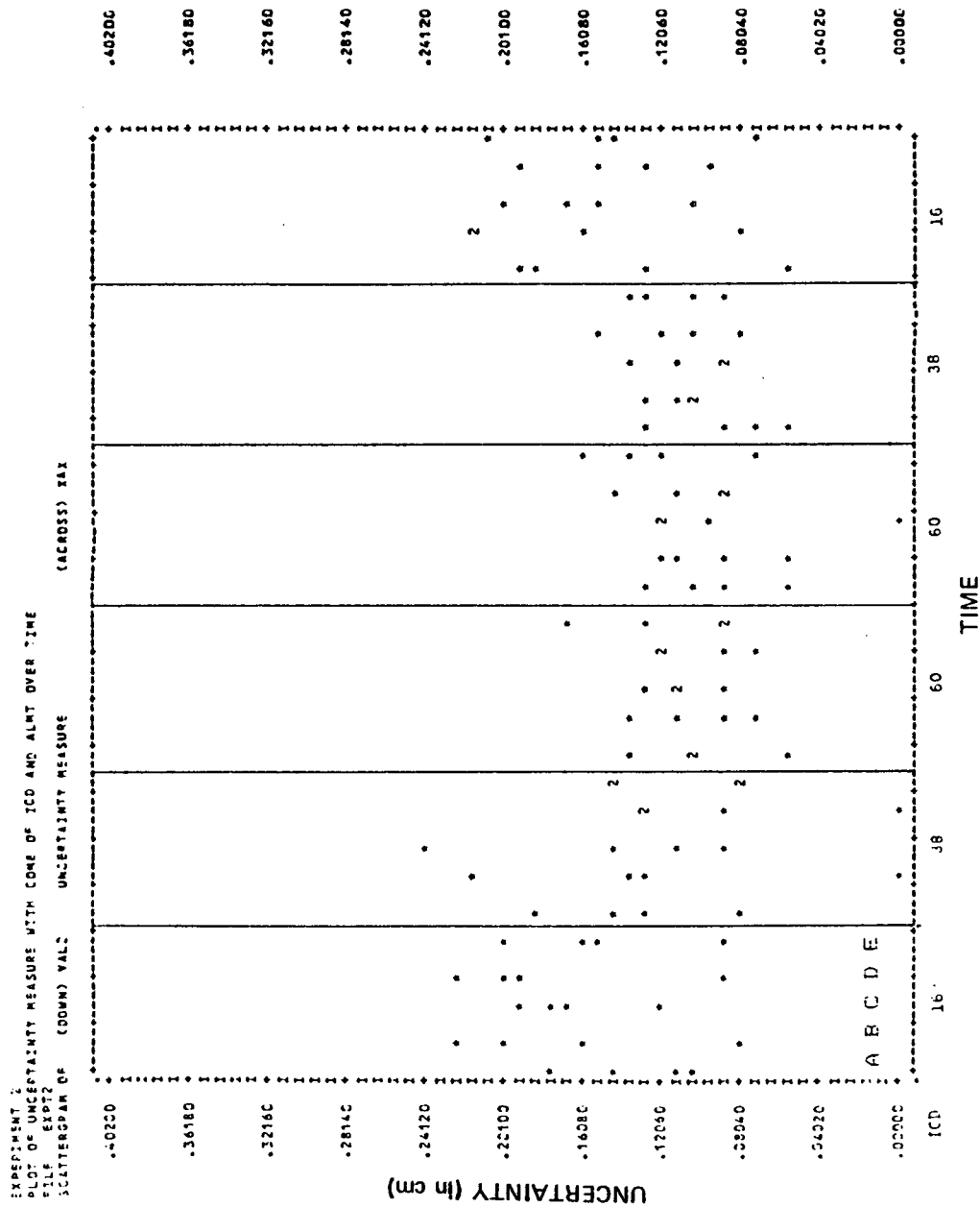
Figure 14. Uncertainty measurements as a function of order of presentation of ICD for experiment 2.

6. DISCUSSION

The stereo depth distortion can be analyzed by breaking it into static and dynamic components. By static, we mean the distortion that is present when we do not move the cameras. It comes from the camera alignment geometry. By dynamic, we mean the change in the static distortion as the stereo camera system scans the work space.

Figure 3 shows the nature of the static stereo depth distortions. Figure 3 represents two CCD cameras converged and viewing a work space. Each lozenge represents the region in space that is seen by a pair of pixels, one on each camera.

In Figure 3, all the shaded lozenges have the same number of pixels difference. Lozenges with equal number of pixels difference will present equal depth cues to the human observer.

The centers of the lozenges with 0 pixels difference lie on a circle. This circle goes through the convergence point and the first nodal points of the lenses of the cameras. We shall refer to it as the Vieth-Mueller circle of the cameras.

Consider now the lozenges of a fixed, non-zero number of pixels difference (for example, 3). The centers of these lozenges lie on a curve. This curve also goes through the centers of the lenses of the cameras. However, this curve and all other curves with a non-zero number of pixels difference are not circles.

Minimization of the Static Depth Distortion

Let us now discuss the $1/D^3$ relation which resulted from Formulas (1) and (2). This shall lead us to a way to greatly minimize static depth distortions without loss of stereo depth resolution.

Let us look at Formula (2). Suppose we viewed one bar at the convergence point, and a second bar at k = ITD. In this case, Formula (2) = Formula (1), (with the exception of the $k^2 * w^2$ term, which we can ignore) because ALIGN = ITD/2. Now let us ask what would happen if we double the viewing distance D, and double the ICD (which of course doubles w), and also double the focal length. In this case, our cameras would now view the work space from the same angle as before the doubling. We leave k unchanged (which of course leaves ITD unchanged), and we converge on the same convergence point (which leaves ALIGN unchanged). What happens to the depth signal at the monitor? In other words, what is the effect on the number of pixels difference?
Formulas (1) and (2) predict the number of pixels difference would be halved. That is, the distortion would be halved.

Let us look at Figure 15. Here we have the two camera configurations in question. We have labelled the cameras Rn, Rf, Ln, and Lf for Right camera in Near configuration, Right camera in Far configuration, etc. We have also drawn two lines parallel to the camera CCD chips which we shall call the lines of equidistant projection. On these lines, every pixel sees a unit length segment of (L/f)*(width/pixel at CCD), where

$$L^2 = D^2 + w^2.$$

Because we doubled D, w and f, for cameras Rf and Lf, every pixel on each of the 4 cameras sees the same size unit length segment for the line of equidistant projection parallel to its CCD chip.

We have labelled the projection points on the corresponding lines of equidistant projection as Rf', Rn', Lf', and Ln'.

Let us first look at the near cameras. Clearly, the length Ln' to C is larger than Rn' to C. The number of pixels difference will be strictly proportional to (Ln' - Rn').

Now let us look at the far cameras. Clearly the length Lf' to C will be less than Ln' to C. Also, the length Rf' to C will be greater than Rn' to C. Thus, the number of pixels difference, which will be proportional to (Lf' - Rf'), is less than (Ln' - Rn').

We have qualitatively shown that the number of pixels difference for the far cameras will be less than for the near cameras. The quantitative demonstration of this is exactly Formulas (1) and (2).

The importance of this point must not be overlooked. By increasing the camera-to-object viewing distance, the ICD, and the focal lengths of the camera lenses, we can maintain image field size and stereo depth resolution, while significantly decreasing the static stereo depth distortion!

Minimization of Dynamic Depth Distortions

We have shown that panning about point A in Figure 16 produces less distortion than translating horizontally. However, it is easy to see theoretically that panning about point B in Figure 17 (the center of the V.-M. circle) should produce hardly any distortion at all. If the curves of equal number of pixels difference were circles with center B, no dynamic distortion at all would be so produced. As is, the only dynamic distortion produced would be the difference between circles with center at B and the actual curves. The center of the Vieth-Mueller circle is less than half the distance between the cameras and the convergence point. For close teleoperation, it would be easy to compute this point and devise a method to pan about it.
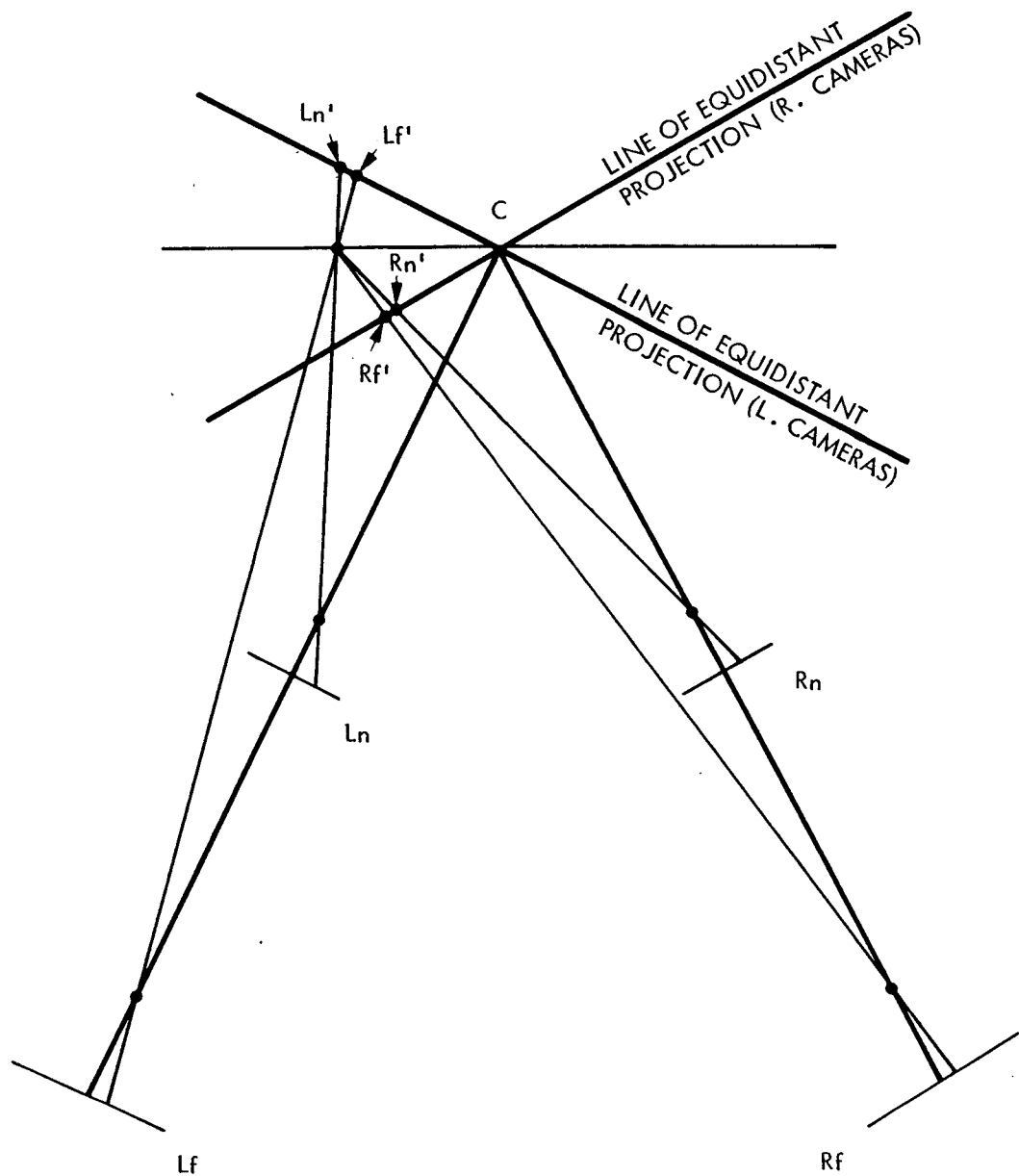
Figure 15. Minimization of static depth distortion. By
doubling the camera-to-object viewing distance, the intercamera
distance and the focal length of the camera lenses, one can
maintain image field size and stereo depth resolution, while
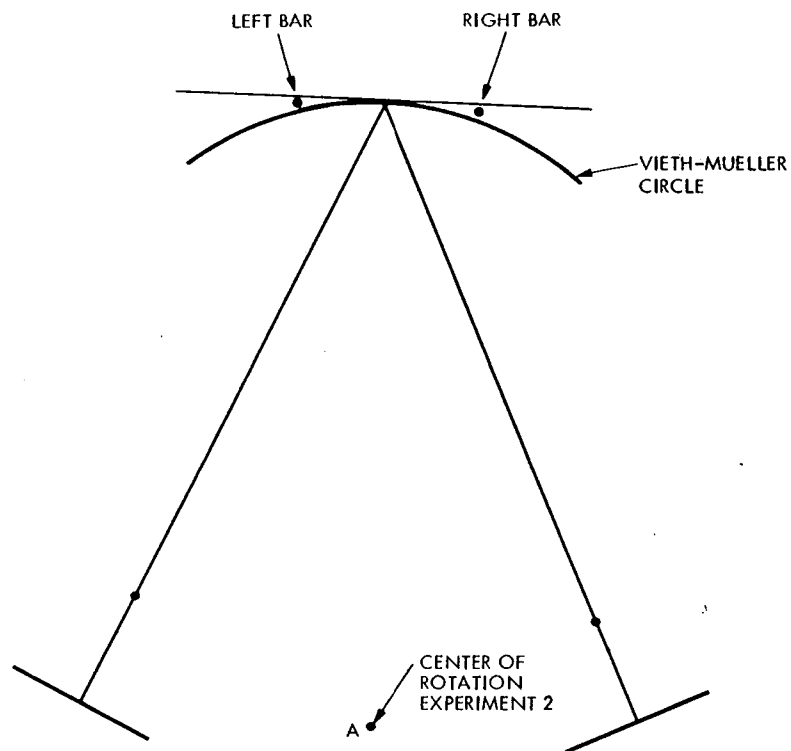cutting the static stereo depth distortion in half.

Figure 16. Partial minimization of dynamic depth distortion. Point A represents the center of rotation for experiment 2.
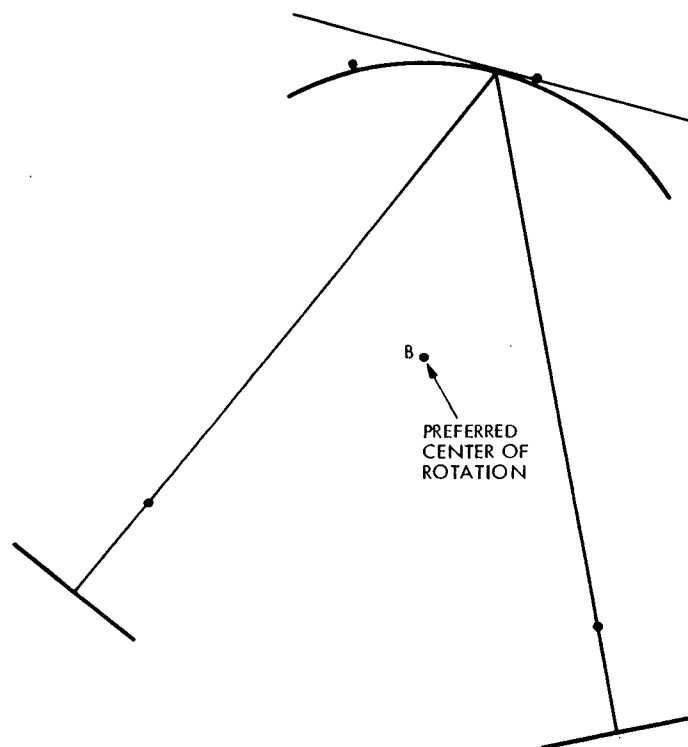

Figure 17. Minimization of dynamic depth distortion. Point B represents the preferred center of rotation, i.e., the center of the Vieth-Mueller circle. Panning the camera pair about this point will minimize dynamic distortion.

7. CONCLUSION

A geometric analysis without small angle approximations has been shown to predict distortions of the FPP which otherwise might not be adequately predicted. These distortions have been demonstrated to be perceived by four human observers.

Our human observers' responses follow the stereo information on the TV monitor. Internal perceptual corrections and/or distortions do not invalidate the usefulness of our geometric analysis to predict optimal camera configurations.

Our analysis predicts that static stereo depth distortion may be greatly decreased, without decreasing the stereo depth resolution, by increasing the camera-to-object viewing distance, the intercamera distance, and the focal length of the TV camera lenses.

Our analysis further predicts that dynamic stereo depth distortion may be greatly reduced by rotating about the center of the Vieth-Mueller circle when panning the stereo cameras.

8. POTENTIAL APPLICATIONS

In the final approach and close-up work of free-flying or stationary teleoperation, stereo TV vision systems may be used to provide necessary depth information.

In order to eliminate the stereo depth distortion errors from teleoperation task performance, a supervised automated system can be built which will adjust the stereo camera configuration on line as the end effector moves through the work space. Different tasks and different people may require different depth resolutions and may tolerate different depth distortions. This may well entail on-line adjustments of the intercamera distance. As the intercamera distance between converged stereo cameras is changed, different distortions of the three spatial axes may be produced. The system should provide the optimal trade-off between stereo depth resolution and stereo depth distortions for a specific task and operator and should automatically adjust the translational axes gains of the hand controller to counteract any remaining visual distortions. For example, if an operator were viewing a meter stick stereoscopically, and the meter stick appeared to be curved convexly away from the operator, the operator need move the hand controller along an identical convex curve, and the end effector would move along the surface of the truly uncurved meter stick.

This translational axes gain adjustment technique has been employed in stereo microscopes with joystick-driven micro-surgery tools, and has demonstrated remarkable improvement in the performance of trained personnel. (D. H. Fender, personal communication.)

Other adjustment or compensation procedures are also possible.

Such an automated system should be designed to allow the operator to function with a distorted percept of space as if it were not distorted at all.

9. ACKNOWLEDGEMENTS

10. REFERENCES

1. Shields, N.L., Kirkpatrick, M., Malone, T.B., and Huggins, C.T. Design parameters for a stereoptic television system based on direct depth perception cues. Washington, D.C.: Proceedings of the Human Factors Society 19th Annual Meeting, 1975, pp. 423-427.

2. Grant, C., Meirick, R., Polhemus, C., Spencer, R. Swain, D., and Tewell, R. Conceptual design study for a teleoperator visual system report. Denver, CO: Martin Marietta Corporation Report NASA CR-124273, April 1973.

3. Upton, H.W. and Strother, D.D. Design and flight evaluation of a helmet-mounted display and control system. In Birt, J.A. & Task, H.L. (Eds.) A symposium on visually coupled systems: Development and application (AMD-TR-73-1). Brooks Air Force Base, TX, September, 1973.

4. Zamarian, D.M. Use of stereopsis in electronic displays: Part II - Stereoscopic threshold performance as a function of system characteristics. Douglas Aircraft Company Report MDC J7410, December, 1976.

5. Pepper, R.L., Cole, R.E., and Spain, E.H. The influence of camera separation and head movement on perceptual performance under direct and TV-displayed conditions. Proceedings of the Society for Information Display, 1983, 24, pp. 73-80.

6. Spain, E.H. A psychophysical investigation of the perception of depth with stereoscopic television displays. University of Hawaii doctoral dissertation, May 1984.

7. Bejczy, A.K., Performance evaluation of computer-aided manipulator control. IEEE International Conference on Systems, Man and Cybernetics, 1976.

8. Fender, D.H., Professor, Biological Information Systems California Institute of Technology, Pasadena, Calif. 91125. Personal communication.

11. LIST OF FIGURES

12. LIST OF TABLES

Table 1. Pixel characteristics of the depth distortions of converged cameras at the three intercamera distances tested.

Table 2. Measured distortions and corresponding uncertainties of experiment 1 for four observers.

Table 3. Measured distortions and corresponding uncertainties of experiment 2 for four observers.

Table 4. Measured distortions and corresponding uncertainties shifted to the 0.0 cm aligned position as origin. Data from experiment 1.

Table 5. Measured distortions and corresponding uncertainties shifted to the 0.0 cm aligned position as origion. Data from experiment 2.

Table 6. F and p values from Regression analysis. Experiment 1, non-shifted and shifted data.

Table 7. F and p values from Regression analysis. Experiment 2, non-shifted and shifted data.

Table 8. Statistics of differences in perceived depth distortions of the -5.5 cm and 5.5 cm camera alignment test conditions.

APPENDIX 1

In Figure 18, the lines of equidistant projection are drawn for both cameras. For a point on the fronto-parallel plane of convergence located a distance k horizontally to the left of the camera convergence point, it's projection on the left camera line of equidistant projection will be Pl' from the camera convergence point, where

$$Pl' \; = \; \tan(\text{alpha}) * L$$

$$= \; \tan [\; \arctan(w/D) - \arctan(\; (w-k)/D \;) \;] * L$$

$$= \; \tan \left[\; \arctan \left(\frac{w/D \; - \; (w-k)/D}{1 \; + \; w/D \; * \; (w-k)/D} \right) \; \right] * L$$

$$= \; \frac{[\; w/D \; + \; (k-w)/D \;] * L}{1 \; - \; w \; * \; (k-w)/D^2}$$

$$= \; \frac{k * L * D}{D^2 \; + \; w^2 \; - \; k * w}$$

Similarly, Pr', the projection on the right camera line of equidistant projection, will be:

$$Pr' \; = \; \frac{k * L * D}{D^2 \; + \; w^2 \; + \; k * w}$$

The difference between the two projections will be:

$$Pl' \; - \; Pr' \; = \; \frac{2 * k^2 * D * L * w}{(D^2 \; + \; w^2 \; - \; k * w) * (D^2 \; + \; w^2 \; + \; k * w)}$$

386

The number of pixels difference will be:

$$\text{number of pixels diff} = \frac{(Pl' - Pr') * f}{L * (\text{width per pixel at camera plate})}$$

$$= \frac{2 * k * D * f * w^{2}}{(D^{4} + w^{4} + 2*D^{2}*w^{2} - k^{2}*w^{2}) * (\text{width per pixel})}$$
at camera plate

NOTE: Small angle approximations (x = tan x), would yield

$$Pl' = Pr' = \frac{k * L}{D}$$

or, equivalently, Pl' - Pr' = 0. This is how the small angle approximations can obscure the nature of the stereo depth distortion of the fronto-parallel plane of convergence.
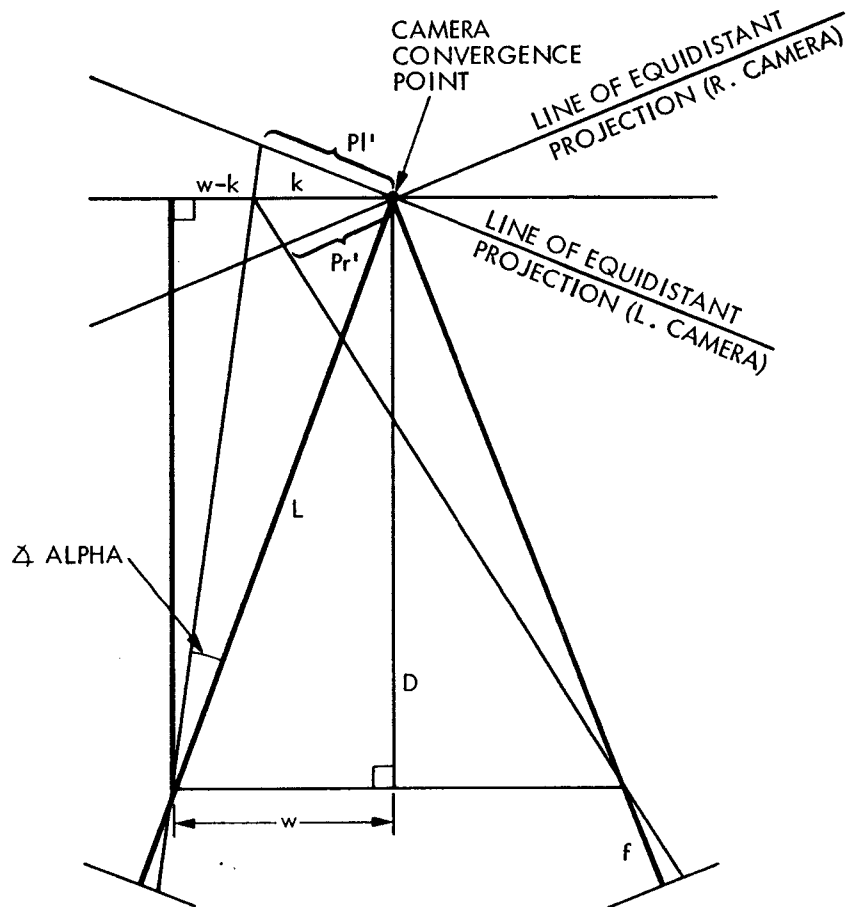
Figure 18. The geometry of converged stereo cameras. On the lines of equidistant projection, every pixel sees a unit length segment of (L/f) * (width/pixel at CCD). The # pixels difference presented to the monitor by the two cameras will be proportional to (Pl' - Pr').

APPENDIX 2

In each experimental run (one ICD and one alignment), 19
test locations were judged 5 times to be in front of, behind or
equal to a fixed location. This gave us a measurement of the
probability that each position would be perceived in front of
the fixed location. We computed that probability as follows:

$$P(front) = \frac{N("1") + N("2") + N("3")/2}{N("1") + N("2") + N("3") + N("4") + N("5")}$$

where $N("I")$ is the number of responses of "I" for $I = 1$ to 5.

    Thus, if an observer answered all "1" and "2" for location
18, we would compute P(front) for location 18 to be 1.0. If an
observer answered "3" twice, and "5" three times, for location 7,
we would compute P(front) for location 7 to be 0.2. (See Figs.
9B and 10B, where location 7 in Figure 9B corresponds to -1 cm on
Figure 10B.) NOTE: we count each "3" response as 1/2 in front
and 1/2 behind. We count "4" and "5" responses as behind, and
therefore they do not show up in the numerator.

    By breaking our responses into two categories, we had a
binomial distribution of P(front) about each location. We
estimated the uncertainty about this point by $(P*(1-P))/N$, where
N is the number of responses at that location, (in this case 5).
The only time an uncertainty could be non-zero is when P is not
equal to 0 or 1. This can only occur when a particular location
was either reported as "3" (equal depth or the observer is
uncertain) or when that location was reported as sometimes in
front and sometimes behind. (NOTE: we did not count reports of
"probably" as adding to the uncertainty).

    We next graphed the P(front) as a function of the distance
between the test location and the right (fixed) bar location,
and computed the area under the curve. We computed a rectangle
of equal area and probability 1.0, which gave an estimate
of the depth distortion between the two bars for that ICD and
at that particular alignment. See Figure 10

    Using the uncertainties of each of the 19 P(front)
measurements, we approximated the uncertainty of the width
of a rectangle of equal area. We first found the area and
standard deviation of each trapezoid under the curve. We
summed the areas, and we used the sums-of-squares rule to
combine the standard deviations. The uncertainty bars on
the rectangles of equal area may, at first glance, appear too
small. They are not. To see this, one must realize that the
Y axis is probability, with a maximum value of 1.0. Thus an
error bar of + or - 1.0 (twice the height of the Y axis) would
contribute between 1/2 cm and 1 cm (depending on the test
location) to the standard deviation of a rectangle of equal area.